Targeting ATM/ATR signalling in lung cancer

Anika Maria Weber

Keble College, University of Oxford

Thesis submitted for the degree of Doctor of Philosophy in Radiobiology
Hilary Term 2015

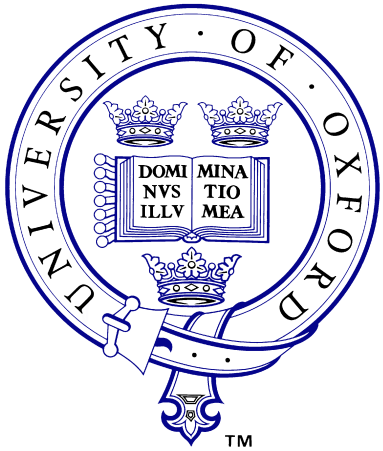

CRUK/MRC Oxford Institute for Radiation Oncology
Department of Oncology, University of Oxford

Targeting ATM/ATR signalling in lung cancer

Anika Maria Weber
Keble College, University of Oxford
Thesis submitted for the degree of Doctor of Philosophy in Radiobiology
Hilary Term 2015

Abstract

Cells respond to the induction of DNA damage with activation of the DNA damage response (DDR), a complex signalling network which orchestrates cell cycle arrest and DNA repair in order to maintain genomic stability and cell viability. Activation of these signalling pathways enables cancer cells to survive DNA damaging chemo- or radiotherapy and contributes to the development of therapy resistance. Therefore, components of the DDR have become attractive targets for chemo- or radiosensitisation. Furthermore, cancer cells frequently exhibit defects in certain DDR components and may, as a consequence, become highly dependent on remaining DDR pathways to survive DNA damage.

Two apical mediators of the DDR are the serine/threonine protein kinases ATM and ATR. ATM is frequently mutated in non-small cell lung cancer (NSCLC), and defects in ATM may render the tumour cells dependent on ATR signalling for survival. In this study, we characterised the functional consequences of ATM mutations in NSCLC cell lines and established an immunohistochemistry-based assay to identify patients with loss of ATM expression. As a single agent, pharmacological ATR inhibition (ATRi) was selectively cytotoxic for cells deficient in both ATM and p53. Furthermore, ATRi in combination with either ATM or PARP inhibition selectively killed tumour cells with mutant p53.

We show that following ATR inhibition, ATM and p53 perform critical cell cycle checkpoint functions, independently of each other. Our results suggest that while retained function in any of these pathways is sufficient to maintain cell viability, functional loss of ATM, ATR and p53 results in premature mitotic entry, chromosome fragmentation and mitotic catastrophe.

We conclude that in NSCLC the functional status of both ATM and p53 determines the cellular response to ATR inhibition, and propose that a combination of ATR inhibition with ATM or PARP inhibition may have broad utility for the treatment of p53-mutated NSCLC.

Acknowledgements

Firstly, I would like to thank my supervisor Dr. Anderson Ryan for sharing his knowledge and experience with me, for guidance, support and many interesting scientific discussions throughout the project.

Many thanks to all the members of the Ryan lab: Aoife, Sivan, Rekha, Yanyan, Neele, Luiza, Amalina, Fiona, John, Agata and Sam who taught me many valuable research skills, made the lab life (and often the after work social life) exciting and have become very dear friends. A special thanks to Agata for proof-reading this thesis despite her own workload and a lot of great support and friendship.

I am very grateful to my wonderful boyfriend, who supported me and took care of me, especially during thesis writing; who listened to my complaints every day, calmed me down, bravely bore my mood swings and managed to make me laugh.

And finally, I would like to thank my parents, my sister and the rest of my family, who have always taken care of me, cheered for me and supported me. Without them I would have never made it this far.

Contents

1 INTRODUCTION 15

1.1 LUNG CANCER 15

1.2 THE DNA DAMAGE RESPONSE 20

1.3 DETECTION AND REPAIR OF DNA DOUBLE STRAND BREAKS (DSBS) 21

1.3.1 DNA DSB repair through non-homologous end-joining (NHEJ) 22

1.3.2 DNA DSB repair through homologous recombination 24

1.4 BASE EXCISION REPAIR 30

1.5 DETECTION AND REPAIR OF DNA SINGLE STRAND BREAKS 33

1.6 CELLULAR RESPONSE TO REPLICATION STRESS 34

1.7 CELL CYCLE CHECKPOINTS 37

1.7.1 The G1/S cell cycle checkpoint 37

1.7.2 The intra-S-phase checkpoint 39

1.7.3 The G2/M cell cycle checkpoint 41

1.8 INTERPLAY BETWEEN THE ATM AND ATR SIGNALLING PATHWAYS 43

1.9 THE ROLE OF THE DDR IN CANCER DEVELOPMENT 45

1.10 THE ROLE OF THE DDR IN THE RESPONSE OF TUMOUR CELLS TO GENOTOXIC THERAPY 47

1.11 THE DDR AS THERAPEUTIC TARGET IN CANCER 47

1.12 POLY(ADP-RIBOSE) POLYMERASE AS THERAPEUTIC TARGET 49

1.13 THE PIKK KINASES: MASTER REGULATORS OF THE DDR AND THEIR POTENTIAL AS THERAPEUTIC TARGETS 51

1.13.1 Targeting the ATM signalling pathway 53

1.13.2 Targeting the ATR signalling pathway 57

1.13.1 Synthetic lethal approaches involving ATM and ATR 62

1.14 AIMS OF THIS STUDY 63

2 MATERIALS AND METHODS 64

2.1 BUFFERS, SOLUTIONS AND CHEMICALS 64

2.2 TISSUE CULTURE 65

2.2.1 Maintenance of cell lines 65

2.2.2 Cryostorage and thawing of cells 67

2.3 ATM GENE SEQUENCING 68

2.3.1 PolyPhen scoring 69

2.4 MYCOPLASMA TESTING 70

2.5 siRNA TRANSFECTIONS 71
2.6 BACTERIAL TRANSFORMATION AND PLASMID PURIFICATION 74
2.6.1 Transformation of bacteria using heat-shock 74
2.6.2 Plasmid purification 75
2.7 GENERATION OF STABLE ATM KNOCKDOWN CELL LINES 76
2.7.1.1 Design of short hairpin RNA sequences 76
2.7.2 Plasmid preparation 77
2.7.3 Transfection and selection of stably transfected clones 78
2.8 LIVE CELL IMAGING 78
2.8.1 Generation of cell lines stably expressing mCherry-conjugated histone H2B 78
2.8.2 Cell imaging 79
2.8.3 Data analysis 80
2.9 DRUG TREATMENTS AND IRRADIATION 80
2.10 PROTEIN DETECTION BY WESTERN BLOTTING 81
2.10.1 Preparation of cell extracts and SDS-polyacrylamide gel electrophoresis 82
2.10.2 Immunoblot 82
2.11 CELL VIABILITY, SPHEROID AND CLONOGENIC SURVIVAL ASSAY 85
2.11.1 Cell viability assay 85
2.11.2 Spheroid growth assay 86
2.11.3 Clonogenic survival assay 87
2.12 FLOW CYTOMETRY 88
2.12.1 DNA content analysis/cell cycle analysis 88
2.12.2 BrdU incorporation analysis 89
2.12.3 BrdU chase assay 90
2.13 IMMUNOFLUORESCENCE 90
2.13.1 Quantitative γH2AX, 53BP1 and RPA32 foci staining 91
2.14 CHROMOSOME ANALYSIS 92
2.14.1 Calculation of mitotic index 93
2.15 HUMAN TUMOUR XENOGRAFT STUDIES 93
2.15.1 Xenograft implantation 93
2.15.2 Formulation of the drugs and treatments 94
2.16 IMMUNOHISTOCHEMISTRY 96
2.16.1 Preparation of cell pellet microarrays for immunohistochemistry 96
2.16.2 Immunohistochemical staining for total ATM in human cancer specimen 97
2.16.3 Immunohistochemistry for pharmacodynamics (PD) studies 98
2.17 DATA ANALYSIS AND STATISTICS 100

3 FUNCTIONAL CONSEQUENCES OF ATM MUTATIONS IN NON-SMALL CELL LUNG CANCER (NSCLC) 101

3.1 DISTRIBUTION AND TYPES OF SOMATIC ATM MUTATIONS IN NSCLC 101

3.2 PHENOTYPIC EFFECTS OF ATM DEFICIENCY 103

3.2.1 Biomarkers of ATM kinase activity 103

3.2.2 Impact of ATM depletion on radiosensitivity and DNA damage induced cell cycle checkpoint activation. 106

3.3 FUNCTIONAL CONSEQUENCES OF ATM MISSENSE MUTATIONS IN NSCLC 110

3.3.1 ATM-deficient cancer cells are highly sensitive to ionising radiation and exhibit cell cycle checkpoint defects. 113

3.4 IDENTIFICATION OF ATM DEFICIENCY IN A CLINICAL SETTING 117

3.4.1 ATM protein expression is frequently lost or reduced in human NSCLC 117

3.5 ROLE OF ATM IN THE CELLULAR RESPONSE TO CHEMOTHERAPEUTIC DRUGS. 123

3.6 DISCUSSION 126

4 TARGETING ATR AS TREATMENT STRATEGY FOR ATM- OR P53-DEFICIENT NSCLC 131

4.1 THE EFFECT OF ATR INHIBITION ON GEMCITABINE-INDUCED CHK1 PHOSPHORYLATION 133

4.2 SIMULTANEOUS LOSS OF ATM AND P53 FUNCTION INCREASES THE CYTOTOXICITY OF PHARMACOLOGICAL ATR INHIBITION. 136

4.3 SIRNA-MEDIATED ATR DEPLETION HAS A DIFFERENT EFFECT ON CELL PROLIFERATION THAN PHARMACOLOGICAL ATR INHIBITION 142

4.4 ASSESSMENT OF RADIOSENSITISATION BY ATR INHIBITORS 145

4.4.1 ATR inhibition leads to attenuation of the DNA damage induced G2/M cell cycle checkpoint 149

4.5 ATR INHIBITION SENSITISES NSCLC CELLS TO GEMCITABINE AND CISPLATIN TREATMENT 157

4.6 DISCUSSION 163

5 COMBINED PHARMACOLOGICAL INHIBITION OF ATM AND ATR FOR THE TREATMENT OF P53-DEFICIENT NSCLC 167

5.1 COMBINED PHARMACOLOGICAL INHIBITION OF ATM AND ATR IS SELECTIVELY CYTOTOXIC FOR P53-DEFICIENT CELLS. 168

5.2 THE INCREASED SENSITIVITY OF ATM- AND P53-DEFICIENT NSCLC CELLS TO PHARMACOLOGICAL INHIBITION OF ATR IS NOT CAUSED BY REPLICATION STRESS 174

5.3 CONCOMITANT DEFICIENCY IN ATM, ATR AND P53 CAUSES ABERRATIONS IN MITOSIS AND CELL DEATH THROUGH MITOTIC CATASTROPHE. 179

5.4 COMBINED INHIBITION OF ATM AND ATR INDUCES DNA DAMAGE IN P53-DEFICIENT CELLS PREDOMINANTLY IN MITOSIS. 187
5.5 ATR INHIBITION IN CELLS WITH FUNCTIONAL LOSS OF BOTH ATM AND P53 INDUCES SEVERE CHROMOSOMAL DAMAGE. 193
5.6 ATM CONTRIBUTES TO THE REGULATION OF CHK1 PHOSPHORYLATION UNDER PHYSIOLOGICAL CONDITIONS 198
5.7 DISCUSSION 201

6 COMBINED PHARMACOLOGICAL INHIBITION OF ATR AND PARP FOR THE TREATMENT OF NSCLC 208

6.1 PARP INHIBITION SENSITISES P53-DEFICIENT NSCLC CELLS TO ATR INHIBITORS. 210
6.2 OLAPARIB ENHANCES ATRI-MEDIATED REPLICATION STRESS AND DNA DSB INDUCTION, PARTICULARLY IN P53-DEFICIENT NSCLC CELLS 214
6.3 COMBINED INHIBITION OF ATR AND PARP INDUCES DNA DAMAGE AND MITOTIC DEFECTS IN P53-DEFICIENT NSCLC CELLS 218
6.4 CELL DEATH IN COMBINATION TREATED CELLS IS DRIVEN BY MULTIPLE MODES OF DEATH. 221
6.5 *IN VIVO* ANTI-TUMOUR ACTIVITY OF COMBINED ATR AND PARP INHIBITION IN P53-DEFICIENT HUMAN NSCLC TUMOUR XENOGRAFTS 225
6.6 *IN VIVO* PHARMACODYNAMICS AND BIOMARKERS OF ATR INHIBITION IN CALU-6 XENOGRAFT MODELS. 229
6.7 DISCUSSION 234

7 GENERAL DISCUSSION AND CONCLUSION 239

8 REFERENCES 249

9 APPENDIX 274

Final word count: approximately 50,000

List of Figures

FIGURE 1.1: THE NHEJ PATHWAY OF DNA DSB REPAIR IN MAMMALIAN CELLS. 23
FIGURE 1.2: HOMOLOGOUS RECOMBINATION REPAIR OF DNA DSBS. 28
FIGURE 1.3: BASE EXCISION REPAIR PATHWAYS 32
FIGURE 1.4: MECHANISM OF PARP1-MEDIATED DNA REPAIR. 34
FIGURE 1.5: A MODEL FOR ATR ACTIVATION BY SINGLE-STRANDED DNA STRUCTURES. 36
FIGURE 1.6: ENFORCEMENT OF THE DNA DAMAGE INDUCED G1 CELL CYCLE CHECKPOINT.. 38
FIGURE 1.7: ENFORCEMENT OF THE INTRA-S-PHASE CHECKPOINT. 40
FIGURE 1.8: ENFORCEMENT OF THE G2/M CELL CYCLE CHECKPOINT. 42
FIGURE 1.9: THE CONCEPT OF SYNTHETIC LETHALITY. 49
FIGURE 1.10: THE PIKK FAMILY MEMBERS. 52
FIGURE 2.1: THE PRINCIPLE OF RNA INTERFERENCE. 73
FIGURE 3.1: DISTRIBUTION AND TYPES OF ATM MUTATIONS IN NSCLC 102
FIGURE 3.2: ATM KNOCKDOWN LEADS TO A REDUCTION IN THE IR-INDUCED PHOSPHORYLATION OF KAP1 AND SMC1. 105
FIGURE 3.3: PHARMACOLOGICAL ATM INHIBITION ATTENUATES ATM AUTOPHOSPHORYLATION AND PHOSPHORYLATION OF THE ATM DOWNSTREAM TARGETS KAP1 AND CHK2. 106
FIGURE 3.4: DOWN-REGULATION OF ATM INCREASES THE SENSITIVITY OF NSCLC CELLS TO IONISING RADIATION. 107
FIGURE 3.5: ATM KNOCKDOWN CAUSES DEFECTS IN THE ENFORCEMENT OF THE G1/S AND INTRA-S-PHASE CELL CYCLE CHECKPOINTS FOLLOWING DNA DAMAGE INDUCTION. .. 108
FIGURE 3.6: PHARMACOLOGICAL ATM INHIBITION ATTENUATES THE G1/S- AND INTRA-S-PHASE DNA DAMAGE CHECKPOINTS. 110
FIGURE 3.7: ATM MISSENSE MUTATIONS CAN LEAD TO A REDUCTION IN ATM PROTEIN LEVELS AND IMPAIRMENT OF THE ATM SIGNALLING PATHWAY IN NSCLC. 112
FIGURE 3.8: ATM DEFICIENCY CONFERS SENSITIVITY TO IONISING RADIATION. 115
FIGURE 3.9: ATM DEFICIENCY LEADS TO ATTENUATION OF THE G1/S AND INTRA-S-PHASE CHECKPOINTS. 116
FIGURE 3.10: ATM PROTEIN EXPRESSION IN NSCLC CELL LINES ASSESSED BY IMMUNOHISTOCHEMISTRY. 118
FIGURE 3.11: IMMUNOHISTOCHEMICAL ANALYSIS OF ATM PROTEIN EXPRESSION IN NSCLC SAMPLES AND NORMAL LUNG TISSUE. 120
FIGURE 3.12: IDENTIFICATION OF TUMORAL LOSS OF ATM PROTEIN EXPRESSION IN COLORECTAL CANCER. 122

FIGURE 3.13: ATM KNOCKDOWN DOES NOT SENSITISE NSCLC CELLS TO CISPLATIN, GEMCITABINE, ETOPOSIDE OR IRINOTECAN. 125
FIGURE 4.1: THE EFFECTS OF ATR INHIBITOR TREATMENT ON THE ACTIVITY OF THE ATR AND ATM SIGNALLING PATHWAYS IN RESPONSE TO GEMCITABINE TREATMENT. 135
FIGURE 4.2: RESPONSE OF NSCLC CELLS AND NORMAL TISSUE CONTROLS TO PHARMACOLOGICAL ATR INHIBITION. 138
FIGURE 4.3: SENSITIVITY OF CELLS TO PHARMACOLOGICAL ATR INHIBITION DOES NOT CORRELATE WITH EXPRESSION LEVELS OF ATR OR CHK1. 140
FIGURE 4.4: PHARMACOLOGICAL ATR INHIBITION IS PARTICULARLY CYTOTOXIC FOR CELLS WITH LOSS OF BOTH ATM AND P53 FUNCTION. 141
FIGURE 4.5: EFFECT OF SIRNA-MEDIATED DEPLETION OF ATR ON ACTIVITY OF THE ATM SIGNALLING PATHWAY AND CELL PROLIFERATION. 143
FIGURE 4.6: VE-821 MEDIATED RADIOSENSITISATION OF NSCLC AND NORMAL BRONCHIAL EPITHELIAL CELLS. 146
FIGURE 4.7: RADIOSENSITISATION OF ATM-DEFICIENT CELLS BY ATRI IS DEPENDENT ON THE FUNCTIONAL STATUS OF P53. 147
FIGURE 4.8: ATM KNOCKDOWN INCREASES THE RADIOSENSITISING EFFECT OF VE-822 TREATMENT. 148
FIGURE 4.9: VE-821 ATTENUATES THE IR-INDUCED G2/M CELL CYCLE CHECKPOINT. 150
FIGURE 4.10: VE-822 ATTENUATES THE IR-INDUCED G2/M CELL CYCLE CHECKPOINT. 151
FIGURE 4.11: VE-821 TREATMENT ABROGATES THE IR-INDUCED G2/M CELL CYCLE ARREST, BUT CELLS WITH RETAINED P53 FUNCTION INDUCE A POST-MITOTIC G1 CELL CYCLE ARREST. 153
FIGURE 4.12: P53-PROFICIENT CELLS SHOW SIGNS OF G1 CHECKPOINT ACTIVATION IN RESPONSE TO IR, IRRESPECTIVE OF THE FUNCTIONAL STATUS OF ATM. 155
FIGURE 4.13: ATM-DEFICIENT CELLS ACTIVATE P53 IN RESPONSE TO IR, INDEPENDENTLY OF DNA-PKCS OR ATR ACTIVITY. 156
FIGURE 4.14: AZD6738 BROADLY SENSITISES P53-DEFICIENT NSCLC CELLS TO GEMCITABINE TREATMENT. 158
FIGURE 4.15: ATR INHIBITION LEADS TO ABROGATION OF GEMCITABINE INDUCED CELL CYCLE ARREST IN P53-DEFECTIVE CELLS 160
FIGURE 4.16: ATR INHIBITION SENSITISES NSCLC CELLS TO CISPLATIN. 162
FIGURE 5.1: PHARMACOLOGICAL INHIBITION OF ATM SELECTIVELY SENSITISES P53-DEFICICIENT CELLS TO VE-821. 169
FIGURE 5.2: THE ATM INHIBITOR KU55933 SELECTIVELY SENSITISES P53-DEFICIENT CELLS TO VE-822. 170

FIGURE 5.3: PHARMACOLOGICAL INHIBITION OF ATR DECREASES CLONOGENIC SURVIVAL OF NSCLC CELLS WITH LOSS OR INHIBITION OF BOTH ATM AND P53 FUNCTION. 171
FIGURE 5.4: SIMULTANEOUS INHIBITION OF ATM AND ATR CAUSES ONLY MINIMAL GROWTH INHIBITION IN NSCLC SPHEROIDS WITH WILD-TYPE P53. 173
FIGURE 5.5: COMBINED INHIBITION OF ATM AND ATR IS SELECTIVELY CYTOTOXIC FOR NSCLC CELLS DEFICIENT IN P53. 175
FIGURE 5.6: INDUCTION OF REPLICATION STRESS BY PHARMACOLOGICAL INHIBITION OF ATR. 178
FIGURE 5.7: CONCOMITANT INHIBITION OF ATM AND ATR RESULTS IN MITOTIC ABERRATIONS AND INDUCTION OF MITOTIC CATASTROPHE IN P53-DEFICIENT CELLS... 180
FIGURE 5.8: PHARMACOLOGICAL ATR INHIBITION INDUCES MICRONUCLEI FORMATION IN CELLS WITH CONCOMITANT DEFICIENCY IN ATM AND P53. 181
FIGURE 5.9: COMBINED ATM AND ATR INHIBITION PROLONGS THE MITOTIC RESIDENCE TIME, INDUCES MICRONUCLEI FORMATION AND CELL DEATH IN P53-DEFICIENT NSCLC CELLS. 184
FIGURE 5.10: COMBINED ATM AND ATR INHIBITION IN P53-DEFICIENT CELLS PROLONGS THE MITOTIC RESIDENCE TIME AND INDUCES CELL DEATH. 185
FIGURE 5.11 COMBINED ATM AND ATR INHIBITION DOES NOT AFFECT MITOTIC FIDELITY OR RESIDENCE TIME IN P53-PROFICIENT CELLS. 186
FIGURE 5.12: ATR INHIBITION INDUCES PAN-NUCLEAR AND PAN-MICRONUCLEAR H2AX PHOSPHORYLATION, PARTICULARLY IN CELLS DEFICIENT IN BOTH ATM AND P53. 188
FIGURE 5.13: INTERPHASE CELLS SHOW ONLY A MODERATE INCREASE IN DNA DSB FORMATION FOLLOWING COMBINED INHIBITION OF ATM AND ATR. 190
FIGURE 5.14: CONCOMITANT INHIBITION OF ATM AND ATR INDUCES γH2AX FOCI FORMATION IN P53-DEFICIENT CELLS PARTICULARLY IN MITOSIS. 192
FIGURE 5.15: CELLS WITH RETAINED P53 FUNCTION SHOW NO INCREASE IN γH2AX FOCI FORMATION IN MITOSIS. 193
FIGURE 5.16: VE-821 INDUCES CHROMOSOMAL DAMAGE AND FRAGMENTATION IN CELLS WITH FUNCTIONAL LOSS OF BOTH ATM AND P53. 195
FIGURE 5.17: CONCOMITANT DISRUPTION OF ATM AND ATR FUNCTION INDUCES CHROMOSOMAL DAMAGE SELECTIVELY IN P53-DEFICIENT CELLS. 197
FIGURE 5.18: P53-PROFICIENT CELLS SHOW A DECREASE IN THE PERCENTAGE OF MITOTIC CELLS WHEN ATM AND/OR ATR SIGNALLING ARE DISRUPTED. 198
FIGURE 5.19: ATM CONTRIBUTES TO THE REGULATION OF CHK1 PHOSPHORYLATION AND ACTIVITY UNDER PHYSIOLOGICAL CONDITIONS. 200

FIGURE 5.20: PROPOSED MECHANISM UNDERLYING THE INCREASED SENSITIVITY OF ATM AND P53 DEFICIENT CELLS TO PHARMACOLOGICAL ATR INHIBITION. 207
FIGURE 6.1: MODE OF ACTION OF OLAPARIB AND RATIONALE FOR THE COMBINATION WITH PHARMACOLOGICAL ATR INHIBITION. 209
FIGURE 6.2: EFFECT OF OLAPARIB ON THE SENSITIVITY OF P53-PROFICIENT AND -DEFICIENT NSCLC CELLS TO AZD6738 TREATMENT. 212
FIGURE 6.3: OLAPARIB SELECTIVELY SENSITISES P53-MUTATED NSCLC CELLS TO AZD6738 IN 3D SPHEROID MODELS. 215
FIGURE 6.4: COMBINED ATR AND PARP INHIBITION INDUCES REPLICATION STRESS AND PAN-NUCLEAR H2AX PHOSPHORYLATION. 217
FIGURE 6.5: COMPARISON OF DNA DSB INDUCTION AND CELL CYCLE CHECKPOINT ACTIVATION BY VE-821 +/- OLAPARIB OR AZD6738 +/- OLAPARIB TREATMENT. 219
FIGURE 6.6: AZD6738 TREATMENT ALONE OR IN COMBINATION WITH OLAPARIB CAUSES THE INDUCTION OF DNA DSBS AND ACTIVATION OF THE ATM SIGNALLING PATHWAY SELECTIVELY IN P53-DEFICIENT NSCLC CELLS. 222
FIGURE 6.7: COMBINED ATR AND PARP INHIBITION CAUSES FORMATION OF MICRONUCLEI IN P53-DEFICIENT NSCLC CELLS. 223
FIGURE 6.8: P53-PROFICIENT NSCLC CELLS SHOW NO MICRONUCLEI FORMATION FOLLOWING COMBINED INHIBITION OF ATR AND PARP. 224
FIGURE 6.9: *IN VIVO* ANTI-TUMOUR ACTIVITY OF AZD6738 AND AZD2281 ALONE AND IN COMBINATION IN A HUMAN XENOGRAFT MODEL OF H1975 NSCLC CELLS. 226
FIGURE 6.10: *IN VIVO* ANTI-TUMOUR ACTIVITY OF AZD6738 AND AZD2281 ALONE AND IN COMBINATION IN A HUMAN XENOGRAFT MODEL OF CALU-6 NSCLC CELLS. 228
FIGURE 6.11: EFFECT OF AZD6738 AND/OR OLAPARIB TREATMENT ON TUMOUR CYCLIN A AND PHOSPHO-HISTONE H3 LEVELS IN CALU-6 HUMAN NSCLC XENOGRAFTS 231
FIGURE 6.12: AZD6738 TREATMENT ALONE AND IN COMBINATION WITH OLAPARIB INDUCES PAN-NUCLEAR H2AX PHOSPHORYLATION IN CALU-6 XENOGRAFTS *IN VIVO*. 232
FIGURE 6.13: PAN-NUCLEAR H2AX PHOSPHORYLATION IN CALU-6 XENOGRAFT CELLS IN RESPONSE TO AZD6738+OLAPARIB TREATMENT OCCURS MORE FREQUENTLY IN HIGHLY VASCULARISED TUMOUR AREAS. 233

List of Tables

TABLE 1.1: NSCLC STAGE AT DIAGNOSIS AND 5-YEAR SURVIVAL RATES. 17

TABLE 1.2: TREATMENT OPTIONS FOR NSCLC PATIENTS ACCORDING TO STAGE AT DIAGNOSIS. 18

TABLE 1.3: ATM INHIBITORS 54

TABLE 1.4: ATR INHIBITORS 60

TABLE 2.1: BUFFERS AND SOLUTIONS FREQUENTLY USED THROUGHOUT THIS STUDY 64

TABLE 2.2: CELL LINES USED IN THIS STUDY 66

TABLE 2.3: ANTIBODIES USED FOR IMMUNOBLOT ANALYSIS. 83

TABLE 2.4: ANTIBODIES USED FOR IMMUNOHISTOCHEMISTRY 99

TABLE 3.1: ATM PROTEIN EXPRESSION IS FREQUENTLY LOST OR REDUCED IN NSCLC. 121

TABLE 3.2: SENSITIVITY OF NORMAL BRONCHIAL EPITHELIAL CONTROL AND NSCLC CELL LINES TO GEMCITABINE, CISPLATIN, ETOPOSIDE AND IRINOTECAN. 124

TABLE 4.1: SENSITIVITY OF NSCLC CELL LINES AND NORMAL TISSUE CONTROLS TO PHARMACOLOGICAL ATR INHIBITION. 139

TABLE 4.2: SENSITISATION OF NSCLC CELL LINES TO GEMCITABINE BY ATR INHIBITORS. 159

TABLE 4.3: SENSITISATION OF NSCLC CELL LINES TO CISPLATIN BY ATR INHIBITORS. 161

TABLE 6.1: IC_{50} VALUES FOR VE-821 ALONE OR IN COMBINATION WITH OLAPARIB. 211

TABLE 6.2: IC_{50} VALUES FOR AZD6738 ALONE OR IN COMBINATION WITH OLAPARIB. 213

Abbreviations

2D	two-dimensional
3D	three-dimensional
53BP1	tumour protein p53 binding protein 1
A	adenine
ADP	adenosine diphosphate
AP	apurinic/apyrimidinic
A-T	Ataxia-telangiectasia
ATCC	American Type Culture Collection
ATM	Ataxia-telangiectasia mutated
ATMi	ATM inhibitor/ pharmacological ATM inhibition
ATP	adenosine triphosphate
ATR	Ataxia-telangiectasia and Rad3-related
ATRi	ATR inhibitor/ pharmacological ATR inhibition
ATRIP	ATR interacting protein
BER	base excision repair
BRCA1	breast cancer type 1 susceptibility protein
BRCA2	breast cancer type 2 susceptibility protein
BrdU	bromodeoxyuridine
BSA	bovine serum albumin
C	cytosine
CDC25	Cell division cycle 25
CDK	Cyclin dependent kinase
CHK1	checkpoint kinase 1
CHK2	checkpoint kinase 2
CFS	common fragile site
CPT	Camptothecin
CtIP	CTBP interacting protein
DAPI	4’,6-diamidino-2-phenylindole
DDR	DNA damage response
DMEM	Dulbecco's modified Eagle's medium
DMSO	dimethyl sulfoxide
DNA	deoxyribonucleic acid
DNA-PK	DNA-dependent protein kinase
DNA-PKcs	DNA-dependent protein kinase catalytic subunit
DSB	double-strand break
dsDNA	double-stranded DNA
EDTA	Ethylenediaminetetraacetic acid
FACS	fluorescence-activated cell sorting
FBS	foetal bovine serum

G	guanine
G1-phase	gap phase of cell cycle before DNA replication
G2-phase	gap phase of cell cycle before mitosis
GFP	green fluorescent protein
h	hour(s)
dH_2O	distilled water
HR	homologous recombination
HRP	horseradish peroxidase
IC_{50}	half-maximal inhibitory concentration
IR	ionising radiation
KAP1	Krüppel-associated box-associated co-repressor 1
kd	kinase-dead
MDC1	mediator of DNA damage checkpoint protein 1
MI	mitotic index
min	minute(s)
M-phase	mitosis
mRNA	messenger RNA
MRN	Protein complex including Mre11, Rad50 and Nbs1
mut	mutated
N/A	not analysed/ excluded from analysis
NBS1	Nijmegen break syndrome 1
ND	not detectable
NGS	normal goat serum
NHEJ	non-homologous end joining
ON	overnight
p53	tumour protein 53
PAR	poly(ADP-ribose)
PARP	poly(ADP-ribose)-polymerase
PARPi	PARP inhibitor/pharmacological PARP inhibition
PBS	phosphate buffered saline
PCR	polymerase chain reaction
PD	pharmacodynamics
PFA	Paraformaldehyde
PI	propidium iodide
PIKK	phosphatidylinositol 3-kinase-related kinase
p.o.	orally
Polβ/ Polδ/ Polε	DNA polymerase β/ δ/ ε
PolyPhen	polymorphism phenotyping
RAD51	radiation sensitivity abnormal 51
RISC	RNA-induced silencing complex
RNA	ribonucleic acid
RNAi	RNA interference
RPA	replication protein A

RT	room temperature
S	serine
s.c.	sub cutaneous
S-phase	DNA replication or synthesis phase of the cell cycle
SDSA	synthesis-dependent strand annealing
SDS	sodium dodecyl sulphate
SEM	standard error of the mean
SER	sensitisation enhancement ratio
SF	surviving fraction
shRNA	short-hairpin RNA
siRNA	small interfering ribonucleic acid
SMC1	structural maintenance of chromosomes protein 1
SR	sensitisation ratio
SSB	single-strand break
ssDNA	single-stranded DNA
T	thymine
TBS	Tris-buffered saline
Thr	Threonine
wt	wild-type
x g	times gravity
XRCC	X-ray cross complementing protein
γH2AX	phosphorylated histone H2AX

CHAPTER 1

1 Introduction

1.1 Lung cancer

Lung cancer is the most common type of cancer worldwide with 1.8 million new cases diagnosed in 2012, equalling 13% of total cancer diagnoses (American Cancer Society, 2014). The term lung cancer refers to carcinomas that originate from the respiratory epithelium of the lung. There are two major types of lung cancer: non-small cell lung cancer (NSCLC), which accounts for approximately 85% of all lung cancers, and small cell lung cancer (10-15% of cases). The distinction is based on histological features of the tumours and is important for the purpose of prognosis and to determine treatment options. NSCLC is further sub-divided into histological subtypes, of which adenocarcinoma, squamous cell carcinoma and large cell carcinoma (approximately 30-45%, 33% and 9% of cases, respectively) are the most common (Davidson *et al*, 2013; Vaporciyan *et al*, 2003). These histologies are grouped together as NSCLC because approaches to diagnosis, staging, prognosis, and treatment are similar.

Several risk factors contribute to the development of lung cancer, however tobacco smoking is the single most important factor. The risk increases with both quantity and duration of smoking. Additional risk factors include occupational or environmental exposure to asbestos, certain metals (chromium, cadmium, arsenic, nickel), some organic chemicals, radiation or air pollution (American Cancer Society, 2014).

Lung cancer has one of the lowest survival outcomes of any cancer, accounting for 27% of all cancer-related deaths - equal to prostate, breast, colon and pancreatic

cancer combined (American Cancer Society, 2014). Only one third of patients survive one year after diagnosis and the 5-year survival rate is only 17% in the USA and 10% in the UK (National Collaborating Centre for Cancer (UK), 2011; American Cancer Society, 2014). The poor prognosis can be attributed to the frequently advanced stage of the disease at the point of diagnosis (for 5-year survival rates according to stage at diagnosis see Table 1.1). As lung cancer generally does not cause any specific symptoms during its early stages, more than one third of NSCLC patients are diagnosed with late stage metastatic disease (stage IV), which thus far remains incurable and has a 5-year survival rate of ≤ 1% (Howlader *et al*, 2013; The Information Centre for Health and Social Care, 2006) (Table 1.1). Approximately one third of NSCLC patients first present with locally advanced or advanced disease, which remains local to the thorax but is in most cases considered unresectable due to the tumour size and the extent of normal tissue invasion (Stage IIIA and IIIB) (National Collaborating Centre for Cancer (UK), 2011). Only about 22% of patients are diagnosed at a sufficiently early stage (I or II) to have a reasonable possibility of long-term survival or cure.

Treatment options largely depend on the histological subtype of the tumour, the stage at the point of diagnosis and the performance status of the patient. Surgical resection is the standard treatment for patients with early-stage (I–II) NSCLC and selected patients with stage IIIA disease (locally advanced disease, with lymph node involvement on the same side of the chest as the tumour). Surgery remains the best treatment option for curative intent, but only about 20% of tumours are suitable for resection (Non-Small Cell Lung Cancer Collaborative Group, 2010). Therefore, DNA-damaging modalities such as chemotherapy and radiation represent the cornerstone of treatment for the majority of lung cancer patients (O'Rourke *et al*, 2010; Non-Small Cell Lung

Cancer Collaborative Group, 2010; Reck *et al*, 2013; National Collaborating Centre for Cancer (UK), 2011) (see Table 1.2).

Table 1.1: NSCLC stage at diagnosis and 5-year survival rates.

Cancer stage	Brief description	Stage at first diagnosis in UK (%)	5-year survival rate UK (%) [1]	5-year survival rate USA (%) [2]
IA/IB	Tumour localised in lung - no spread to lymph nodes	14.5	35	47
IIA/IIB	Tumour localised in lung – spread to lymph nodes	7.3	21	30
IIIA/IIIB	Tumour spread locally in the lung and to lymph nodes	31.8	6	9.5
IV	Cancer has metastasised to the other lung or distant organs	35.8	N/A [3]	1
Stage unknown	Stage not reported	10.6	6	7.4

Radiation therapy may be recommended for patients with stage I/II tumours who are not good candidates for surgery, for example due to underlying medical problems. In some cases, the initial surgery or radiation therapy may be followed by adjuvant chemotherapy. Patients with stage III lung tumours are generally treated with radio- or chemotherapy or a combination of both (O'Rourke *et al*, 2010). Palliative chemotherapy or radiotherapy is offered to patients with stage IV disease with the aim

1. (The Information Centre for Health and Social Care, 2006)
2. The numbers are survival rates published in 2007. They are calculated from the National Cancer Institute's Surveillance, Epidemiology, and End Results (SEER) database, based on people who were diagnosed with non-small cell lung cancer between 1998 and 2000.(Howlader *et al*, 2013)
3. Data not available due to the small number of patients surviving > 2 years.

of improving disease-related symptoms and delaying disease progression (Table 1.2). Patients with good performance status will usually be offered doublet chemotherapy comprising a platinum agent (cisplatin or carboplatin) combined with another agent (most commonly paclitaxel, docetaxel, gemcitabine, irinotecan, pemetrexed or vinorelbine). Patients who have poor performance status, or who have good performance status but whose disease has progressed on a platinum-based doublet, will be offered single agent chemotherapy (most commonly docetaxel or pemetrexed).

Table 1.2: Treatment options for NSCLC patients according to stage at diagnosis[4].

Stage	Standard treatment options
IA/IB	Surgical resection, definitive radiotherapy (curative intent)
IIA/IIB	Surgical resection or definitive radiotherapy followed by adjuvant chemotherapy
IIIA/IIIB	Multimodality treatment: Chemotherapy, definitive radiotherapy +/- surgical resection, or concurrent chemoradiotherapy
IV	Chemotherapy; possibly targeted therapies according to driver mutations (e.g. gefitinib or erlotinib). Radiotherapy (palliative intent).

Despite many efforts to improve the treatment and outcome of patients with NSCLC over the past decades, overall survival rates have only marginally increased (Schiller *et al*, 2002; Howlader *et al*, 2013). Improvements in diagnostics and treatments are urgently needed, yet there is a sense that the use of traditional chemotherapeutic agents may have reached a plateau of efficacy, which cannot be improved further with conventional chemotherapeutic drugs (Carney, 2002). However, advances in our understanding of the molecular biology of cancer and the mechanisms underlying

4. References: (Non-Small Cell Lung Cancer Collaborative Group, 2010; National Collaborating Centre for Cancer (UK), 2011; Reck *et al*, 2013; O'Rourke *et al*, 2010)

tumorigenesis have enabled the development of novel therapeutic approaches. It is well established that cancer results from multiple complex combinations of molecular and genetic alterations, which ultimately lead to a malignant mass of cells bearing the phenotypic hallmarks of cancer (Hanahan & Weinberg, 2011). One of the most prominent features of malignant cells is their ability to sustain unrestrained proliferation, which results from a deregulation of tumour suppressor genes and tumour promoting oncogenes. Identification and characterisation of such cancer-promoting oncogenic driver-mutations has contributed to the development of targeted therapies that inhibit signalling pathways involved in the development and progression of cancer (Hanahan & Weinberg, 2011).

The best-established oncogenic target for the management of advanced NSCLC so far is the epidermal growth factor receptor (EGFR). 10% of Caucasian NSCLC patients and 20-40% of Asian NSCLC patients have tumours which harbour genetic alterations in the tyrosine kinase domain of the EGFR gene that lead to sustained activity of this receptor and consequently promotion of survival and proliferation of the cancer cells (Chung, 2015). Several small molecules targeting EGFR have been developed (e.g. gefitinib and erlotinib), which competitively inhibit ATP binding at the tyrosine kinase domain of the receptor and block oncogenic signalling. Clinical trials have demonstrated that patients with EGFR mutation positive NSCLC receive greater benefit from EGFR inhibitors compared with standard platinum-based chemotherapy in terms of improved response rate and progression-free survival. In contrast, patients with tumours without activating EGFR mutations receive greater benefit from chemotherapy (Lynch *et al*, 2004; Paez *et al*, 2004; Mok *et al*, 2009; Mitsudomi *et al*, 2010; Maemondo *et al*, 2010).

In addition to therapeutic approaches targeting oncogenic driver mutations, a new class of small molecule inhibitors has been developed in recent years, which aim to enhance the efficacy of standard chemo- or radiotherapy and improve treatment outcome and patient survival. This new group of compounds selectively target the DNA damage response - the cellular signalling pathways that allow a cell to repair and consequently survive the DNA damage induced by chemo- or radiotherapy.

1.2 The DNA damage response

In every cell, tens of thousands of DNA lesions are generated each day, which threaten the integrity of the genome (Lindahl, 1993). This DNA damage can be caused exogenously by exposure to environmental factors such as different types of radiation or genotoxic agents. It can also occur endogenously through, for example, reactive by-products of the cellular metabolism (Lindahl & Barnes, 2000; De Bont & van Larebeke, 2004). If unrepaired or aberrantly repaired, such lesions may prove lethal to the cell or give rise to deleterious mutations that can affect cell viability or induce aberrant cellular behaviour leading to the development of cancer. Because genetic alterations have such a significant potential impact on survival and viability of a cell, as well as the organism as a whole, cells have developed a complex network of signalling pathways – collectively known as the DNA damage response (DDR) - that orchestrates the detection and repair of DNA damage with transient cell cycle arrest to ensure maintenance of genomic stability and cell viability (Jackson & Bartek, 2010; Ciccia & Elledge, 2010). A detailed description of all the proteins and mechanisms involved in the DDR is beyond the scope of this introduction, therefore the focus will

be on some of the key players and pathways which have attracted interest as potential targets for cancer treatment in recent years.

1.3 Detection and repair of DNA double strand breaks (DSBs)

Of the many different types of DNA lesions, DNA double strand breaks (DSBs) are amongst the most deleterious. It has been suggested that a single unrepaired DSB may be sufficient to induce cell death (Bennett *et al*, 1993), whereas misrepaired DSBs can result in loss of genetic information, potentially harmful mutations or chromosomal rearrangements, which can lead to cancer development. DNA DSBs can arise, for example, intrinsically through the collapse of stalled replication forks or from damage by reactive oxygen species produced during cellular metabolism, or extrinsically through exposure to ionising radiation (IR) (O'Driscoll & Jeggo, 2006).

There are two main pathways which mediate the repair of DNA DSBs: Non-homologous end joining (NHEJ), which links together the two broken DNA ends by direct ligation, and homologous recombination (HR), which is only available during the S- and G2-phases of the cell cycle when a sister chromatid can be used as a template for the repair reaction (Helleday *et al*, 2007; O'Driscoll & Jeggo, 2006).

It should be noted that at least two additional pathways for the detection and repair of DNA DSBs have been reported, namely micro-homology mediated end-joining and single-strand annealing (Ciccia & Elledge, 2010). However, these pathways are thought to play a minor role in comparison to NHEJ and HR and will not be discussed further.

1.3.1 DNA DSB repair through non-homologous end-joining (NHEJ)

As NHEJ repairs DNA DSBs through direct ligation of the broken DNA ends it requires no sister chromatid as a template and is active in all phases of the cell cycle.

NHEJ is initiated when DNA DSBs are sensed and bound by the ring-shaped Ku heterodimer, which consists of the Ku70 and Ku80 subunits (Figure 1.1a) (Griffith *et al*, 1992; Mari *et al*, 2006). The Ku heterodimer slides onto the ends of the broken DNA in a sequence independent manner, as it interacts with the DNA sugar backbone and not with the bases (Walker *et al*, 2001). DNA-bound Ku recruits the DNA-protein kinase catalytic subunit (DNA-PKcs), to form the DNA-PK holoenzyme (Figure 1.1b) (Gottlieb & Jackson, 1993). DNA-PKcs is a large (469 kDa) serine threonine protein kinase of the phosphatidylinositol 3-kinase-related-kinase (PIKK) family. Its interaction with DSB-bound Ku leads to activation of the DNA-PKcs kinase activity, which is required for NHEJ (Gottlieb & Jackson, 1993; Kurimasa *et al*, 1999; Zhao *et al*, 2006). The DNA-Ku-DNA-PKcs complex also protects and stabilises the two ends of the broken DNA molecule, and holds them together (Walker *et al*, 2001; DeFazio *et al*, 2002). Furthermore, the complex functions as a scaffold to attract other NHEJ factors to the DSB, including those involved in the enzymatic processing of DNA ends, the second step in the NHEJ process (Mahaney *et al*, 2009).

DNA termini at sites of DNA DSBs are often complex, especially those induced by IR or reactive oxygen species, and may require processing to create DNA ends that can be ligated (Mahaney *et al*, 2009; O'Driscoll & Jeggo, 2006). Depending on the nature of the break, different processing enzymes may be required to remove non-ligatable end groups (e.g. 3'-phosphate groups) or incompatible single-strand overhangs, to fill in gaps or to remove secondary structure elements surrounding the break (Mahaney *et*

al, 2009). The processing of 3' or 5' single-strand overhangs is performed either by filling, using the nucleotide sequence of the overhang as a template to duplicate a complementary strand, or by resection of the overhang (Figure 1.1c).

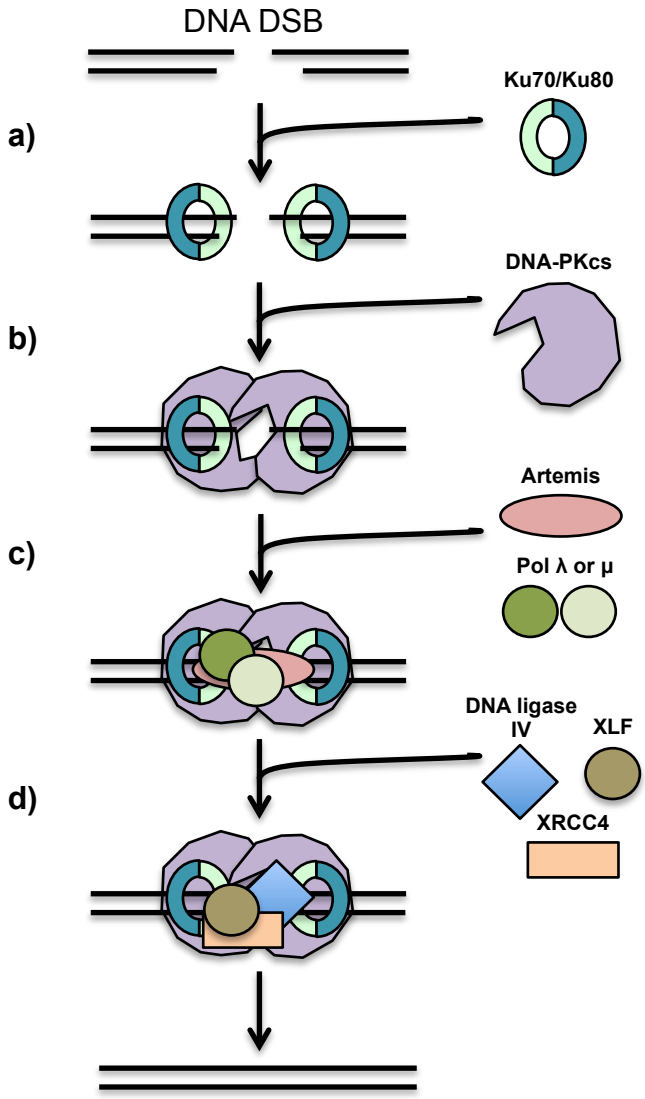

Figure 1.1: The NHEJ pathway of DNA DSB repair in mammalian cells.

a) DNA DSBs are sensed by the ring shaped Ku70/Ku80 heterodimer, which then recruits and activates DNA-PKcs forming the DNA-PK holoenzyme (**b**). DNA-PK stabilises the two ends of the broken DNA molecule and keeps them in close proximity. **c)** Processing enzymes (including polymerases λ or μ and Artemis) are recruited to create ligatable DNA ends. **d)** Finally, the complex of DNA ligase IV, XRCC4 and XLF forms at the site of the DNA DSB and re-ligates the broken DNA strands.

Several enzymes with single-strand filling capability, including polymerase λ and polymerase μ, have been suggested to play a role as DNA processing enzymes during NHEJ (Lee *et al*, 2004; Mahajan *et al*, 2002). The resection of DNA ends for NHEJ is performed by the endonuclease Artemis, which is likely recruited to the repair complex by interaction with the DNA-Ku-DNA-PKcs complex (Ma *et al*, 2002; Povirk *et al*, 2007). Artemis activity is regulated by DNA-PKcs through both complex formation and phosphorylation (Ma *et al*, 2002).

DSB-bound Ku also serves to recruit the repair factors mediating the final step of NHEJ: the re-ligation (Mari *et al*, 2006). DNA ligase IV provides the catalytic activity for the re-joining of the DNA ends (Figure 1.1d). It forms a complex with XRCC4 and XLF, which stabilise DNA ligase IV and stimulate its activity (Grawunder *et al*, 1997; Ahnesorg *et al*, 2006).

NHEJ is inherently error prone, as the processing of DSB ends can result in the loss of nucleotides and the re-ligation is performed in a template-independent manner (Mahaney *et al*, 2009).

1.3.2 DNA DSB repair through homologous recombination

Homologous recombination (HR) repairs DNA DSBs with high fidelity using an undamaged sister chromatid as a template, but can only operate following DNA replication in the S- and G2-phases of the cell cycle. Compared to NHEJ, HR is a slow process that involves a coordinated series of complex events: DNA end resection, RAD51 filament formation on the resulting ssDNA, search for homologous DNA sequence and strand invasion (heteroduplex formation), repair synthesis, and resolution of the heteroduplex (Helleday *et al*, 2007; Krejci *et al*, 2012).

HR is initialised by the recognition of DNA DSBs through the MRE11-RAD50-NBS1 (MRN) complex. The MRN complex assembles at sites of DNA DSBs, where it acts as a damage sensor that can also form a physical bridge spanning the DSB (Stracker & Petrini, 2011). The MRN complex then recruits Ataxia-telangiectasia mutated (ATM; Figure 1.2a) which, like DNA-PKcs, is a member of the PIKK family of serine/threonine kinases (Lee & Paull, 2005).

In its inactive state, ATM forms homodimers or higher order multimers which dissociate into active monomers following rapid intermolecular autophosphorylation at serine 1981 (S1981) upon ATM activation (Bakkenist & Kastan, 2003). This S1981 autophosphorylation is considered a hallmark of activated human ATM (Shiloh & Ziv, 2013) and several studies have demonstrated that mutation of this site to alanine (S1981A) leads to defects in the monomerisation of ATM, the stabilisation of ATM at sites of DNA DSBs and the efficient phosphorylation of its downstream targets after DNA damage induction (Berkovich et al, 2007; So et al, 2009; Kozlov et al, 2006). It should be noted however, that the physiological significance of this autophosphorylation event *in vivo* is still controversial, as mutation of mouse ATM at S1987 (the mouse homologue of human S1981) to alanine did not affect the localisation of ATM to DNA DSBs or the phosphorylation of its downstream targets when expressed in an ATM knockout background (Pellegrini et al, 2006). Several other ATM autophosphorylation sites have also been shown to be dispensable for the function and activity of murine ATM *in vivo* (Daniel *et al*, 2008). Further studies will need to address the question whether these differential observations are due to species-specific differences in ATM activation, or whether they reflect S1981 autophosphorylation to be a consequence of, rather than a requirement for, ATM activation.

ATM recruitment to sites of DNA DSBs has been shown to require its binding to the C-terminus of NBS1, an interaction that also enhances the kinase activity of ATM (You et al, 2005). Immediately following its recruitment to sites of DNA DSBs, ATM contributes to the phosphorylation of the histone variant H2AX on serine 139 (referred to as γH2AX) (Burma *et al*, 2001). Depending on the cellular context and the source of DNA damage, H2AX phosphorylation can also be mediated through ATR or DNA-PKcs, highlighting the complex interactions and overlapping functions of these kinases in orchestrating the cellular response to DNA damage (Hammond *et al*, 2003; Stiff *et al*, 2004; An *et al*, 2010; Ward & Chen, 2001). H2AX phosphorylation in turn initiates a cascade which assembles DDR components at the breakage site (Figure 1.2b) (Scully & Xie, 2013; Paull *et al*, 2000).

In addition to histone H2AX, activated ATM phosphorylates numerous DNA repair and cell cycle checkpoint proteins including: CHK2, p53, (CtBP)-interacting protein (CtIP) and breast cancer type 1 susceptibility protein (BRCA1) (Cortez *et al*, 1999; Canman *et al*, 1998; Banin *et al*, 1998; Siliciano *et al*, 1997; Matsuoka *et al*, 1998; Wang *et al*, 2013). Interestingly, MRN complex components not only modulate the activity of ATM, but are also amongst its downstream targets (Di Virgilio *et al*, 2009; Lim *et al*, 2000; Gatei *et al*, 2011, 2000). This suggests that ATM and the MRN complex work together at the sites of DNA DSBs to fine-tune the recruitment and dissociation of DDR factors and promote effective DNA damage repair.

The adaptor protein mediator of DNA damage checkpoint protein 1 (MDC1) is recruited to DNA DSB through direct interaction with γH2AX (Stucki *et al*, 2005). MDC1 in turn is recognised by the E3 ubiquitin ligase RNF8, which ubiquitinylates histones in the vicinity of the DSB (Mailand *et al*, 2007). This ubquitinylation signal is

further amplified by the E3 ubiquitin ligase RNF168 and eventually leads to the recruitment of tumour protein p53 binding protein 1 (53BP1) and BRCA1 to the DSB (Figure 1.2b) (Mailand *et al*, 2007; Doil *et al*, 2009).

In addition to stabilising DNA ends, MRE11 possesses endo- and exonuclease activities and initiates DSB end resection (Buis *et al*, 2009). Other proteins are also involved in this process including CtIP and BRCA1 (Chen *et al*, 2008). CtIP directly interacts with NBS1 and BRCA1 and is essential for the DNA end resection processes required for HR (You & Bailis, 2010; Sartori *et al*, 2007; Huertas & Jackson, 2009; Chen *et al*, 2008). In the S- and G2-phases of the cell cycle, CtIP undergoes CDK-dependent phosphorylation[5], which promotes its binding to BRCA1 and the MRN complex (Chen *et al*, 2008; Wang *et al*, 2013). This phosphorylation furthermore facilitates ATM-dependent phosphorylation of CtIP, which has been shown to be important for promoting CtIP-mediated end resection, helping elucidate the role of ATM in DSB repair (Wang *et al*, 2013). Following the initial 5' to 3' DNA end resection by CtIP and MRE11, which generates a 3' single-stranded DNA (ssDNA) overhang, extensive resection is performed by the exonuclease EXO1 with the help of the Bloom syndrome helicase (BLM; Figure 1.2c) (Nimonkar *et al*, 2008). The ssDNA generated by resection is rapidly coated by replication protein A (RPA) (Wold, 1997; Wold & Kelly, 1988), which stabilises the ssDNA and results in the activation of the PIKK family member ATR (ATR activation and function is discussed in more detail in section 1.6) (Jazayeri *et al*, 2006; Myers & Cortez, 2006).

5. CDK1 in yeast, CDK2 in mammals (You & Bailis, 2010).

The initial recombination step requires the RAD51 recombinase, which, with the help of BRCA2, replaces RPA coating on the ssDNA (Davies *et al*, 2001; Tarsounas *et al*, 2004).

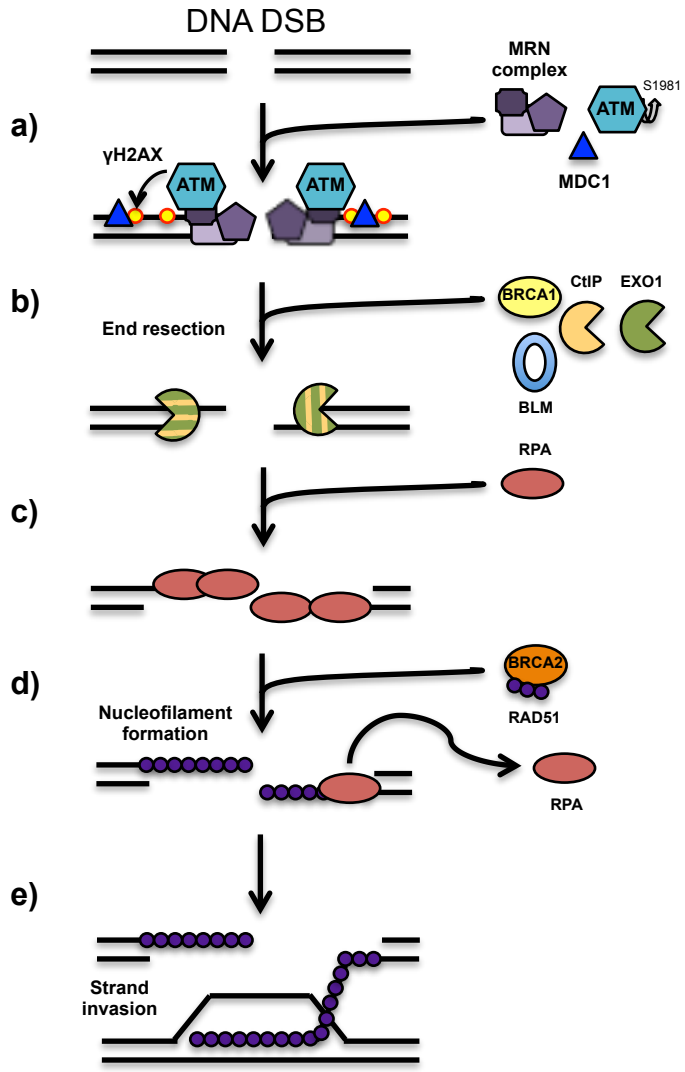

Figure 1.2: Homologous recombination repair of DNA DSBs.

a) The MRN complex assembles at sites of DNA DSBs and recruits the ATM kinase. Activated ATM phosphorylates numerous substrates including histone H2AX, which leads to recruitment of MDC1 and, subsequently, BRCA1 and CtIP.
b) In a reaction that depends on several endo- and exonucleases (including MRE11, CtIP and EXO1, which is supported by the BLM helicase), DSBs are resected forming ssDNA ends, which are rapidly coated by RPA **(c)**.
d) RPA is replaced by RAD51, which together with associated proteins forms a nucleoprotein filament that invades the undamaged sister-chromatid forming a D-Loop structure **(e)**.

Together with other associated proteins (including RAD52 and RAD54), RAD51 forms a nucleoprotein filament that mediates strand invasion of the sister chromatid to form a displacement loop ("D-loops"; Figure 1.2d) (West, 2003; Baumann *et al*, 1996). Several models for the next steps in homology directed repair have been described, most notably the formation of a double Holliday junction or synthesis-dependent strand annealing (SDSA).

SDSA is believed to be the main HR repair mechanism and results in a non-crossover product, as following homology-directed DNA synthesis, the invading strand is directly re-annealed to the other end. After D-loop formation, the annealed 3' end is extended by repair synthesis, performed by DNA polymerase η (McIlwraith *et al*, 2005). The newly synthesised end is released by the Holliday junction sliding towards the 3' end in a process referred to as branch migration, which is facilitated by the RAD54, BLM and WRN (Werner syndrome helicase) proteins (Bugreev *et al*, 2006; Constantinou *et al*, 2000). Final processing to remove flaps, fill in gaps, and ligate remaining nicks completes this pathway (Helleday *et al*, 2007).

According to the double Holliday junction model, both DNA ends invade the homologous DNA template and form a double Holliday junction that may be resolved by creating a crossover or a non-crossover product. Several proteins have been implicated in the regulation of this process (Fekairi *et al*, 2009; Raynard *et al*, 2006; Wu & Hickson, 2003), however, the complex mechanisms involved are not yet fully understood.

The choice whether a DNA DSB is repaired via NHEJ or HR depends on several factors, most obviously the cell cycle stage at which the DSB is induced. Therefore, as mentioned above, one important mediator of the pathway choice is CDK2, which

prevents resection of DNA ends outside the S- and G2-phases of the cell cycle (Ira et al, 2004; Aylon et al, 2004; Chen et al, 2008; Wang et al, 2013).

As a first responder to DNA DSBs, the MRN complex is another important factor in the pathway choice. Depending on the type of the break and the chromatin context, it acts together with ATM and DNA-PKcs to promote repair by either HR or NHEJ through the endo- and exonuclease activities of MRE11 (Zhou & Paull, 2013; Shibata *et al*, 2011, 2014). MRE11 was also demonstrated to regulate CtIP-dependent DSB repair via interaction with CDK2 (Buis et al, 2012).

Additional DNA repair factors which have been linked to the choice between NHEJ and HR include 53BP1 and BRCA1 (Kakarougkas & Jeggo, 2014; Daley & Sung, 2014). Despite many advances in recent years, however, many aspects of how DSB repair pathway choice is determined at the molecular level are still unresolved and remain the subject of intense study.

1.4 Base excision repair

Base excision repair (BER) is a DDR pathway that corrects non-bulky damage to bases, which can result from, for example, oxidation, deamination, or spontaneous loss of the DNA base itself (Lindahl & Barnes, 2000; Lindahl, 1993). There are two alternative forms of this pathway, which differ in the number of nucleotides replaced during the repair process: 1 nucleotide for short-patch and 2-10 nucleotides for long-patch repair (Figure 1.3) (Frosina *et al*, 1996; Sancar *et al*, 2004).

BER is initiated by DNA glycosylases, which recognise and remove specific damaged bases, forming apurinic/apyrimidinic (AP) sites (Huffman *et al*, 2005). AP

endonuclease (APE1) recognises the AP site, displaces the DNA glycosylase and cleaves the DNA sugar-phosphate backbone at a position 5' of the AP sites to prime DNA repair synthesis (Mol *et al*, 2000). The resulting single nucleotide gap is filled-in using information from the complementary strand with the help of DNA polymerase β (Polβ) (Bennett *et al*, 1997). Polβ also mediates recruitment of the XRCC1/DNA Ligase III complex, which re-seals the sugar-phosphate backbone (Figure 1.3) (Kubota *et al*, 1996).

Long-patch repair is usually employed for the repair of more complex lesions, for example those where both a base and the adjacent deoxyribose residue have been damaged. This sub-pathway requires many of the same factors involved in short-patch repair, including a DNA glycosylases and APE1 (Lindahl & Barnes, 2000). In long-patch BER, APE1 makes the 5' incision to the AP site, followed by the recruitment of a complex consisting of replication factor C, proliferating cell nuclear antigen (PCNA) and DNA polymerases δ and ε (Frosina *et al*, 1996; Matsumoto *et al*, 1994; Sancar *et al*, 2004). This complex adds several nucleotides to the repair gap, thus displacing the damaged nucleotide as part of a flap of 2–10 nucleotides. The resulting oligonucleotide overhang is cut at the junction of the single- to double-strand transition by the endonuclease FEN1 (Klungland & Lindahl, 1997) and the gap is sealed by Ligase I (Figure 1.3).

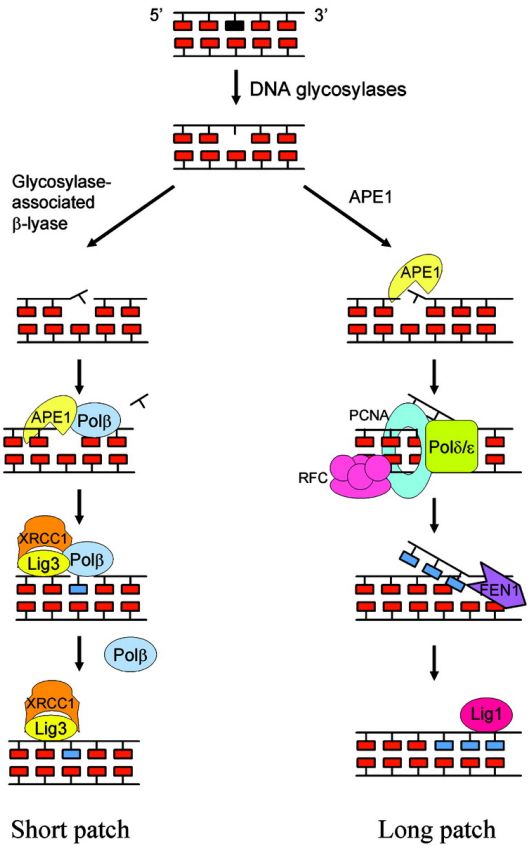

Figure 1.3: Base excision repair pathways.

A damaged base is removed by a DNA glycosylase to generate an AP site. The lesion is then repaired by short patch (single nucleotide replacement) or long-patch (2–10 nucleotides) BER. **Short patch BER:** APE1 cleaves the 5' phosphodiester bond and recruits Polβ to fill in the gap that is then ligated by the DNA LigIII/XRCC1 complex.
Long patch BER: Following APE1 cleavage of the 5' phosphodiester bond, the RFC/PCNA-Polδ/ε complex carries out repair synthesis, displacing several nucleotides. The resulting flap structure is cleaved off by FEN1, and the DNA backbone is ligated by Ligase 1. Figure derived from (Sancar *et al*, 2004) with permission.

1.5 Detection and repair of DNA single strand breaks

DNA single-strand breaks (SSBs) can arise in a variety of ways, including by disintegration of deoxyribose following oxidation, by reactive oxygen species, as normal intermediates of the BER pathway, or as abortive intermediates of topoisomerase I activity (Caldecott, 2008). When DNA SSBs occur they are rapidly recognised and bound by poly(ADP-ribose)-polymerase 1 (PARP1), which activates its catalytic activity[6]. PARP subsequently modifies itself and other target proteins, including histones, with branched chains of poly(ADP-ribose) (PAR) of up to several hundred ADP-ribose units in length, by using NAD^+ as a cofactor (Mendoza-Alvarez & Alvarez-Gonzalez, 1993; Caldecott, 2008; Burzio *et al*, 1979; Satoh & Lindahl, 1992). This PARylation serves as a signal for the recruitment of chromatin remodelling or DNA repair factors to the SSB, including XRCC1, Polβ and DNA ligase III (Okano *et al*, 2003; El-Khamisy *et al*, 2003; Leppard *et al*, 2003; Chou *et al*, 2010; Ohashi *et al*, 1986) (Figure 1.4). The binding and activity of PARP1 at DNA breaks is transient, because PARylated PARP1 rapidly dissociates from DNA and the PAR polymers are degraded by poly(ADP-ribose) glycohydrolase (Davidovic *et al*, 2001). This restores PARP1 and other PARylated proteins to their de-ribosylated state in preparation for subsequent rounds of SSB detection and signalling.

In addition to the role of PARP in SSB and BER, it has also been demonstrated that PARP facilitates the repair of DNA strand breaks induced by topoisomerase I malfunction and has been implicated in the detection and repair of DNA DSBs through an alternative NHEJ pathway (Audebert *et al*, 2004; Dantzer *et al*, 2000; Malanga & Althaus, 2004; Fisher *et al*, 2007).

---

6. The DDR functions are mainly carried out by PARP1, however, contribution of other PARP family members, particularly PARP2, are possible (Caldecott, 2008).

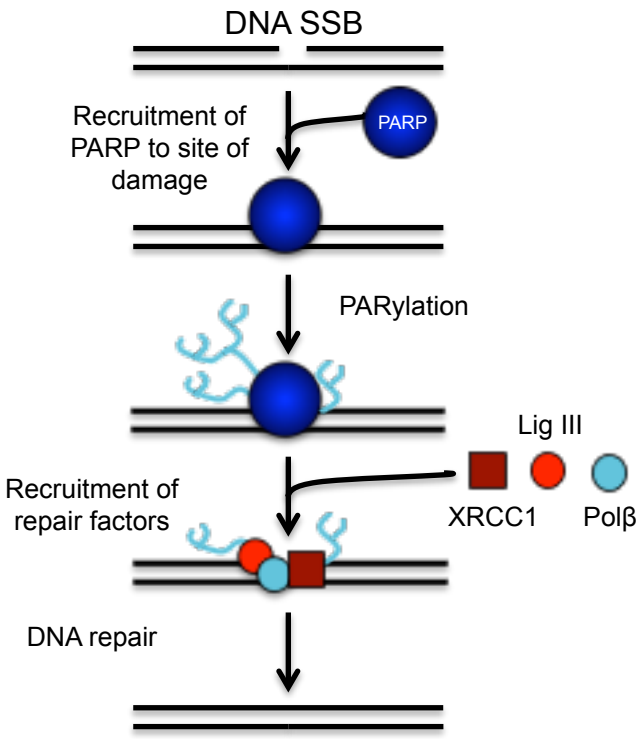

Figure 1.4: Mechanism of PARP1-mediated DNA repair.

The binding of PARP to DNA SSBs activates its catalytic activity. PARP then modifies itself as well as numerous acceptor proteins through PARylation, which serves as a signal for the recruitment of DNA repair factors that mediate the SSB repair.

1.6 Cellular response to replication stress

Accurate duplication of genetic information and subsequent transfer to daughter cells is a fundamental process in living cells and of vital importance for the viability of multicellular organisms. Various perturbations can threaten genome integrity through interference with proper progression and completion of the DNA replication. Replication stress can be defined as slowing or stalling of replication fork progression. It can arise from endogenous or exogenous sources including DNA lesions or nicks (caused for example by exposure to genotoxic agents), secondary DNA structures, collisions between DNA replication and transcription complexes, repetitive DNA

sequences and aberrant activation of oncogenes (Mazouzi *et al*, 2014; Zeman & Cimprich, 2014). Failure to overcome the stalling of replication forks results in an inability to complete chromosome duplication and can lead to the induction of complex chromosomal rearrangements, replication fork associated DNA DSBs, mitotic catastrophe, and cell death (Mazouzi *et al*, 2014; Zeman & Cimprich, 2014; Hills & Diffley, 2014).

A hallmark of replication stress is the accumulation of long stretches of single-stranded DNA (ssDNA) at replication forks, which form as a consequence of replicative helicases continuing to unwind the DNA ahead of the replication fork while the replicative DNA polymerases are stalled (Byun *et al*, 2005). These regions of ssDNA are then bound and stabilised by replication protein A (RPA; Figure 1.5a) (Wold, 1997). This is followed by the recruitment of ATR, a PIKK family DDR kinase, which is mediated by direct interaction of its obligate binding partner ATRIP (ATR interacting protein) with ssDNA-bound RPA (Zou & Elledge, 2003; Cortez *et al*, 2001). Furthermore, RPA-ssDNA complexes stimulate the binding of the RAD17/RFC2-5 clamp loader complex to the damage sites (Figure 1.5b). The presence of a dsDNA–ssDNA junction activates this complex to load the RAD9-HUS1-RAD1 (9-1-1) heterotrimer onto the DNA ends (Ellison & Stillman, 2001; Bermudez *et al*, 2003). The 9-1-1 complex in turn recruits TOPBP1 which activates ATR (Figure 1.5c) (Kumagai *et al*, 2006; Lee *et al*, 2007; Delacroix *et al*, 2007). Alternatively, long stretches of ssDNA can form during DNA DSB resection and also result in activation of ATR (see section 1.3.2). Once activated, ATR acts via its downstream targets to promote DNA repair, as well as stabilisation and restart of stalled replication forks (Cimprich & Cortez, 2008; Errico & Costanzo, 2012; Chen, 2000; Tibbetts *et al*, 2000).

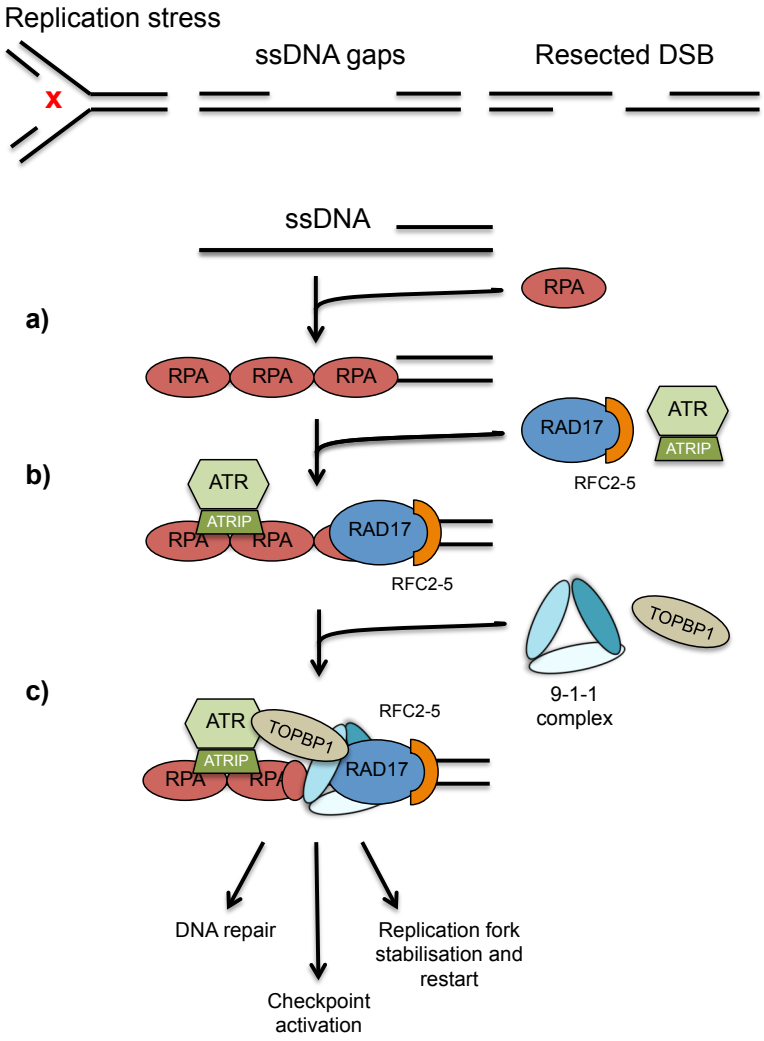

Figure 1.5: A model for ATR activation by single-stranded DNA structures.

a) ssDNA is recognised and coated by RPA. **b)** RPA-coated ssDNA constitutes the signal for recruitment of ATR/ATRIP. In the presence of ssDNA-dsDNA junctions and RPA, the Rad17–RFC clamp loader complex loads the 9-1-1 complex onto the ssDNA. **c)** The 9-1-1 complex then brings TOPBP1 to the lesion, which activates ATR.

ATR is also involved in the inhibition of replication origin firing. Although ATR per se remains confined to stalled forks, its downstream target CHK1 diffuses globally throughout the nucleus, where it inhibits new origin firing. This limits the number of stalled forks to those that were active at the onset of the replication stress and ensures that RPA remains in excess over ssDNA, which is important to avoid the collapse of stalled forks and induction of DNA DSBs (Toledo *et al*, 2013; Syljuåsen *et al*, 2005).

1.7 Cell cycle checkpoints

In addition to mediating DNA damage detection and repair, the DDR halts cell cycle progression, thereby allowing time for appropriate repair mechanisms to correct genetic lesions. This is of particular importance as it prevents DNA lesions from being passed on to the next generation of daughter cells.

Following their activation (see sections 1.3.2 and 1.6), ATM and ATR are the two most important apical mediators of the activation and enforcement of DNA damage induced cell cycle checkpoints (Kastan & Bartek, 2004; Bartek *et al*, 2004).

1.7.1 The G1/S cell cycle checkpoint

DNA replication in the presence of DNA damage can lead to replication fork stalling and the accumulation of even more DNA lesions. Cells with damaged DNA are therefore prevented from entering S-phase through activation of the G1/S cell cycle checkpoint. At the heart of this checkpoint lies a series of signalling events that lead to accumulation of the tumour suppressor protein p53. This response is primarily mediated through ATM. In response to the induction of DNA DSBs, ATM directly phosphorylates p53 on serine 15 (Siliciano *et al*, 1997; Kastan *et al*, 1992; Banin *et al*,

1998; Canman *et al*, 1998). Checkpoint kinase 2 (CHK2) a key downstream target of ATM (Matsuoka *et al*, 1998) and mediator of ATM signalling also phosphorylates p53, on serine 20 (Figure 1.6) (Chehab *et al*, 1999, 2000). This phosphorylation of p53 leads to its stabilisation by preventing its MDM2-mediated ubiquitinylation and degradation (Chehab *et al*, 1999; Haupt *et al*, 1997; Marine & Lozano, 2010).

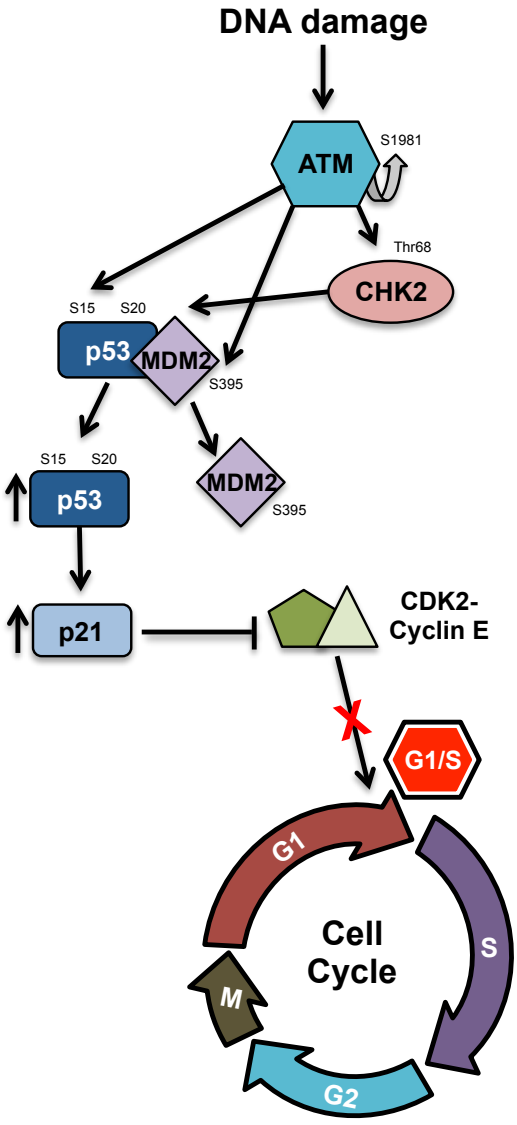

Figure 1.6: Enforcement of the DNA damage induced G1 cell cycle checkpoint.

ATM further contributes to the accumulation and stabilisation of p53 by directly phosphorylating MDM2 (Khosravi *et al*, 1999). Upon activation and accumulation in the nucleus, p53 acts as transcription factor and drives the expression of genes involved in cell cycle checkpoint activation and apoptosis (Sullivan *et al*, 2012). Among the genes induced by p53 is the cyclin-dependent kinase 2 (CDK2) inhibitor p21 (CDKN1A), which prevents damaged cells from entering S-phase (Figure 1.6) (El-Deiry *et al*, 1994). Although ATM is generally considered the most important mediator of p53 phosphorylation after DNA damage, both ATR and DNA-PKcs are able to directly phosphorylate and stabilise p53 in response to DNA damage (Tibbetts *et al*, 1999; Lakin *et al*, 1999; Lees-Miller *et al*, 1992; Shieh *et al*, 1997).

1.7.2 The intra-S-phase checkpoint

A link between ATM and activation of an intra-S-phase checkpoint was predicted on the basis of early studies, which demonstrated that cells deficient in ATM do not reduce DNA synthesis rates following induction of DNA DSBs, a phenotype referred to as radioresistant DNA synthesis (Houldsworth & Lavin, 1980). It has since been established that the S-phase checkpoint functions of ATM in response to IR are partly mediated through phosphorylation of NBS1 and SMC1, a component of the cohesin complex (Figure 1.7) (Kitagawa *et al*, 2004; Lim *et al*, 2000). Additional enforcement of the intra-S-phase checkpoint by ATM is mediated through its activation of CHK2, which induces ubiquitinylation and degradation of the S-phase-promoting phosphatase CDC25A (Figure 1.7) (Falck *et al*, 2001). CDC25A promotes S-phase progression through activation of CDK2, which is required for DNA synthesis.

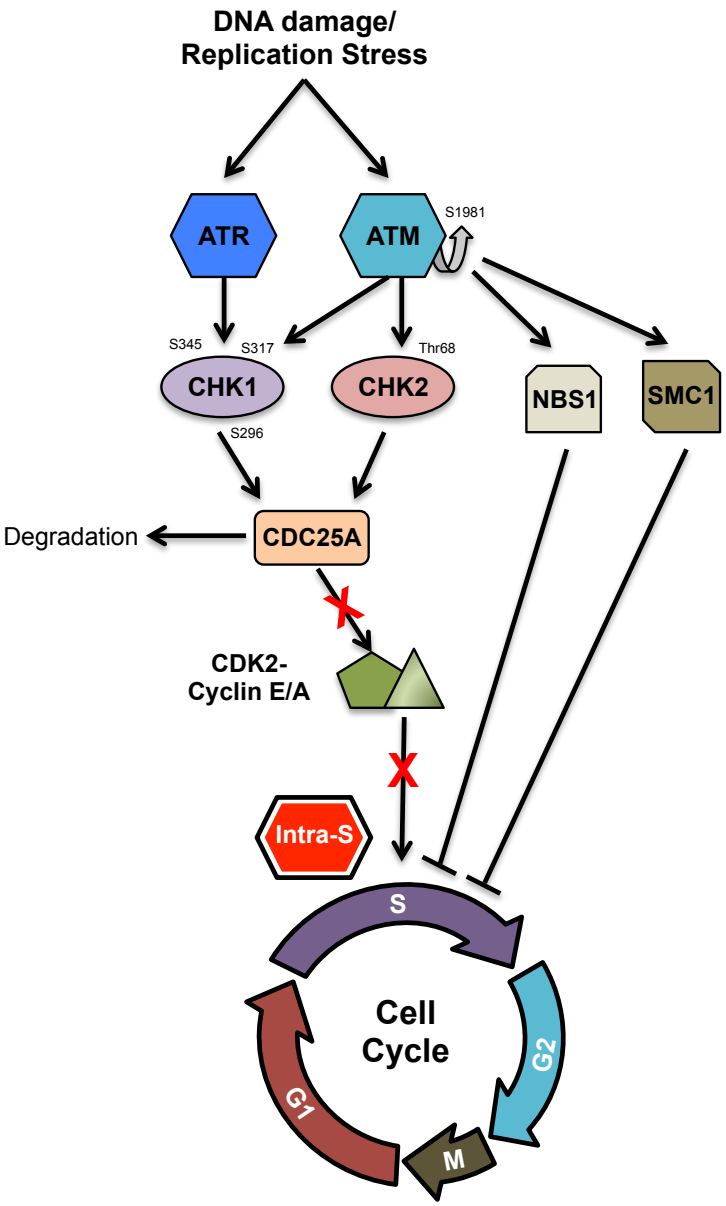

Figure 1.7: Enforcement of the intra-S-phase checkpoint.

In addition to ATM, ATR plays a major role in the enforcement of the intra-S-phase cell cycle checkpoint following DNA damage. ATR activity inhibits the firing of replication origins via degradation of CDC25A mediated through its downstream target CHK1 (Figure 1.7) (Xiao *et al*, 2003; Bartek *et al*, 2004; Sørensen *et al*, 2003).

This in turn slows the progression of DNA replication and provides time for resolution of the stress source.

1.7.3 The G2/M cell cycle checkpoint

The role of the G2/M checkpoint is to delay or prevent mitosis in the presence of DNA lesions, thus avoiding mitotic segregation of damaged chromosomes, which could lead to loss of genetic material or other genomic rearrangements. ATR is a principal mediator of the G2/M cell cycle checkpoint to prevent the premature entry of cells into mitosis, before DNA replication is completed or in the presence of DNA damage. This ATR-dependent G2/M cell cycle arrest is primarily mediated through two mechanisms: (i) the degradation of CDC25A (Xiao *et al*, 2003; Zhao *et al*, 2002) and (ii) the phosphorylation of the CDC25C phosphatase by CHK1, which creates a binding site for 14-3-3 proteins (Peng *et al*, 1997; Sanchez *et al*, 1997). The binding of CDC25C to 14-3-3 proteins facilitates its export from the nucleus and cytoplasmic sequestration (Figure 1.8). As CDC25C is responsible for removing two inhibitory phosphates from CDK1, its inactivation prevents the cell from entry into mitosis (Kumagai & Dunphy, 1999; Graves *et al*, 2001). Importantly, ATM has also been demonstrated to mediate phosphorylation of CDC25C via CHK2, thus contributing to the activation of the G2/M cell cycle checkpoint (Figure 1.8) (Shiloh, 2003; Matsuoka *et al*, 1998; Shiloh, 2001). A parallel ATM-mediated pathway that ensures the maintenance of G2 arrest involves the activation of p53 (Bunz *et al*, 1998). P53 supports G2/M arrest through transcriptional regulation of 14-3-3σ, which inhibits G2/M progression by cytoplasmatic sequestration of CDK1/cyclin B complexes (Hermeking *et al*, 1997; Hermeking & Benzinger, 2006). Furthermore, p53 induces p21 expression which has been proposed to sustain G2 arrest by inhibiting cyclin B1

and CDK1 expression and by promoting cyclin B1 degradation (Figure 1.8) (Flatt *et al*, 2000; Gillis *et al*, 2009). Entry into mitosis is furthermore delayed through WEE1-mediated inhibition of CDK1 (Parker & Piwnica-Worms, 1992; Beck *et al*, 2012; McGowan & Russell, 1995).

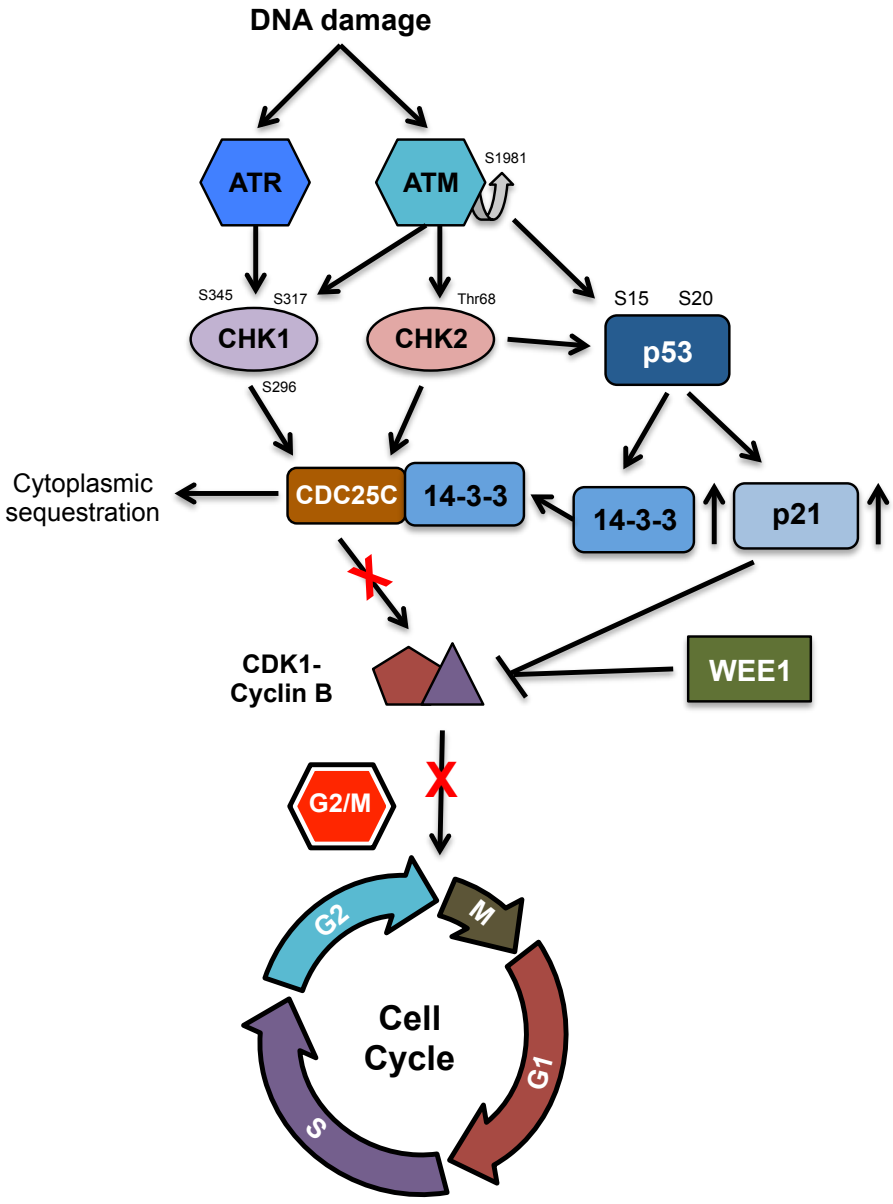

Figure 1.8: Enforcement of the G2/M cell cycle checkpoint.

1.8 Interplay between the ATM and ATR signalling pathways

The ATM and ATR kinases are central to the DDR and together they ensure the maintenance of genomic stability by coordinating cell cycle progression with DNA repair (Cimprich & Cortez, 2008; Shiloh, 2003; Abraham, 2001).

Although ATM and ATR are activated by different types of DNA damage and act in distinct pathways, their downstream targets and the responses they mediate are partially overlapping and dependent on the type of genotoxic stress (Helt *et al*, 2005). The ATM and ATR kinases share a consensus protein phosphorylation site (the SQ/TQ motif[7]), and a large-scale phospho-proteomic study identified over 700 proteins which are phosphorylated at ATM/ATR consensus sites in response to DNA damage (Kim *et al*, 1999; O'Neill *et al*, 2000; Matsuoka *et al*, 2007). A large proportion of the targets, including p53, the histone variant H2AX and BRCA1, are common targets of both kinases (Banin *et al*, 1998; Canman *et al*, 1998; Tibbetts *et al*, 1999; Burma *et al*, 2001; Friesner *et al*, 2005; Ward & Chen, 2001; Gatei *et al*, 2001). Even CHK1, which is usually considered to be the most specific ATR downstream target, can be phosphorylated by ATM on both serine 317 and serine 345 in response to genotoxic stress (e.g. exposure to IR or aphidicolin) (Sørensen *et al*, 2003; Helt *et al*, 2005; Gatei *et al*, 2003; Ozeri-Galai *et al*, 2008).

Although ATM and ATR are recruited to different types of DNA lesions, the overlap in substrates and the partial convergence of the two signalling pathways in their downstream effectors suggests that deficits in one pathway might be, at least to some extent, compensated for by the activity of the respective other pathway.

---

7. ATM and ATR preferentially phosphorylate serine or threonine residues followed by glutamine.

One example is the above mentioned enforcement of the intra-S-phase checkpoint (see section 1.7.2), where both ATM and ATR can target the CDC25A phosphatase for ubiquitin-dependent degradation thereby regulating the timing of replication origin firing in response to DNA damage (Xiao *et al*, 2003; Bartek *et al*, 2004; Falck *et al*, 2001). Indeed, it has been demonstrated that overexpression of wild-type ATR can complement the radioresistant DNA synthesis phenotype of cells lacking ATM (Cliby *et al*, 1998).

Furthermore, both ATM and ATR have been shown to mediate G2/M cell cycle checkpoint activation through phosphorylation of CDC25C via their downstream effectors CHK1 and CHK2 (Shiloh, 2003; Matsuoka *et al*, 1998; Shiloh, 2001; Peng *et al*, 1997; Sanchez *et al*, 1997). ATM also blocks the G2 to M transition through activation of p53 and subsequent increase in p21 (Bunz *et al*, 1998). A recent study has shown that under conditions of continuous genotoxic stress, ATR and CHK1 are dispensable for activation of the G2 cell cycle checkpoint, providing that the ATM-p53-p21 pathway is functional (Lossaint *et al*, 2011).

Another functional interplay between ATM and ATR has been identified in the maintenance of common fragile site (CFS) stability (Ozeri-Galai *et al*, 2008). CFSs are large chromosomal regions that are thought to be particularly difficult to replicate, replicate late during S-phase and tend to undergo frequent breakage under conditions of partial replication stress that slows (but does not arrest) DNA replication (Debatisse *et al*, 2012; Glover *et al*, 2005; Hills & Diffley, 2014). Of particular interest is the observation that the role of ATM in maintaining CFS stability was only revealed in the absence of functional ATR (Ozeri-Galai *et al*, 2008). It was further demonstrated that following induction of replication stress both ATR and ATM phosphorylate CHK1,

suggesting that both proteins work together to regulate fragile site expression via their effect on CHK1 activation (Ozeri-Galai *et al*, 2008).

These observations indicate that even though the ATM and ATR signalling pathways are not completely redundant, they are partially overlapping. Given the central importance of the DDR and DNA damage checkpoints, there may be an evolutionary imperative for parallel pathways and backup mechanisms in case defects in one of the signalling pathways arise. At the same time the functional overlap between DDR pathways might have important implications for cancer therapy, as it could allow for specific targeting of tumour cells with defects in certain components of the DDR through synthetic lethal interactions, as will be discussed below.

1.9 The role of the DDR in cancer development

The DDR has been linked to several aspects of tumour development. Numerous hereditary cancer predisposition syndromes result from mutations in DDR genes (Curtin, 2012; Negrini *et al*, 2010). For example, women who carry a defective allele of the BRCA1 or BRCA2 genes, which encode for proteins centrally involved in homologous recombination repair of DNA DSBs (see section 1.3.2), are at much higher risk of developing breast and ovarian cancers than women in the general population (Pal *et al*, 2005; Levy-Lahad & Friedman, 2007). Another example is Li-Fraumeni syndrome, which is caused by inherited mutations in the p53 gene and is associated with a very high risk of developing cancer early in life (<45 years) (Olivier *et al*, 2003).

Furthermore, several studies have demonstrated that during early stages of tumorigenesis several DDR signalling pathways are activated (Bartkova *et al*, 2005; Gorgoulis *et al*, 2005). This response has been linked to the induction of replication stress and DNA damage caused by aberrant oncogene activation (Bartkova *et al*, 2006; Di Micco *et al*, 2006). It has been suggested that activation of DDR pathways may act as a barrier for tumour development in its early stages by limiting the proliferation of aberrant cells (Bartkova *et al*, 2005; Gorgoulis *et al*, 2005). Activation of the tumour suppressor protein p53 may be of particular importance for this mechanism, which would explain the very high frequency of inactivating p53 mutations observed in certain human cancers (Halazonetis *et al*, 2008). Many malignant tumours also show functional loss or deregulation of other key proteins involved in the DDR and cell cycle regulation, including ATM (Cancer Genome Atlas Research Network, 2012c, 2012b, 2014, 2012a; Kandoth *et al*, 2013), MRE11 (Ottini *et al*, 2004; Choudhury *et al*, 2010; Bartkova *et al*, 2008), BRCA1/2 (Cancer Genome Atlas Research Network, 2012c; Kandoth *et al*, 2013) or SMC1 (Kandoth *et al*, 2013). Such mutations may allow pre-cancerous cells to overcome the proliferation barrier posed by the DDR and thereby allow pre-malignant lesions to progress to malignant carcinomas.

Furthermore, a key characteristic of human cancers is genomic instability, which accelerates the accumulation of genetic alterations that drive tumour progression. Evidence suggests that genomic instability occurs early during cancer development (Shih *et al*, 2001) and that deregulation of components of the DDR contributes to its development (Hanahan & Weinberg, 2011; Negrini *et al*, 2010; Bouwman & Jonkers, 2012; Curtin, 2012).

1.10 The role of the DDR in the response of tumour cells to genotoxic therapy

Standard cancer treatments, such as radio- and chemotherapy, rely on the induction of DNA damage, which is cytotoxic for proliferating cells and hence effective in targeting highly proliferative cancer cells. However, since genotoxic therapies generally lack selectivity towards cancer cells, the toxicity induced in normal tissues and the resulting side effects are limiting factors for both the dose and duration of therapy. This is one of the reasons why these cytotoxic therapies, though effective, usually are rarely curative. Furthermore, tumours can develop resistance to radio- or chemotherapy allowing tumour recurrence following an initial response to therapy.

The DDR plays a central role in the effectiveness of cancer treatment, as it can enable cancer cells to resist the lethal effects of genotoxic cancer therapy (Myers *et al*, 2009; Karnitz *et al*, 2005; Woods & Turchi, 2013; Curtin, 2012). Several studies have shown, that the development of resistance to different types of genotoxic therapy can be caused by deregulation or overexpression of different components of the DNA damage response (Bao *et al*, 2006; Bobola *et al*, 2012; Oliver *et al*, 2010; Martin *et al*, 2008).

1.11 The DDR as therapeutic target in cancer

Since up-regulation of DNA repair pathways can cause resistance to DNA-damaging chemo- or radiotherapy, inhibition of these pathways may have the potential to sensitise cells to these modalities. Regulators of the DDR have therefore become attractive targets for chemo- or radiosensitisation. This approach may allow for enhancement in the effectiveness of standard genotoxic treatments and help to either

prevent or overcome the development of resistance. In support of this concept, numerous studies have demonstrated that inhibition of components of the DDR machinery can sensitise cancer cells to DNA damaging treatments, including PARP (Miknyoczki *et al*, 2003; Vance *et al*, 2011; Tuli *et al*, 2014), DNA-PKcs (Zhao *et al*, 2006), ATM (Golding *et al*, 2012; Rainey *et al*, 2008), ATR (Prevo *et al*, 2012; Fokas *et al*, 2012; Pires *et al*, 2012; Huntoon *et al*, 2013), or their downstream targets CHK1 and CHK2 (Mitchell *et al*, 2010; Riesterer *et al*, 2011; Matthews *et al*, 2007; Blasina *et al*, 2008).

Defects in DDR mechanisms may also be exploitable as potentially targetable weaknesses through synthetic lethal approaches. Two genes are considered synthetically lethal, if mutation or inactivation of either gene or gene product alone has no effect on cellular viability, whereas simultaneous defects in both genes/gene products lead to cell death (Kaelin, 2005). While defects in DDR components may, on the one hand, give cancer cells a growth advantage, allowing them to survive and proliferate despite oncogene-induced replication stress and genomic instability, they may also drive a reliance of cancer cells on any remaining DDR pathways in order to survive DNA damage. Targeting of such remaining pathways through pharmacological inhibition may therefore be selectively toxic to cancer cells with mutations in certain DDR genes (Figure 1.9). Some examples for this approach are discussed below.

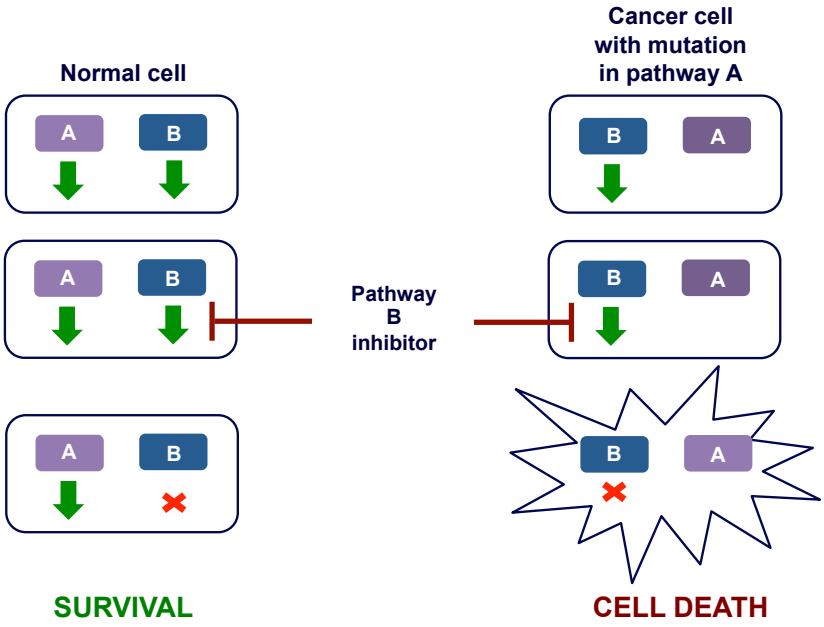

Figure 1.9: The concept of synthetic lethality.

Cancer cells harbouring somatic mutations in a certain signalling pathway (pathway A) may become reliant on an alternative signalling pathway (pathway B) for survival. Pharmacological inhibition of this pathway would then induce cell death selectively in those cancer cells, while non-tumour cells with retained function of pathway A would be spared.

1.12 Poly(ADP-ribose) polymerase as therapeutic target

The potential of the approach of inducing synthetic lethality for cancer therapy was first demonstrated in cells harbouring mutations in the breast and ovarian cancer susceptibility genes BRCA1 and BRCA2, which were shown to be highly sensitive to small molecule inhibitors of PARP (Bryant *et al*, 2005; Farmer *et al*, 2005). As PARP plays important roles in the detection and repair of DNA SSBs, as well as BER (see sections 1.4 and 1.5), its inhibition leads to the accumulation of DNA SSBs. Such SSBs can be converted to DNA DSBs at replication forks during S-phase (Ciccia & Elledge, 2010; Kuzminov, 2001). Interestingly, recent studies have demonstrated that

the cytotoxicity of several PARP inhibitors is not merely based on the blocking of the DNA repair function of PARP, but also on the trapping of PARP at sites of DNA damage (Murai *et al*, 2012). Trapped PARP/DNA complexes are thought to induce replication fork stalling and replication stress following collision with active replication forks and thereby promote the generation of replication associated DNA DSBs. As HR plays a vital role in the repair of such replication associated DNA DSBs (Arnaudeau *et al*, 2001; Helleday *et al*, 2007), this might explain the increased sensitivity of BRCA1/BRCA2 mutated cells to PARP inhibitors, as BRCA1/BRCA2 deficiency causes defects in HR (Gudmundsdottir & Ashworth, 2006). In agreement with this notion, defects in other components of the HR pathway also sensitise cells to pharmacological PARP inhibition (McCabe *et al*, 2006). Furthermore, loss of PARP1 has been shown to cause an increase in RAD51 foci formation, a biomarker of homologous recombination repair (Schultz *et al*, 2003; Bryant *et al*, 2005; Farmer *et al*, 2005). The PARP inhibitor olaparib (AZD2281, LYNPARZA^{TM}) has since shown great promise for the treatment of BRCA1/2 mutated breast or ovarian cancer in clinical trials (Fong *et al*, 2009; Tutt *et al*, 2010; Audeh *et al*, 2010) and was FDA approved in the EU and the USA in 2014 for the treatment of BRCA-mutation positive advanced ovarian cancer.

Furthermore, there is abundant pre-clinical data demonstrating that concurrent PARP inhibition sensitises tumour cells to genotoxic therapy, including ionising radiation, DNA alkylating agents (temozolomide) and topoisomerase inhibitors (Senra *et al*, 2011; Boulton *et al*, 1995; Patel *et al*, 2012; Calabrese *et al*, 2004; Curtin, 2005; Curtin & Szabo, 2013; Sandhu *et al*, 2010). Each of these treatments induces DNA lesions that require either SSB-repair or BER, thereby explaining the sensitising effects of PARP inhibitors. More than a dozen potent and selective PARP inhibitors

have been developed and 152 clinical trials involving PARP inhibitors are listed on ClinicalTrials.gov[8]. Reviewing them in detail is beyond the scope of this introduction and readers are referred to recent detailed reviews on the therapeutic applications for PARP inhibitors as monotherapy, as well as in combination with genotoxic modalities (Curtin & Szabo, 2013; Sonnenblick *et al*, 2015; Sandhu *et al*, 2010).

1.13 The PIKK kinases: Master regulators of the DDR and their potential as therapeutic targets

The role of ATM, ATR and DNA-PKcs in the detection and repair of DNA damage has identified them as attractive potential targets for cancer treatment. All three kinases are members of the phosphatidylinositol 3-kinase-related kinase (PIKK) family of serine/threonine protein kinases, which also comprises mammalian target of rapamycin (MTOR/FRAP), suppressor of morphogenesis in genitalia (SMG1) and transformation/transcription associated protein (TRRAP) (Lempiäinen & Halazonetis, 2009). The cellular functions of these protein kinases range from regulation of the DNA damage response (ATM, ATR and DNA-PKcs) to cell survival, proliferation, metabolism, differentiation, motility, nonsense-mediated mRNA decay and epigenetic regulation of transcription (Jackson & Bartek, 2010; Ciccia & Elledge, 2010; Lempiäinen & Halazonetis, 2009).

The members of the PIKK kinase family show considerable similarities in their domain architecture and extensive sequence homology, particularly in their kinase domain (Keith & Schreiber, 1995; Bosotti *et al*, 2000) (Figure 1.10), which has

8. Search result for "PARP inhibitor" on www.clinicaltrials.gov; accessed in April 2015.

hindered the development of selective PIKK-family inhibitors. Many of the early inhibitors that were identified were non-specific and inhibited several members of the PIKK family (e.g. caffeine and Wortmannin; (Sarkaria *et al*, 1999, 1998)). However, through the improvement and optimisation of chemical structures and screening of compound libraries increasingly potent and specific inhibitors of PIKK family kinases have been developed in recent years.

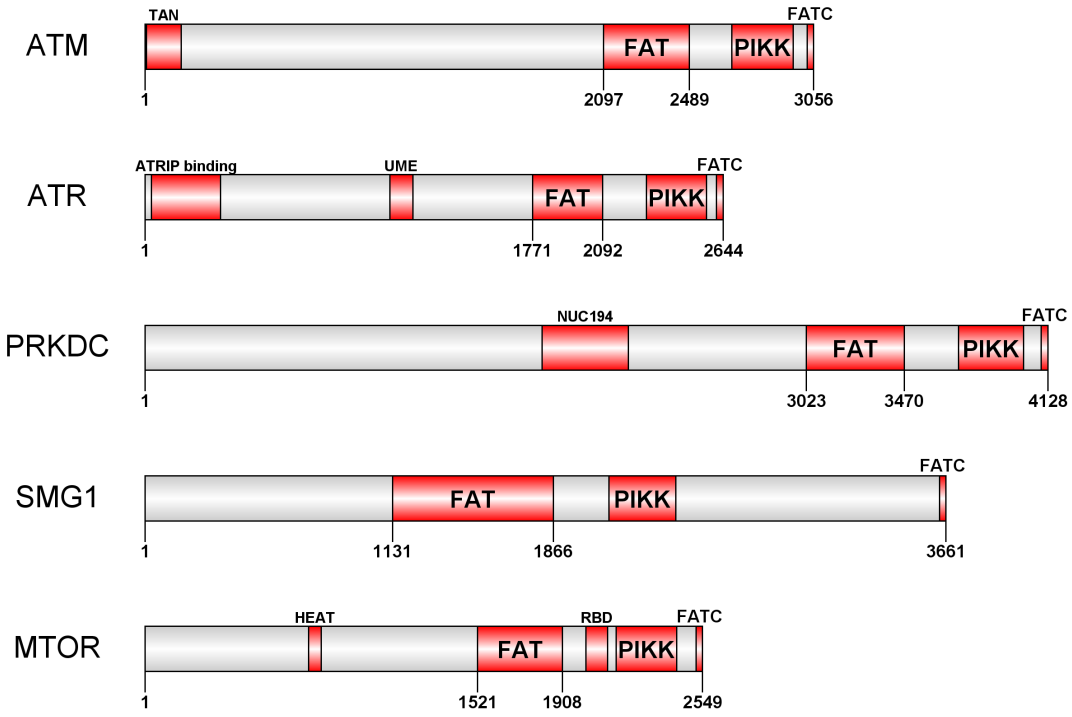

Figure 1.10: The PIKK family members.

Schematic diagrams of domain structure of the PIKK family members are shown with the known structural domains highlighted in red for each protein. PRKDC (DNA-dependent protein kinase catalytic subunit; DNA-PKcs), FAT (FRAP-ATM-TRRAP domain), FATC (FAT C-terminal domain), PIKK (phosphatidylinositol 3-kinase-related kinase domain), TAN (Tel1/ATM N-terminal motif), ATRIP (ATR interacting protein), UME (UVSB PI3 kinase, MEI-41 and ESR1 domain), NUC194 (domain B in the catalytic subunit of DNA-dependent protein kinase), RBD (rapamycin binding domain), HEAT (Huntingtin, elongation factor 3, protein phosphatase 2A , and the yeast kinase TOR1 –like repeat).

1.13.1 Targeting the ATM signalling pathway

ATM was first described in 1995 as the gene defective in the autosomal recessive human hereditary disorder Ataxia-telangiectasia (A-T) (Savitsky *et al*, 1995). This disease is caused by a loss of ATM function and is characterised by progressive cerebellar degeneration, telangiectasia, immunodeficiency, genomic instability, cancer susceptibility and cellular defects in the repair of DNA DSBs, conferring a profound sensitivity to ionising radiation (Taylor *et al*, 1975; Lavin, 2008). It is primarily this hypersensitivity of ATM-defective cells to IR that has sparked considerable interest in ATM as therapeutic target for cancer therapy.

Numerous ATM inhibitors with increasing potency and specificity have been developed (see Table 1.3). Pre-clinical studies have demonstrated that pharmacological ATM inhibition has great potential as a cancer therapy in combination with radiotherapy and certain chemotherapeutic drugs (like topoisomerase inhibitors), encouraging the further development of ATM inhibitors for the clinic. Table 1.3 summarises the ATM inhibitors developed to date and important findings from pre-clinical studies. For a more detailed description see our recent review (Weber & Ryan, 2015) (see Appendix).

ATM plays a vital role in the cellular response to DNA DSB formation in normal as well as cancer cells, which raises concerns that the chemo- and radiosensitising properties of pharmacological ATM inhibition will also increase normal tissue toxicity. However, a recent study has demonstrated that the radiosensitisation conferred by depletion of ATM may be significantly greater in proliferating cells (Moding *et al*, 2014).

Table 1.3: ATM inhibitors (adjusted from (Weber & Ryan, 2015) with permission)

Caffeine	**Wortmannin**	**CP-466722**
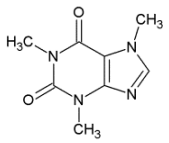	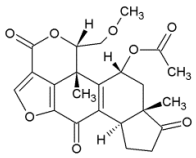	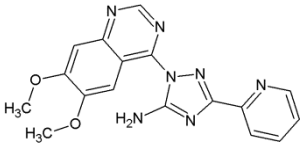
KU-55933	**KU-60019**	**KU-59403**
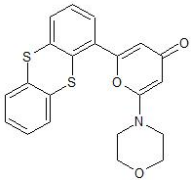	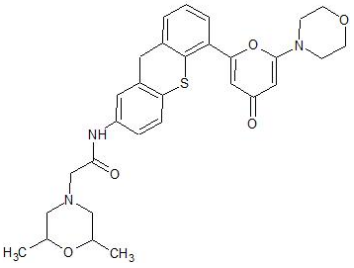	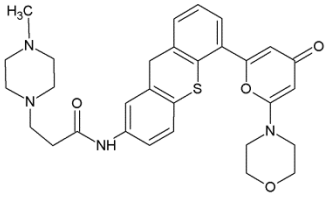

Compound	**Targets *(IC_{50})*[9]**	**Description**	**References**
Caffeine	ATM *(0.2 mM)*/ ATR *(1.1 mM)*/ mTOR *(0.4 mM)*	Caffeine sensitises cells to genotoxic modalities, particularly IR. Caffeine shows an increased radiosensitising effect in cells with p53-deficiency.	(Blasina *et al*, 1999; Sarkaria *et al*, 1999; Powell *et al*, 1995; Bracey *et al*, 1997; Yao *et al*, 1996)
Wortmannin	ATM *(150 nM)*/ PI3K *(3 nM)*/ DNA-PKcs *(16 nM)*	Radiosensitises cells in vitro through inhibition of both ATM and DNA-PKcs. Highly toxic *in vivo*.	(Price & Youmell, 1996; Sarkaria *et al*, 1998; Karve *et al*, 2012)
CP-466722	ATM *(410 nM)*	Highly selective ATM inhibitor. Radiosensitises cells *in vitro*. First report that transient inhibition of ATM is sufficient to confer radiosensitivity.	(Rainey *et al*, 2008)
KU-55933	ATM *(12.9 nM)*	First potent and selective ATM inhibitor. Confers marked sensitisation to IR and DNA DSB inducing chemo-therapeutics. Not suitable for *in vivo* use.	(Hickson *et al*, 2004)

9. IC_{50} values are based on cell-free kinase assays and were derived from the listed references or from the selleckchem.com homepage.

Table 1.3: ATM inhibitors (continued)

Compound	Targets *(IC_{50})*[10]	Description	References
KU-60019	ATM *(6.3 nM)*	Analogue of KU-55933 with improved potency and solubility in aqueous solutions. Potently inhibits ATM downstream signalling and sensitises cells to IR *in vitro*.	(Golding *et al*, 2009, 2012)
		Radiosensitised glioblastoma cells to *IR in vivo* following injection of the compound directly into the tumour. Possesses poor bioavailability *in vivo*.	(Biddlestone-Thorpe *et al*, 2013)
KU-59403	ATM *(3 nM)*	First potent and selective ATM inhibitor with good enough solubility and bioavailability to allow for *in vivo* studies. Confers radiosensitivity *in vitro* Greatly increased the anti-tumour activity of etoposide and irinotecan in xenograft models.	(Batey *et al*, 2013)

As normal tissue is generally less proliferative active than tumour tissue, this suggests that there might be a possibility of differential responses in tumour versus non-tumour tissue. Furthermore, the observations that (i) transient inhibition of ATM is sufficient to achieve radiosensitisation *in vitro* (Rainey *et al*, 2008) and (ii) ATM must be inhibited at the time of chemotherapy exposure (Batey *et al*, 2013) to achieve chemosensitisation *in vivo*, suggest that short-term treatment with ATM inhibitors might be sufficient to achieve clinically relevant chemo- or radiosensitisation. Taken together these findings suggest that a favourable therapeutic index could be achieved and encourage further development of ATM inhibitors for the clinic.

10. IC_{50} values are based on cell-free kinase assays and were derived from the listed references or from the selleckchem.com homepage.

Of note, pharmacological inhibition of ATM kinase activity appears to cause a different cellular phenotype than lack of ATM protein expression. A recent study showed that following exposure to IR, repair of damaged DNA replication forks is normal in A-T cells, which lack ATM protein, but is defective in wild-type cells when ATM is inhibited by KU55933 or KU60019 (White *et al*, 2010). The authors hypothesised that "kinase-inhibited ATM" presents a physical impediment to homologous recombination repair of DSBs at damaged replication forks (White *et al*, 2010; Choi *et al*, 2010). Furthermore, expression of kinase dead (kd) ATM protein has been shown to be more detrimental to cells than its loss, as expression of physiological levels of kd ATM leads to early embryonic lethality in mice, while ATM knockout mice are viable (Yamamoto *et al*, 2012; Barlow *et al*, 1996; Elson *et al*, 1996).

It has been suggested that the binding of catalytically inactive ATM to sites of DNA DSBs blocks those sites for proteins mediating alternative routes of DNA damage repair thereby causing persistence of DNA damage (Yamamoto *et al*, 2012). Thus, ATP-competitive ATM inhibitors might act in a similar way as kd ATM protein and, upon prolonged exposure, may have the potential to cause greater normal tissue effects *in vivo* than a loss of ATM protein expression. Future studies will need to address this question, but the possibility should be taken under consideration for the clinical development of ATM inhibitors.

ATM is also frequently mutated in a broad range of human cancers including lung (Cancer Genome Atlas Research Network, 2014, 2012b), colorectal (Cancer Genome Atlas Research Network, 2012a), breast (Cancer Genome Atlas Research Network, 2012c) and haematopoietic cancers (Landau & Wu, 2013; Beà *et al*, 2013). This raises the possibility that ATM deficiency in tumours might be exploitable as an intrinsic

radio- or chemosensitiser. However, to our knowledge no studies on the functional consequences of ATM mutations in cancer or a possible correlation between ATM function and patient responses to radio- or chemotherapy have been carried out to date.

1.13.2 Targeting the ATR signalling pathway

Concerns revolving around the potential normal tissue effects of functional inhibition of ATR kinase activity have hindered the exploitation of ATR as therapeutic target in cancer therapy, and delayed the development of specific ATR kinase inhibitors. It was anticipated that pharmacological inhibition of ATR might not be tolerated *in vivo* since ATR function is essential for the cellular response to replication stress (Bartek *et al*, 2012). Even in the absence of replication stress-inducing agents, some replication fork stalling can occur during normal replication, for example at common fragile sites or repetitive sequences (Mirkin & Mirkin, 2007). It has been shown that ATR is critical for fragile-site stability and that ATR-deficient cells have high levels of fragile site breakage resulting in the induction of DNA double strand breaks (Casper *et al*, 2002). This finding is consistent with the observation that ATR knockout leads to chromosomal fragmentation and cell death (Brown & Baltimore, 2000), which are thought to be the underlying reason for the early embryonic lethality observed in ATR knockout mice (Brown & Baltimore, 2000; de Klein *et al*, 2000). In humans, mutations in ATR lead to a rare hereditary disorder, Seckel syndrome (O'Driscoll *et al*, 2003; Alderton *et al*, 2004). However, the ATR mutations causing Seckel syndrome are hypomorphic, with only a partial loss of gene function. It thus appears

that mutations in ATR are only compatible with viability when heterozygous or hypomorphic.

Depletion of ATR in adult mice has been shown to cause defects in tissue homeostasis through induction of acute cytotoxicity in tissues in which continuous cell proliferation is required (Ruzankina *et al*, 2007). Furthermore, in a mouse model of Seckel syndrome, the partial loss of ATR causes accelerated aging through the induction of substantial replication stress, thereby limiting the lifespan of the mice (Murga *et al*, 2010).

The effects of ATR depletion on DNA replication and the induction of DNA damage in normal tissues raised concerns that pharmacological ATR inhibition could cause severe side effects due to toxicity on highly proliferative normal tissues, especially if ATR inhibition was combined with modalities that induce replication stress. However, several studies have indicated that ATR inhibition might be preferentially cytotoxic for cancer cells, thereby raising the possibility of a therapeutic window for ATR inhibitors in cancer therapy.

Recent studies in mice demonstrated that the detrimental effects of ATR-deficiency on cell viability may be ameliorated by wild-type p53 activity, since loss of p53 function exacerbated the accumulation of replication stress and tissue degeneration when ATR signalling was compromised (Murga *et al*, 2010; Ruzankina *et al*, 2009). These findings point towards an important role of p53 in the cellular response to ATR inhibition and raise the possibility that p53-deficient tumours, which comprise a large proportion of cancer cases, may show increased sensitivity to ATR inhibition compared with non-tumour tissue.

Furthermore, several studies have demonstrated that depletion of functional ATR increases the sensitivity of cancer cells to oncogene-induced replication stress thereby hindering tumour growth and inducing extensive cell death (Gilad *et al*, 2010; Murga *et al*, 2011; Schoppy *et al*, 2012). Importantly, Schoppy et al. found that hypomorphic ATR signalling (reduced to 10% of normal levels) was sufficient to induce synthetic lethality in oncogenic RAS-driven tumours, while only minimally affecting normal bone marrow and intestinal homeostasis (Schoppy *et al*, 2012). This finding suggests that a low level of ATR activity may be sufficient to sustain viability of highly proliferative adult tissues and at the same time indicates that complete inhibition of ATR kinase activity may not be required to cause substantial and selective toxicity in cancer cells.

A number of potent and selective ATR inhibitors have been developed in recent years and pre-clinical *in vitro* and *in vivo* studies have demonstrated that pharmacological ATR inhibition has great clinical potential for chemo- and radiosensitisation, particularly in G1 checkpoint deficient (ATM or p53-deficient) tumours. Several ATR inhibitors have entered clinical development recently and Table 1.4 summarises the most important compounds and pre-clinical studies. A detailed review of the therapeutic applications for ATR inhibitors has recently been published (Weber & Ryan, 2015) (see Appendix).

Table 1.4: ATR inhibitors (adjusted from (Weber & Ryan, 2015) with permission)

Schisandrin B	**NU6027**	**NVP-BEZ235**
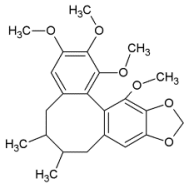	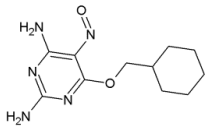	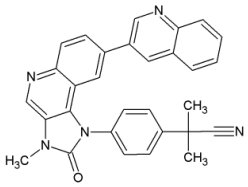

VE-821	**VE-822**	**AZ20**	**AZD6738**
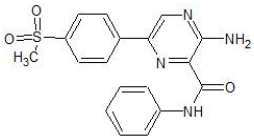	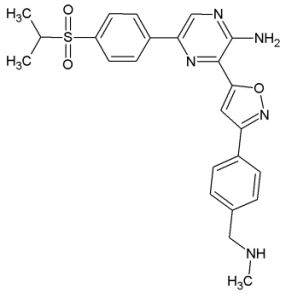	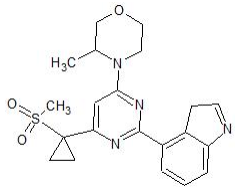	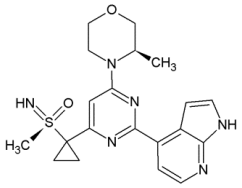

Compound	**Targets *(IC$_{50}$)*[11]**	**Description**	**References**
Schisandrin B	ATR *(7.25 µM)*	Selective, though weak ATR inhibitor. Abrogates the UV-induced S and G2/M cell cycle checkpoints and increases sensitivity of cancer cells to UV radiation.	(Nishida *et al*, 2009)
NU6027	ATR *(0.4 µM)*/ CDK2 *(1.3 µM)*/ DNA-PKcs *(2.2 µM)*	NU6027 was originally developed as CDK2 inhibitor, but also potently inhibits ATR activity. Has been demonstrated to chemo- and radiosensitise several breast and ovarian cancer cell lines.	(Peasland *et al*, 2011)
NVP-BEZ235	PI3Kα *(2 nM)*/ mTOR *(2 nM)*/ DNA-PKcs *(5 nM)*/ ATM *(7 nM)*/ ATR *(21 nM)*	Originally developed as dual PI3K/MTOR inhibitor, also possesses substantial activity against ATM, ATR, and DNA-PKcs. Has been demonstrated to potently radiosensitise RAS-overexpressing tumours.	(Maira *et al*, 2008; Toledo *et al*, 2011) (Konstantinidou *et al*, 2010)

11. IC_{50} values are based on cell-free kinase assays and were derived from the listed references or from the selleckchem.com homepage.

Table 1.4: ATR inhibitors (continued)

Compound	Targets *(IC_{50})*[12]	Description	References
VE-821	ATR *(13 nM)*	First potent and selective ATR inhibitor. Chemosensitises cancer cells to various chemotherapeutics in vitro. Chemosensitisation most potent for cross-linking agents. Potent *in vitro* radiosensitiser. Shows increased single-agent toxicity in hypoxic cells.	(Charrier *et al*, 2011; Reaper *et al*, 2011; Huntoon *et al*, 2013; Pires *et al*, 2012; Prevo *et al*, 2012)
VE-822 **(VX-970)**	ATR *(0.2 nM)*	Analogue of VE-821 with increased potency and improved bioavailability. First ATR inhibitor to enter clinical development. Increased anti-tumour activity with IR and gemcitabine in xenograft models of pancreatic cancer. Chemosensitises lung cancer cells to several chemotherapeutic drugs *in vitro*. Increases the anti-tumour activity of cisplatin *in vivo*.	(Fokas *et al*, 2012; Hall *et al*, 2014) ClinicalTrials.gov: NCT02157792
AZ20	ATR *(5 nM)*	Potent and selective ATR inhibitor. Possesses substantial single agent activity against MRE11-deficient cancer cells *in vivo* at well-tolerated doses.	(Jacq *et al*, 2012; Foote *et al*, 2013)
AZD6738	ATR *(4 nM)*	Analogue of AZ20 with improved solubility, pharmacodynamics and bioavailability. Significantly increases anti-tumour activity of IR or carboplatin *in vivo*. Shows single-agent activity in ATM-deficient xenograft models. Currently in Phase I clinical development.	(Guichard *et al*, 2013; Jones *et al*, 2013) ClinicalTrials.gov: NCT02223923

12. IC_{50} values are based on cell-free kinase assays and were derived from the listed references or from the selleckchem.com homepage.

1.13.1 Synthetic lethal approaches involving ATM and ATR

In addition to the potential utility of ATM and ATR as chemo- or radiosensitisers, recent studies suggest that such compounds may have single agent activity in certain subsets of patients through induction of synthetic lethality. The ATR inhibitor AZD6738 has shown single-agent anti-tumour activity in ATM-deficient but not ATM-proficient xenograft models, suggesting that a synthetic lethal interaction could exist between the ATM and ATR signalling pathways (Jones *et al*, 2013; Guichard *et al*, 2013), potentially due to the overlapping and cooperating roles of these pathways in coordinating cell cycle progression with DNA repair.

Furthermore, inhibition of ATM kinase activity or knockdown of ATM protein expression has been shown to be synthetically lethal in cells with defects in the Fanconi anaemia pathway, components of which are commonly mutated or lost in cancer (Kennedy *et al*, 2007; Kennedy & D'Andrea, 2006). ATM inhibition or -deficiency has also been shown to be synthetically lethal in cells with deficiency in the BER pathway, including APE1 (Sultana *et al*, 2012), XRCC1 (Sultana *et al*, 2013a) and PARP (Gilardini Montani *et al*, 2013; Weston *et al*, 2010; Williamson *et al*, 2010).

ATR inhibition also shows a synthetic lethal interaction with XRCC1 loss (Sultana *et al*, 2013b). Furthermore, the ATR inhibitors AZ20 and AZD6738 conferred increased cytotoxicity in MRE11A mutated cells *in vitro* and in *vivo* (Jacq *et al*, 2012; Foote *et al*, 2013; Guichard *et al*, 2013) pointing towards a potential synthetic lethal interaction between ATR inhibition and functional loss of MRE11. This synthetic lethality may also include other components of the MRN complex (Al-Ahmadie *et al*, 2014). Hence, pharmaceutical inhibition of ATM and/or ATR may provide the basis for the selective treatment of DDR pathway-deficient cancers.

1.14 Aims of this study

1. Analysis of the functional consequences of ATM missense mutations in NSCLC and establishment of an assay for the identification of patients with tumoral loss of ATM function for use in a clinical setting.

2. Pre-clinical evaluation of novel small molecule ATR inhibitors as single agents and in combination with other therapeutic interventions, including radiotherapy, chemotherapy and targeted agents in NSCLC, and to assess the influence of the functional status of ATM and/or p53 on the response of NSCLC cells to these treatments.

3. Analysis of the cellular mechanisms underlying the increased sensitivity of cells with deficiency in both ATM and p53 to pharmacological ATR inhibition as a single-agent and in combination with ionising radiation.

4. Pre-clinical evaluation of the anti-tumour activity of combined PARP and ATR inhibition in NSCLC, with particular regard to the role of p53 in the cellular response to this treatment.

CHAPTER 2

2 MATERIALS AND METHODS

2.1 Buffers, solutions and chemicals

Unless otherwise stated, all chemicals were purchased from Sigma-Aldrich (St. Louis, USA).

Table 2.1: Buffers and solutions frequently used throughout this study

Buffer	Composition
Carnoy's fixative (prepared fresh before use)	75% (v/v) methanol, 25% (v/v) glacial acetic acid
Citrate antigen retrieval buffer	10 mM citric acid and 0.05% Tween-20 in distilled water (dH_2O) pH adjusted to 6.0 with 1 M NaOH.
Fixative solution for clonogenic assays	0.5% (w/v) crystal violet (Merck KGaA, Darmstadt, Germany) 75% methanol 4.5% acetic acid (VWR International Ltd., Poole, UK) 20% dH_2O
10% (2-Hydroxypropyl)-β-cyclodextrin	10% (w/v) (2-Hydroxypropyl)-β-cyclodextrin in sterile dH_2O (5 g dissolved in 41.8 ml dH_2O = total volume of 50 ml)
LB-broth	2.5 g LB-broth high salt dissolved in 100 ml dH_2O and autoclaved
Lysis buffer (for western blot)	50 mM Tris-HCl pH 7.6, 137 mM NaCl, 10% (v/v) glycerol (VWR), 0.1% (v/v) Igepal, 0.1% (v/v) SDS (AppliChem GmbH, Darmstadt, Germany) 50 mM sodium fluoride 1 mM sodium orthovanadate and cOmplete protease inhibitor cocktail (Roche, Basel, Switzerland) in dH_2O [13]

13. Sodium orthovanadate and protease inhibitors were freshly added before use. The lysis buffer containing the remaining components was aliquoted and stored at 4°C.

Table 2.1 (continued)

Buffer	Composition
1x Phosphate buffered saline (PBS)	5x PBS tablets dissolved in 1 litre dH_2O
PBS-T	1x PBS, 0.1% (v/v) Tween-20
3% Paraformaldehyde (PFA)	3% PFA (w/v; VWR) dissolved in 1x PBS, pH adjusted to 7.4 with 5 M NaOH.
Resazurin stock solution	125 μg/ml resazurin in dH_2O
1x Tris-buffered saline (TBS)	1x pack OmniPur® TBS 20x Ready Pack Powder (Calbiochem, Darmstadt, Germany) dissolved in 20 litres of dH_2O
TBS-T	1x TBS, 0.1% (v/v) Tween-20
Tris-EDTA antigen retrieval buffer	10 mM Tris, 1 mM EDTA (VWR), 0.05% (v/v) Tween-20 in dH_2O; pH adjusted to 9 with 1M HCl

2.2 Tissue culture

2.2.1 Maintenance of cell lines

The cell lines used in this study are listed in Table 2.2. All cell lines were cultured in advanced DMEM/F12 (Life technologies, Carlsbad, USA), supplemented with 5% foetal bovine serum (FBS; Sigma-Aldrich), 2 mM GlutaMAX™ (Life technologies) and 50 U penicillin / 50 μg/ml streptomycin (Life technologies) in a standard humidified incubator at 37°C and 7.5% CO_2. The culture medium was changed every two to four days and cells were passaged at sub-confluence (70-80%). Routine passaging of the cells involved the preparation of a cell suspension by removal of the medium, washing with PBS and trypsinisation with 0.025% Trypsin/EDTA (Life technologies).

Table 2.2: Cell lines used in this study.

For each cell line, the designation used throughout the study is highlighted in bold. All cell lines are of human origin.

Cell line	Histological subtype	Obtained from	ATM mutation status	p53 mutation status	Ras mutation status	EGFR mutation status
A549	Lung carcinoma not specified (NSCLC)	ATCC[14] # CCL-185	wild-type (wt) [15]	wt	KRAS p.G12S homozygous	wt
A427	Lung carcinoma not specified	ATCC # HTB-53	wt	wt	KRAS p.G12D heterozygous	wt
Calu-6	Anaplastic carcinoma	ATCC # HTB-56	wt	(p.R196*) homozygous	KRAS p.Q61K heterozygous	wt
COR-L105	Lung adenocarcinoma	ECACC[16] # 92031918	wt	wt	wt	wt
HCC827	Lung adenocarcinoma	ATCC # CRL-2868	wt	(p.V218del) homozygous	wt	del (E746_A750)
NCI-**H1299**	Lung carcinoma not specified (NSCLC)	ATCC # CRL-5803	wt	homozygous deletion	NRAS p.Q61K heterozygous	wt
NCI-**H1395**	Lung adenocarcinoma	ATCC # CRL-5868	(p.T2666A); homozygous	wt	wt	wt
NCI-**H1975**	Lung adenocarcinoma	ATCC # CRL-5908	wt	(p.R273H) homozygous	wt	(p.L858R) (p.T790M)
NCI-**H2087**	Lung adenocarcinoma	ATCC # CRL-5922	(p.E848Q) heterozygous	(p.V157F) homozygous	NRAS p.Q61K heterozygous	wt
NCI-**H23**	Lung adenocarcinoma	ATCC # CRL-5800	(p.Q1919P); homozygous	(p.M246I) homozygous	KRAS p.G12C heterozygous	wt
PC-9	Lung adenocarcinoma	[17]	wt	(p.R248Q) homozygous	wt	del (E746_A750)
GM16666 (Ziv *et al*, 1997)	Fibroblast cell line derived from an Ataxia-telangiectasia patient	Coriell Institute (Camden, USA)	homozygous frameshift mutation at codon 762	SV-40 transformed	wt	wt
LIMM-**NBE1** (Stead *et al*, 2012)	Telomerase immortalised normal bronchial epithelial cells	[18]	wt [19]	wt	wt	wt
MRC-5 SV2	Lung fibroblast cell line	ECACC # 84100401	wt	SV-40 transformed	wt	wt

14. ATCC = American type culture collection (Manassas, USA)
15. It should be noted that wt refers to "no mutations reported to date".
16. ECACC = European collection of cell cultures (Salisbury, UK)
17. Kindly provided by Dr. Kazuto Nishio, Kinki University, Osaka, Japan.
18. Kindly provided by Dr. Pamela Rabbitts, Leeds Institute of Molecular Medicine, University of Leeds, UK
19. Presumed wild-type as derived from normal cells, but sequencing data has not been reported.

Cell density and viability was measured by adding a 1:1 mixture of cell suspension and 0.4% trypan blue solution to a Countess® cell counting chamber slide and carrying out standard cell counting using the Countess® automated cell counter (Life technologies). The desired cell numbers were seeded in fresh culture media prior to any experiments.

Upon receipt, all cell lines were authenticated by sequencing of highly polymorphic loci in the mitochondrial DNA as described in (Hutter *et al*, 2004). Authentication was carried out by Joe Ryan. Cells were passaged for no more than 25 passages post-authentication (approximately 3 months).

2.2.2 Cryostorage and thawing of cells

Cells from liquid nitrogen stocks were thawed rapidly at 37°C for 2 minutes (min). The cell suspension was diluted in 12 ml pre-warmed (37°C) complete culture medium and cells were pelleted by centrifugation at 225 x g for 5 min. The supernatant was discarded and the cell pellet re-suspended in 12 ml complete medium at 37°C and transferred to a T75 flask.

Cell lines to be frozen were grown until they reached approximately 80-90% confluence and then trypsinised as described in section 2.2.1. Cells were collected by centrifugation for 5 min at 225 x g, followed by re-suspension in 3 ml of complete culture medium containing 10% (v/v) dimethyl sulfoxide (DMSO; VWR). 500 μl aliquots were transferred to cryogenic tubes which were then frozen at -80°C overnight in an isopropanol container, before being transferred into liquid nitrogen.

2.3 ATM gene sequencing

In order to validate the presence of ATM missense mutations in the NSCLC cell lines H23, H1395 and H2087, Sanger sequencing of the respective genomic loci was performed. The protocol for ATM gene sequencing was adjusted from (Sandoval *et al*, 1999). In short, the regions of interest in exons 17, 38 and 54 of the ATM gene were pre-amplified from genomic DNA samples of H2087, H1395 and H23 cells using polymerase chain reaction (PCR). PCR is a technique for the amplification of DNA, which employs a heat-stable DNA polymerase. During a PCR, changes in temperature are used to control the activity of the polymerase and the binding of primers - short DNA fragments that contain sequences complementary to the DNA target region of interest. To begin the reaction the temperature is raised to 95°C, which allows all double stranded DNA (dsDNA) to be melted into single strands. The temperature is then lowered to ~60°C to allow for the primers to bind to the gene of interest. The primers are required for the initiation of DNA synthesis, as they provide a basis for the DNA polymerase to bind to and begin DNA synthesis. The optimal temperature for the polymerase to operate is 72°C so the temperature is raised for DNA synthesis ("elongation"). Repetition of these temperature changes for 30-40 cycles allows for the exponential replication of the DNA template of interest.

The primers used for ATM gene sequencing were[20]:

Exon 17: Forward: 5'-GTACTGTAGTTTTCATACTTACAC-3',

Reverse: 5'-GGAACAATCCTAAAAGGCTATAC-3'

Internal sequencing primer for Exon 17: 5'-GATTAGGTAAATTTTGACTACAG-3'

20. Exon numbering differs from (Sandoval *et al*, 1999) as the designation of exon boundaries has been changed since 1999, according to the National Center for Biotechnology information (NCBI).

Exon 38: Forward 5'-TATCATATTGTGTTGTAATGTCCC-3',

Reverse 5'-ATCATGTTAAAATTCAGCCGATAG-3'

Exon 54: Forward 5'-CTGCTGACTATTCCTGCTTGACC-3',

Reverse 5'-GCCAATATTTAACCAATTTTGACC-3'

PCR reactions were carried out on an Applied Biosystems® thermal cycler (Life technologies). The PCR amplification was performed in 25 μl reactions containing 2 units MiFi DNA polymerase, 0.1 μg genomic DNA and 0.5 μM of each primer in 1x MiFi reaction buffer (Bioline Reagents Ltd, London, UK). The following conditions were used:

Activation (hotstart)	95°C	3 min	
Denaturation	94°C	1 min	35x
Annealing	59°C	1 min	
Elongation	72°C	1 min	
Final extension	72°C	10 min	

Sanger DNA sequencing of the resulting PCR-products was performed commercially by SourceBioscience (Oxford, UK) and the resulting reads analysed for the presence of the reported missense changes.

2.3.1 PolyPhen scoring

The possible impact of the amino acid substitutions identified in the NSCLC cell lines H23, H1395 and H2087 on ATM structure and function was evaluated using the program PolyPhen-2, which predicts the possible consequences of amino acid substitutions on protein stability and function based on structural and comparative

evolutionary considerations (Adzhubei et al, 2010). PolyPhen-2 was accessed through the web interface at http://genetics.bwh.harvard.edu/pph2/index.shtml. The protein sequence for ATM (FASTA format) was derived from the National Center for Biotechnology information (NCBI; accession number: AAB65827.1).

2.4 Mycoplasma testing

All cell lines were tested for mycoplasma infection using a quantitative real-time PCR based assay. Real-time PCR follows the same principle as PCR (see section 2.3), but it allows for the amplification and simultaneous quantification of a target DNA molecule. The quantification is facilitated through the binding of a dsDNA-intercalating agent (e.g. SYBR Green), which generates a fluorescent signal that is proportional to the amount of dsDNA in the sample. As the target sequence is amplified exponentially with each cycle, this fluorescence signal increases with the amount of target DNA in the sample and can be detected with a camera. Calculation of the threshold cycle (C_T) value for each reaction then serves as a measure for the DNA copy number and allows for comparison between samples. The C_T is defined as the cycle number, at which the level of fluorescence signal first crosses a fixed threshold and is considered to be sufficiently above background levels to represent a specific signal.

The assay used for mycoplasma testing was performed as described in (Ishikawa *et al*, 2006) with a few modifications. In short, DNA was isolated from cell pellets using the MasterPure™ DNA purification kit (Epicentre, Madison, USA) according to the manufacturer's instructions. The primers used were designed to amplify a section of the 23S ribosomal RNA gene, which is known to contain species-specific regions,

from eight different mycoplasma subspecies that account for over 95% of isolates from cultured cells (for primer sequences see (Ishikawa *et al*, 2006)).

The real-time PCR reactions were carried out on a MiniOpticon real-time PCR System (BioRad, Hemel Hempstead, UK) in a 20 μl reaction containing 0.1 μg sample DNA, 1x Power SYBR Green PCR Master Mix (Applied Biosystems, Carlsbad, USA) and 300 nM of each primer/primer mix. Samples were measured in triplicates. Thermal cycling conditions were as follows:

Activation (hotstart)	95°C	1 min	
Amplification	95°C	15 s	} 40x
	60°C	30 s	
Melting curve	55°C to 95°C		
	increment (0.5°C)	10 s	
Cooling	4°C	∞	

Appropriate non-template controls were included and melting point analysis was performed at the end of each run to confirm the specificity of the reaction and to rule out possible contamination of the reagents used. Amplification of a positive control (0.1 pg of M. orale DNA; Minerva Biolabs GmbH, Berlin, Germany, #51-0112) was performed to define the threshold for a positive reaction result. The threshold cycle (C_T) values were calculated using the BioRad CFX Manager software.

2.5 siRNA transfections

Transfection of cells with small interfering RNAs (siRNAs) is a commonly used method, which allows for the highly specific and selective downregulation of the

expression of a gene of interest through RNA interference (RNAi). RNAi is a naturally occurring biological process that is usually employed to defend a cell against RNA viruses or to help regulate gene expression. During RNAi, RNA molecules cause sequence-specific gene silencing at the post-transcriptional level by mediating the destruction of specific messenger RNA (mRNA) molecules (Figure 2.1).

When double-stranded RNA is introduced into a cell (e.g. through expression of a short hairpin RNA, see section 2.7), it is recognised and processed into smaller intermediates known as small interfering RNAs (siRNAs) by the ribonuclease enzyme Dicer. Each siRNA consists of a short double-stranded fragment of ~20 nucleotides, which is then separated into two single-stranded RNAs: the passenger strand and the guide strand. The passenger strand is degraded and the guide strand is incorporated into the RNA-induced silencing complex (RISC), which binds to mRNAs and cleaves them if they are complementary to the incorporated guide strand. The cleaved mRNA is rapidly destroyed, leaving the RISC-guide strand complex available for additional cycles of mRNA binding and cleavage (Figure 2.1).

In our studies, the siGenome ATR siRNA SMART pool from Dharmacon was used for downregulation of ATR (#M-003202-05-0005; GE Healthcare UK, Little Chalfont, UK). The siGenome non-targeting siRNA SMART pool #1 served as control (#D-001206-13-05; Dharmacon; GE Healthcare UK). Two days before transfection, cells were seeded in 6-well plates for western blot analysis ($1x10^5$ cells/well) or 96-well plates for proliferation assays ($1x10^3$ or $2x10^3$ cells/well, depending on cell line). Cells were transfected with 25 nM siRNA using the DharmaFECT 2 (Dharmacon) transfection reagent according to the manufacturer's instructions.

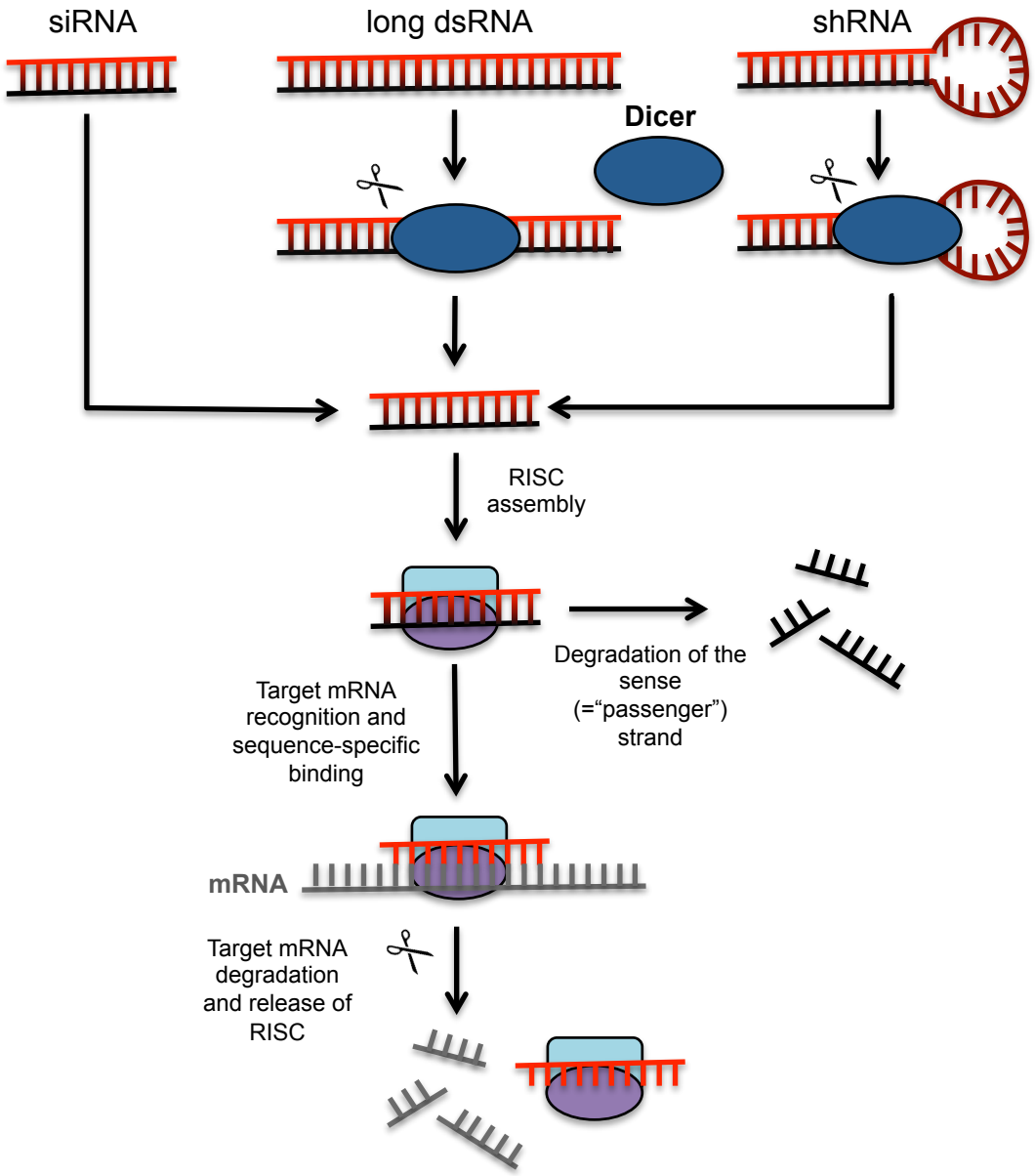

Figure 2.1: The principle of RNA interference.

Long double-stranded RNA (dsRNA) or short hairpin RNA, introduced into the cytoplasm of a cell, is cleaved into siRNA by the ribonuclease Dicer. Alternatively, siRNA can be introduced directly into the cell. The siRNA sense (="passenger") strand is then cleaved and degraded while the anti-sense (="guide") strand is incorporated into the RISC. The activated RISC–siRNA complex then recognises, binds to and degrades complementary mRNA, which leads to the silencing of the target gene. Following mRNA degradation, the RISC–siRNA complex can be recycled for the destruction of identical mRNA targets.

In short, the transfection mix was produced in two stages, with separate mixing of the DharmaFECT2-Opti-MEM® (Life technologies) and siRNA-Opti-MEM® components before 5 min incubation at room temperature (RT). The two solutions were combined, vortexed and left to incubate for another 20 min at RT. The complexes were then added to each well containing cells and culture medium. To reduce the cytotoxicity of the procedure, the transfection medium was removed and fresh culture medium was added 5 h after transfection. Cells were harvested at the indicated times post-transfection and processed for western blot analysis (see section 2.10) or cell viability was assessed by quantification of resazurin metabolism 5 days after transfection (see section 2.11.1).

2.6 Bacterial transformation and plasmid purification

2.6.1 Transformation of bacteria using heat-shock

We aimed to generate NSCLC cell lines that stably express fluorescently labelled histone H2B, or a short hairpin RNA directed against ATM (see sections 2.7 and 2.8.1). To produce sufficient quantities of the plasmids required for transfection, we used bacterial transformation. This technique allows for the amplification of plasmids in bacteria, which can be subsequently extracted and used for transfection of mammalian cells.

Chemically competent DH5α E.coli cells (Invitrogen) were used for plasmid amplification. The bacterial cells were removed from the -80°C freezer, thawed on ice and aliquoted into 50 μl volumes. 1-50 ng of plasmid DNA was added to each 50 μl aliquot of bacteria and incubated on ice for 30 min. Heat shock was performed in a 42°C water bath for 20 s, followed by 2 min incubation on ice. 950 μl LB medium was

added to each tube and bacteria were incubated for 1 h at 37°C while shaking at 250 rpm. 20-200 μl of the resulting bacterial culture was spread on LB agar plates containing 100 μg/ml ampicillin (Calbiochem) and incubated overnight at 37°C.

2.6.2 Plasmid purification

Single bacterial colonies were picked from the LB agar plates, transferred to selective LB medium (containing 100 μg/ml ampicillin) and incubated at 37°C and 250 rpm over night. For isolation of small amounts of plasmid DNA, 5 ml liquid cultures were used and plasmid DNA was purified using the QIAprep spin MiniPrep kit (Qiagen) according to the manufacturer's instructions. For extraction of larger amounts of plasmid DNA, 100 ml liquid cultures were prepared and the QIAGEN Plasmid Midi kit was used. In short, following over night growth in selective LB medium, bacterial cells were pelleted by centrifugation at 6,000 x g for 15 min at 4°C. The pellet was re-suspended in buffer P1 containing RNase A and cells were lysed by addition of buffer P2 and mixed by inverting the tube several times. The lysis buffer was then neutralised by addition of chilled buffer P3 (buffers P1, P2 and P3 are included in the kit). When the Plasmid Midi kit was used, this was followed by 15 min incubation on ice. Cell debris was precipitated by centrifugation (16,100 x g at 4°C) and the plasmid DNA containing supernatant was applied to a QIAprep spin column (MiniPrep kit) or an equilibrated QIAGEN-tip 100 column (Plasmid Midi kit). Following centrifugation (QIAprep spin column) or emptying of the QIAGEN-tip 100 column by gravity flow, the flow through was discarded and the plasmid DNA bound to the silica membranes of the columns was washed several times using the supplied washing buffers to remove impurities. The plasmid DNA was eluted using 50 μl TE-buffer (MiniPrep kit), or buffer QF (Plasmid Midi kit) followed by alcohol precipitation and re-

suspension in TE-buffer. DNA concentrations were determined using a NanoDrop 1000 spectrophotometer (Thermo Fisher Scientific).

2.7 Generation of stable ATM knockdown cell lines

2.7.1.1 Design of short hairpin RNA sequences

We aimed to generate NSCLC cell lines with stable knockdown of ATM protein expression. For this purpose, expression plasmids were generated that mediate intracellular synthesis of short hairpin RNAs (shRNAs) directed against ATM. Following processing in the cytoplasm, such shRNAs mediate gene knockdown via RNA interference (as described in section 2.5).

The pSuperRetro.puro vector was used for the expression of shRNAs (OligoEngine, Seattle, USA). In addition to ATM knockdown plasmids, plasmids carrying shRNA directed against green fluorescent protein (GFP), a gene not present in mammalian cells, were generated as non-targeting controls. Short-hairpin RNA sequences directed against ATM (NM_000051.3) and GFP (M62654.1) were designed using the Dharmacon *siDESIGN Center* software (Thermo Fisher Scientific, Lafayette, USA) and the *2-shRNA Oligo Designer* online tool (University of North Carolina, USA). The sequences were designed to hold restriction sites for BamH1 and HindIII at their 5' and 3' end, respectively. Published criteria for design of functional shRNA sequences were taken into account (Brummelkamp *et al*, 2002; Birmingham *et al*, 2007), as well as guidelines provided by the pSuperRetro.puro supplier. All oligonucleotides were purchased from Sigma-Aldrich. For each gene, three shRNA sequences were tested. For ATM, the sequence achieving the highest degree of protein knockdown was chosen for transfection and used in subsequent experiments. None of

the shGFP sequences appeared to cause changes in morphology, growth rate or activation of the ATM signalling pathway following exposure of the cells to ionising radiation (IR). Therefore the sequence with the closest similarity to the chosen shATM sequence, based on the GC content, was selected. The selected shRNA target sequences were:

5'- GCAACATACTACTCAAAGA –3' (ATM)

5'- GCATGGATGAACTATACAA –3' (GFP)

2.7.2 Plasmid preparation

Cloning of the generated oligonucleotides into the pSuperRetro.puro vector backbone was performed as described in the protocol provided by OligoEngine. In short, pSuperRetro.puro plasmid DNA was linearised by incubation with the restriction enzymes BglII and HindIII (Fermentas, St. Leon-Rot, Germany) for 3 h at 37°C, as per the manufacturer's protocol. The linearised vector was purified on a 1% agarose gel to remove the fragment, and plasmid DNA cut out from the gel was extracted using a gel extraction kit from Qiagen (Hilden, Germany). Oligonucleotides containing the shRNA coding sequences were annealed and inserted into the linearised vector backbone using T4 DNA ligase (Fermentas). Following transformation into bacteria (DH5α; Invitrogen; see section 2.6), the presence of positive colonies was tested by BglII digest of isolated plasmids and agarose gel electrophoresis of the digestion products.

2.7.3 Transfection and selection of stably transfected clones

The day before transfection, COR-L105, H1299, H2087 or H1975 cells were seeded in 6-well plates at a density of $2x10^5$ cells/well. The pSuperRetro.puro vector constructs were linearised through digestion with the restriction enzyme XbaI, to increase the efficiency of stable integration of plasmid DNA into the genome of the cells. Transfections were carried out with Lipofectamine 2000 transfection reagent (Invitrogen) as described by the manufacturer. 1-2 μg of linearised plasmid DNA were used per transfection. 48 h after transfection, medium was exchanged for selection medium containing 1-2 μg/ml puromycin. During the selection period of approximately 14 days, medium was changed every two to four days. Following selection, individual colonies were picked, separately trypsinised and transferred to new plates where they were expanded for further experiments. To assess efficiency of gene knockdown, total ATM protein levels, as well as phosphorylation of ATM and several downstream targets following exposure of cells to IR were measured by western blot analysis.

Stably transfected cells were maintained in culture medium supplemented with 0.5 μg/ml puromycin. At least 24 h prior to any experiments, the selection medium was removed and replaced by puromycin-free medium.

2.8 Live cell imaging

2.8.1 Generation of cell lines stably expressing mCherry-conjugated histone H2B

In order to study the cellular responses to DDR inhibitors in more detail, in particular the dynamics of mitosis, we generated cell lines expressing a red-fluorescent

(mCherry-tagged) version of histone H2B, which allows for the indirect visualisation of DNA in live cell imaging. For this purpose, the pH2B_mCherry_IRES_puro2[21] plasmid was used and amplified in bacteria as described in section 2.6. The day before transfection, A427 or H1299 cells were seeded in 6-well plates at a density of $2x10^5$ cells/well. Transfections were carried out using 1 μg of plasmid DNA with the Lipofectamine 2000 transfection reagent (Invitrogen) as described by the manufacturer. 48 h after transfection, medium was exchanged for selection medium containing 1-2 μg/ml puromycin. During the selection period of approximately 10 days, medium was changed every two to four days. Following selection, cells were trypsinised, seeded in 6-well plates at a density of 500 cells/well and allowed to form colonies for approximately 10 days. Individual colonies were selected based on nuclear fluorescence intensity, separately trypsinised and transferred to new plates.

Stably transfected cells were maintained in HEPES and sodium bicarbonate buffered OptiMEM (Life technologies) supplemented with 10% FBS, 2 mM GlutaMAX™ (Life technologies), 50 U penicillin / 50 μg/ml streptomycin (Life technologies) and 0.5 μg/ml puromycin in a standard humidified incubator at 37°C and 7.5% CO_2. At least 24 h prior to any experiments, the selection medium was removed and replaced by puromycin-free medium.

2.8.2 Cell imaging

Cells were seeded in puromycin-free medium in 8-well μ-slides (ibidi GmbH, Martinsried, Germany) at a density of 5,000 cells/well (A427) or 1,000 cells/well (H1299). Cells were then incubated at 37°C and 7.5% CO_2 for three (A427) to five

21. The pH2B_mCherry_IRES_puro2 plasmid was a gift from Daniel Gerlich (Addgene plasmid #21045) (Steigemann *et al*, 2009).

(H1299) days before imaging. Cells were treated with the indicated drugs diluted in complete puromycin-free OptiMEM medium (see section 2.8.1) and imaging was commenced within 1 h of drug addition. Cells were imaged for 72 h at 15 min intervals unless otherwise stated. An inverted TE2000-E Nikon Eclipse microscope (Nikon UK Limited, Kingston Upon Thames, UK) was used for imaging with an ORCA-ER camera (Hamamatsu) and a motorised microscope stage system from Prior Scientific (Rockland, USA). Pictures were taken at a 100x or 200x magnification (10x or 20x objective) using the NIS-Elements Advanced Research software (Nikon UK Limited). During imaging, cells were kept in a microscope incubator setup (Solent Scientific Ltd., Segensworth, UK) at 37°C and 5% CO_2 in a humidified atmosphere.

2.8.3 Data analysis

The pictures acquired during live cell imaging were used for single-cell tracking of 50 mitotic cells per cell line and treatment condition. The analysis included quantification of the average residence time of each cell in mitosis, the percentage of cells progressing through mitosis with obvious nuclear fragmentation or formation of micronuclei as well as the percentage of cells that underwent cell death during mitosis or shortly after mitotic exit. Mitotic residence time was defined as the timespan from the beginning of chromosomal condensation up to the point where DNA decondensation occurred.

2.9 Drug treatments and irradiation

Stock solutions of gemcitabine (LC Laboratories; Woburn, USA), KU55933 (TOCRIS Bioscience; Bristol, UK), AZD2281, AZD6738 (AstraZeneca, Macclesfield, UK),

etoposide, irinotecan, NU7441, KU60019, VE-821 and VE-822 (Selleck chemicals; Houston, USA) were prepared in 100% DMSO at a concentration of 10 mM. Cisplatin (Sigma-Aldrich) was prepared at 3.3 mM in 0.9% sterile saline solution. All stock solutions were aliquoted and stored at –20°C until use. Dilutions of the drugs for the treatment of cells were made using DMSO and/or culture media.

Irradiations were carried out using a Gamma Service® GSR D1 irradiator (Gamma-Service Medical GmbH; Leipzig, Germany) containing a ^{137}Cs source. The dose rates of the system were 1.938 Gy/min and 1.233 Gy/min, respectively, depending on the distance from the source.

2.10 Protein detection by western blotting

Western blotting is an analytical technique used to detect specific proteins or modified proteins (e.g. ubiquitinylated or phosphorylated) from a complex mixture of proteins extracted from cells. It uses SDS-polyacrylamide gel electrophoresis (SDS-PAGE) to separate proteins contained in a cell or tissue homogenate according to molecular weight. The proteins are then transferred onto a matrix (e.g. a nitrocellulose membrane) where they are incubated with antibodies specific to the protein or modified protein of interest. The membrane-bound antibodies can then be detected and expression levels of the target proteins and/or modifications in the given sample can be obtained by analysing the location and intensity of the specific reaction.

2.10.1 Preparation of cell extracts and SDS-polyacrylamide gel electrophoresis

For western blot analysis, cells were washed in ice-cold (4°C) PBS and whole-cell lysates were prepared on ice in lysis buffer supplemented with sodium orthovanadate and cOmplete protease inhibitor cocktail (see Table 2.1). Lysates were homogenised by brief sonication and cleared by centrifugation at 16,100 x g for 15 min at 4°C. Protein concentrations were determined using a NanoDrop 1000 spectrophotometer. Samples were diluted in PBS and 2x Laemmli sample loading buffer to equal protein concentrations and heated to 95°C for 10 min. A molecular weight ladder (BioRad) and 50 μg of protein per lane were loaded onto a 4-15% or 4-20% gradient precast Mini-PROTEAN® TGX gel (gel dimensions: 8.6 x 6.7 x 0.1 cm; BioRad) and separated at 150-200V.

2.10.2 Immunoblot

The proteins resolved via SDS-PAGE were then transferred to nitrocellulose membranes (0.45 μm pore size; BioRad) in 1x tris-glycine buffer (BioRad) containing 20% methanol (v/v) for 1 h at 150 V (high molecular weight proteins) or 35-45 min at 150 V (low molecular weight proteins). Membranes were incubated in 5% (w/v) non-fat skimmed milk powder in 1xTBS-T or PBS-T (0.1% Tween-20) for 1 h at room temperature (RT) to block non-specific binding of antibodies to the membrane. Exposure to primary antibodies (listed in Table 2.3), diluted in the same blocking solution, was carried out overnight at 4°C, with the exception of the pCHK1 antibodies which were incubated at 4°C for 48 h.

Table 2.3: Antibodies used for immunoblot analysis.

Specification (Name)	**Species/ clonality**	**Dilution**	**Manufacturer and *catalogue number***
α-Tubulin	Mouse monoclonal	1:5,000	Sigma-Aldrich (St. Luis, USA) ***# T6074***
total ATM	Mouse monoclonal	1:1,000	Sigma-Aldrich ***#A1106***
phospho-ATM Ser1981	Rabbit monoclonal	1:10,000	Epitomics Inc. (Burlingame, USA) ***#2152-1***
ATR	Goat polyclonal	1:500	Santa Cruz Biotechnology (Santa Cruz, USA) ***#sc-1887***
β-Actin	Mouse monoclonal	1:5,000	Sigma-Aldrich ***# A1978***
total CHK1	Mouse monoclonal	1:2,000	Santa Cruz Biotechnology ***#sc-8408***
phospho-CHK1 Ser317	Rabbit polyclonal	1:500	Cell Signaling Technology Inc. (Danvers, USA) ***#2344***
phospho-CHK1 Ser345	Rabbit polyclonal	1:500	Cell Signaling ***#2341***
phospho-CHK1 Ser296	Rabbit polyclonal	1:500	Cell Signaling ***#2349***
phospho-CHK2 Thr68	Rabbit polyclonal	1:1,000	Cell Signaling ***#2661***
cleaved Caspase-3 (Asp175)	Rabbit polyclonal	1:500	Cell Signaling ***#9661***
Cyclin A	Mouse monoclonal	1:2,000	Abcam ***#ab16726***
Cyclin D1	Rabbit monoclonal	1:10,000	Abcam ***#ab134175***
phospho-H2AX Ser139	Mouse monoclonal	1:1,000	Upstate-Millipore (Billerica, USA) ***#05-636***
Phospho-histone H3 Ser10	Rabbit polyclonal	1:2,000	Upstate-Millipore ***#06-570***
total KAP1	Rabbit polyclonal	1:10,000	Bethyl Laboratories (Universal Biologicals, Cambridge, UK) ***#A300-274A***
phospho-KAP1 Ser824	Rabbit polyclonal	1:2,000	Bethyl Laboratories ***#A300-767A***
PARP	Rabbit polyclonal	1:2,000	Cell Signaling ***#9542***
p21	Rabbit polyclonal	1:1,000	Santa Cruz Biotechnology ***#sc-397***
total p53	Mouse monoclonal	1:500	Santa Cruz Biotechnology ***#sc-126***
phospho-p53 Ser15	Rabbit polyclonal	1:1,000	Cell Signaling ***#9284***
phospho-SMC1 Ser966	Rabbit polyclonal	1:2,000	Bethyl Laboratories ***#A300-050A***

Table 2.3 (continued)

Specification (Name)	Species/ clonality	Dilution	Manufacturer and *catalogue number*
Secondary antibodies:			
Anti-goat-HRP	donkey	1:5,000	Jackson Immunoresearch Laboratories (West Grove, USA)
Anti-mouse-HRP	goat	1:5,000	Sigma-Aldrich
Anti-rabbit-HRP	goat	1:5,000	Sigma-Aldrich

After several washes in TBS-T or PBS-T, membranes were incubated with appropriate HRP-conjugated secondary antibodies for 1 h at RT, diluted in the same blocking solution as the primary antibodies. Following additional three washes in TBS-T or PBS-T (5-10 min) and two washes in TBS/PBS, detection was carried out by chemoluminescence and film exposure. Depending on the strength of the signal, the Pierce® ECL Western Blotting substrate (Thermo Scientific, Rockford, USA) or the Amersham™ ECL™ Prime Western Blotting detection reagent from GE Healthcare UK (Little Chalfont, UK) was used.

Densitometric quantification of protein bands was performed using the ImageJ software. The numbers reflect the relative intensity of each band normalised to a reference sample and expressed as a ratio of each band relative to the loading control of the respective lane.

2.11 Cell viability, spheroid and clonogenic survival assay

2.11.1 Cell viability assay

To assess the impact of chemotherapeutic drugs or DDR inhibitors on cell proliferation and viability, resazurin-based cell viability assays were performed (O'Brien *et al*, 2000). Following seeding of cells into 96-well plates, cells are allowed to grow for several days in the presence of a dilution series of the compound(s) of interest. At the end of the treatment period, the metabolic activity of the cells in each well is assessed through quantification of resazurin metabolism as an indirect measure of cell numbers. Resazurin is a blue non-fluorescent dye, which is reduced to the highly fluorescent product resorufin in metabolically active cells, rendering the resulting fluorescent signal proportional to the number of viable cells. The signal intensity obtained for each treatment condition then allows for the assessment of cell viability relative to vehicle control treated cells and thus gives an estimate of the response of the cell line to the respective drug at the given concentration.

Cells were seeded in triplicate into 96-well plates, incubated overnight to allow for re-attachment and then treated with dilution series of the respective compounds or compound combinations. Following incubation at 37°C for three or five days, quantification of resazurin metabolism (12.5 μg/ml final concentration per well) was used to measure cell viability and proliferation (O'Brien *et al*, 2000). Fluorescence intensity was measured on a POLARstar Omega plate reader (BMG Labtech GmbH, Ortenberg, Germany) with excitation at 544 nm and emission at 585–595 nm. The half-maximal inhibitory concentration (IC_{50}) was determined from at least three independent experiments, unless otherwise stated, using the Origin software (OriginLab Corporation, Northampton, USA). For the single-treatments, IC_{50} values

represent the concentration of compound, which is required to reach 50% inhibition of cell viability relative to vehicle-treated control. To calculate IC_{50} values for drug combination treatments, data was normalised to cells treated with the combination agent alone (the compound which was added at a fixed concentration).

2.11.2 Spheroid growth assay

Results obtained from cell viability assays indicated that certain combinations of DDR inhibitors were particularly cytotoxic for NSCLC cell lines with defects in p53 signalling. To further validate these results, we generated a three-dimensional spheroid assay. Spheroid models possess many of the elements of *in vivo* xenograft models and are thus improved *in vitro* models for the assessment of cellular responses to small molecule inhibitors or chemotherapeutic drugs. In addition to cell-cell interactions, spheroids possess a spatial geometry that produces drug and nutrient concentration gradients as well as subpopulations of cells that are hypoxic, quiescent or necrotic (Phung *et al*, 2011).

Spheroid production was performed as described previously (Phung *et al*, 2011). In short, $1x10^3$ (H23 and H1299), $2x10^3$ (A549, H2087) or $3x10^3$ (H1395 and COR-L105) cells were seeded in each well of a low-binding Lipidure-Coat 96-well plate (AMS Biotechnology Ltd., Abingdon, UK; #A-U96) in 200 μl cell culture medium per well. Plates were centrifuged at 250 x g at RT for 10 min and incubated for 48 h at 37°C and 7.5% CO_2 to allow for spheroid formation.

For treatment, 100 μl of medium was removed from each well and replenished with 100 μl culture medium containing 2x concentrated drug or vehicle (DMSO).

For experiments with short-term treatment (48 h or 72 h), 150 μl of culture medium was removed and replenished with fresh drug-free culture medium at the end of the treatment period. These washes were performed several times (5x) to remove/dilute residual inhibitor. Spheroids were then allowed to grow in drug-free culture medium for an additional 7-day (for 72 h treatments) or 8-day (for 48 h treatments) period before assessment of spheroid growth and viability through quantification of resazurin metabolism (see section 2.11.1). For continuous treatments, cells were exposed to the respective inhibitors for 10 days before assessment of cell viability. To maintain optimal treatment and growth conditions 100 μl of culture medium was replaced with fresh medium (with or without the respective drug) every 2-3 days for all spheroid experiments, irrespective of treatment duration.

Pictures of the spheroids were taken at a 40x magnification on a TE2000-E Nikon Eclipse microscope using the NIS-Elements Advanced Research software.

2.11.3 Clonogenic survival assay

The clonogenic survival assay is the standard technique to evaluate radiation sensitivity of cell lines. It assesses the relative reproductive capacity - the ability of a single cell to form a colony of 50 or more cells - of control and irradiated cells with or without potential radiosensitising agents.

To assess radiosensitisation, cells were plated in triplicate in 6-well plates and allowed to re-attach (depending on cell line for 3 to 16 h). One hour prior to irradiation, cells were pre-incubated with 0.1% DMSO (vehicle control), NU7441 (500 nM), KU55933 (10 μM), VE-821 (1 μM) or VE-822 (0.1 μM). 24 h post irradiation, cells were washed with PBS and then incubated in drug-free medium at 37°C to allow for colony

formation. Once colonies reached a size of 50 or more cells, cells were fixed and stained with a 0.5% (w/v) crystal violet/ 75% (v/v) methanol/ 4.5% acetic acid (v/v) solution for 30 min at RT and air dried before colony counting. The plating efficiency (PE) for each cell line was calculated using the following equation:

PE = number of colonies counted / number of cells seeded

The PE was then used to calculate a surviving fraction (SF) for each irradiated population normalised to mock-irradiated vehicle control or mock-irradiated inhibitor treated and expressed as mean ± SEM (standard error of the mean).

SF = number of colonies counted after IR/ (number of cells seeded x PE)

2.12 Flow cytometry

2.12.1 DNA content analysis/cell cycle analysis

Measurement of the cellular DNA content by flow cytometry is one of the most commonly used methods to assess the cell cycle distribution of a given cell population. During this process, a DNA-binding fluorescent dye (e.g. propidium iodide) is incubated with a single cell suspension of fixed and permeabilised cells. Since the dye binds to DNA stoichiometrically, the amount of fluorescent signal is directly proportional to the amount of DNA. Due to the DNA-content alterations that occur during the cell cycle, this allows discrimination between G1-, S-, G2- and M-phase cells.

For DNA content analysis by flow cytometry, cells were treated as indicated, harvested by trypsinisation and collected at 225 x g for 5 min. The supernatant was

discarded and cell pellets were fixed by drop-wise addition of 1 ml ice-cold 70% ethanol while vortexing, followed by 30 min incubation on ice. Cells were washed in PBS and incubated in PBS containing 100 μg/ml RNase A (Qiagen) for 30 min at 37°C. For the staining of DNA, propidium iodide (PI, Calbiochem) was added at a final concentration of 20 μg/ml. DNA content was determined using a FACScan Flow Cytometer (BD Biosciences, San Jose, USA) and BD CellQuest™ Pro software. The proportion of cells in G1, S or G2/M was determined using the ModFit LT software (Verity Software House, Topsham, USA).

2.12.2 BrdU incorporation analysis

The thymidine analogue bromodeoxyuridine (BrdU) can be used to detect DNA synthesis in cells *in vitro*, as well as *in vivo*. BrdU is incorporated into DNA during replication as a substitute for thymidine and represents a molecular label of newly synthesised DNA that can be detected using anti-BrdU antibodies.

We used BrdU incorporation assays to assess the activation of the G1/S- and intra-S-phase cell cycle checkpoints in response to IR, through quantification of cell populations in early S-, mid S- and late S-phase at different time points post-irradiation. For this purpose, asynchronous cell populations were mock-irradiated or irradiated with 10 Gy. 6 or 24 h after irradiation, cells were pulse labelled with 20 μM BrdU for 20 min at 37°C and protected from light. After harvesting by trypsinisation and fixation in 70% ethanol (4°C), cells were re-suspended in 2 M HCl and incubated for 20 min at RT. Following centrifugation at 225 x g for 5 min, cells were first washed in PBS and then PBS containing 2% FBS. The cell pellets were re-suspended in PBS+ 2% FBS containing mouse anti-BrdU antibody (1:100 dilution; #347580; BD

Biosciences). Incubation in primary antibody was performed for 90 min at RT, followed by a washing step in PBS+ 2% FBS. This was followed by incubation in goat anti-mouse Alexa 488 secondary antibody (1:200 dilution; Invitrogen) for 1 h at RT in the dark, before washing in PBS and re-suspension in PBS containing 20 μg/ml PI. DNA content and BrdU incorporation were assessed using a FACSCalibur Flow Cytometer (BD Biosciences) and BD CellQuest^{TM} Pro software. Analysis of the data was carried out using the FlowJo software (Tree Star Inc.).

2.12.3 BrdU chase assay

We also used BrdU labelling to allow for the following of cells through the cell cycle. To label the S-phase population of the cell lines at the beginning of the treatment period, asynchronous cell populations were pulse labelled with 20 μM BrdU for 30 min. After washing with PBS, complete cell culture medium was added containing vehicle (0.01% DMSO) or 1 μM VE-821. Cells were treated with vehicle, 1 μM VE-821 (for 1 h prior to IR), 10 Gy or a combination of VE-821 and IR and incubated at 37°C for the indicated time periods. Cells were then fixed and stained for BrdU and PI to assess to which stage of the cell cycle the originally BrdU labelled (S-phase) cells had progressed. BrdU staining and FACS analysis were performed as described in section 2.12.2.

2.13 Immunofluorescence

Immunofluorescence is a technique that utilises antibodies conjugated with a fluorescent dye to detect specific target proteins in fixed cells using fluorescence microscopy.

For this purpose, cells were grown on poly-L-lysine coated coverslips (BD Biosciences) and treatments were carried out for 48 h. Cells were then fixed for 20 min in 3% paraformaldehyde (PFA; see Table 2.1) in PBS at RT and permeabilised with 0.1% Triton X-100 (VWR) in PBS for 1 h at RT. 1% normal goat serum (NGS; Millipore) and 1% BSA were added to the buffer to block non-specific protein binding. Cells were incubated in primary antibodies directed against histone H3 S10 (1:2,000; #06-570; Upstate Millipore), γH2AX S139 (1:1,500; clone JBW301, #05-636; Upstate Millipore) and/or α-Tubulin (1:2,000; Sigma-Aldrich; # T6074) diluted in 1% NGS and 1% BSA in PBS overnight at 4°C. After washing and incubation with goat anti-rabbit Alexa 555 and goat anti-mouse Alexa 488 secondary antibodies (Invitrogen; 1:1,200 dilution in 1% NGS/1% BSA in PBS), coverslips were mounted with Fluoroshield mounting medium containing DAPI (Sigma). Images were acquired with a Nikon Eclipse 90i microscope using the NIS-Elements Advanced Research software.

2.13.1 Quantitative γH2AX, 53BP1 and RPA32 foci staining

For the quantification of nuclear γH2AX, 53BP1 or RPA32 foci following immunofluorescence labelling of the respective target protein, cells were seeded in triplicate in 96-well plates and allowed to re-attach before treatment as indicated (for 48 h). Following treatment, cells were fixed in 3% PFA in PBS at RT for 20 min and permeabilised with 0.1% Triton X-100 in PBS for 1 h at RT. 1% NGS and 1% BSA were added for blocking. Cells were incubated with primary antibodies recognising γH2AX S139 (1:1,500; #05-636; Upstate Millipore), RPA32 (1:200; #ab2175; Abcam) or 53BP1 (1:800; #4937; Cell Signaling) diluted in 1% NGS and 1% BSA in

PBS overnight at 4°C. After washing, cells were incubated with goat anti-rabbit Alexa 555 or goat anti-mouse Alexa 488 secondary antibodies (Invitrogen; diluted in 1% NGS/ 1% BSA in PBS). Hoechst 33258 was added to the secondary antibody solution for nuclear counterstain (1:1,000 dilution of a 25 μM stock solution). Images were acquired using the INCell Analyzer 1000 automated epifluorescence microscope and foci quantification was carried out with the associated analysis software (GE Healthcare UK Ltd).

2.14 Chromosome analysis

To assess the amount of chromosomal abnormalities and DNA DSBs carried through into - or introduced during - mitosis, metaphase chromosome spreads were analysed. For this technique, cells were treated with vehicle control or the respective compounds for 48 h. Colcemid (0.1 μg/ml; KaryoMAX®, Life technologies) was added for 2 h before harvesting of the cells by trypsinisation. Colcemid arrests cells at metaphase by inhibiting spindle formation, thereby increasing the number of metaphase spreads available for analysis in each sample. After 20 min of hypotonic treatment in 0.075% potassium chloride solution (Life technologies), which facilitates better chromosome spreading, cells were fixed in 7 ml Carnoy's fixative (75% methanol, 25% glacial acetic acid). Cells were collected by centrifugation (225 x g for 5 min), the supernatant discarded and the cell pellet re-suspended in 7 ml Carnoy's fixative. This washing step was repeated four times before re-suspension of the pellet in 0.5-1 ml Carnoy's fixative solution. The suspension was then dropped onto glass slides using a pasteur pipette and air-dried. Slides were stained with KaryoMAX® Giemsa stain (Life technologies) according to the manufacturer's instructions, air-dried and mounted with

DPX mounting medium. Chromosome spreads were examined under oil using an Olympus BX60 microscope (x100 objective) and chromosomal abnormalities were counted. At least 30 well-spread metaphases were analysed per cell line and treatment condition.

2.14.1 Calculation of mitotic index

The mitotic index (MI) for each cell line and condition was scored from the prepared metaphase spread slides as the number of mitotic cells (prophase and metaphase) per 1,000 cells (including interphase nuclei) and expressed as percentage of mitotic cells. The nuclei of at least 1,000 cells were assessed and grouped as prophase (P), metaphase (M) or interphase (I). The MI was then calculated as

MI = (number of P+M)/total number of nuclei counted (I+P+M) x 100

2.15 Human tumour xenograft studies

All animal procedures were performed under a project license issued by the UK Home Office after local ethical committee review and in accordance with the U.K. legal requirements under the Animals (Scientific Procedures) Act of 1986.

2.15.1 Xenograft implantation

To study the *in vivo* anti-tumour activity of combined pharmacological inhibition of ATR and PARP, human NSCLC xenograft models were established.

Six- to eight-week old female Balb/c nude mice were purchased from Charles River Laboratories and housed in individually ventilated cages with food and water provided *ad libitum*. For the implantation of xenografts, NSCLC cells (Calu-6 or H1975) of approximately 70% confluence were washed with PBS and trypsinised. The resulting cell suspension was diluted in pre-warmed medium and centrifuged (5 min at 225 x g). After re-suspension in pre-warmed serum- and antibiotic free cell culture medium, cell concentrations were measured using the Countess® automated cell counter and the appropriate dilution was calculated for the viable cell fraction. Cells were centrifuged again and re-suspended in culture medium (serum- and antibiotic free) and 50% Matrigel™ (BD Biosciences, #3129934) at a concentration of 5x 10^7 cells/ml. Cells were transported and stored on ice until injection.

Mice were anesthetised with isoflurane in air/oxygen. 5x10^6 human Calu-6 or H1975 cells (0.1ml of the 5x 10^7 cells/ml cell suspension per mouse) were implanted subcutaneously (s.c.) into the back of the anesthetised mice. Tumour size was measured three times per week in three dimensions (length, width and height) using a caliper. Volumes were calculated from the measurements according to the formula:

$V\ (mm^3) = ½ \times [length\ (mm) \times width\ (mm) \times height\ (mm)]$.

2.15.2 Formulation of the drugs and treatments

The ATR inhibitor AZD6738 was formulated in 2.5% DMSO/40% propylene glycol in sterile distilled water. The powder was first dissolved in 2.5% volume of DMSO and mixed thoroughly by vortexing. A solution of 40% volume of propylene glycol and 57.5% volume of sterile dH_2O was added slowly while vortexing, resulting in a clear solution.

The PARP inhibitor AZD2281 (olaparib) was dissolved in 2.5% DMSO/10% (2-Hydroxypropyl)-β-cyclodextrin in sterile dH_2O. The powder was first dissolved in 2.5% volume of DMSO and mixed thoroughly by vortexing. Pre-warmed (37°C) 10% (2-Hydroxypropyl)-β-cyclodextrin solution (see Table 2.1) was added drop-wise while vortexing to ensure that the drug dissolved properly without precipitation. The AZD2281 solution was prepared freshly every day to avoid precipitation of the drug, which generally occurred within a day of formulation, particularly when the solution was stored at 4°C.

Mice were randomised into treatment cohorts when tumours reached a size of approximately 100 mm^3 (5-8 mice for efficacy and 3-4 (Calu-6) mice for pharmacodynamics (PD) studies). AZD2281 and AZD6738 were dosed at 50 mg/kg, administered via oral gavage, once daily. For the combination studies, AZD6738 was administered first followed by AZD2281 two hours later. Control animals received both vehicles (2 h apart). Tumour volumes, body weight and clinical signs of adverse effects were monitored three times per week to assess efficacy and tolerability of the drugs.

Mice were culled by schedule 1 when tumours reached a size of 400 mm^3 or at 42 days after the first treatment. For PD studies, tumours were collected two hours after administration of the last dose of treatment.

Tumour volumes are expressed as means ± SEM (n=5 per group for H1975, n=8 per group for Calu-6 xenografts). Statistical comparison of tumour growth inhibition between the treatment groups was performed by univariate analysis of variance (ANOVA). Differences were considered statistically significant for $p < 0.05$.

Oral gavage was performed by Dr. Yanyan Jiang. The remaining procedures including drug formulation, tumour cell implantation, tumour volume measurements, monitoring of the animals, schedule 1 and tumour collection/processing I carried out myself.

2.16 Immunohistochemistry

2.16.1 Preparation of cell pellet microarrays for immunohistochemistry

Immunohistochemistry is a microscope-based technique that is widely used to study the differential expression, distribution and localisation of certain proteins of interest in different parts of a biological tissue. This assay utilises the specific binding of antibodies to the target antigen in a tissue section. The tissue-bound primary antibody is generally detected using an enzyme-conjugated[22] secondary antibody. Following addition of a substrate and chromogen, the enzyme catalyses the generation of a coloured deposit at the sites of antibody-antigen binding, which can then be visualised under the microscope.

To first validate the specificity of the ATM antibody used in our studies and the suitability of the antibody for use on paraffin embedded tissue, a cell line tissue microarray was generated using cell pellets from cell lines that had been cultured *in vitro*. Cell lines were harvested by trypsinisation as described above (see section 2.2.1) and centrifuged in 15 ml Falcon tubes for 5 min at 225 x g. The supernatant was discarded and cells were fixed in 10% neutral buffered formalin overnight at 4°C. Following another centrifugation step (5 min at 225 x g), the formaldehyde solution was discarded and 70% chilled ethanol (4°C) was added to the tubes. The cell pellets

22. Secondary antibodies are usually conjugated to horseradish peroxidase (HRP) or alkaline phosphatase (AP).

were then stored at 4°C until paraffin embedding. The embedding in paraffin and the preparation of microarrays were carried out by Rekha Wadekar. For the staining procedure, 5 μm thick sections were cut from the TMA.

2.16.2 Immunohistochemical staining for total ATM in human cancer specimen

Immunohistochemical analysis of ATM protein expression was carried out on a lung carcinoma and normal tissue array (#BC041115a) purchased from US Biomax,Inc. (Rockville, USA) and 5 μm sections prepared from paraffin-embedded lung cancer specimens derived from ProteoGenex, Inc. (Culver City, USA) and the Oxford Radcliffe Biobank (Oxford, UK). Tissue microarrays containing quadruple cores from 180 colorectal cancer specimen derived from the COIN clinical trial (Maughan *et al*, 2011) were kindly provided by Professor Tim Maughan (University of Oxford, UK) and Dr. Richard Adams (Cardiff University, Institute of Cancer & Genetics, Cardiff, UK).

For the staining procedure, the EnVision+ detection system (#K4065; Dako Denmark A/S, Glostrup, Denmark) was used according to the manufacturer's instructions with a few modifications. In short, 5 μm thick tissue sections were deparaffinised in xylene and cleared in a graded ethanol series. Antigen retrieval was performed in Tris-EDTA buffer, pH 9 (see Table 2.1) in a decloaker (BIOCARE MEDICAL, Concord, USA) for 2 min at 125°C. The sections were allowed to cool down in the antigen retrieval buffer for 30 min before being washed twice in dH_2O (5 min). Endogenous peroxidase activity was quenched through 20 min incubation in 3% H_2O_2 in PBS, followed by 2x 5 min washing in PBS. Non-specific antibody binding was blocked through incubation

in protein blocking solution (Abcam #ab64226) for 30 min at RT. Following 5 min washing in PBS, primary antibody specific for ATM (clone Y170; #04-200; Upstate Millipore) diluted 1:500 in antibody diluent solution (Abcam #ab64211) was incubated with the sections overnight at 4°C. Sections were then washed three times in PBS and incubated in Polymer/HRP solution for 30 min at RT (provided in EnVision+ kit). Following an additional three washes in PBS (5-10 min) and one in tap water, the chromogen reaction was carried out with diaminobenzidine for approximately 2 min. Counterstaining was done with Harris hematoxylin. Stained tissues were dehydrated through ascending grades of ethanol (50% to 100%) and incubated in xylene (2x 3 min) before mounting with DPX mounting medium. Slides were then left to harden overnight at RT. Stained slides were digitised using an Aperio ScanScope CS digital slide scanner and analysed utilising the ScanScope software (Aperio, Vista, USA).

The intensity of staining was graded on a scale of 0–3 (0 = negative, 1 = weak staining, 2 = moderate staining, and 3 = strong staining). The staining intensity in the tumour stroma was used as the basis for moderate staining in each case.

2.16.3 Immunohistochemistry for pharmacodynamics (PD) studies

Tumours were collected and fixed in 4% PFA in PBS overnight. The tumour tissue was then transferred to 70% ethanol and stored at 4°C until embedding in paraffin. The embedding was performed at the Sir William Dunn School of Pathology (Oxford, UK). 5 μm thick sections were cut and processed for immunohistochemistry as described above (see section 2.16.2) with modifications to the antigen retrieval conditions used and primary antibody incubation times and conditions. For details on the primary antibodies used, dilutions, incubation times and antigen retrieval

conditions see Table 2.4. Stained slides were digitised using an Aperio ScanScope CS digital slide scanner and analysed utilising the ScanScope software.

For the quantification of tumour cell numbers staining positive for pan-nuclear γH2AX, pHH3 or cyclin A, five random fields of view per tumour were selected under low power magnification (10x objective). Each field contained at least 1,000 tumour cells, necrotic tumour areas were excluded and n= 3–4 tumours analysed per group. Scoring was carried out under a high power magnification (200 or 400x). The number of cells staining positive for the respective marker were counted as well as the total number of tumour cells in each field. Data is expressed as the mean percentage of positive cells relative to the total number of tumour cells ± SEM.

Table 2.4: Antibodies used for immunohistochemistry

Specification	**Antigen retrieval[23]**	**Dilution/ incubation**	**Manufacturer and *catalogue number***
total ATM	2 min 125°C	1:500 ON[24] 4°C	Upstate Millipore ***#04-200***
cleaved caspase-3	2 min 125°C	1:600 2 h at RT[25]	Cell Signaling Technology ***#9661***
Cyclin A	2 min 125°C	1:1,000 1 h at RT	Abcam ***#ab16726***
phospho-H2AX S139	2 min 110°C	1:2,000 ON 4°C	Upstate-Millipore ***#05-636***
Phospho-histone H3 (S10)	2 min 125°C	1:5,000 1 h at RT	Upstate-Millipore ***#06-570***

23. Antigen retrieval for total ATM staining on human tissues was performed in Tris/EDTA pH 9.0 buffer. Antigen retrieval for IHC staining on xenograft tissues (all other antibodies) was carried out in citrate buffer pH 6.0 (see Table 2.1).
24. ON = overnight
25. RT = room temperature

2.17 Data analysis and statistics

All values are expressed as the mean ± SEM of at least three independent experiments unless otherwise stated. All statistical analyses were performed using the SPSS 20.0 software package (SPSS Inc.). For data comparison between two groups (inhibitor treated vs. vehicle control treated or combination treatment vs. single-agent treatments) two-sided Student's t-test was used.

Radiation dose responses were compared by univariate analysis of variance (ANOVA) to detect statistically significant differences between drug+IR and IR-only treated controls. Unless otherwise stated, no correction for multiple testing was made and differences were considered significant for values of $p<0.01$.

CHAPTER 3

3 Functional consequences of ATM mutations in non-small cell lung cancer (NSCLC)

3.1 Distribution and types of somatic ATM mutations in NSCLC

ATM is a key regulator of the cellular response to genotoxic stress, particularly DNA double strand breaks, and is frequently mutated in a broad range of human cancers, including NSCLC (Cancer Genome Atlas Research Network, 2014, 2012b, 2012a, 2012c; Landau & Wu, 2013; Beà *et al*, 2013). Several studies have implicated ATM as a potential tumour suppressor protein. This notion is partly based on the cancer-predisposition observed in Ataxia-telangiectasia (A-T) patients and the observation that ATM knockout mice develop thymic lymphomas with a high frequency (Barlow *et al*, 1996). Furthermore, several known tumour suppressor proteins are downstream targets of ATM, in particular BRCA1 or p53 - one of the most frequently mutated tumour suppressor proteins in human cancers (Matsuoka *et al*, 2007; Shiloh, 2003). Therefore it seems likely, that at least a proportion of the somatic ATM mutations found in cancer result in an impairment of ATM function. But, to our knowledge, no experimental studies on the functional and phenotypic consequences of such mutations in NSCLC have been carried out to date.

Amongst the ATM mutations identified in NSCLC are several frame-shift deletions, splice site mutations and mutations resulting in a truncation of the protein due to introduction of a premature stop codon (nonsense mutations; Figure 3.1). When homozygous or occurring coincidentally with heterozygous loss of the ATM gene

locus, these mutations are likely to affect ATM protein expression and function (Mitui *et al*, 2009). However, a substantial proportion of the cancer-associated ATM mutations reported to date are missense variants, which occur scattered across the entire length of the ATM protein with no apparent hotspots (Figure 3.1). Distinguishing deleterious missense mutations from benign nonsynonymous polymorphisms or passenger mutations is challenging, if not impossible, without functional studies (Gnad *et al*, 2013).

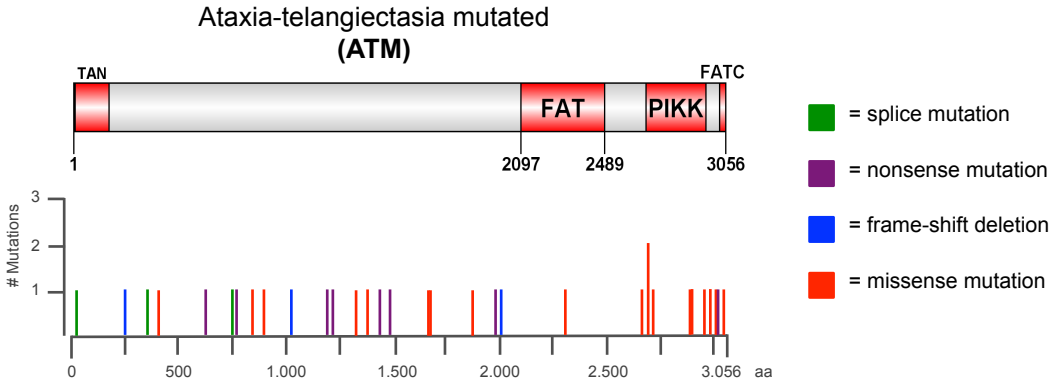

Figure 3.1: Distribution and types of ATM mutations in NSCLC.

Schematic representation of the ATM protein with the positions of ATM mutations reported in NSCLC highlighted below. Mutations identified in two representative studies are shown (Cancer Genome Atlas Research Network, 2012b, 2014). The scale represents the amino acid positions and lines indicate the positions of the reported splice site, frame-shift, missense or nonsense mutations (see legend for colour coding). The length of the lines specifies the number of samples in which the respective mutation occurred (see scale on the left). FAT (FRAP-ATM-TRRAP domain), FATC (FAT C-terminal domain), PIKK (phosphatidylinositol 3-kinase-related kinase domain), TAN (Tel1/ATM N-terminal motif).

The studies described in this chapter aimed to elucidate the functional consequences of ATM missense mutations in NSCLC and to develop a method for the identification of patient subsets with tumoral loss of ATM function in a clinical setting.

3.2 Phenotypic effects of ATM deficiency

3.2.1 Biomarkers of ATM kinase activity

Numerous studies in cells derived from Ataxia-telangiectasia patients have focussed on the characterisation of cellular defects caused by ATM deficiency. This has led to the discovery of several phenotypes and biomarkers associated with functional impairment of ATM (Lavin, 2008). In order to analyse the functional consequences of ATM mutations in NSCLC, we first aimed to establish experimental tools and assays that would allow us to validate some of the reported biomarkers and to assess the phenotypic effects of ATM loss of function.

For this purpose, isogenic pairs of stable ATM knockdown (shATM) and corresponding shGFP control cell lines were generated, derived from p53 wild-type (COR-L105) and p53-mutant (H2087, H1299 and H1975) cell lines (Figure 3.2). Stable ATM knockdown was achieved through constitutive expression of short hairpin RNA directed against ATM, which results in cleavage of the ATM mRNA through RNA interference and thus downregulation of ATM protein levels. A short hairpin RNA construct directed against GFP, a gene not present in human cells, served as a non-targeting control.

Assessment of ATM protein expression by western blot analysis demonstrated a substantial reduction in the levels of total ATM in all cell lines transfected with the shATM construct (Figure 3.2). Widely used biomarkers to evaluate functionality of the ATM signalling pathway include ATM autophosphorylation at serine 1981, which has been shown to be a hallmark of activated human ATM (Shiloh & Ziv, 2013; Bakkenist & Kastan, 2003), as well as IR-induced phosphorylation of the ATM downstream targets KAP1, SMC1 and CHK2 (Rainey *et al*, 2008; Olcina *et al*, 2013;

Barone *et al*, 2009; Jacquemin *et al*, 2012; Verhagen *et al*, 2012; Guo *et al*, 2014). Therefore, to assess ATM kinase activity, we determined ATM autophosphorylation levels as well as phosphorylation of KAP1, SMC1 and CHK2 in cells exposed to 10 Gy γ-radiation (henceforth referred to as ionising radiation; IR) by western blot analysis.

All control cell lines (shGFP) showed a marked increase in the phosphorylation of ATM itself, as well as its downstream targets, in response to IR (Figure 3.2). As expected, no or very low levels of ATM S1981 were detected following ATM knockdown. This was associated with a marked reduction in the phosphorylation levels of KAP1 and SMC1, supporting the utility of KAP1 (S824) and SMC1 (S966) levels as readout for ATM kinase activity. Phosphorylation of CHK2 (Thr68), on the other hand, was not consistently reduced. In fact, in H2087 and H1299 cells IR-induced pCHK2 levels were rather increased following ATM knockdown (Figure 3.2).

In contrast to the response observed following shRNA-mediated ATM depletion, we found that exposure of H1299 cells to the selective ATM inhibitor KU60019 reduced the radiation-induced phosphorylation of CHK2 in a dose-dependent manner (Figure 3.3). It should be noted that many of the studies which used CHK2 phosphorylation as readout for ATM activity assessed the effects of transient siRNA mediated ATM knockdown or pharmacological ATM inhibition (Rainey et al, 2008; Hickson et al, 2004; Golding et al, 2012; Helt et al, 2005).

It is therefore possible that the observed differential CHK2 phosphorylation response between ATM knockdown cells and cells treated with an ATM inhibitor could be due to a compensatory up-regulation of an alternative DDR signalling pathway after prolonged impairment of ATM function through stable shRNA knockdown. DNA-

PKcs, for example, has been shown to contribute to CHK2 activation in response to DNA damage (Shang et al, 2010; Zannini et al, 2014) and could be responsible for the observed sustained IR-induced activation of CHK2 following ATM knockdown.

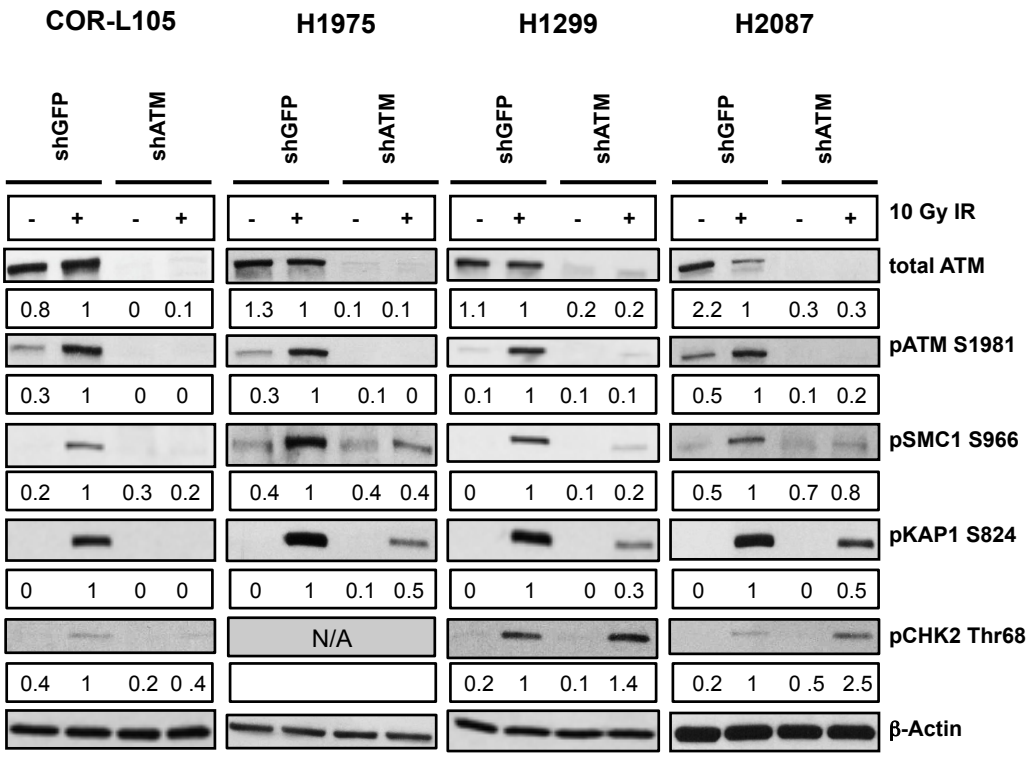

Figure 3.2: ATM knockdown leads to a reduction in the IR-induced phosphorylation of KAP1 and SMC1.

COR-L105, H1975, H1299 and H2087 cells, stably transfected with ATM short hairpin RNA (shATM) or the respective control plasmid (shGFP), were mock-irradiated (control) or irradiated with 10 Gy followed by preparation of protein lysates 60 min after irradiation. β-Actin was used to ensure equal loading. For H1975, pCHK2 levels were not analysed = N/A. The results from densitometric quantification of the protein bands are shown underneath each blot. For each isogenic pair of cell lines, the numbers reflect the relative intensity of the respective band, normalised to the shGFP sample derived from irradiation treated cells, and expressed as the ratio of each band relative to the loading control of the respective lane.

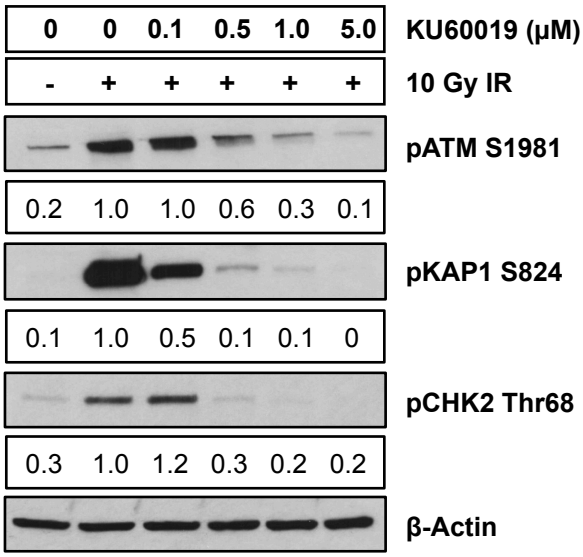

Figure 3.3: Pharmacological ATM inhibition attenuates ATM autophosphorylation and phosphorylation of the ATM downstream targets KAP1 and CHK2.

H1299 cells were exposed to 10 Gy IR, or a combination of 10 Gy and increasing doses of the selective ATM inhibitor KU60019, followed by preparation of protein lysates 60 min after irradiation. ATM autophosphorylation and phosphorylation of the ATM downstream targets KAP1 and CHK2 were included to assess activity of the ATM signalling pathway. β-Actin served as loading control. The results from densitometric quantification of the protein bands are shown underneath each blot. The numbers reflect the relative amounts of the respective protein, normalised to the sample derived from cells treated with irradiation only, and expressed as the ratio of each band relative to the loading control of the respective lane.

3.2.2 Impact of ATM depletion on radiosensitivity and DNA damage induced cell cycle checkpoint activation

One of the most prominent phenotypes of ATM-deficient cells described to date is a strong sensitivity to ionising radiation (Taylor *et al*, 1975). In order to assess the effect of ATM protein expression levels on radiation sensitivity, we compared the clonogenic survival capacity of ATM knockdown cell lines and the corresponding controls following exposure of the cells to a dose-range of IR (Figure 3.4). We found that ATM knockdown markedly increased the cytotoxic effects of IR in all cell lines, consistent with an important role of ATM in the cellular response to IR.

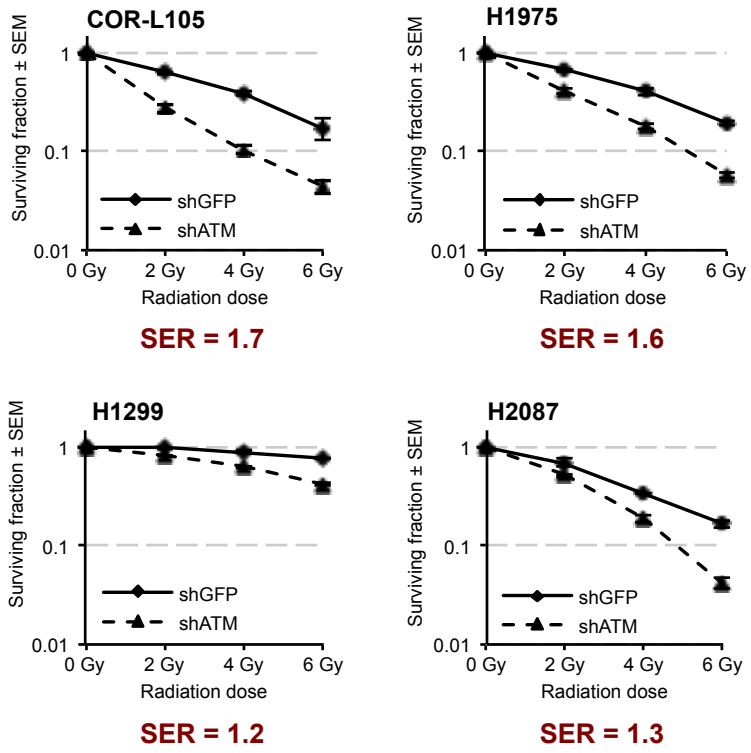

Figure 3.4: Down-regulation of ATM increases the sensitivity of NSCLC cells to ionising radiation.

Clonogenic survival of stable ATM knockdown cell lines (shATM), or the respective shGFP controls, following exposure to the indicated doses of IR. Each point represents the mean of at least three independent experiments, each performed in triplicate. Error bars = SEM.
SER indicates the sensitisation enhancement ratio at 2 Gy.

Furthermore, loss of ATM function has been shown to cause defects in cell cycle checkpoint activation in response to DNA damage. In particular, these checkpoint defects include an impairment to arrest at the G1/S-boundary following DNA DSB induction, as well as an inability to slow on-going DNA replication in cells exposed to IR, a phenomenon referred to as radioresistant DNA synthesis (Kastan *et al*, 1992; Houldsworth & Lavin, 1980; Falck *et al*, 2001). The first is also a characteristic of p53-deficient cells (Kastan *et al*, 1991).

To assess the impact of ATM depletion on the enforcement of DNA damage-induced cell cycle checkpoints, H1299 and COR-L105 shGFP and shATM cells were irradiated and harvested 24 or 48 h post-irradiation for analysis of cell cycle distribution by flow cytometry. Following ATM knockdown, COR-L105 cells showed a moderate increase in the G2 cell population within 24 h post-irradiation, indicating attenuation of the IR-induced G1 cell cycle arrest (Figure 3.5a, b). However, the changes in cell cycle distribution were overall small in this cell line, which could be related to retained p53-activity.

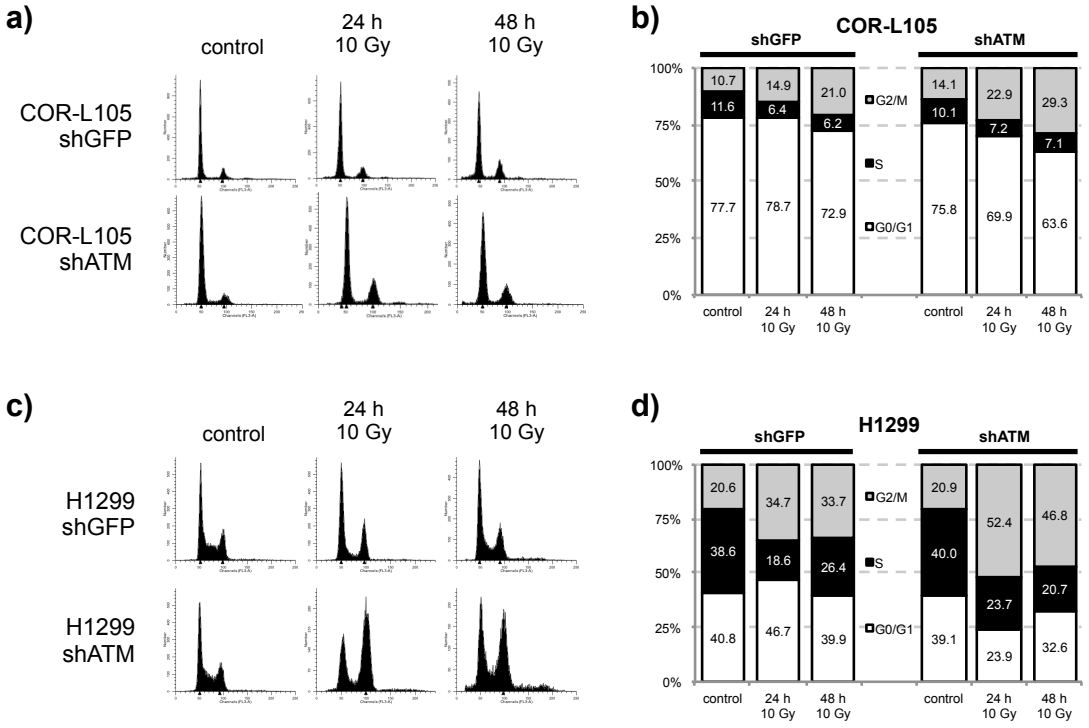

Figure 3.5: ATM knockdown causes defects in the enforcement of the G1/S- and intra-S-phase cell cycle checkpoints following DNA damage induction.

a) and **b)** COR-L105 and **c)** and **d)** H1299 shGFP and shATM cells were mock-irradiated (control) or irradiated with 10 Gy IR. 24 h and 48 h after irradiation, cells were harvested, fixed and stained with propidium iodide to assess cell cycle distribution through DNA content analysis. Representative images of three independent experiments are shown in a) and c). The diagrams in b) and d) summarise the average G0/G1, S and G2/M cell population values obtained from the three experiments.

Cells deficient in p53 (H1299), on the other hand, showed more prominent changes in cell cycle distribution. Within 24 h, an increase in the G2 cell population was evident in IR-treated shGFP control cells, consistent with a loss of the G1 cell cycle checkpoint due to impairment of p53 function (Figure 3.5c, d). This phenotype was considerably exacerbated following ATM depletion. Within 24 h after irradiation, more than 50% of shATM cells had accumulated in the G2-phase of the cell cycle. As the shGFP and shATM cell lines are both defective in p53 - and hence the G1 cell cycle checkpoint - this accelerated accumulation of cells in G2 suggests an attenuation of the intra-S-phase checkpoint following DNA damage induction.

We obtained similar results when combining pharmacological ATM inhibition with radiation treatment. Exposure of p53-proficient COR-L105 cells to the ATM inhibitor KU55933 attenuated the IR-induced G1 cell cycle checkpoint and caused an increase in the G2 cell population within 24 h (Figure 3.6a). This phenotype was also markedly exacerbated in p53-deficient H1299 cells, providing further evidence for intra-S-phase checkpoint defects following impairment of ATM function (Figure 3.6b).

Taken together these results demonstrate that phosphorylation levels of ATM (S1981), KAP1 (S824) and SMC1 (S966) are useful biomarkers of ATM kinase activity in response to IR. Supportive of previous reports, we found that impairment of ATM signalling leads to an increase in the cellular sensitivity to IR and defects in cell cycle checkpoint activation following induction of DNA damage. The attenuation of the G1/S- and intra-S-phase checkpoints was, however, much more pronounced in p53-deficient cells. This may indicate that p53 can, at least to some extent, perform ATM-independent checkpoint functions.

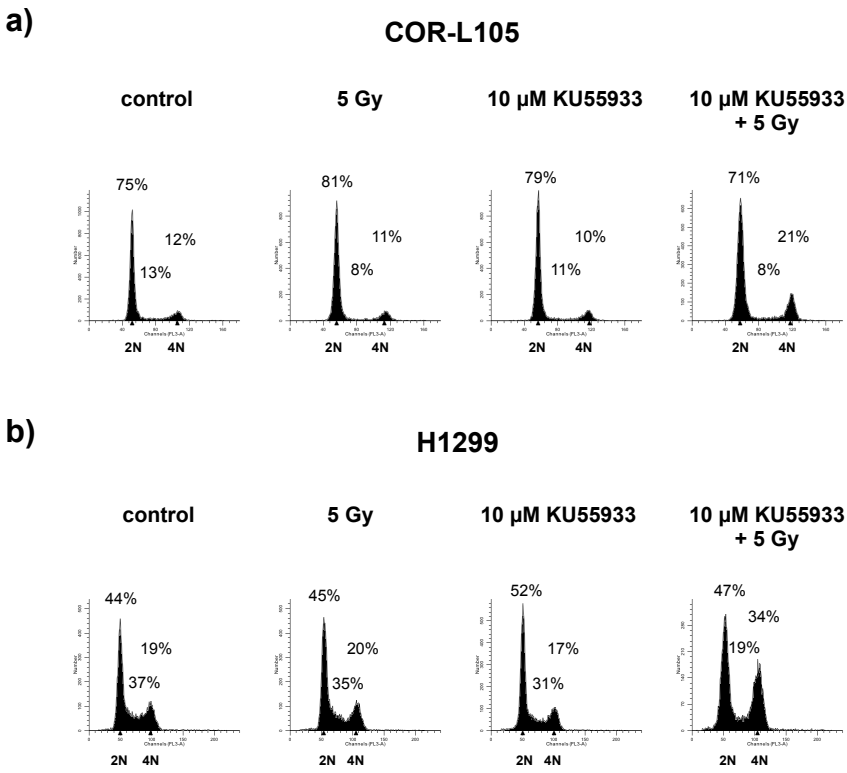

Figure 3.6: Pharmacological ATM inhibition attenuates the G1/S- and intra-S-phase DNA damage checkpoints.

a) COR-L105 and **b)** H1299 cells were exposed to the ATM inhibitor KU55933 (10 μM) and/or 5 Gy IR. 24 h after irradiation, cells were harvested, fixed and stained with propidium iodide to assess cell cycle distribution through DNA content analysis. Images of n=1 experiments are shown.

3.3 Functional consequences of ATM missense mutations in NSCLC

Next, we aimed to assess the functional consequences of somatic ATM missense substitutions in NSCLC cells, through a combination of biomarker and phenotypic studies.

Several NSCLC cell lines have been reported to carry homo- or heterozygous mutations in the ATM gene. We selected two of those cell lines, H1395 and H23, which have been reported to harbour a homozygous p.T2666A (H1395) and p.Q1919P (H23) missense substitution, respectively (Davies et al, 2005; Barretina et al, 2012). We verified the presence of the reported mutations by Sanger sequencing (Figure 3.7a) and calculated the PolyPhen scores for the missense changes (Adzhubei et al, 2010). Both mutations were predicted to affect protein function. The NSCLC cell line H2087 has been reported to carry a heterozygous p.E848Q ATM missense substitution, which we also validated by DNA sequencing. However, according to PolyPhen this mutation is predicted to be benign and our previous results had demonstrated that this cell line exhibits normal ATM kinase activity in response to IR, as well as increased radiosensitivity and intra-S-phase checkpoint defects (data not shown) following ATM knockdown. These observations suggest that the ATM missense substitution present in this cell line is a passenger mutation rather than a deleterious mutation (Stratton *et al*, 2009).

To study the functional consequences of the identified ATM missense substitutions, we determined total ATM protein levels, as well as ATM kinase activity by western blot analysis. Cells were exposed to 10 Gy IR and autophosphorylation levels of ATM as well as phosphorylation of the ATM downstream targets KAP1, SMC1, p53 and CHK2 were determined. In addition to the ATM mutated H23, H2087 and H1395 cell lines, the ATM and p53 wild-type cell line COR-L105 and the p53 null-mutant cell line H1299 were used as controls. Levels of the respective total and phospho-proteins in these cell lines served as reference level for normal ATM kinase activity.

Notably, only trace-detectable amounts of total ATM protein were evident in the H1395 and H23 cell lines (Figure 3.7b). Following exposure to IR, a robust increase in

the levels of ATM activation and phosphorylation of ATM downstream targets was evident in COR-L105 within 30 min post-irradiation. In agreement with our previous results, H1299 and H2087 cells also displayed normal kinase activity for both, ATM itself, as well as its downstream targets. However, both of these cell lines carry p53 mutations and show either no (H1299) or aberrant p53 protein levels (H2087), independent of radiation treatment.

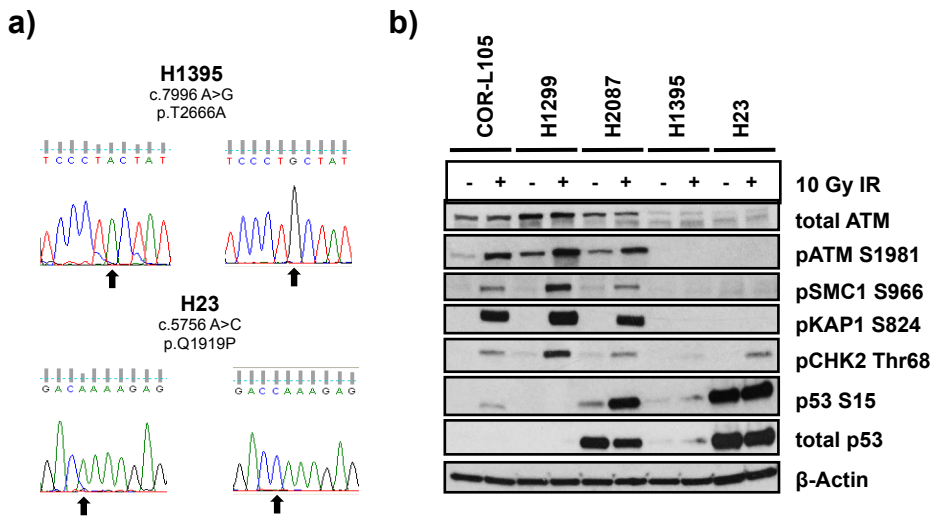

Figure 3.7: ATM missense mutations can lead to a reduction in ATM protein levels and impairment of the ATM signalling pathway in NSCLC.

a) DNA sequencing results demonstrating the presence of a homozygous c.7996 A>G (p.T2666A) and c.5756 A>C (p.Q1919P) missense mutation in the ATM gene in the H1395 and H23 cell line, respectively. Wild-type sequences derived from H1299 cells are shown on the left. Arrows indicate the positions of the respective missense change.
b) To determine activity of the ATM signalling pathway, ATM auto-phosphorylation (S1981) and phosphorylation of ATM downstream targets were monitored by western blot analysis. Cells were mock-irradiated (control) or irradiated with 10 Gy followed by preparation of protein lysates 30 minutes after IR. Representative blots of two experiments are shown. β-Actin was determined to ensure equal loading.

Consistent with the low total ATM protein levels observed in H1395 and H23 cells, the radiation-induced kinase activity of ATM was severely impaired, as seen by a loss of ATM autophosphorylation and a marked reduction in the phosphorylation of KAP1 and SMC1. As the H23 cell line also harbours a mutation in the TP53 gene (p.M246I), aberrant levels of total and phosphorylated p53 were observed in this cell line (Figure 3.7b).

Despite the lack of ATM protein expression, H23 cells exhibited CHK2 phosphorylation levels similar to those observed in ATM wild-type COR-L105 cells. H1395 cells, on the other hand, showed no CHK2 phosphorylation. This observation is consistent with our previous results from ATM knockdown cell lines and further supports the concept that CHK2 phosphorylation in response to IR might not be a reliable readout for ATM kinase activity. Phosphorylation levels of KAP1 and SMC1, on the other hand, correlated well with the levels of ATM autophosphorylation.

3.3.1 ATM-deficient cancer cells are highly sensitive to ionising radiation and exhibit cell cycle checkpoint defects.

Clonogenic survival assays further supported a functional loss of ATM in H1395 and H23 cells, as both cell lines exhibited substantial radiosensitivity. H2087 cells showed intermediate sensitivity to IR (Figure 3.8a).

In order to validate that the observed high degree of radiosensitivity in H1395 and H23 cells was due to impaired ATM function, we assessed clonogenic survival of cells treated with a combination of IR and the specific ATM inhibitor KU55933, or the DNA-PKcs inhibitor NU7441, which served as a radiosensitiser control (Zhao *et al*, 2006). We hypothesised that, if the observed radiosensitivity of H1395 and H23 cells

was due to defects in ATM signalling, treatment of cells with an ATM inhibitor would produce no additional effect on radiation-induced cytotoxicity in these cells.

Consistent with loss of ATM function, exposure of H1395 and H23 cells to the ATM inhibitor did not significantly further increase the cytotoxic effects of IR (H23 p=0.06; H1395 p=0.8), (Figure 3.8b). Normal bronchial epithelial cells (NBE1), as well as COR-L105, H1299 and H2087 cells, on the other hand, were profoundly radiosensitised by KU55933 treatment (p-values <0.001 for all four cell lines). DNA-PKcs inhibition significantly radiosensitised all cell lines (Figure 3.8b, p-values <0.001 for all cell lines).

To further evaluate potential defects in ATM function, we analysed cell cycle checkpoint activation in cells exposed to IR, using flow cytometry. We performed BrdU pulse labelling of COR-L105 ($^{ATM+/p53+}$), H1395 ($^{ATM-/p53+}$) and H2087 ($^{ATM+/p53-}$) cells to detect S-phase populations following IR treatment (Figure 3.9). In COR-L105, a reduction in the proportion of BrdU-labelled cells in early S-phase within 6 h post-irradiation was evident, indicating activation of the G1/S checkpoint, which prevents cells with damaged DNA from entering S-phase (Figure 3.9a). In contrast, H1395 and H2087 cells showed no or only a minimal decrease in BrdU-labelled cells in early S-phase after irradiation, suggesting that these cells failed to induce the G1/S cell cycle checkpoint. Over time, an accumulation of cells in G2 was evident in both cell lines (Figure 3.9b, c), consistent with the activation of a G2/M cell cycle arrest following IR. While H2087 cells displayed a significant increase in the overall S-phase population during early time-points after IR, indicating a slowdown of S-phase progression, this effect was less pronounced in H1395 cells (Figure 3.9b).

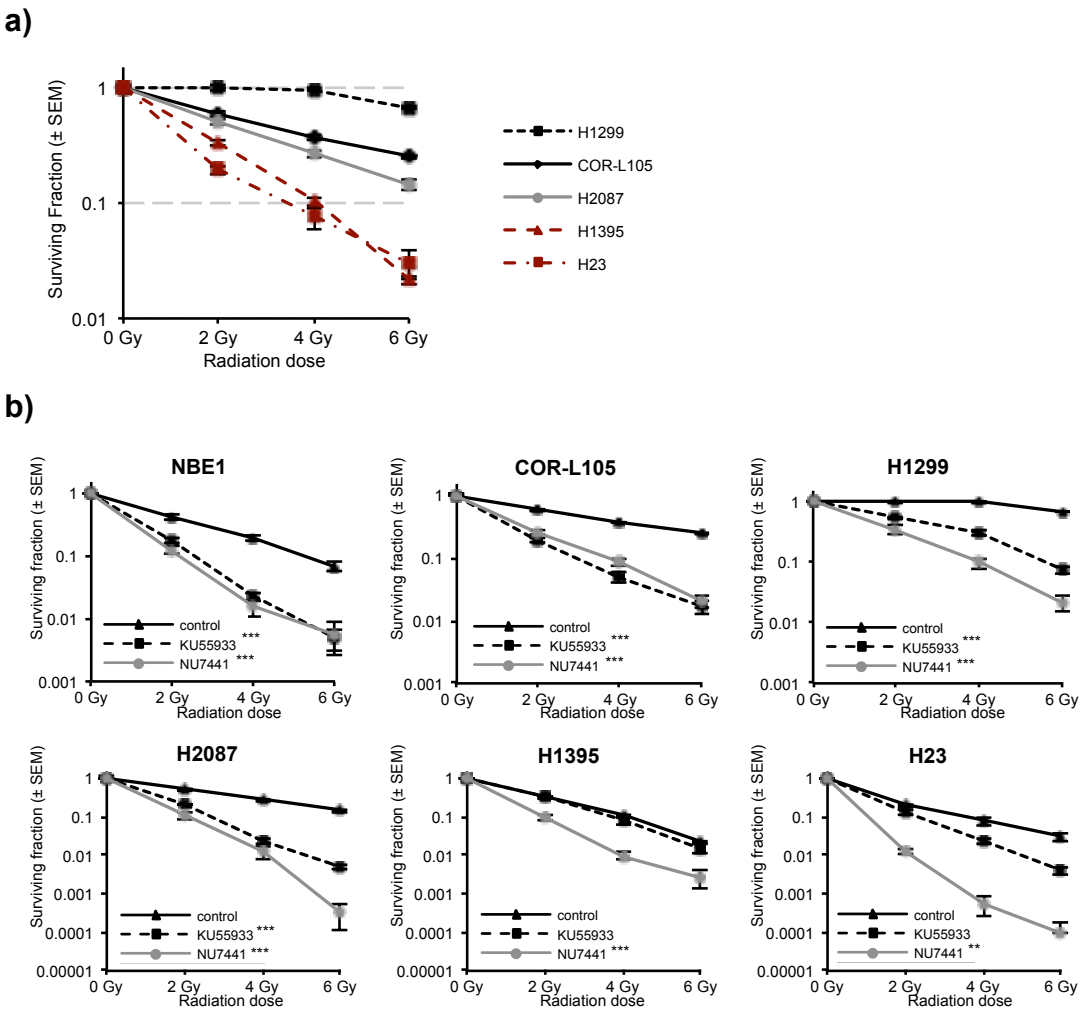

Figure 3.8: ATM deficiency confers sensitivity to ionising radiation.

a) Clonogenic survival of COR-L105, H1299, H2087, H1395 and H23 cells following exposure to the indicated doses of IR. Each point represents the mean of at least three independent experiments, each performed in triplicate ± SEM.
b) Clonogenic survival of NBE1, COR-L105, H1299, H2087, H1395 and H23 cells following exposure to IR alone, or in combination with ATM (KU55933; 10 μM) or DNA-PK (NU7441; 500 nM) inhibition. Cells were pre-treated with the inhibitors for 1 h prior to irradiation and treatment was continued for 24 h. Each point represents the mean of at least three independent experiments, each performed in triplicate. Radiation dose responses of vehicle treated controls and inhibitor treated cells were compared by univariate analysis of variance (ANOVA). Statistically significance differences between survival curves are indicated with **= p-values <0.001 and ***= p-values <0.0001.

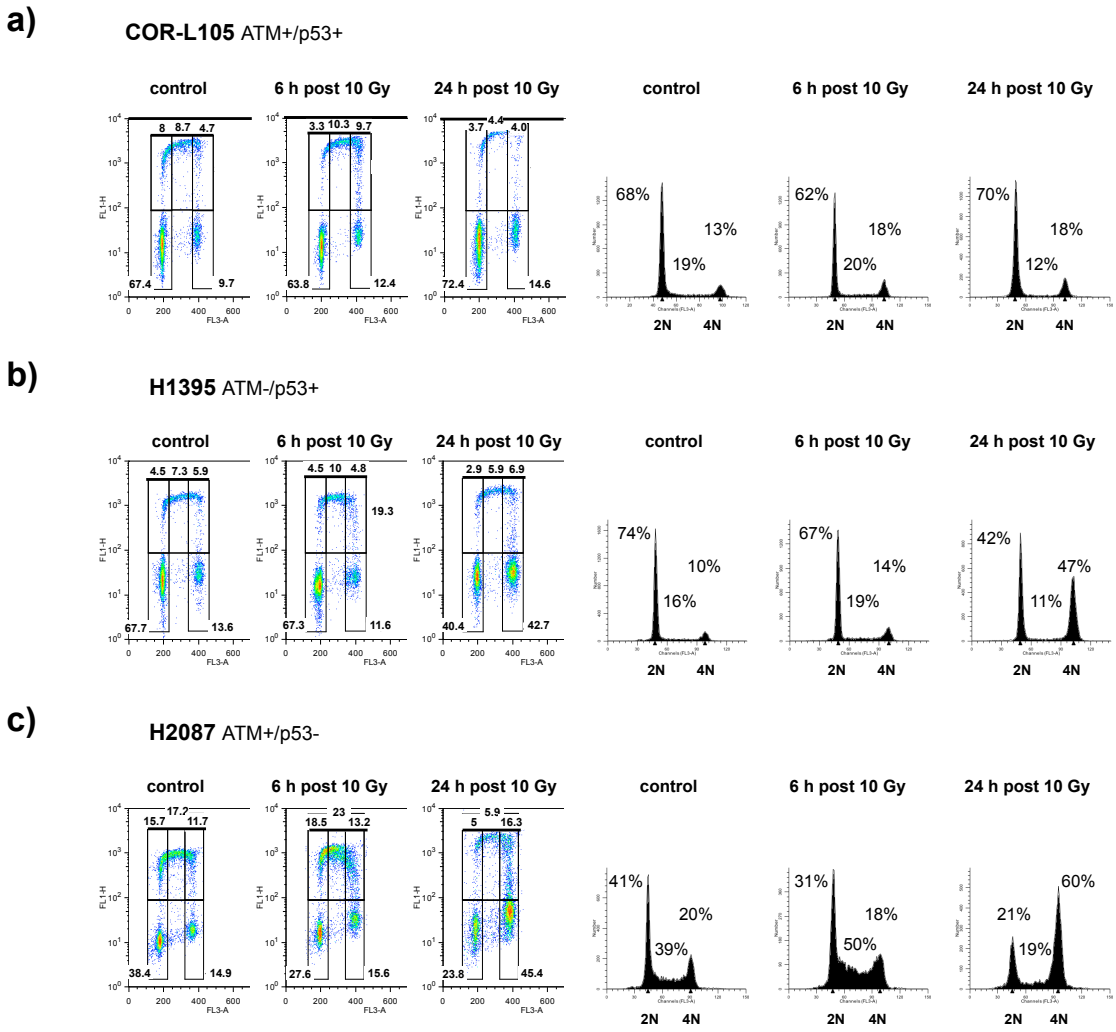

Figure 3.9: ATM deficiency leads to attenuation of the G1/S and intra-S-phase checkpoints.

Asynchronous populations of **a)** COR-L105, **b)** H1395 and **c)** H2087 cells were mock-irradiated or irradiated with 10 Gy. After irradiation, cells were incubated at 37°C for the indicated times before being pulse labelled with BrdU for 20 min. Cells were then harvested, fixed, and stained with PI and anti-BrdU antibody for FACS analysis. BrdU diagrams are representative of two, DNA content histograms (PI-staining) of at least three independent experiments. The two bottom gates in the BrdU diagrams represent unlabelled cell populations in G1- and G2/M-phase of the cell cycle, respectively. The upper gates represent (from left to right) early-S-, intra-S- and late-S- /early G2-phase cell populations.

Taken together these results demonstrate that the p.T2666A (H1395) and p.Q1919P (H23) missense substitutions in the ATM gene lead to a strong reduction in ATM protein levels and severe impairment of the ATM signalling pathway, indicating that

these are deleterious mutations. The heterozygous p.E848Q missense substitution found in H2087 cells, on the other hand, did not appear to affect ATM function.

3.4 Identification of ATM deficiency in a clinical setting

3.4.1 ATM protein expression is frequently lost or reduced in human NSCLC.

Loss of ATM function confers a high sensitivity to ionising radiation (Taylor *et al*, 1975; Barlow *et al*, 1996) and may define a subset of cancer patients that could get increased benefit from radiation therapy. However, the ATM gene extends over approximately 150 kb of genomic DNA, contains 66 exons and encodes for a 3056 amino acid protein (350kDa) (Uziel *et al*, 1996). This large size of the ATM gene renders routine DNA sequencing a challenging diagnostic tool to identify patients with ATM deficiency. Furthermore, a large proportion of the mutations reported in cancer to date are missense variants and as our results clearly show, the presence of an ATM mutation does not necessarily imply that there will be a functional impairment of ATM. Therefore, we aimed to address the question how patients with tumoral loss of ATM function could be identified in a clinical setting.

Studies on ATM missense mutations found in Ataxia-telangiectasia patients have shown that such changes can lead to a destabilisation of the protein product and thereby reduction in ATM protein expression and that loss of ATM activity is in most cases associated with reduced ATM protein levels (Sandoval *et al*, 1999; Mitui *et al*, 2009; Jacquemin *et al*, 2012; Lavin *et al*, 2004; Verhagen *et al*, 2012; Barone *et al*, 2009). Our own results provide supportive evidence for this concept, as we found that

the p.T2666A (H1395) and p.Q1919P (H23) missense substitutions in the ATM gene, which result in ATM-deficiency, lead to a loss of ATM protein expression.

To address this possibility further, we evaluated immunohistochemical (IHC) staining of ATM in human tumour samples as a potential method for the identification of patients with a loss or reduction of ATM protein expression. For the optimisation of the staining procedure we generated a cell line microarray from paraffin-embedded cell pellets derived from a panel of 35 NSCLC cell lines.

Following immunohistochemical labelling of ATM, we detected specific nuclear staining in 33 out of 35 cell lines. No staining for ATM could be observed in two cell lines (5.7%) – H23 and H1395 (Figure 3.10; Supplementary Table 1).

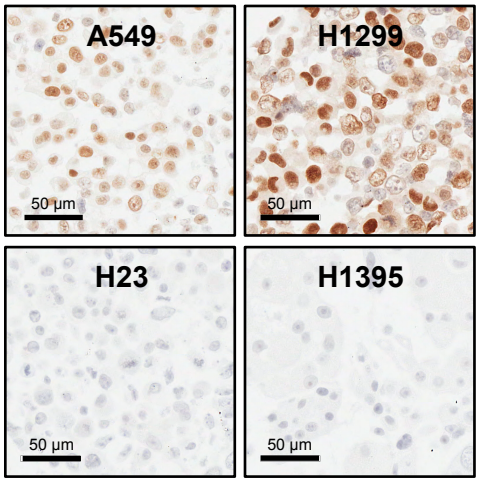

Figure 3.10: ATM protein expression in NSCLC cell lines assessed by immunohistochemistry.

A panel of 35 NSCLC cell lines was analysed for ATM protein expression by IHC. Representative images of two ATM positive (A549 and H1299) and two ATM negative (H23 and H1395) cell lines are shown. Pictures were taken at a 400x magnification. Scale bar indicates 50 μm.

This is in agreement with our previous findings from western blot analysis, which demonstrated a loss of ATM protein expression in both cases, and confirms the specificity of the antibody on paraffin-embedded material.

We then proceeded with the analysis of ATM protein expression in human NSCLC tumour specimens (n=156) by IHC. The staining intensity of tumour cells was graded relative to the intensity observed in the tumour stroma (e.g. endothelial cells or fibroblasts), which was used as the basis for moderate staining in each case (Figure 3.11a, c). The intensity of staining in tumour cells was scored independently by two observers on a scale of 0–3 (0= negative, 1= weaker than stroma, 2= same as stroma or moderate, and 3= stronger staining than in stroma). Specimens, in which no or only very weak staining was observed in the tumour stroma were excluded from analysis (N/A; n=19). Normal lung tissue was stained to assess ATM protein expression in the lung parenchyma under physiological conditions (n= 8; Figure 3.11b). Lymphocytes and macrophages show higher ATM staining than stromal or lung parenchyma cells (e.g. pneumocytes) and were therefore, where present, considered a measure for high staining intensity (Figure 3.11).

We found that in 13/137 (9.5%) cases, ATM protein expression in tumour cells was not detectable. In 76.6% of cases, ATM protein levels were similar to those seen in the stroma (moderate). In 13 cases (9.5%), tumour cells exhibited weaker staining than stromal cells and in 6 cases (4.4%), higher ATM protein levels were observed (Figure 3.11c; Table 3.1).

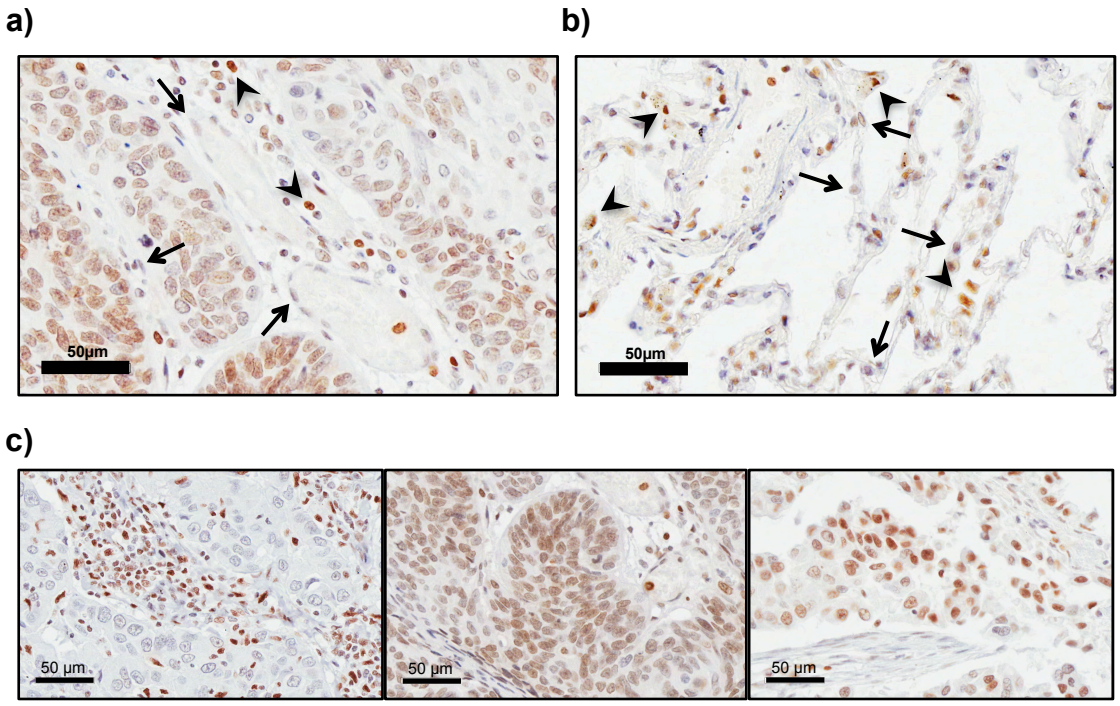

Figure 3.11: Immunohistochemical analysis of ATM protein expression in NSCLC samples and normal lung tissue.

a) Representative image of an adenocarcinoma specimen with moderate ATM protein expression, in which the nuclear staining for ATM in tumour cells is similar to that observed in stromal cells (arrows). Lymphocytes (arrowheads) were used as basis for strong staining intensity.
b) Representative image of ATM IHC staining in normal lung tissue. Note the higher staining intensity in resident macrophages (arrowheads), compared to pneumocytes (arrows).
c) Representative images of negative (left), moderate (middle) and strong (right) staining for ATM in NSCLC tumour samples.
Pictures were taken at a 400x magnification. Scale bar = 50 μm.

Table 3.1: ATM protein expression is frequently lost or reduced in NSCLC.

Table summarising the results of ATM protein expression analysis in 156 human NSCLC samples by immunohistochemistry. N/A= excluded from analysis due to poor staining or tissue quality.

Histological subtype	# of samples	N/A		negative (0)	weak (1)	moderate (2)	strong (3)
Squamous carcinoma	**71**	3	n	6	7	54	1
		4.2	%	8.8	10.3	79.4	1.5
Adenosquamous carcinoma	**2**	0	n	0	0	1	1
		0	%	0	0	50	50
Adenocarcinoma	**67**	11	n	7	5	42	2
		16.4	%	12.5	8.9	75	3.6
Bronchioalveolar carcinoma	**5**	3	n	0	0	2	0
		60	%	0	0	100	0
Carcinoid	**7**	0	n	0	0	6	1
		0	%	0	0	85.7	14.3
Large cell carcinoma	**4**	2	n	0	1	0	1
		50	%	0	50	0	50
Total (n) (excluding N/A)		137		13	13	105	6
Total (%)		100		9.5	9.5	76.6	4.4

We further evaluated the clinical utility of this method for identifying cancer patients with tumoral loss of ATM function, by analysing ATM protein expression in 168 human colorectal cancer specimen. 162 of the samples had been classified as adenocarcinoma, while for 6 of the samples no histological subtype had been specified. ATM immunohistochemistry was performed on tissue microarrays containing quadruple cores of each sample. 14 of the 168 samples were excluded from analysis due to poor stromal staining or insufficient tumour material.

Scoring of ATM staining intensity was performed as for the lung cancer specimen. In 77.9% (120/154) of cases, the ATM expression observed in tumour cells was similar to that observed in the stroma (moderate). We found that in 16 cases, tumour cells exhibited weaker staining than stromal cells (10.4%) and in 6/156 (3.9%) specimens, no ATM protein expression could be detected in tumour cells. In 7.8% (12/154) of cases, tumour cells showed higher ATM staining than stromal cells indicating increased ATM protein expression in these tumours. Figure 3.12 shows representative images for negative, moderate and strong staining.

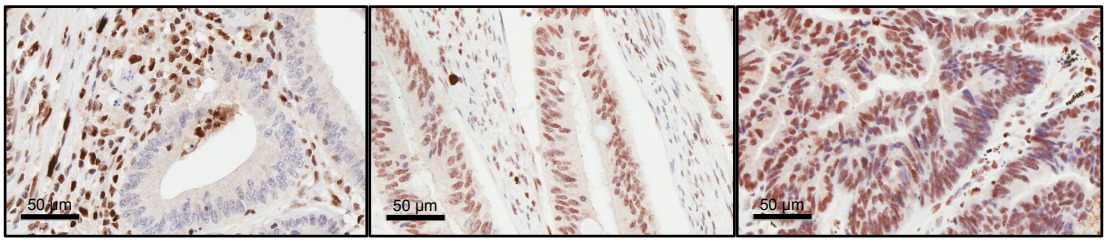

Figure 3.12: Identification of tumoral loss of ATM protein expression in colorectal cancer.

Human colorectal carcinoma specimen were analysed for ATM protein expression by IHC. Representative images of negative (left), moderate (middle) and strong (right) ATM staining are shown. Pictures were taken at a 400x magnification. Bars indicate 50 μm.

In conclusion, our results indicate that analysis of ATM protein expression by IHC, for example in biopsy samples, could be a valuable clinical tool to identify cancer patients with tumoral loss of ATM function. This could help guide the process of deciding on optimal cancer treatment, especially in those cases where radiotherapy is an option. Unfortunately, no data on pre-treatment of patients, treatment responses or survival outcome is available for the samples used in this study. Therefore no prediction for a

potential correlation between ATM protein expression levels and response to chemo- and/or radiotherapy, or overall survival, can be made at this point.

3.5 Role of ATM in the cellular response to chemotherapeutic drugs

In addition to the increased radiosensitivity conferred by ATM deficiency, defects in ATM function could render cells particularly sensitive to certain chemotherapeutic drugs or small molecule inhibitors. For instance, it has been proposed that ATM inhibition enhances the cytotoxicity of the topoisomerase I inhibitor irinotecan (Batey *et al*, 2013). Furthermore, it has been suggested that cells deficient in both ATM and p53 are particularly sensitive to the DNA crosslinking agent cisplatin and the topoisomerase II inhibitor doxorubicin (Jiang *et al*, 2009). Additional studies have demonstrated an increased sensitivity of cells to gemcitabine or topoisomerase I (irinotecan or camptothecin) and II (etoposide or doxorubicin) inhibitors when these modalities were combined with pharmacological or genetic ATM depletion (Batey *et al*, 2013; Fedier *et al*, 2003).

To assess such a potential vulnerability of ATM-deficient cells, we analysed the sensitivity of NSCLC cell lines, stable ATM knockdown cell lines and normal bronchial epithelium control cells (NBE1), to a variety of commonly used chemotherapeutic drugs. For this purpose, cells were treated with dilution series of gemcitabine, cisplatin, etoposide and irinotecan for 3 or 5 days before assessment of cell viability by resazurin assay. Comparison of IC_{50} values showed, that there was no clear association between functional status of ATM and sensitivity of cells to any of

these drugs (Table 3.2). Furthermore, no differential response could be observed in isogenic ATM knockdown or shGFP control cell lines - neither in a p53-proficient (COR-L105; Figure 3.13a), nor in a p53-deficient background (H1299; Figure 3.13b).

For our further studies, we therefore focused on potential synthetic lethal interactions with targeted therapies, particularly small molecule inhibitors of DDR components.

Table 3.2: Sensitivity of normal bronchial epithelial control and NSCLC cell lines to gemcitabine, cisplatin, etoposide and irinotecan.

H1299, COR-L105, H2087, H1395, H23, NBE-1, COR-L105 shGFP and shATM as well as H1299 shGFP and shATM cells were treated with dilution series of the drugs for 3 days (gemcitabine and cisplatin) or 5 days (etoposide and irinotecan). Cell viability and proliferation was assessed by resazurin assay. IC_{50} values ± SEM were calculated from at least three independent experiments, each performed in triplicate.

Cell line	ATM/ p53 status	Cisplatin mean IC_{50} [μM] (-/+ SEM, range)	Gemcitabine mean IC_{50} [nM] (-/+ SEM, range)	Etoposide mean IC_{50} [μM] (-/+ SEM, range)	Irinotecan mean IC_{50} [μM] (-/+ SEM, range)
NBE1	ATM+/ p53+	8.3 (7.7-8.9)	11.6 (9.1-14.6)	6.7 (6.0-7.5)	2.3 (2.0-2.6)
COR-L105	ATM+/ p53+	3.0 (2.8-3.2)	50.8 (42.9-60.2)	9.1 (8.5-9.7)	4.4 (4.1-4.8)
H1299	ATM+/ p53-	7.5 (7.0-8.1)	27.7 (23.0-33.5)	0.6 (0.58-0.63)	0.65 (0.62-0.67)
H2087	ATM+/ p53-	3.2 (3.0-3.5)	26.9 (22.0-33.0)	1.1 (0.9-1.2)	0.5 (0.47-0.53)
H1395	ATM-/p53+	6.9 (6.5-7.2)	75.1 (64.9-87.0)	3.0 (2.6-3.6)	1.1 (1.0-1.2)
H23	ATM-/p53-	3.0 (2.8-3.2)	4.7 (4.2-5.4)	0.24 (0.23-0.25)	0.7 (0.67-0.72)
COR-L105 (shGFP)	ATM+/ p53+	5.2 (5.0-5.5)	111.2 (90.3-136.8)	10.1 (8.8-11.7)	3.1 (2.9-3.4)
COR-L105 (shATM)	ATM-/p53+	4.9 (4.5-5.2)	294.9 (218.8-397.4)	9.2 (8.8-9.7)	3.8 (3.5-4.1)
H1299 (shGFP)	ATM+/ p53-	13.5 (12.4-14.8)	55.8 (44.6-69.7)	0.71 (0.67-0.74)	0.85 (0.79-0.9)
H1299 (shATM)	ATM-/p53-	13.3 (12.1-14.7)	35.6 (28.3-44.7)	0.66 (0.63-0.68)	0.88 (0.80-0.98)

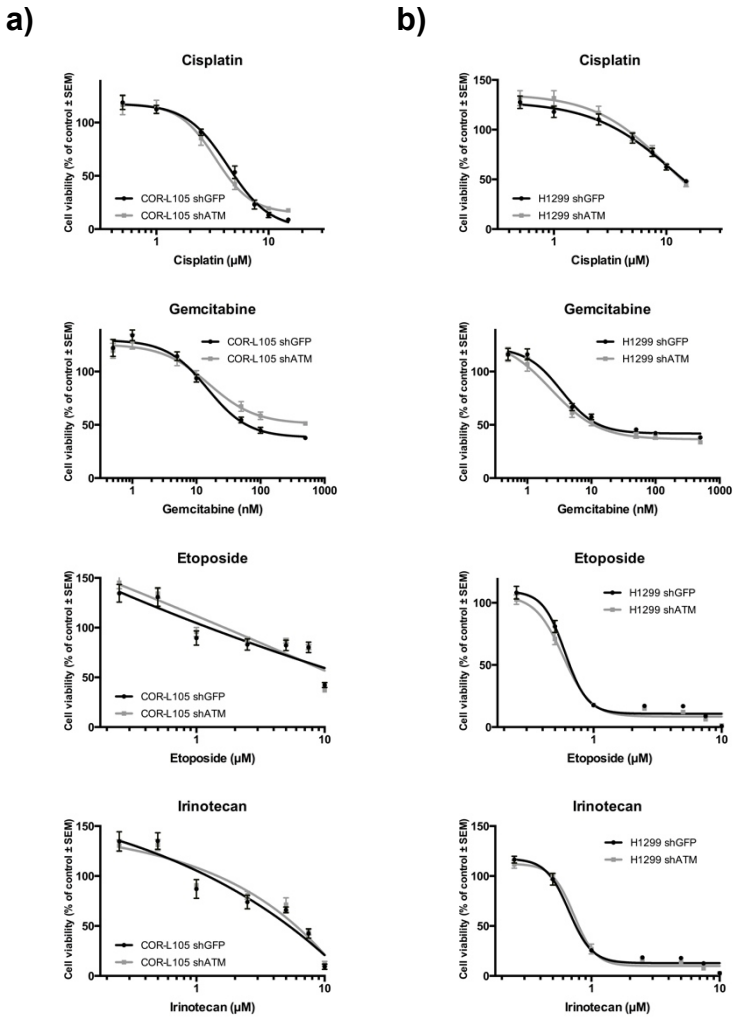

Figure 3.13: ATM knockdown does not sensitise NSCLC cells to cisplatin, gemcitabine, etoposide or irinotecan.

a) P53-proficient COR-L105 and **b)** p53-deficient H1299 shGFP and shATM cells were exposed to dilution series of the drugs for 3 days (gemcitabine and cisplatin) or 5 days (etoposide and irinotecan). Cell viability and proliferation was assessed by resazurin assay. Graphs represent means of at last three independent experiments each performed in triplicate ±SEM.

3.6 Discussion

Somatic mutations in the ATM gene have been identified in a variety of cancer types, but as a large proportion of these mutations are missense variants, the prediction of their consequences on protein stability and activity is challenging without functional studies. However, studies in cells derived from Ataxia-telangiectasia patients have shown that the vast majority of missense mutations which lead to functional impairment of ATM do so by destabilising the protein, leading to reduced or absent protein levels (Jacquemin *et al*, 2012; Sandoval *et al*, 1999; Mitui *et al*, 2009; Lavin *et al*, 2004).

Our data supports this concept as we identified two NSCLC cell lines harbouring homozygous missense mutations in the ATM gene (H1395 and H23) with impaired ATM function. In both cases, mutation was associated with markedly reduced ATM protein expression. To our knowledge, mutations leading to expression of a kinase-dead (kd) ATM protein have only rarely been reported in cancer (Scott *et al*, 2002) and none of them in NSCLC. We also compared the sequence variants that have been reported to cause expression of kd ATM in A-T patients with the reported NSCLC associated ATM missense mutations, but found no overlap ((Barone *et al*, 2009; Scott *et al*, 2002; Mitui *et al*, 2009; Barretina *et al*, 2012; Cancer Genome Atlas Research Network, 2012b, 2014; Ding *et al*, 2009); data not shown).

When studying ATM protein expression in human NSCLC tumour samples, we found that ATM protein expression was not detectable in 9.5% of cases, which is a higher proportion than the percentage of reported ATM mutations in NSCLC (5.1-9.1%; (Cancer Genome Atlas Research Network, 2012b, 2014)). This discrepancy could be

due to the small sample size in our study. In addition to point mutations, loss or rearrangement of the ATM gene could also contribute to the loss of ATM protein expression, as could epigenetic silencing of gene expression. Indeed, hypermethylation of the ATM promoter resulting in decreased protein levels and increased radiosensitivity has been described for colorectal and glioma cell lines (Kim *et al*, 2002; Roy *et al*, 2006). Furthermore, studies in locally advanced breast cancer have shown that the ATM gene is a target for epigenetic silencing (Vo *et al*, 2004).

Interestingly, it has been shown that the expression of kd ATM protein is more detrimental to cells than its loss (Yamamoto et al, 2012). While ATM knockout mice are viable and recapitulate many of the symptoms characteristic for A-T (Elson et al, 1996; Barlow et al, 1996), expression of physiological levels of kd ATM was found to be lethal during mouse embryogenesis, without displaying dominant-negative interfering activity (Daniel *et al*, 2012). It has been suggested that catalytically inactive ATM binds to sites of DNA DSBs, thereby "blocking" those sites for DNA repair, and causing disturbance of the DDR and persistence of DNA damage (Yamamoto *et al*, 2012). This observation may in part explain why loss of ATM function is generally associated with loss of protein expression in A-T and, as far as we can tell from our studies, cancer.

We have not yet obtained data to investigate the correlation between loss of ATM protein expression in immunohistochemistry and the presence of ATM mutations or epigenetic changes in clinical samples. However we would anticipate ATM IHC negative samples to be enriched for ATM mutations and possibly also markers of epigenetic silencing of ATM (e.g. promoter hypermethylation).

The DDR forms a barrier for tumour development during its early stages and deficiencies in DDR components are believed to allow the progression of pre-cancerous lesions to malignant carcinomas ((Bartkova *et al*, 2005; Gorgoulis *et al*, 2005; Halazonetis *et al*, 2008); see section 1.9). It is therefore likely, that mutations affecting key regulators of the DDR, such as ATM or p53, occur early during tumorigenesis and would therefore be found in a large proportion of the tumour cells at later stages, despite the occurrence of considerable heterogeneity. Our observations from IHC analysis of ATM protein expression support this concept, as we found that weak or negative staining in tumour cells was found homogenously across the tumour samples. However, more extensive work and comparison of primary and metastatic tumours will be needed to confirm this hypothesis.

In our studies we also assessed ATM activity in the NSCLC cell line H2087, which has been reported to carry a heterozygous p.E848Q ATM missense substitution. Functional analysis suggests that the mutation is benign and does not interfere with ATM function. It is however possible that the wild-type ATM allele in this cell line is sufficient to allow for normal ATM expression levels and function. This raises the question, whether heterozygosity of ATM mutations in cancer cells is generally associated with retained ATM function. However, there is at least one case reported in the literature where a heterozygous missense mutation causes severe deficiency in ATM signalling. The human mantle cell lymphoma cell line GRANTA-519 carries a heterozygous p.R2832C ATM missense mutation which results in a reduction of ATM protein expression and loss of ATM function (Williamson *et al*, 2010; Menezes *et al*, 2014; Barretina *et al*, 2012), demonstrating that heterozygosity may not be a general indicator of retained ATM function.

We conclude that immunohistochemical analysis of ATM protein expression in tumour samples may be a valuable tool to identify a patient subgroup with impairment of ATM function. It may not be able to identify the rare cases where a mutation causes expression of a kd protein, but it would allow for the detection of patients with loss of ATM function due to deletion of the gene locus, epigenetic changes or mutations that lead to loss of ATM expression, including truncating, missense or frameshift mutations. As hypersensitivity to ionising radiation is one of the most prominent phenotypes of ATM-deficient cells this may help to identify patients, which could get increased benefit from radiation therapy.

Several studies have also suggested that defects in ATM function could render cells particularly sensitive to certain chemotherapeutic drugs, including gemcitabine, cisplatin and topoisomerase I and II inhibitors (Jiang *et al*, 2009; Batey *et al*, 2013; Fedier *et al*, 2003). However, in our own studies we found no correlation between the functional status of ATM and the cellular sensitivity to cisplatin, gemcitabine, irinotecan (topoisomerase I inhibitor) or etoposide (topoisomerase II inhibitor).

A potential reason for these differential findings could be the differences in assays used to assess the cytotoxicity of these compounds. In our studies we used proliferation assays that determine cellular viability based on the quantification of resazurin metabolism. One potential drawback of this assay is that there is no differentiation between cells that are actively dividing and those that are quiescent which may result in an over-estimation of proliferating cell numbers. Furthermore, differences in the doubling times and the percentages of cells, which are actively dividing during the course of the treatment period, may impact on the results. Alternative assays to assess the cytotoxicity of these compounds, such as clonogenic assays, which are based on the clonogenicity of a given cell population and are less

affected by differences in doubling times between cell lines, may thus give different results.

It should also be noted that at least in the case of cisplatin, the role of ATM in mediating the cellular response remains controversial. While Jiang et al. show that depletion of ATM confers sensitivity to cisplatin (Jiang *et al*, 2009), others demonstrate that inhibition or depletion of ATM has no effect (Fedier *et al*, 2003) or even confers resistance (Wang *et al*, 2012; Lundholm *et al*, 2013; Teng *et al*, 2015). These differences between studies could be related to the different cellular models and experimental assays used. Further studies will be required to determine, whether the functional status of ATM plays a role in the therapeutic response of tumour cells to these chemotherapeutic agents.

In addition to a potential role in the response of tumours to chemo- or radiotherapy, ATM-deficiency may also identify a patient subset that could benefit from small molecule inhibitors in the context of inducing a synthetic lethal response. This question will be addressed in the following chapters.

CHAPTER 4

4 Targeting ATR as treatment strategy for ATM- or p53-deficient NSCLC

A previous report suggested that pharmacological ATR inhibition (ATRi) has the potential to selectively kill cells deficient in either ATM or p53 when combined with genotoxic agents (Reaper *et al*, 2011). This hypothesis is based on the observation that ATM- or p53-deficient cancer cells are defective in the G1 cell cycle checkpoint and therefore rely on the intra-S and G2/M checkpoints to arrest cell cycle progression following induction of DNA damage (Kastan *et al*, 1992). Thus, inhibition of ATR, which is an important mediator of the intra-S and G2/M cell cycle arrest in such cells, would lead to a loss of DNA damage checkpoints. In cells exposed to genotoxic agents, ATRi would further promote the induction of DNA damage, such as formation of DNA DSBs through collapse of stalled replication forks. In cancer cells where ATM or p53 signalling is defective, this would cause DNA damage accumulation and mitotic entry in the presence of DNA damage, resulting in mitotic catastrophe and cell death. Non-tumour cells, however, are ATM- and p53-proficient and would be spared.

Two potent and selective ATP-competitive inhibitors of ATR are currently in clinical development. After showing promising anti-tumour activity in xenograft models in combination with cisplatin, gemcitabine and IR, VE-822 (also known as VX-970) was the first ATR inhibitor to enter clinical development (Charrier *et al*, 2011; Fokas *et al*, 2012). A phase I clinical trial to assess the safety, tolerability and pharmacokinetics (PK) of VE-822 in combination with cytotoxic chemotherapy (cisplatin, gemcitabine and etoposide) is currently ongoing (ClinicalTrials.gov: NCT02157792). AZD6738,

an ATR inhibitor developed by AstraZeneca, has entered clinical development more recently. Notably, AZD6738 has shown single-agent anti-tumour activity in ATM-deficient but not ATM-proficient xenograft models (Jones *et al*, 2013; Guichard *et al*, 2013). Furthermore, *in vivo* combination studies with carboplatin or IR demonstrated significantly increased anti-tumour growth inhibitory activity with this compound. Two phase I clinical trials involving AZD6738 are currently recruiting. The first trial is assessing the safety of AZD6738 alone and in combination with radiotherapy in patients with solid tumours (ClinicalTrials.gov: NCT02223923). The second trial is assessing the efficacy of AZD6738 in combination with carboplatin in ATM-deficient NSCLC and advanced solid malignancies (ClinicalTrials.gov: NCT02264678).

These data are of particular interest for two reasons. Firstly, because both ATM and p53 are commonly mutated in NSCLC - in 5.1-9.1% and 46-90% of cases, respectively (Cancer Genome Atlas Research Network, 2014, 2012b) - suggesting that targeting ATR to confer synthetic lethality might have utility for the treatment of a large number of NSCLC patients. Secondly, gemcitabine, platinum-based chemotherapy and IR are commonly used modalities for the treatment of NSCLC. Identifying strategies to improve the anti-tumour activity of these therapies without increasing normal tissue toxicity would be beneficial for improving treatment outcome and could be readily incorporated into the clinic.

The studies described in this chapter aimed to evaluate the potential of pharmacological ATR inhibition for the treatment of ATM- or p53-deficient NSCLC, as single agent as well as in combination with IR or the chemotherapeutic drugs cisplatin and gemcitabine.

4.1 The effect of ATR inhibition on gemcitabine-induced CHK1 phosphorylation

To date, phosphorylation of the ATR downstream target CHK1 is the most widely used preclinical biomarker of ATR kinase activity (Fokas *et al*, 2012; Hall *et al*, 2014; Pires *et al*, 2012). We therefore used immunoblot analysis of pCHK1 as readout for ATR kinase activity to confirm that the ATR inhibitors used in our studies potently attenuate ATR activity. In addition to the two clinical compounds AZD6738 and VE-822, we also used VE-821, the first selective ATR inhibitor to be reported, as it has been extensively studied (Pires *et al*, 2012; Prevo *et al*, 2012; Huntoon *et al*, 2013; Reaper *et al*, 2011). The tested dose-ranges for this experiment and the concentrations used for subsequent experiments were chosen based on recommendations from the manufacturers and from published literature (Fokas *et al*, 2012; Prevo *et al*, 2012).

CHK1 is phosphorylated on S345 (and S317) predominantly by ATR (Zhao & Piwnica-Worms, 2001), though it has been suggested that ATM contributes to phosphorylation of these sites, albeit to a lesser extent (Sørensen *et al*, 2003; Helt *et al*, 2005; Gatei *et al*, 2003; Ozeri-Galai *et al*, 2008). These phosphorylation events in turn facilitate autophosphorylation at S296, which is important for the cell cycle checkpoint functions of CHK1 (Kasahara *et al*, 2010). Furthermore, CHK1 S296 phosphorylation appears to correlate with CHK1 activity, as it has been shown that S296 phosphorylation is depleted following CHK1 inhibition, while phosphorylation of the ATR (and ATM) phosphorylation sites S345 and S317 is elevated (Montano *et al*, 2012).

As phosphorylation levels of CHK1 are generally very low under physiological conditions, we used gemcitabine treatment to induce activity of the ATR signalling

pathway. Gemcitabine is a nucleoside analogue of deoxycytidine, which is incorporated into the DNA during replication. This incorporation blocks the proceeding of DNA polymerases leading to stalling of replication forks, which in turn induces profound activation of the ATR signalling pathway.

As expected, treatment of cells with gemcitabine induced phosphorylation of CHK1 at serine 296, 345 and 317. These changes were evident at 3 h after beginning treatment, but were generally less pronounced than at 24 h, when a substantial increase in CHK1 phosphorylation was evident (Figure 4.1).

While VE-821 potently attenuated the phosphorylation of CHK1 at both S296 and S345 (Figure 4.1a), VE-822 only minimally reduced CHK1 (S345) phosphorylation (Figure 4.1b). AZD6738 potently inhibited CHK1 S345 phosphorylation in both H1299 and A427 cell lines. The effect on S317 and S296 levels were, however, less pronounced, particularly in H1299 cells (Figure 4.1c, d).

After 24 h of treatment, the combination of gemcitabine with ATRi led to a strong and dose dependent induction of the ATM signalling pathway (increase in ATM S1981, KAP1 S824 and γH2AX levels). This observation was similar for all three ATR inhibitors and occurred in both H1299 and A427 cells. The observed increase in ATM activity and γH2AX levels, a known marker for DNA DSBs (Scully & Xie, 2013; Löbrich *et al*, 2010), points towards an increase in the induction of DNA damage in cells co-treated with gemcitabine and ATRi, compared with gemcitabine treatment alone.

Importantly, none of the compounds inhibited ATM kinase activity at the doses chosen for further experiments (1 μM for VE-821, 100 nM for VE-822 and 1 μM for AZD6738).

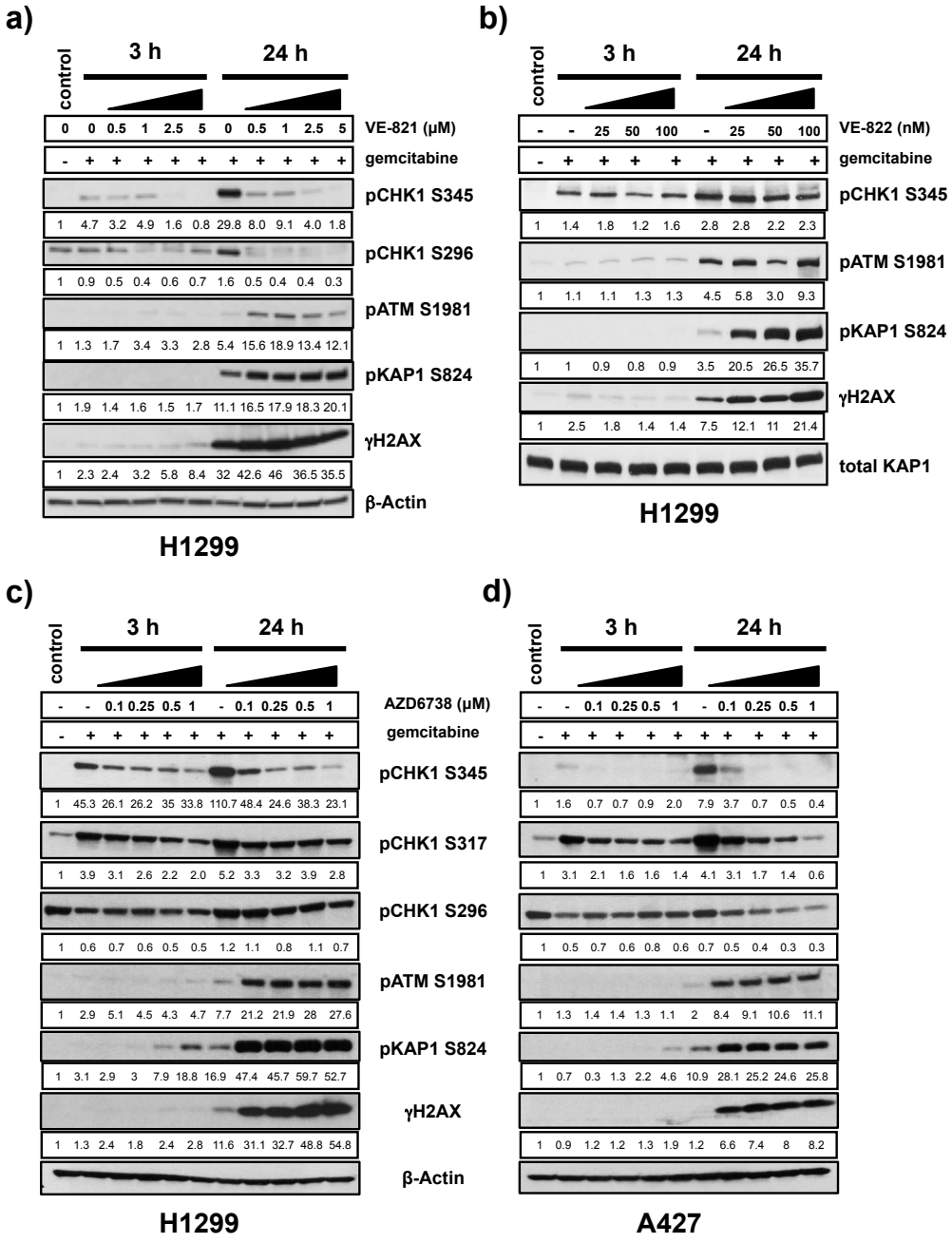

Figure 4.1: The effects of ATR inhibitor treatment on the activity of the ATR and ATM signalling pathways in response to gemcitabine treatment.

Phosphorylation of CHK1 (S345, S317 and S296) was determined to assess ATR kinase activity (for VE-821 only S345 and S296 were assessed; for VE-822 only S345). pATM (S1981) and pKAP1 (S824) were used as a measure of ATM activity, while H2AX (S139) served as an indicator for the induction of DNA DSBs. β-Actin or total KAP1 were used as loading control. Relative amounts of the respective protein, determined through densitometric quantification of the protein bands, are shown underneath each blot. Values are normalised to untreated control and expressed as the ratio of each band relative to the loading control of the respective lane. **a) to c)** H1299 cells were treated with gemcitabine (50 nM), or a combination of gemcitabine and **a)** VE-821 (0.5 - 5 μM) **b)** VE-822 (25 -100 nM) or **c)** AZD6738 (0.1 - 1 μM). **d)** A427 cells were treated with gemcitabine (50 nM), or a combination of gemcitabine and AZD6738 (0.1 - 1 μM). Protein lysates were prepared 3 h and 24 h after beginning treatment, respectively.

The variability in reduction of CHK1 phosphorylation levels between ATR inhibitors and cell lines raised the question of incomplete ATR inhibition at the tested dose range, particularly in the case of VE-822. All three ATR inhibitors used in this study have been shown to potently and specifically inhibit ATR kinase activity in cell-free kinase assays. However, there is incomplete knowledge about possible off-target effects, modes of action and kinetics of inhibition in cells. Differences in these properties could be responsible for the observed differential effects on CHK1 phosphorylation levels observed in our studies.

Furthermore, a study conducted by Huntoon et al. suggested that CHK1 phosphorylation levels may not offer a reliable marker for inhibition of the ATR pathway, as they demonstrated that ATRi blocks gemcitabine induced phosphorylation of CHK1 (Ser296 and Ser345) in some cell lines, but not others (Huntoon *et al*, 2013). In agreement with this notion, a recent study assessing CHK1 phosphorylation following ATR knockdown suggested that phospho-CHK1 levels may only reflect ATR kinase activity for a short period of time (3 h) after ATR depletion (Chen *et al*, 2014). Therefore, the timepoints chosen for this assay may not have been optimal and the effects of the inhibitors on ATR kinase activity could have been masked by compensatory mechanisms.

4.2 Simultaneous loss of ATM and p53 function increases the cytotoxicity of pharmacological ATR inhibition.

Before investigating the ability of ATR inhibitors to act as chemo- or radiosensitisers, we sought to assess a potential link between the sensitivity of cells to single-agent

ATR inhibitor treatment and the functional status of ATM and p53. For this purpose, we determined the impact of ATRi on cell proliferation and viability in resazurin assays. In addition to a panel of NSCLC cell lines, we included the telomerase immortalised normal bronchial epithelial cell line NBE1 ($^{ATM+/p53+}$), the SV-40 transformed human fibroblast cell line MRC5 SV2 ($^{ATM+/p53-}$) and the SV-40 transformed A-T fibroblast cell line GM16666 ($^{ATM-/p53-}$) as non-tumour-cell controls.

We found no clear association between the sensitivity of cells to VE-821 (Figure 4.2a), VE-822 (Figure 4.2b) or AZD6738 (Figure 4.2c) and mutation status of either ATM or p53 alone (Figure 4.2; Table 4.1). Although ATRi was generally more cytotoxic for p53-deficient than for p53-proficient tumour cells, the cytotoxicity observed in p53 wild-type NBE1 cells was similar to that observed in p53-mutated tumour cells for all three ATR inhibitors. H1395 cells, which express wild-type p53 but lack functional ATM, were not particularly sensitive to any of the ATR inhibitors. At the same time, cells with deficiency in both ATM and p53 consistently showed substantially higher sensitivity to all three ATR inhibitors than cells deficient in either ATM or p53 alone (IC_{50} values of 1.28 μM (VE-821), 60.32 nM (VE-822) and 0.50 μM (AZD6738) for H23 and 2.42 μM (VE-821), 91.33 nM (VE-822) and 0.32 μM (AZD6738) for GM16666; Figure 4.2).

We examined whether the difference in sensitivity to ATRi between cell lines could be related to expression levels of ATR or CHK1. All cell lines tested, however, showed similar ATR protein expression. Though CHK1 protein levels differed between cell lines, there was no correlation with sensitivity to ATRi (Figure 4.3).

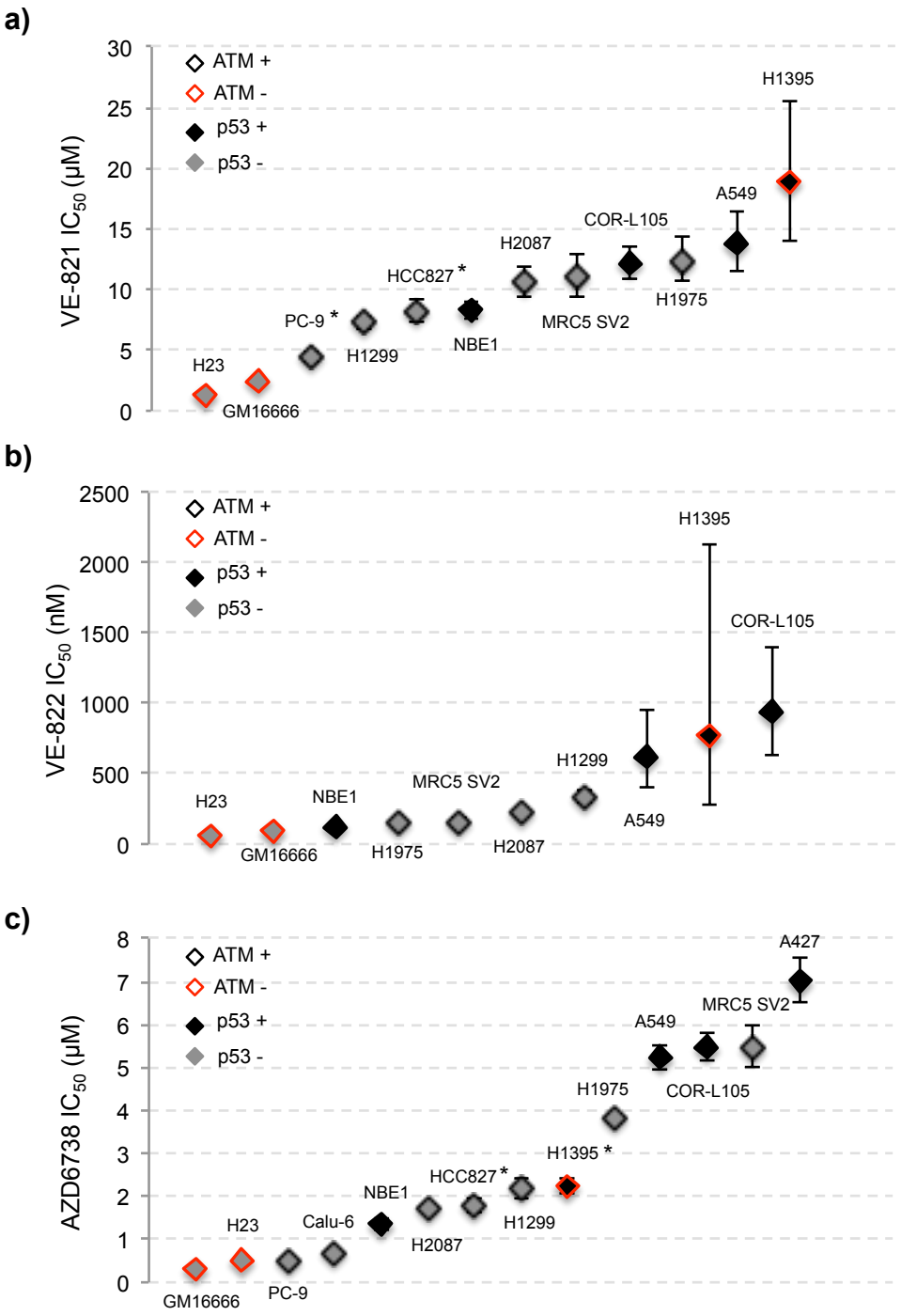

Figure 4.2: Response of NSCLC cells and normal tissue controls to pharmacological ATR inhibition.

Graphs summarising absolute IC_{50} values for **a)** VE-821, **b)** VE-822 and **c)** AZD6738 ± SEM. Values were calculated from two (*), or at least three independent experiments, each performed in triplicate. Functional status for ATM and p53 are indicated (see legend).

Table 4.1: Sensitivity of NSCLC cell lines and normal tissue controls to pharmacological ATR inhibition.

Cell line	ATM status	p53 status	VE-821 mean IC_{50} [μM] (-/+ SEM, range)	VE-822 mean IC_{50} [nM] (-/+ SEM, range)	AZD6738 mean IC_{50} [μM] (-/+ SEM, range)
A549	wt (+)	wt (+)	13.8 (11.5-16.5)	621.2 (404-955)	5.2 (5.0-5.5)
A427	wt (+)	wt (+)	N/A	N/A	7.0 (6.5-7.5)
COR-L105	wt (+)	wt (+)	12.2 (10.9-13.6)	940.2 (629-1406)	5.5 (5.1-5.8)
NBE1	wt (+)	wt (+)	8.3 (7.6-9.0)	122.1 (113-132)	1.4 (1.2-1.5)
MRC5 SV2	wt (+)	SV-40 transf. (-)	11.0 (9.4-13.0)	159.8 (138-185)	5.5 (5.0-6.0)
H2087	wt (+)	mut. (-)	10.6 (9.4-12.0)	214.7 (197-234)	1.7 (1.65-1.8)
H1975	wt (+)	mut. (-)	12.4 (10.7-14.3)	148.4 (126-175)	2.2 (2.1-2.4)
H1299	wt (+)	mut. (-)	7.2 (6.8-7.8)	333.5 (295-377)	2.2 (1.9-2.4)
HCC827	wt (+)	mut. (-)	8.2 (7.3-9.1)	N/A	1.8 (1.6-1.9)
Calu-6	wt (+)	mut. (-)	NA	N/A	0.7 (0.64-0.72)
PC-9	wt (+)	mut. (-)	4.5 (4.1-4.9)	N/A	0.5 (0.5-0.52)
H1395	mut. (-)	wt (+)	18.9 (14.0-25.4)	772.3 (280-2127)	3.8 (3.7-3.9)
H23	mut. (-)	mut. (-)	1.3 (1.2-1.4)	60.3 (54.1-67.3)	0.5 (0.47-0.52)
GM16666	mut. (-)	SV-40 transf. (-)	2.4 (2.3-2.5)	91.3 (87.2-95.7)	0.32 (0.3-0.33)

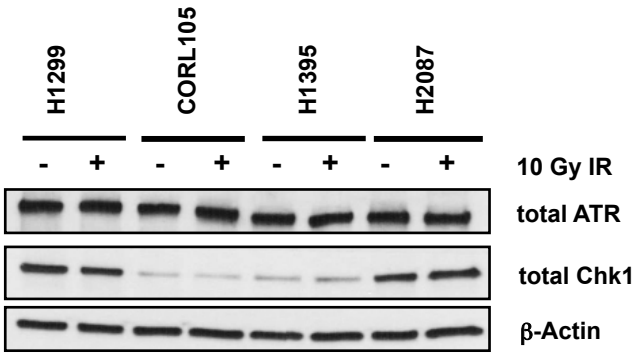

Figure 4.3: Sensitivity of cells to pharmacological ATR inhibition does not correlate with expression levels of ATR or CHK1.

H1299, COR-L105, H1395 and H2087 cells were mock-irradiated (control) or irradiated with 10 Gy followed by incubation at 37°C for 60 min and preparation of protein lysates. Total ATR and CHK1 protein levels were assessed by western blot analysis. β-Actin serves as loading control.

In line with our observations from proliferation assays, exposure of cells to 1 μM VE-821 for 48 h was sufficient to reduce the clonogenic survival of H23 cells to 35% compared with vehicle control (***$p<0.0001$). In cell lines with retained p53 and/or ATM function (COR-L105, H1299 and H1395) on the other hand, VE-821 treatment had no or only little effect on colony formation of the cells (Figure 4.4a).

We aimed to further investigate this increased sensitivity of ATM- and p53- deficient cells in *in vivo* studies. However, we were unable to establish a reliable tumour xenograft model from the H23 cell line, as tumours would only form in approximately 25% of cases (following injection of 1 x 10^7 H23 cells in 50% Matrigel™ per mouse). Therefore, to further validate the observed effect, we established a three-dimensional (3D) spheroid model. Spheroid models possess many of the elements of a tumour xenograft including cell-cell interactions, a spatial geometry that can produce well-

defined drug and nutrient concentration gradients as well as subpopulations of cells that are quiescent, hypoxic or necrotic (Phung *et al*, 2011).

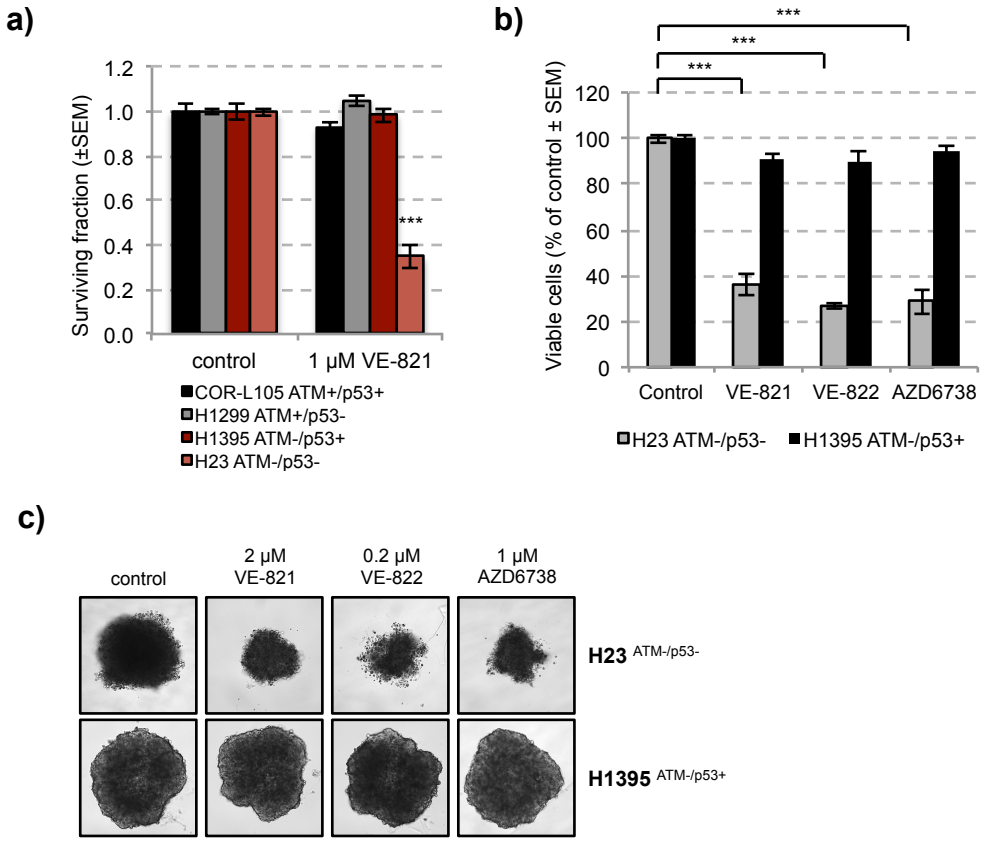

Figure 4.4: Pharmacological ATR inhibition is particularly cytotoxic for cells with loss of both ATM and p53 function.

a) Clonogenic survival of COR-L105, H1299, H1395 and H23 cells following 48 h treatment with 1μM VE-821. Each point represents the mean of three independent experiments ± SEM. ***= p<0.0001 (calculated by Student's t-test).
b) Spheroids of H23 and H1395 cells were treated with DMSO (control), 2 μM VE-821, 0.2 μM VE-822 or 1 μM AZD6738 for 72 h. Following a 7-day recovery period in drug-free culture medium, cell viability was assessed. Data are presented as mean of three independent experiments ± SEM. *** = p-values <0.0001 (calculated by Student's t-test).
c) Representative images of H23 and H1395 spheroids treated as in c). Images were taken at a 40x magnification.

Spheroids of H1395$^{ATM-/p53+}$ and H23$^{ATM-/p53-}$ cells were generated and exposed to ATR inhibitors (2 μM VE-821, 200 nM VE-822 or 1 μM AZD6738) for 72 h. Drugs were then removed through several washes and spheroids were allowed to grow in drug-free cell culture medium for an additional seven days before assessment of cell viability. As expected, in H23$^{ATM-/p53-}$ cells treatment with VE-821, VE-822 or AZD6738 led to a significant reduction in spheroid growth and viability to approximately 36%, 26% and 29% of vehicle treated controls, respectively (***$p<0.0001$). In contrast, spheroids derived from the ATM-deficient, but p53-proficient cell line H1395$^{ATM-/p53+}$, showed little or no reduction in spheroid growth and viability following exposure to any of the ATR inhibitors (Figure 4.4b, c).

4.3 siRNA-mediated ATR depletion has a different effect on cell proliferation than pharmacological ATR inhibition.

To study the cellular response to loss of ATR function in more detail, we utilised siRNA-mediated knockdown of ATR. H1299 and A549 cells were transfected with control siRNA (siCTR) or siRNA directed against ATR (siATR) and processed for western blot analysis. Surprisingly, we found that siRNA transfection, even with the non-targeting control, induced a substantial up-regulation of ATM activity (measured by ATM S1981 and KAP1 S824) 24 h after transfection. Furthermore, high levels of H2AX phosphorylation were evident in siCTR-, as well as siATR-transfected cells (Figure 4.5a, b). These observations suggest induction of a general stress response triggered by siRNA transfection, which involves activation of ATM.

In H1299 cells transfected with siCTR, ATM activity returned to normal levels 48 h after transfection, but were elevated again at 72 h. γH2AX levels remained elevated

until 72 h after transfection (Figure 4.5a). In A549 cells transfected with siCTR, γH2AX, pATM and pKAP1 levels returned to background levels 48 h after transfection (Figure 4.5b).

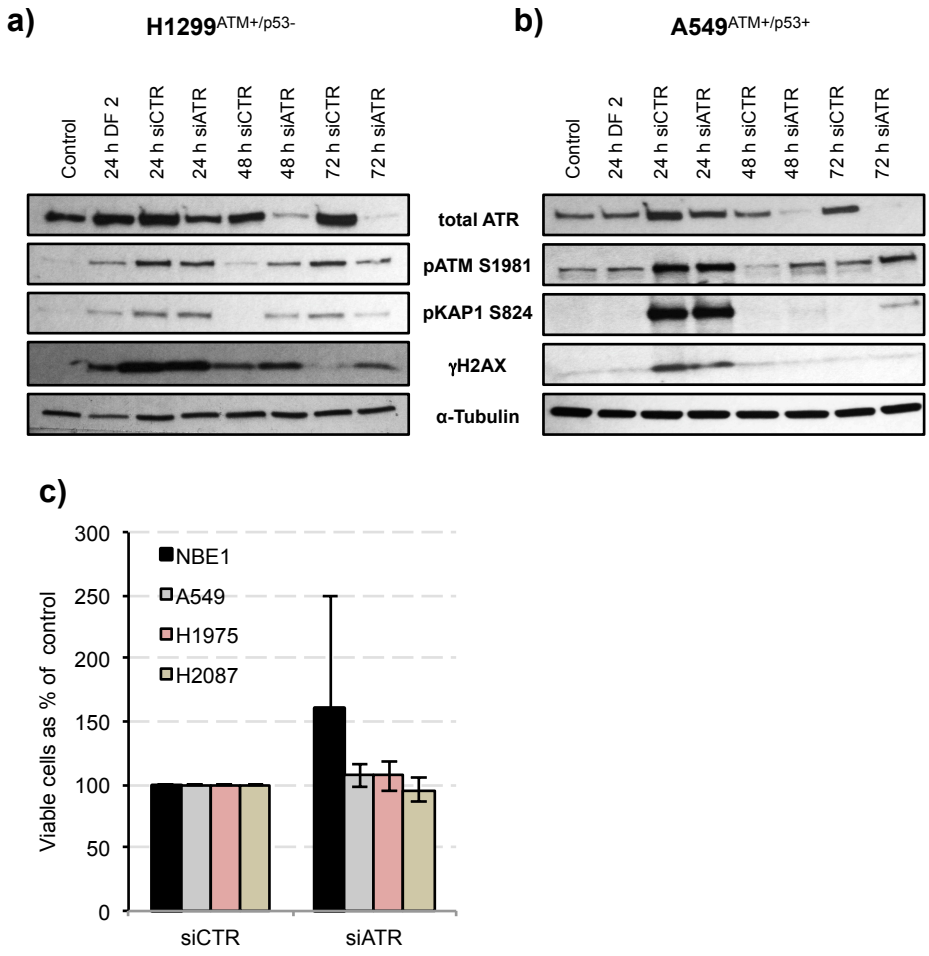

Figure 4.5: Effect of siRNA-mediated depletion of ATR on activity of the ATM signalling pathway and cell proliferation.

a) and b) H1299 (a) and A549 (b) cells were transfected with non-targeting control (siCTR) or ATR siRNAs (siATR) and processed for western blot analysis 24, 48 and 72 h after transfection. Samples of non-transfected cells and cells treated with the transfection reagent only (DF 2) were included as control. α-tubulin served as loading control.
c) NBE1, A549, H1975 and H2087 cells were transfected with siCTR or siATR and cell proliferation and viability was assessed 5 days after transfection by quantification of resazurin metabolism. Bars represent the means of three independent experiments, each performed in triplicate, normalised to siCTR-transfected controls. Error bars=SEM

In both cell lines, transfection with siATR led to a significant decrease in ATR protein levels within 48 h (Figure 4.5a, b). However, given the strong reaction of the cells to siRNA transfection in general, interpreting the effect of ATR knockdown on ATM activity was not possible.

We also assessed the impact of siRNA-mediated ATR depletion on cell proliferation and viability (Figure 4.5c). In contrast to our results obtained with pharmacological ATR inhibition, siRNA mediated knockdown did not significantly affect cell proliferation or viability. This is in agreement with a recent finding reported by Cui et al., who found that inducible shRNA-mediated knockdown of ATR does not affect cell proliferation (Cui *et al*, 2014).

At least for ATM, DNA-PKcs and PARP, it has been reported that pharmacological inhibition causes a different cellular phenotype than lack of protein expression (White *et al*, 2010; Choi *et al*, 2010; Murai *et al*, 2012; Allen *et al*, 2003). It seems possible that ATR inhibitors may, at least in some respects, also have a different impact on cellular biology than genetic depletion. However, future studies will have to address this question.

Considering that the aim of our studies was to investigate the effects of pharmacological ATR inhibition and in light of the observed impediments of siRNA transfection with regard to activation of ATM signalling, we focussed our further studies on the effects of ATR inhibitors only. To avoid misinterpretation of results due to potential off-target effects of the drugs, we used three different ATR inhibitors and chose inhibitor concentrations, which were recommended by the developing companies and which had previously been demonstrated to not inhibit other PIKK family members.

4.4 Assessment of radiosensitisation by ATR inhibitors

Consistent with the cell viability data, when combining VE-821 treatment with IR, neither ATM- (H1395; Figure 4.6b) nor p53-deficient (H1299, H2087, H1975; Figure 4.6g-i) cells showed a higher degree of radiosensitisation by ATRi compared with the p53 wild-type control (COR-L105, A549, H460; Figure 4.6d-f) or the normal bronchial epithelium control (NBE1; Figure 4.6a).

However, in cells deficient in both ATM and p53 ($H23^{ATM-/p53-}$), a marked radiosensitisation was observed with a sensitisation enhancement ratio (SER) of 26.05 based on the surviving fraction at 2 Gy (Figure 4.6c, p=0.001). Consistently, exposure of cells to VE-822 had no effect on the IR-induced cytotoxicity in $H1395^{ATM-/p53+}$ cells (Figure 4.7a). $H23^{ATM-/p53-}$ cells, on the other hand, were profoundly radiosensitised by VE-822 treatment ($p<0.0001$; Figure 4.7b). These results were confirmed in the SV-40 transformed A-T fibroblast cell line $GM16666^{ATM-/p53-}$, which also showed marked radiosensitisation by VE-821, VE-822 and AZD6738 (SER at 2 Gy of 13.7, 111.4 and 345.4, respectively; Figure 4.7c).

These observations raised the possibility that the ability of ATR inhibitors to act as radiosensitisers may be determined by the functional status of ATM and p53, rather than either gene alone. To address this question, we performed clonogenic survival assays in stable ATM knockdown (shATM) cell lines, and the corresponding shGFP controls, derived from the p53-proficient COR-L105 and the p53-deficient H1299 cell line. ATM knockdown had no significant effect on the radiosensitising effect of VE-822 in COR-L105 cells (SER=1.56 in shGFP vs. SER=1.3 in shATM cells; Figure 4.8a). In contrast, down-regulation of ATM in the p53-mutant cell line H1299 markedly potentiated the radiosensitising effect of VE-822 (SER=1.38 in shGFP vs. SER=2.6 in shATM cells; Figure 4.8b).

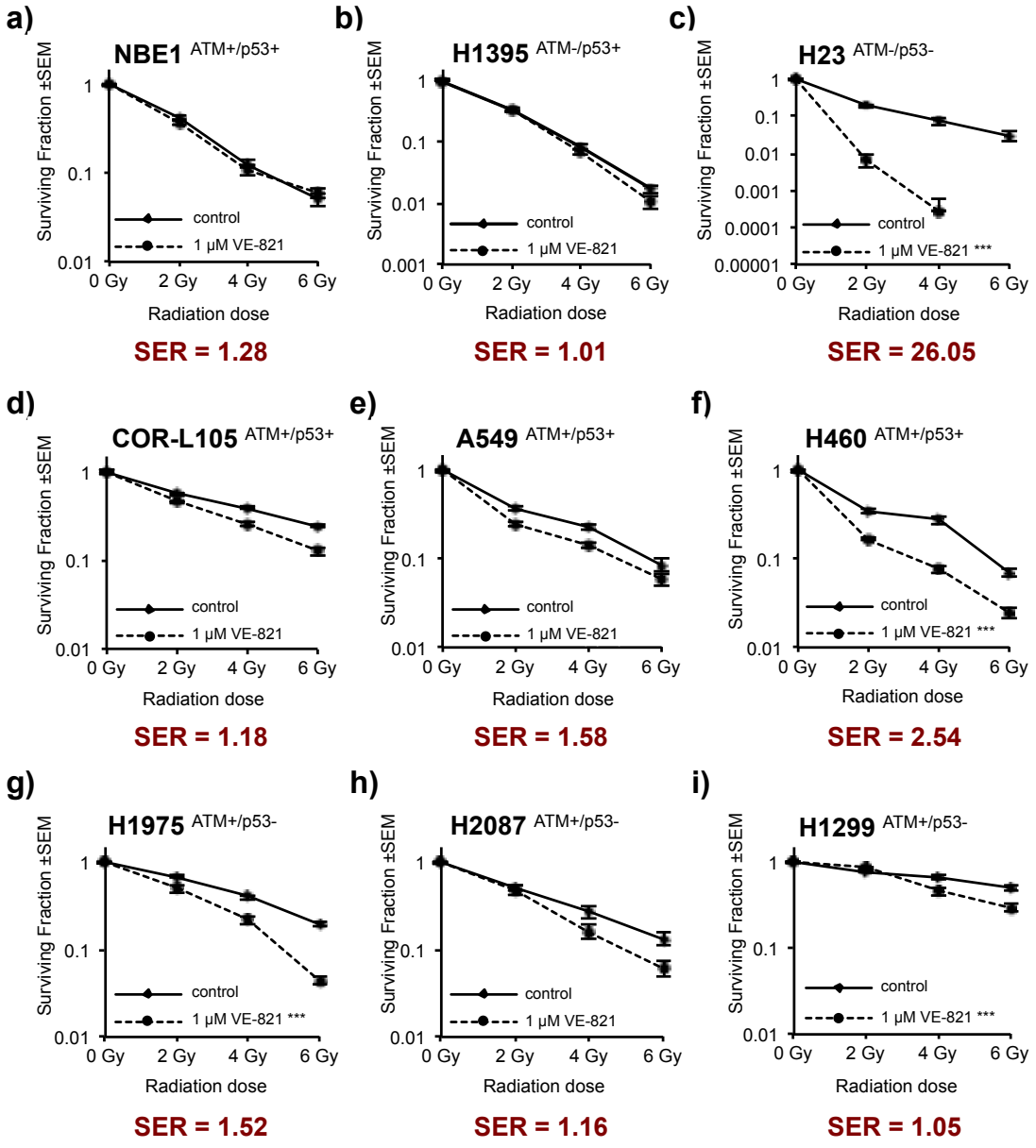

Figure 4.6: VE-821 mediated radiosensitisation of NSCLC and normal bronchial epithelial cells.

Clonogenic survival of **a)** NBE1, **b)** H1395, **c)** H23, **d)** COR-L105, **e)** A549, **f)** H460, **g)** H1975, **h)** H2087 and **i)** H1299 cells following treatment with the indicated doses of IR +/- VE-821. Cells were irradiated after pre-treatment with 1 μM VE-821 for 1 h. 24 h after beginning treatment, the inhibitor was removed to allow for colony formation. Each point represents the mean of three independent experiments, each performed in triplicate. Error bars = SEM. Surviving fractions were normalised to DMSO treated or VE-821 treated mock-irradiated controls, respectively. SER = sensitisation enhancement ratio based on the surviving fraction at 2 Gy IR. Radiation dose responses of vehicle treated controls and inhibitor treated cells were compared by univariate analysis of variance (ANOVA). Asterisks indicate statistical significance between survival curves with p-values <0.001 indicated by ***.

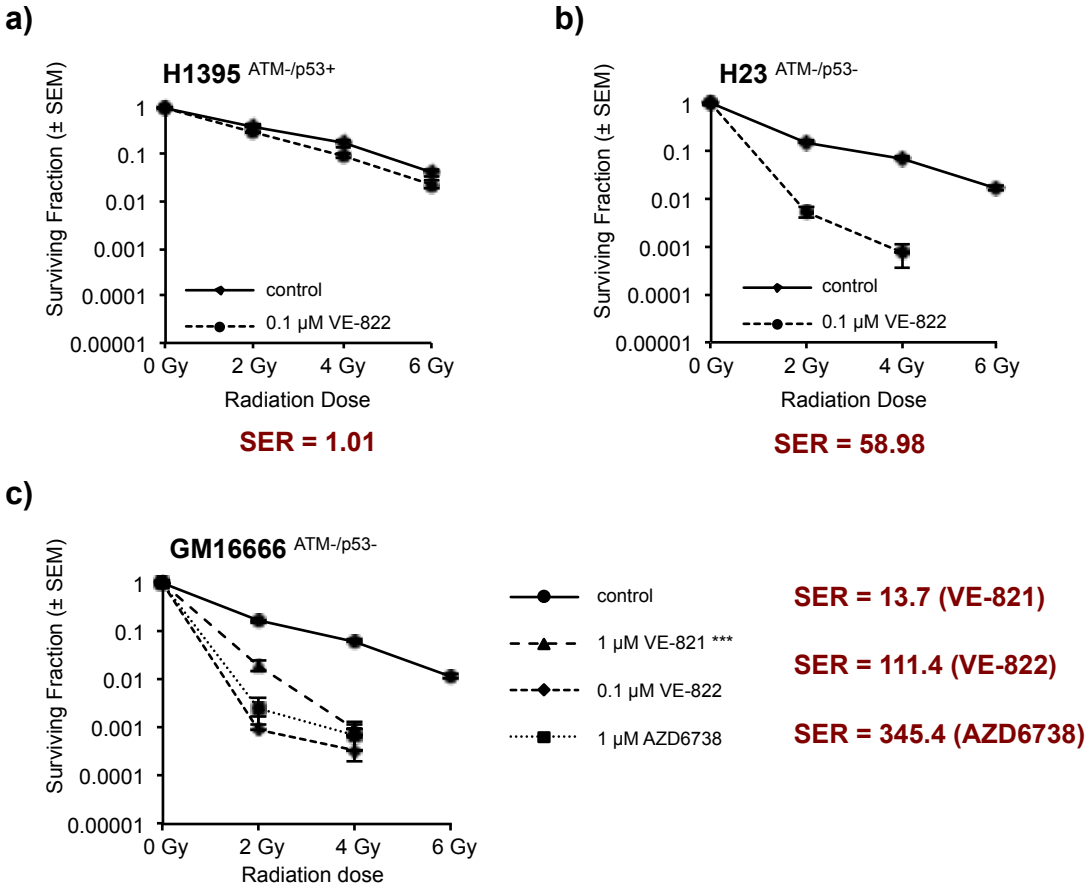

Figure 4.7: Radiosensitisation of ATM-deficient cells by ATRi is dependent on the functional status of p53.

a) and **b)** Clonogenic survival of H1395 and H23 cells following combined treatment with IR and VE-822. Cells were irradiated after pre-treatment with 100 nM VE-822 for 1 h. VE-822 exposure was continued for 23 h after irradiation. Each point represents the mean of three independent experiments, each performed in triplicate. Surviving fractions were normalised to DMSO treated or inhibitor treated mock-irradiated controls, respectively. *** indicates $p<0.0001$ calculated by univariate ANOVA. Error bars = SEM; SER indicates the sensitisation enhancement ratio based on the surviving fraction at 2 Gy.
c) Clonogenic survival of GM16666 cells following combined treatment with the indicated doses of IR and VE-821 (1 μM), VE-822 (0.1 μM) or AZD6738 (1 μM). Treatment and analysis as in a) and b).

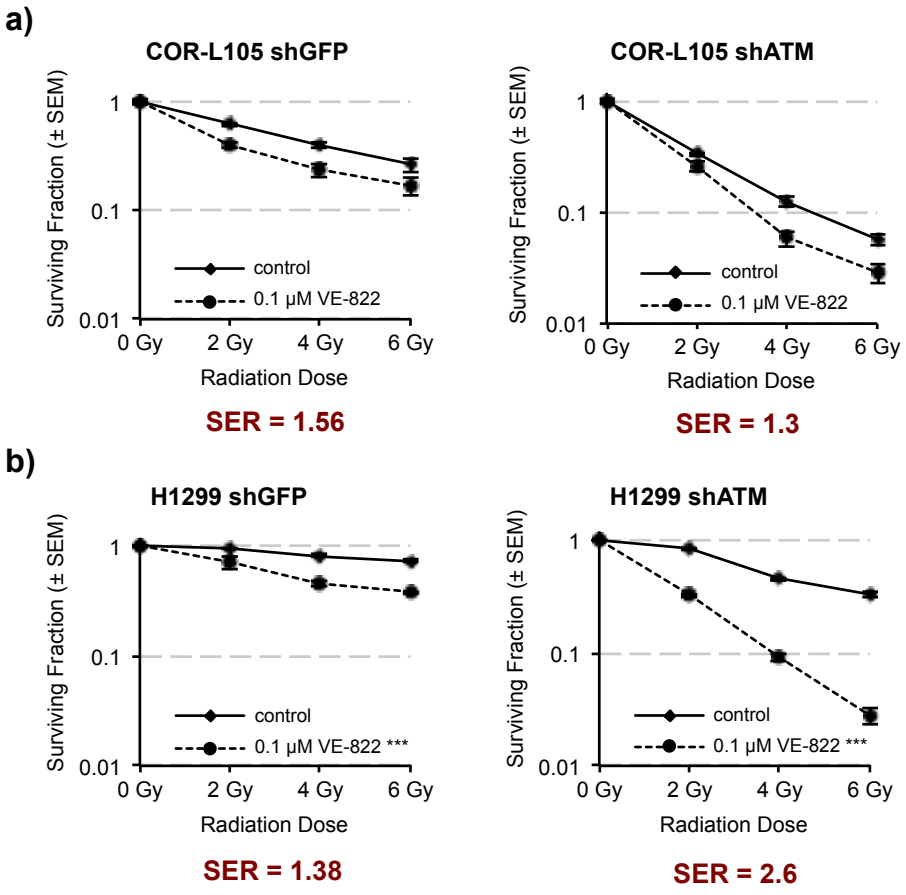

Figure 4.8: ATM knockdown increases the radiosensitising effect of VE-822 treatment.

Clonogenic survival of stable ATM knockdown cell lines and corresponding shGFP controls derived from **a)** COR-L105 and **b)** H1299 cells following combined treatment with IR and 100 nM VE-822. Treatment and statistical analysis as in Figure 4.7a, b. Error bars = SEM, SER = sensitisation enhancement ratio based on the surviving fraction at 2 Gy; *** = p-values <0.0001.

4.4.1 ATR inhibition leads to attenuation of the DNA damage induced G2/M cell cycle checkpoint

In response to IR, particularly in cells deficient in ATM, ATR activation contributes to the induction of the G2/M cell cycle checkpoint to ensure that cells with damaged DNA do not enter mitosis. Several studies have demonstrated that pharmacological or genetic inhibition of ATR function leads to abrogation of the DNA damage induced G2/M cell cycle arrest, thereby allowing transition of cells from G2 to M phase despite the presence of DNA damage, which can result in mitotic errors, chromosome mis-segregation and mitotic catastrophe (Cliby *et al*, 1998; Cui *et al*, 2014; Prevo *et al*, 2012).

To establish, whether the observed differences in response to ATRi treatment between cell lines might be due to differences in cell cycle checkpoint activation following induction of DNA damage, CORL-105 and H1299 shATM and shGFP cells were treated with VE-821 (or VE-822), IR (10 Gy), or a combination of both and harvested for cell cycle profile analysis at 24 h and/or 48 h after commencing treatment (Figure 4.9 and 4.10). Treatment with ATRi alone had little or no effect on cell cycle distribution in any of the cell lines tested. Combined treatment of cells with VE-821 and radiation, however, led to an abrogation of the IR-induced G2/M cell cycle arrest in cells deficient in p53 (H1299 shGFP and shATM). Furthermore, a substantial increase in the aneuploid cell populations with >4N and <2N DNA content could be observed in ATRi + IR treated H1299 shGFP cells. This phenotype was markedly exacerbated following ATM knockdown (Figure 4.9b, c). In COR-L105, no significant changes in cell cycle distribution (by DNA content) between IR-only or

IR+VE-821 treated cells or increase in aneuploidy could be observed, even following ATM knockdown (Figure 4.9a,b).

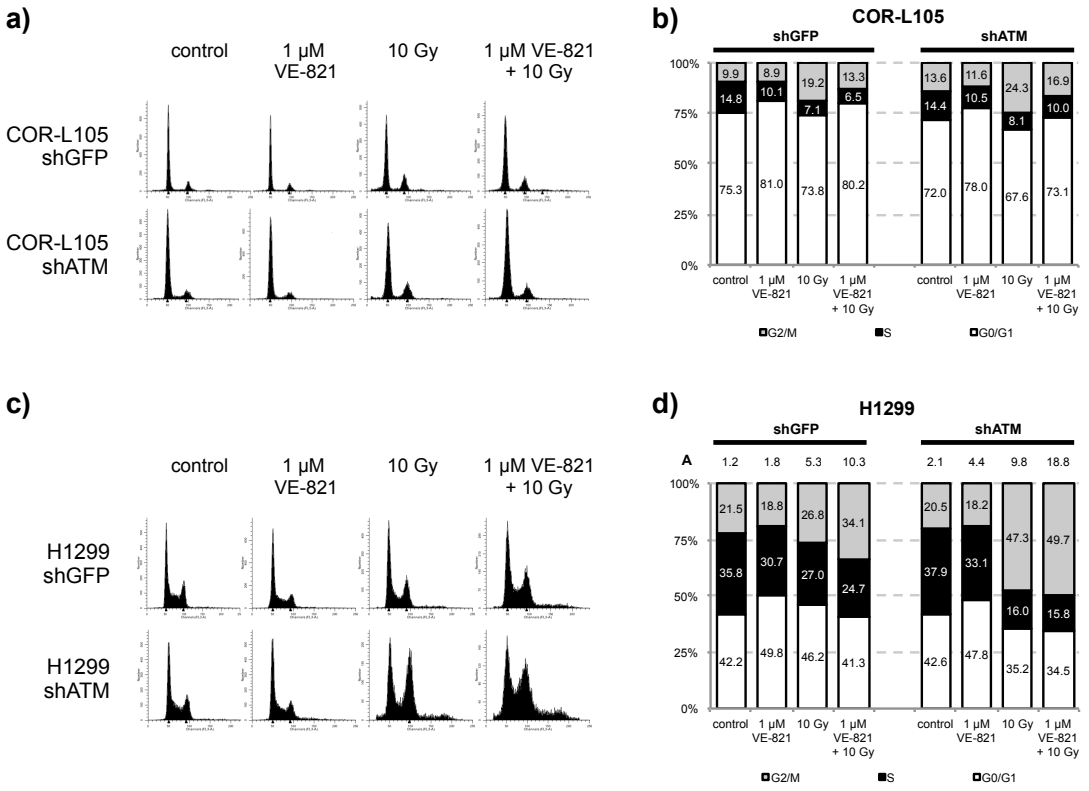

Figure 4.9: VE-821 attenuates the IR-induced G2/M cell cycle checkpoint.

Asynchronous populations of COR-L105 and H1299 shATM knockdown cell lines and corresponding shGFP controls were treated with VE-821 (1 μM), IR (10 Gy) or a combination of both and harvested for assessment of cell cycle distribution by propidium iodide staining and FACS analysis 48 h after beginning treatment. **a)** and **c)** show representative images of n=3 (COR-L105) or n=2 (H1299) independent experiments. Quantification of G0/G1, S and G2/M cell populations, calculated from the diploid cell population (excluding aneuploid cells) and expressed as average of n=3 (COR-L105) or n=2 (H1299) experiments, is shown in the bar graphs in **b)** and **d)**. For H1299, the percentage of aneuploid cells (A) in the overall cell population is shown above the bar for each condition. For COR-L105, the percentages of aneuploid cells were insignificantly low (even following treatment) and were thus not included in the analysis.

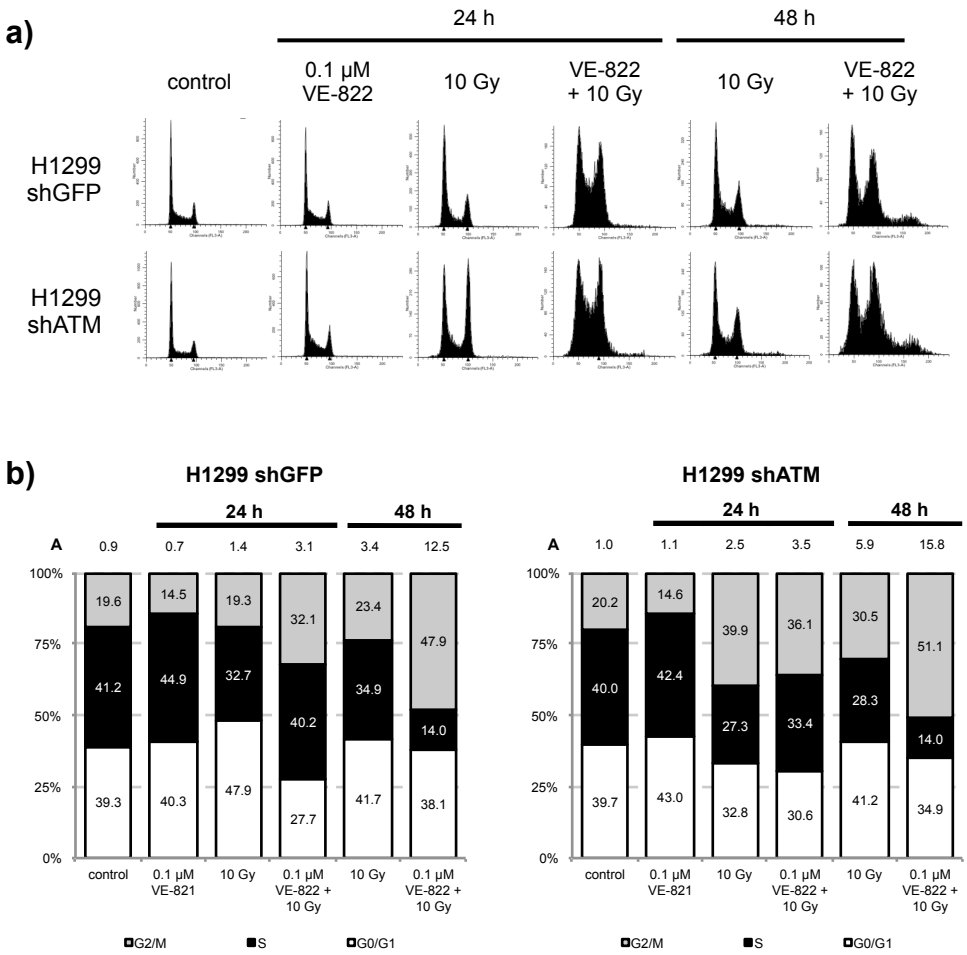

Figure 4.10: VE-822 attenuates the IR-induced G2/M cell cycle checkpoint.

H1299 shGFP and shATM cells were treated with VE-822 (0.1 μM), IR (10 Gy) or a combination of both and harvested 24 h and 48 h after beginning of treatment. Assessment of cell cycle distribution was performed by FACS analysis following propidium iodide staining. **a)** Representative images of two independent experiments. **b)** Bar graphs represent the average percentages of cells in G0/G1-, S- or G2/M-phase of the cell cycle (based on the diploid cell populations) calculated from two experiments. The percentage of aneuploid cells (A) in the overall cell population is shown above the bar for each condition.

To better understand the differences in ATRi-mediated checkpoint abrogation between cell lines, BrdU pulse labelling was performed to allow cell populations to be followed through the cell cycle. For this purpose, ATM-deficient H1395 ($^{ATM-/p53+}$) and p53-deficient H2087 ($^{ATM+/p53-}$) cells were pulse labelled with BrdU followed by treatment

with VE-821 (1 μM), IR (10 Gy), or a combination of both. Cells were analysed by FACS 24 h and 48 h after treatment.

Subsequent to BrdU exposure, the passage of BrdU-labelled cells through G2-phase and mitosis into G1-phase could be followed in vehicle control treated cells in both cell lines within 24 h (Figure 4.11a, b). After irradiation with 10 Gy, both cell lines showed accumulation of BrdU pulse labelled cells in the G2/M-Phase of the cell cycle, indicating activation of the DNA damage-induced G2/M cell cycle checkpoint. When combining radiation treatment with ATRi, BrdU labelled cells continued through mitosis and appeared in G1 within 24 h, consistent with an abrogation of the G2/M cell cycle arrest by VE-821 (Figure 4.11). 48 h post irradiation and VE-821 treatment, further dilution of the BrdU label was observed in p53-deficient H2087 cells, as cells continued to pass through the cell cycle. In particular, a substantial population of S-phase cells was evident (Figure 4.11a). Strikingly, however, cells with retained p53 function ($H1395^{ATM-/p53+}$) remained in G1-phase of the cell cycle, even 48 h after treatment, pointing towards a potential activation of a post-mitotic G1 cell cycle arrest (Figure 4.11b).

To further investigate this possibility, $A549^{ATM+/p53+}$, $H1395^{ATM-/p53+}$ and $H2087^{ATM+/p53-}$ cells were treated as outlined above and processed for immunoblot analysis. The analysis showed an increase in p53 phosphorylation (S15) and protein levels in p53 wild-type $A549^{ATM+/p53+}$ and $H1395^{ATM-/p53+}$ cells following treatment with IR alone or in combination with VE-821. This correlated with an increase in p21 levels, consistent with the induction of a G1 cell cycle arrest - despite the lack of ATM activity in the H1395 cell line (Figure 4.12a). Both cell lines showed a marked reduction in cyclin A and phospho-histone H3 (pHH3 S10) levels, particularly 48 h after treatment.

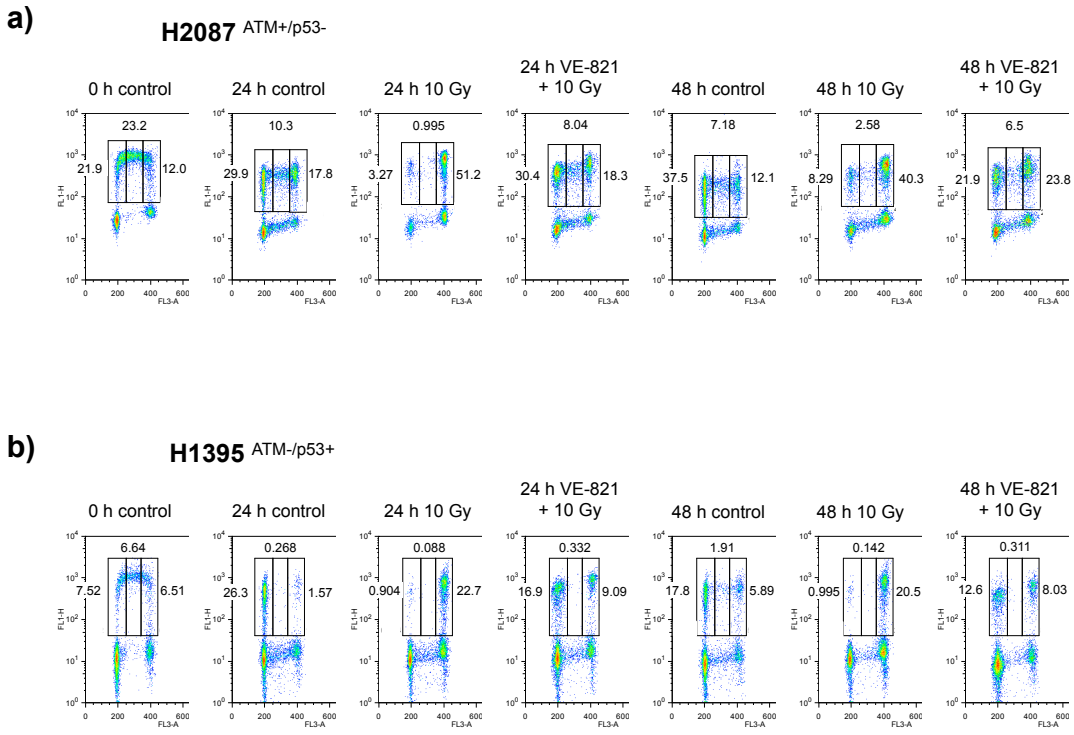

Figure 4.11: VE-821 treatment abrogates the IR-induced G2/M cell cycle arrest, but cells with retained p53 function induce a post-mitotic G1 cell cycle arrest.

To follow cells through the cell cycle, asynchronous populations of **a)** H2087 and **b)** H1395 cells were pulse labelled with BrdU for 30 min before treatment with VE-821 (1 μM), 10 Gy or a combination of both. Cells were harvested, fixed, and stained with PI and anti-BrdU antibody for analysis by flow cytometry at 24 h and 48 h after beginning treatment. Diagrams are representative of two independent experiments. The gates represent BrdU-labelled cell populations (from left to right) - G1/early S-phase, intra-S-phase and late S-/G2/M-phase.

Phosphorylation of histone H3 (HH3) is a marker for mitotic cells, while expression of cyclin A is associated with cells in S- and G2-phase of the cell cycle. This observed decrease in S-/G2- and M-phase cells is in agreement with the observed G1-retention and depletion of S-phase cells observed in H1395 in FACS analysis following co-treatment with IR and VE-821. Interestingly, a similar, yet less pronounced decrease in cyclin A and pHH3 levels could be observed in both p53 wt (A549 and H1395) cell lines following 48 h treatment with VE-821 indicating that the ATR inhibitor may, by

itself, generate low levels of DNA damage leading to activation of a DDR and induction of G1 cell cycle arrest. This is supported by the induction of pATM S1981 in A549 cells treated with VE-821 for 48 h (Figure 4.12a). H2087 cells, on the other hand, showed no significant reduction in pHH3 or cyclin A levels in cells co-treated with 10 Gy and VE-821 compared to control (Figure 4.12b). This finding supports the FACS data showing re-entry of cells into S-/G2-phase following passage through mitosis after DNA damage induction.

These results demonstrate that VE-821 treatment can lead to abrogation of the IR induced G2/M cell cycle arrest in both, p53-proficient and -deficient cells. However, cells proficient in p53 activate a post-mitotic G1 checkpoint, even in the absence of functional ATM (H1395), while p53-deficient cells continue to pass through the cell cycle, entering the next S-phase. DNA replication in the presence of DNA damage, however, could lead to induction of replication stress and, in the presence of an ATR inhibitor, cause more DNA damage due to collapse of stalled replication forks, leading to an accumulation of DNA damage over time.

ATM is believed to be the principal mediator of p53 activation in response to IR, rendering the observed IR-induced phosphorylation and activation of p53 in cells deficient in ATM signalling rather surprising. However, several studies have suggested that ATR (Tibbetts *et al*, 1999; Lakin *et al*, 1999) and DNA-PK (Lees-Miller *et al*, 1992; Shieh *et al*, 1997) also phosphorylate p53 at serine 15 in response to DNA damage. In fact, the observed phosphorylation of p53 following IR was slightly attenuated in H1395 cells when irradiation was combined with VE-821 treatment suggesting that ATR may contribute to this phosphorylation event.

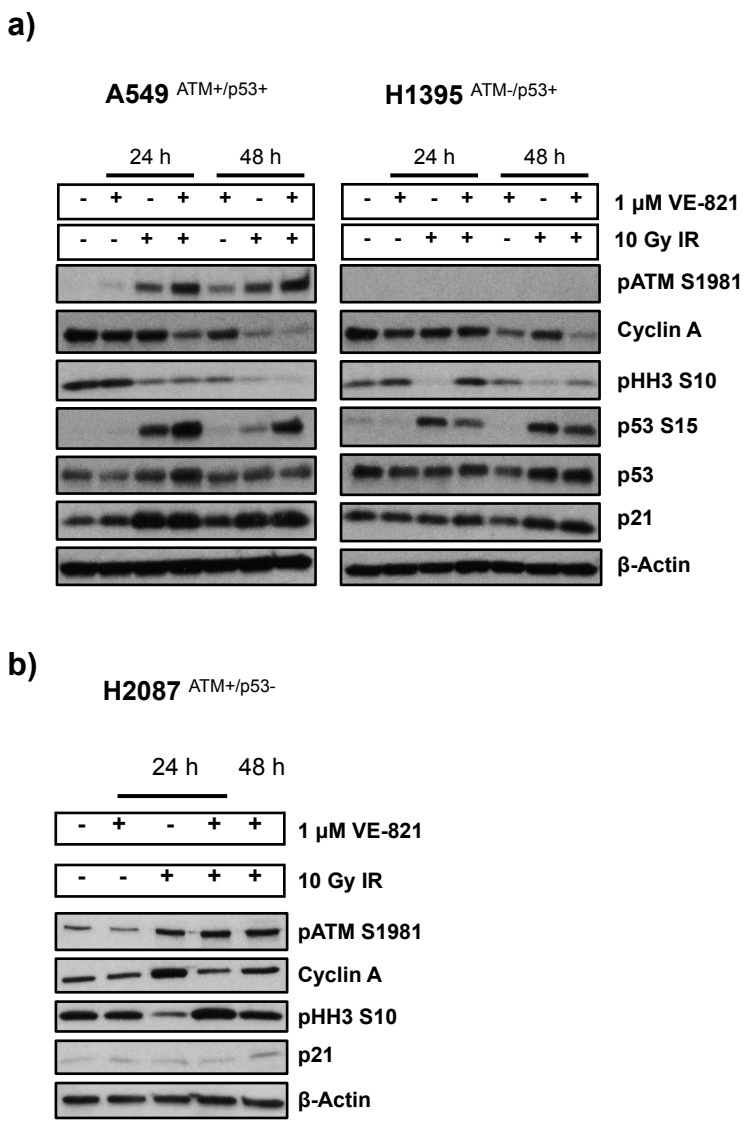

Figure 4.12: P53-proficient cells show signs of G1 checkpoint activation in response to IR, irrespective of the functional status of ATM.

a) p53-proficient H1395 and A549 cells were treated with 1 µM VE-821, 10 Gy or a combination of both. 24 h and 48 h after beginning treatment cells were lysed and processed for western blot analysis. β-Actin served as loading control. **b)** p53-deficient H2087 cells were treated and processed for western blot as in a).

It is also possible that residual amounts of ATM were present in H1395 cells, providing sufficient activity to mediate p53 phosphorylation in response to IR or that VE-821-mediated ATR inhibition was insufficient to completely abolish p53 phosphorylation.

To address this question, H1395 cells were treated with IR and VE-821 as outlined above, but this time an ATM inhibitor (KU55933, 10 μM) or a DNA-PKcs inhibitor (NU7441, 1 μM) were added. However, neither inhibition of ATM, nor DNA-PKcs in addition to ATR was able to reduce or abolish the observed residual phosphorylation and activation of p53 (Figure 4.13a) Furthermore, treatment of cells with IR and another ATR inhibitor (VE-822) also failed to inhibit p53 S15 phosphorylation (Figure 4.13b).

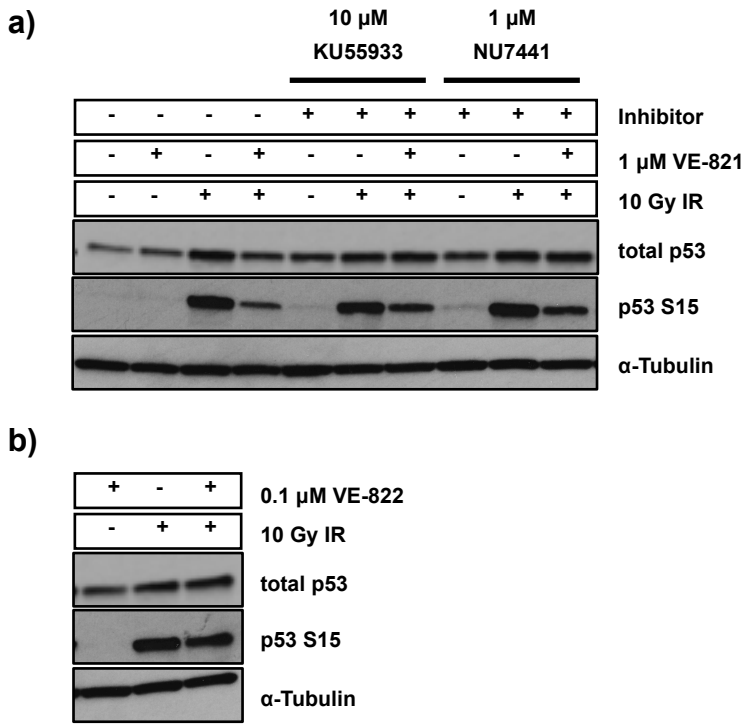

Figure 4.13: ATM-deficient cells activate p53 in response to IR, independently of DNA-PKcs or ATR activity.

a) Western blot analysis demonstrating the occurrence of p53 phosphorylation (S15) in H1395$^{ATM-/p53+}$ cells following 10 Gy IR. This phosphorylation even persisted when IR was combined with VE-821 (1 μM) or a combination of VE-821 and ATMi (KU55933, 10 μM) or DNA-PKi (NU7441, 1 μM). Lysates were prepared 24 h after IR. Images are representative of two experiments. **b)** Western blot analysis following treatment with 10 Gy IR, VE-822 (0.1 μM) or a combination of both. Lysates were prepared 24 h after IR. Images are representative of two experiments. α-Tubulin served as loading control.

These data suggest that p53 may be able to perform ATM- and ATR-independent cell cycle checkpoint functions in response to DNA damage.

4.5 ATR inhibition sensitises NSCLC cells to gemcitabine and cisplatin treatment

We next sought to investigate the impact of ATR inhibition on the cellular response to genotoxic chemotherapy. First, we assessed whether ATRi sensitises NSCLC cells to gemcitabine treatment. For this purpose, a panel of NSCLC and non-tumour cell lines were exposed to dilution series of gemcitabine with or without addition of VE-822 (0.1 μM) or AZD6738 (1 μM) at a fixed concentration. Cell proliferation was assessed 3 days after beginning treatment by resazurin assay.

We found that both ATR inhibitors broadly sensitised NSCLC as well as normal tissue control cell lines to gemcitabine treatment. The sensitising effect was, however, generally more pronounced in p53-defective cell lines compared with p53 wild-type controls (Figure 4.14; Table 4.2).

Our previous results had already demonstrated that combining gemcitabine treatment with ATR inhibition leads to a strong and dose-dependent induction of DNA DSBs (up-regulation of ATM signalling and γH2AX; see Figure 4.1). Furthermore, we found that p53-defective cells showed an increase in the levels of phospho-histone H3 (pHH3) when AZD6738 was added to gemcitabine treatment (Figure 4.15a). As pHH3 (S10) is a biomarker for mitotic cells, this observation indicates that ATR inhibition leads to abrogation of the gemcitabine induced intra-S-phase and G2/M cell cycle checkpoints, thereby promoting premature mitotic entry. Cells with retained p53

function (A427), on the other hand, showed no increase in pHH3 levels, but rather a decrease when compared with the control (Figure 4.15b). This finding further supports our previous results, which demonstrated important DNA damage checkpoint functions of p53 following ATR inhibition.

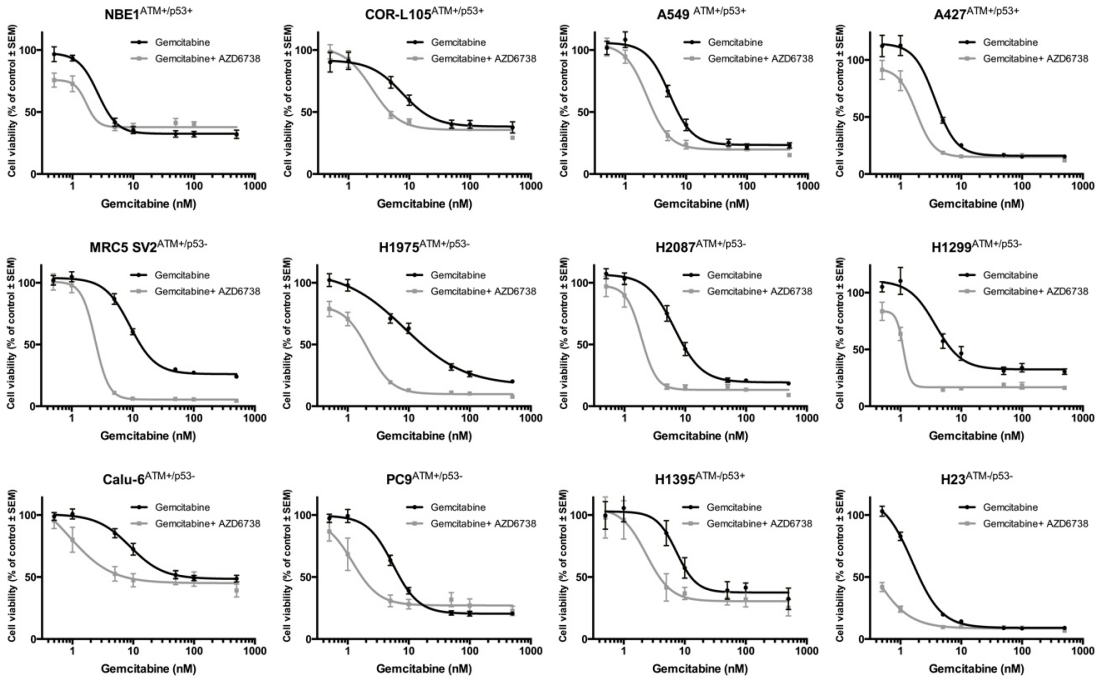

Figure 4.14: AZD6738 broadly sensitises p53-deficient NSCLC cells to gemcitabine treatment.

A panel of NSCLC cell lines and non-tumour cell line controls (NBE1 and MRC5 SV2) were exposed to a dilution series of gemcitabine with or without addition of AZD6738 at a fixed concentration of 1 μM for 3 days. Diagrams show means ± SEM of at least two (COR-L105, H23, A427, H1395) or three (remaining cell lines) independent experiments, each performed in triplicate, respectively.

Table 4.2: Sensitisation of NSCLC cell lines to gemcitabine by ATR inhibitors.

Cell line	ATM status	p53 status	Gemcitabine mean IC_{50} [nM] (-/+ SEM, range)	Gemcitabine mean IC_{50} [nM] in the presence of 0.1 μM VE-822 [26] (-/+ SEM, range)	Gemcitabine mean IC_{50} [nM] in the presence of 1 μM AZD6738 [27] (-/+ SEM, range)
A549	wt (+)	wt (+)	12.8 (10.8-15.2)	4.9 (4.3-5.6)	3.8 (3.4-4.4)
A427	wt (+)	wt (+)	5.3 (4.7-6.0)	3.9 (3.2-4.7)	2.4 (2.1-2.8)
COR-L105	wt (+)	wt (+)	50.8 (42.9-60.2)	27.5 (20.2-37.4)	18.3 (14.0-24.0)
NBE1	wt (+)	wt (+)	11.6 (9.1-14.6)	6.2 (4.5-8.5)	30.2 (22.1-41.1)
MRC5 SV2	wt (+)	SV-40 transf. (-)	26.4 (23.4-29.9)	4.0 (3.7-4.3)	2.8 (2.4-3.2)
H2087	wt (+)	mut. (-)	26.9 (22.0-33.0)	3.3 (3.0-3.6)	7.4 (6.9-7.9)
H1975	wt (+)	mut. (-)	22.8 (20.1-25.9)	4.3 (3.9-4.8)	1.8 (1.7-2.0)
H1299	wt (+)	mut. (-)	27.7 (23.0-33.5)	2.3 (2.0-2.6)	1.7 (1.5-2.0)
Calu-6	wt (+)	mut. (-)	151.1 (119.9-190.4)	10.6 (8.5-13.2)	44.4 (28.6-68.9)
PC-9	wt (+)	mut. (-)	10.3 (9.1-11.7)	3.1 (2.8-3.5)	4.17 (2.9-5.9)
H1395	mut. (-)	wt (+)	75.1 (64.9-87.0)	21.1 (17.2-26.0)	11.1 (9.0-13.7)
H23	mut. (-)	mut. (-)	4.7 (4.2-5.4)	0.66 (0.64-0.68)	0.17 (0.13-0.22)

26. Values were normalised to 0.1 μM VE-822 treated cells.
27. Values were normalised to 1 μM AZD6738 treated cells.

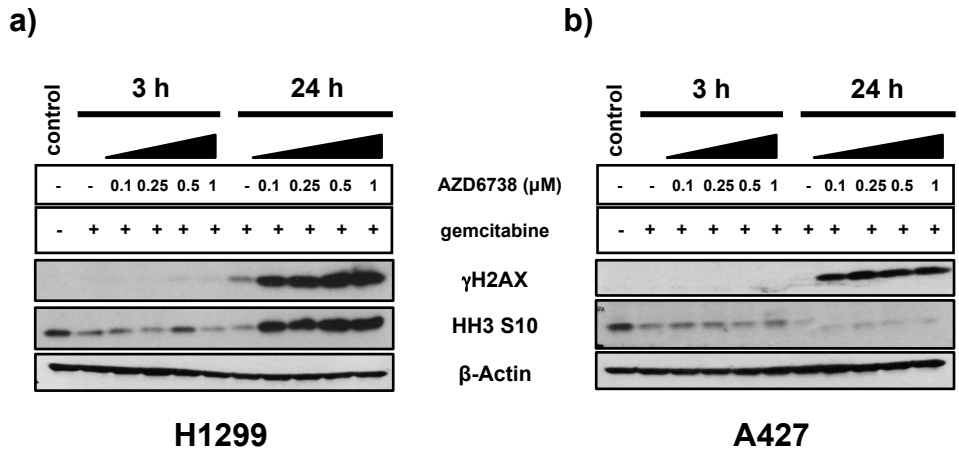

Figure 4.15: ATR inhibition leads to abrogation of the gemcitabine-induced cell cycle arrest in p53-defective cells.

Western blot analysis of **a)** H1299 (p53-) and **b)** A427 (p53+) cells treated with gemcitabine (50 nM), or a combination of gemcitabine and AZD6738 (0.1 - 1 μM) for 3 h or 24 h.

Next, we assessed the impact of ATRi on the sensitivity of cells to cisplatin, which binds DNA to form intra- and inter-strand crosslinks between purine bases. These adducts impair DNA replication and can lead to stalling of replication forks and the formation of DNA DSBs.

Similar to the results obtained using gemcitabine, we found that ATRi broadly sensitised NSCLC cell lines to cisplatin treatment and the sensitising effect was generally more pronounced in p53-defective cell lines compared with p53 wild-type controls. Interestingly, ATR depletion in ATM-defective cells (H1395, H23) resulted in substantial sensitisation to cisplatin, independently of p53 function (Figure 4.16; Table 4.3). This observation suggests that combining pharmacological ATR inhibition with cisplatin treatment may be selectively more cytotoxic for cells defective in ATM or p53 and could therefore have utility for the treatment of ATM- or p53-mutated NSCLC. However, further studies will be required to confirm this hypothesis.

Table 4.3: Sensitisation of NSCLC cell lines to cisplatin by ATR inhibitors.

Cell line	ATM status	p53 status	Cisplatin mean IC_{50} [μM] (-/+ SEM, range)	Cisplatin mean IC_{50} [μM] in the presence of 0.1 μM VE-822 [28] (-/+ SEM, range)	Cisplatin mean IC_{50} [μM] in the presence of 1 μM AZD6738 [29] (-/+ SEM, range)
A549	wt (+)	wt (+)	5.9 (5.4-6.4)	2.8 (2.4-3.3)	3.5 (3.0-4.1)
A427	wt (+)	wt (+)	3.9 (3.6-4.2)	2.2 (1.9-2.6)	1.2 (1.1-1.4)
COR-L105	wt (+)	wt (+)	3.0 (2.8-3.2)	2.9 (2.6-3.2)	1.6 (1.5-1.7)
NBE1	wt (+)	wt (+)	8.3 (7.7-8.9)	8.0 (7.2-8.9)	4.7 (4.4-5.1)
H2087	wt (+)	mut. (-)	3.2 (3.0-3.5)	1.2 (1.0-1.3)	0.65 (0.6-0.7)
H1975	wt (+)	mut. (-)	8.1 (7.6-8.6)	2.0 (1.8-2.2)	1.1 (1.0-1.2)
H1299	wt (+)	mut. (-)	7.5 (7.0-8.1)	2.0 (1.8-2.2)	1.3 (1.2-1.4)
H1395	mut. (-)	wt (+)	6.9 (6.5-7.2)	2.2 (1.9-2.5)	0.5 (0.4-0.6)
H23	mut. (-)	mut. (-)	3.0 (2.8-3.2)	0.7 (0.6-0.8)	0.18 (0.15-0.22)

28. Values were normalised to 0.1 μM VE-822 treated cells.
29. Values were normalised to 1 μM AZD6738 treated cells.

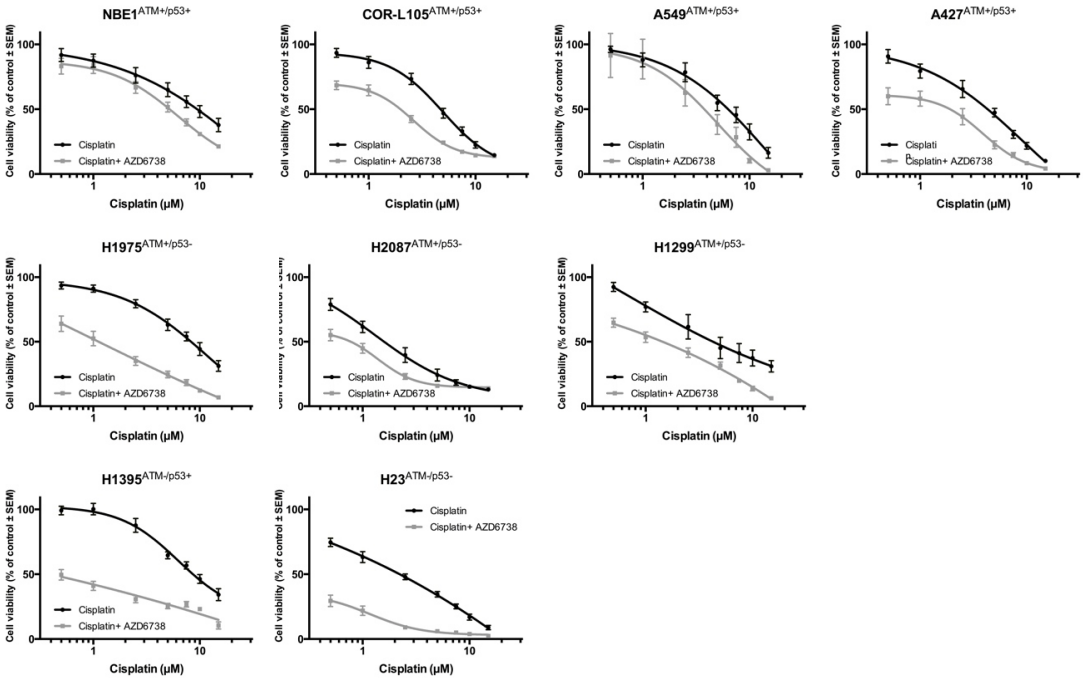

Figure 4.16: ATR inhibition sensitises NSCLC cells to cisplatin.

A panel of NSCLC cell lines and a bronchial epithelial cell line control (NBE1) were exposed to a dilution series of cisplatin with or without addition of AZD6738 at a fixed concentration of 1 μM for 3 days. Diagrams show means ± SEM of at least two (A427, A549) or three (remaining cell lines) independent experiments, each performed in triplicate, respectively.

4.6 Discussion

A previous study suggested that combining genotoxic modalities with pharmacological ATR inhibition (ATRi) has the potential to selectively kill cancer cells deficient in either ATM or p53 (Reaper *et al*, 2011). As both ATM and p53 are frequently mutated and inactivated in NSCLC (Cancer Genome Atlas Research Network, 2014, 2012b), we sought to assess the utility of ATRi for the treatment of NSCLC.

ATR is a central kinase involved in the DDR and is particularly important for responses to DNA replication stress (Cimprich & Cortez, 2008; Nam & Cortez, 2011). Stalling of replication forks due to DNA damage induced by genotoxic agents activates the ATR signalling pathway, which in turn induces transient cell cycle arrest, replication fork stabilisation and restart of DNA replication following resolution of the stress source. In the presence of an ATR inhibitor, however, such stalled replication forks would collapse causing the formation of DNA DSBs, which in turn activate ATM to enforce cell cycle checkpoint activation and facilitate DNA repair to ensure survival of the cells.

The present study provides two pieces of supporting data for this model. Firstly, we observed induction of ATM phosphorylation in A549 cells following treatment with the specific ATR inhibitor VE-821. Secondly, when replication stress was induced by treatment of cells with gemcitabine, the addition of ATR inhibitors (VE-821, VE-822 or AZD6738) led to a significant increase in ATM activation and formation of DNA DSBs, measured by γH2AX levels. This led us to hypothesise that loss of ATM function would lead to accumulation of DNA damage when ATR activity was inhibited.

However, while p53-deficient cells were generally more sensitive to the ATR inhibitors VE-822 and AZD6738 in standard (2D) cell culture proliferation assays, loss of ATM function alone did not confer sensitivity to any of the ATR inhibitors in 2D or spheroid (3D) cell culture assays. At the same time, we found that ATRi induced substantial cytotoxicity in cells deficient in both ATM and p53, as a single agent as well as in combination with IR. This increased sensitivity of ATM- and p53-deficient cells to ATR inhibition will be addressed further in the next chapter.

A limitation of the current work is that the effect of p53-deficiency on ATR inhibitor sensitivity was assessed in a panel of NSCLC cell lines and the presence of other somatic mutations may have masked the effect to some extent. Future studies to confirm the role of p53 in this response could include the use of paired isogenic cell lines with/without functional p53.

Since cells with functional loss of ATM are defective in the G1 checkpoint they are believed to rely on the intra-S and G2/M checkpoints to arrest cell cycle following DNA damage (Kastan *et al*, 1992). ATR is an important mediator of the intra-S and G2/M cell cycle arrest in such cells and consistent with previous reports (Fokas *et al*, 2012; Prevo *et al*, 2012) we were able to show that ATRi abrogates the IR-induced G2/M cell cycle arrest in both p53-proficient and –deficient cells. Surprisingly, however, we found that p53-proficient cells were able to induce a post-mitotic G1 cell cycle arrest following induction of DNA damage by IR, even in the absence of functional ATM.

This G1 cell-cycle arrest was associated with increased p53 and p21 protein levels, increased phosphorylation (S15) of p53 and reduced cyclin A and phospho-histone H3 levels. We only observed induction of this p53-dependent G1 cell-cycle arrest when

ATRi treated ATM-defective cells had passed through the cell cycle including mitosis and not in those cells which were in G1 at the time of irradiation, suggesting an ATM-independent delayed checkpoint response. ATM (Siliciano *et al*, 1997; Canman *et al*, 1998; Banin *et al*, 1998), ATR (Hammond *et al*, 2003; Tibbetts *et al*, 1999) and DNA-PKcs (Lees-Miller *et al*, 1992; Shieh *et al*, 1997) have been shown to be able to phosphorylate p53 on S15. However, we found that neither addition of an ATM or DNA-PKcs, nor of an alternative ATR inhibitor was able to abolish the IR-induced p53 activation. This finding suggests that the observed phosphorylation of p53 is not due to residual amounts of ATM protein in the cells and that in the absence of functional ATM and ATR or DNA-PK, yet another kinase might be able to activate p53 and thus enforce checkpoint function. Further work is required to determine how this p53-dependent post-mitotic G1 cell-cycle arrest is mediated in the absence of functional ATM. This additional work should include the assessment of IR-induced p53 phosphorylation in cells treated with a triple combination of ATR, ATM and DNA-PK inhibitors, to rule out compensation amongst the three pathways when one or two pathways are inhibited. Furthermore, increased concentrations of the inhibitors should be tested to further rule out that incomplete inhibition of ATR or DNA-PK could be responsible for the observed p53 activation.

Furthermore, we found that ATRi (VE-822 or AZD6738) broadly sensitises NSCLC cell lines to gemcitabine and cisplatin treatment. This sensitising effect appeared to be generally more pronounced in p53-deficient cells and was associated with signs of intra-S and G2/M cell cycle checkpoint abrogation (increase in the mitotic cell population) in p53-deficient but not –proficient cells treated with gemcitabine + ATRi. This observation further supports the notion that the cellular response to ATR

inhibitors in combination with replication stress inducing chemotherapy greatly depends on p53 function.

Our conclusion that p53 plays an important role in the cellular response to ATR inhibition is supported by a recent study in mice which demonstrated, that the detrimental effects of ATR-deficiency on cell viability may be ameliorated by p53, since loss of p53 function exacerbated the accumulation of replication stress when ATR signalling was compromised (Murga *et al*, 2010). Functional loss of p53 was also found to profoundly aggravate the severity of ATR loss in adult mice, where simultaneous depletion of p53 and ATR exacerbated tissue degeneration, accompanied by the induction of high levels of DNA damage, and accelerated lethality of the mice (Ruzankina *et al*, 2009).

Pharmacological ATR inhibition furthermore sensitised ATM-deficient cells to cisplatin treatment, independently of the functional status of p53, suggesting that this combination could have clinical utility for the treatment of ATM-deficient NSCLC. However, further studies are required to confirm this observation.

CHAPTER 5

5 Combined pharmacological inhibition of ATM and ATR for the treatment of p53-deficient NSCLC

Our previous results had shown that ATM-defective H23 and GM16666 cells are particularly sensitive to ATR inhibition. As both cell lines are simultaneously deficient in ATM and p53, this observation raised the possibility that the cellular response to pharmacological ATR inhibition is not determined by the functional status of either ATM or p53, but by that of both proteins. This is an intriguing possibility, as ATM and p53 are generally regarded to act in the same signalling pathway, with ATM being the principal mediator of p53 activation in response to DNA damage (Kastan *et al*, 1992; Kastan & Bartek, 2004; Banin *et al*, 1998; Khosravi *et al*, 1999). But, as our previous results had shown, p53 is able to perform ATM independent cell cycle checkpoint functions in response to DNA damage and may therefore protect the cells against the otherwise detrimental effects of ATR inhibition in ATM-deficient cells.

We sought to address this question and to study the molecular mechanisms underlying the increased sensitivity of ATM- and p53-deficient cells to ATR inhibition. Furthermore, we aimed to establish whether p53-deficient cells could be selectively targeted through concomitant inhibition of both ATM and ATR. As p53 is the most commonly mutated tumour suppressor in human cancers, this approach could have broad utility for cancer therapy.

5.1 Combined pharmacological inhibition of ATM and ATR is selectively cytotoxic for p53-deficient cells.

Based on our observations made in cell lines with genetic loss of ATM and p53 activity, we reasoned that combined pharmacological inhibition of ATM and ATR would be selectively cytotoxic for p53-deficient cells. We addressed this possibility by assessing the effect of combined ATM and ATR inhibition on cell proliferation and viability in resazurin assays. P53 wild-type (NBE1, COR-L105 and A549) and p53-deficient (MRC5 SV2, H2087 and H1975) cells were treated with dilution series of VE-821 (1–10 μM dose range) and VE-822 (10-250 nM) with or without addition of the ATM inhibitor KU55933 at a fixed concentration of 10 μM.

We found that addition of the ATM inhibitor markedly increased sensitivity to VE-821 and VE-822 (Figure 5.1; Figure 5.2). Notably, this sensitisation was confined to p53 mutated NSCLC cells (H2087 and H1975) or p53-deficient non-tumour cell controls (MRC5 SV2). In p53 wild-type cells (NBE1, COR-L105 or A549), on the other hand, no or only minimal sensitisation to ATR inhibitor treatment was observed in combination with ATM inhibition (Figure 5.1; Figure 5.2).

a)

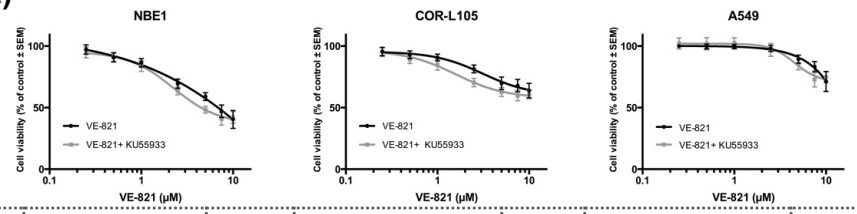

	IC_{50} (μM)	SR	IC_{50} (μM)	SR	IC_{50} (μM)	SR
VE-821	8.3 (7.6-9.0)		12.2 (10.9-13.6)		13.8 (11.5-16.5)	
VE-821 +KU55933	5.4 (4.9-5.9)	1.54	15.2 (12.2-18.9)	0.80	18.3 (25.1-13.4)	0.75

b)

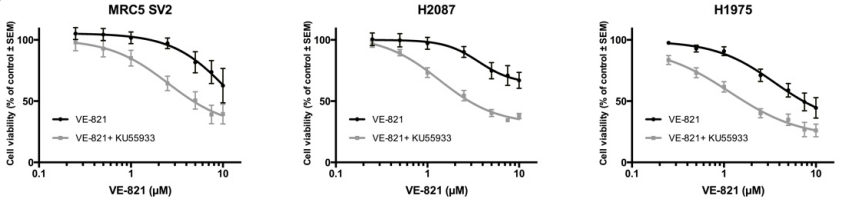

	IC_{50} (μM)	SR	IC_{50} (μM)	SR	IC_{50} (μM)	SR
VE-821	11.0 (9.4-13.0)		10.6 (9.4-12.0)		12.4 (10.7-14.3)	
VE-821 +KU55933	5.3 (4.6-6.1)	2.08	3.8 (3.5-4.0)	2.79	1.9 (1.7-2.1)	6.53

Figure 5.1: Pharmacological inhibition of ATM selectively sensitises p53-deficient cells to VE-821.

a) Assessment of the proliferation response of p53 wild-type (NBE1, COR-L105 and A549) cells to combined inhibition of ATM and ATR. Cells were treated with a dilution series of the ATR inhibitor VE-821 alone or in combination with the ATM inhibitor KU55933 at a fixed concentration (10 μM)[30]. Cell viability was assessed through quantification of resazurin metabolism 5 days after beginning treatment. Points represent the means of three independent experiments each performed in triplicate ± SEM. The table below the graphs summarises the respective IC_{50} values and the sensitisation ratio (SR) for each treatment condition and cell line. The SR represents the -fold sensitisation of VE-821 + KU55933 treatment compared with VE-821 treatment alone and is calculated as the ratio of mean IC_{50} values.
b) Assessment of the response of p53-deficient cells (MRC5 SV2, H2087 and H1975) to combined ATM and ATR inhibition. Treatment and analysis as in a).

30. For the combination treatments, values were normalised to 10 μM KU55933 treated cells.

a)

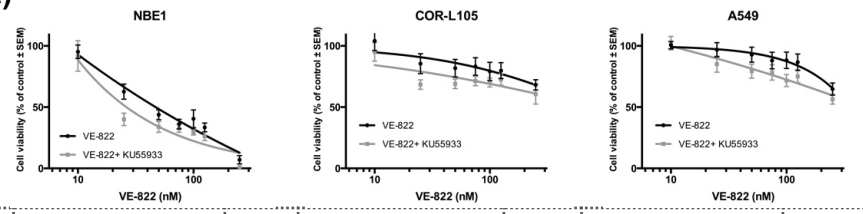

	IC_{50} (nM)	SR	IC_{50} (nM)	SR	IC_{50} (nM)	SR
VE-822	122.1 (112.8-132.3)		940.2 (404.2-954.6)		621.2 (404.2-954.6)	
VE-822 +KU55933	31.8 (27.9-36.2)	3.8	813.8 (367.4-1803)	1.16	364.5 (268-495.7)	1.70

b)

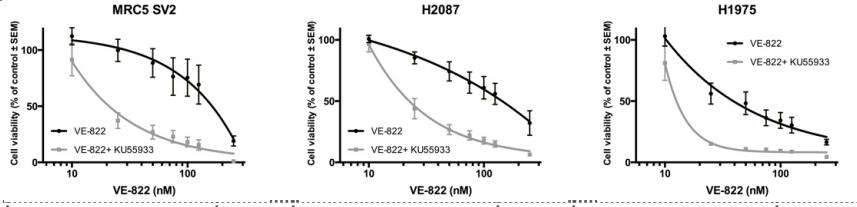

	IC_{50} (nM)	SR	IC_{50} (nM)	SR	IC_{50} (nM)	SR
VE-822	159.8 (138.3-184.8)		214.7 (197-233.9)		148.4 (126.2-174.6)	
VE-822 +KU55933	25.7 (22.4-29.5)	6.22	28.6 (26.2-31.3)	7.51	15.6 (14.4-17.0)	9.51

Figure 5.2: The ATM inhibitor KU55933 selectively sensitises p53-deficient cells to VE-822.

a) p53 wild-type (NBE1, COR-L105 and A549) cells were treated with dilution series of the ATR inhibitor VE-822 with or without addition of KU55933 (10 μM) [31]. Cell viability and proliferation was assessed 5 days after beginning treatment. Points represent the means of three independent experiments each performed in triplicate ± SEM. The table below the graphs summarises the respective IC_{50} values and the SR for each treatment condition and cell line (see Figure 5.1).
b) Assessment of the response of p53-deficient cell lines (MRC5 SV2, H2087 and H1975). Treatment and analysis as in a).

31. For the combination treatments, values were normalised to 10 μM KU55933 treated cells.

Next, we assessed the clonogenic survival of p53 wild-type (A549) and p53 mutant (H2087, H1975 and H23) cells following 48 h treatment with the ATR inhibitor VE-821, the ATM inhibitor KU55933 or a combination of both. In $A549^{ATM+/p53+}$ cells, neither the single nor the combination treatments had a strong effect on clonogenic survival of the cells ($p<0.01$ for VE-821 treatment compared to control; $p<0.01$ for combination of KU55933 and VE-821 compared with KU55933 only, but no statistically significant difference between VE-821 only and the combination; Figure 5.3a).

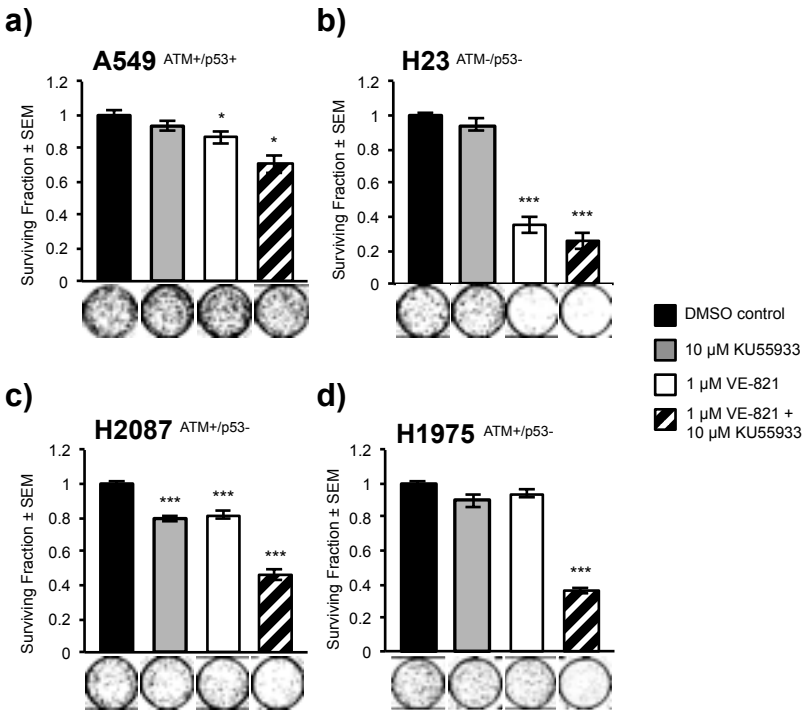

Figure 5.3: Pharmacological inhibition of ATR decreases the clonogenic survival of NSCLC cells with loss or inhibition of both ATM and p53 function.

Clonogenic survival of **a)** A549, **b)** H23, **c)** H2087 and **d)** H1975 cells following 48 h treatment with DMSO (control), 10 μM KU55933, 1 μM VE-821 or a combination of both. Example images of the plates after staining and fixation of the colonies are shown underneath the graph for each condition. Bars represent means of three independent experiments, each performed in triplicate, ± SEM. * = $p<0.01$; *** = $p<0.0001$ calculated by 2-sided Student's t-test (single-treatments were compared to control, combination treatments to each of the single treatments).

As expected from our previous results, KU55933 treatment showed no effect in ATM- and p53-deficient H23 cells, while exposure to VE-821 significantly reduced clonogenic survival by approximately 70% compared with vehicle control or KU55933 treated cells ($p<0.0001$; Figure 5.3b). In the case of $H2087^{ATM+/p53-}$, there was a significant reduction by single-agent treatments (by approximately 20%) but the effect was much less than combination (reduction of clonogenic survival by 55% compared with control; $p<0.0001$ for combination treatment compared with either single agent; Figure 5.3c). In the p53-deficient cell line H1975, neither one of the inhibitors by itself had an effect on colony formation, but the co-treatment with ATM and ATR inhibitors significantly reduced the clonogenic survival by 64% ($p<0.0001$ for combination treatment compared to either single treatment; Figure 5.3d).

Finally, we validated the differential response of p53-proficient and –deficient cells to combined ATM and ATR inhibition in 3D spheroid models. Spheroids of $COR-L105^{ATM+/p53+}$, $A549^{ATM+/p53+}$, $H1299^{ATM+/p53-}$ and $H2087^{ATM+/p53-}$ cells were exposed to the ATR inhibitors VE-821, VE-822 or AZD6738, the ATM inhibitor KU55933 or the combinations for 72 h. Spheroids were then allowed to grow in the absence of the drugs for an additional 7 days. 10 days after beginning treatment, proliferation and cell viability was assessed.

Spheroid growth of p53- and ATM-proficient COR-L105 or A549 cells was not significantly altered by exposure to the ATR inhibitors VE-821 or VE-822 alone, or in combination with KU55933 (Figure 5.4a, b). AZD6738 moderately inhibited spheroid growth by itself (by approximately 25% for COR-L105 and 30% for A549) as well as in combination with the ATM inhibitor (20% for COR-L105 and 40% for A549), however, addition of KU55933 did not significantly increase growth inhibition compared with AZD6738 treatment alone.

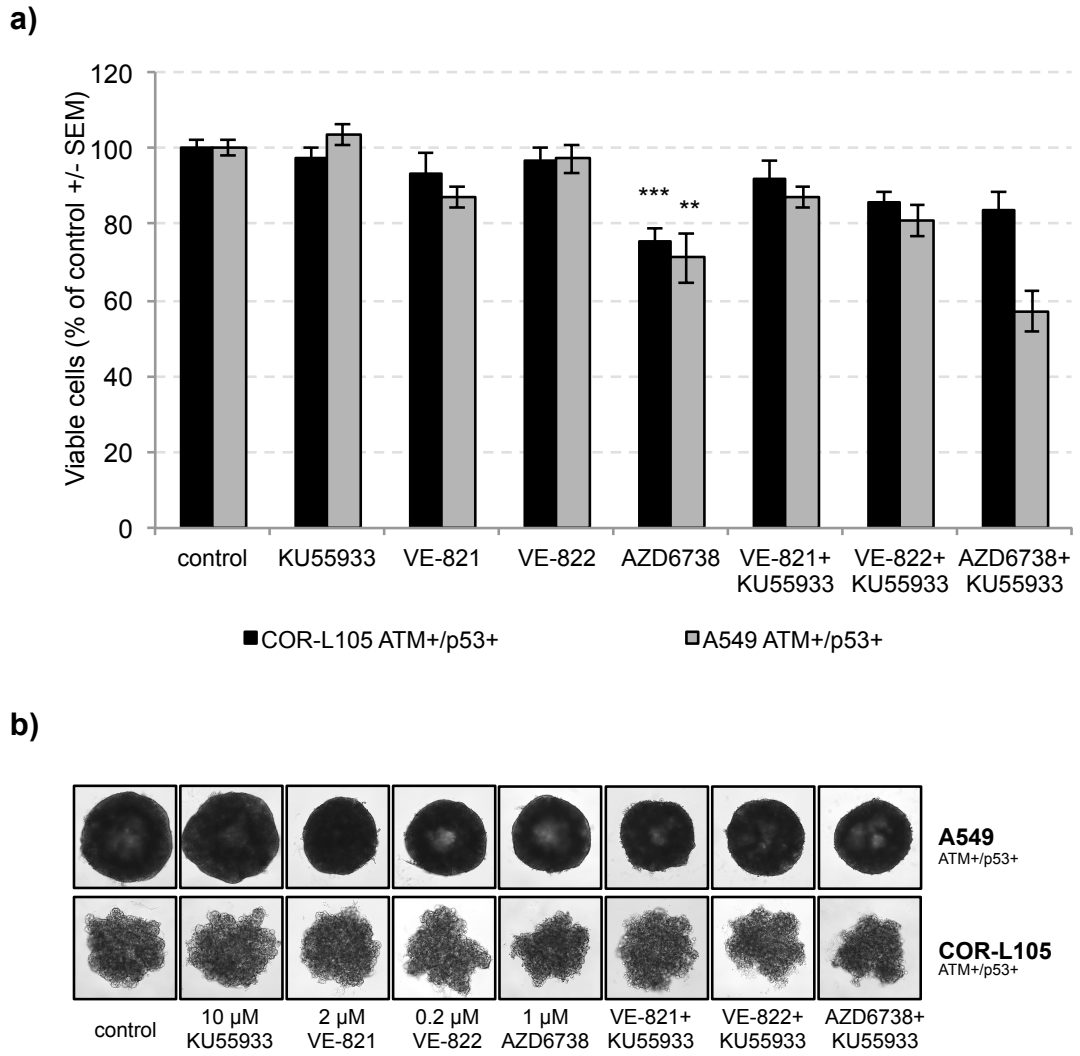

Figure 5.4: Simultaneous inhibition of ATM and ATR causes only minimal growth inhibition in NSCLC spheroids with wild-type p53.

a) Spheroids of COR-L105 and A549 cells were treated with DMSO (control), 2 μM VE-821, 0.2 μM VE-822, 1 μM AZD6738 or 10 μM KU55933, or a combination of the ATM inhibitor (KU55933) with each of the ATR inhibitors, respectively. Treatment was carried out for 72 h. Following a 7-day recovery period in drug-free culture medium, cell viability was assessed by quantification of resazurin metabolism. Bars represent means of three independent experiments, each performed in triplicate, ± SEM. Asterisks indicate statistically significant differences between treatment groups calculated by Student t-test (single treatments were compared with control, combination treatments with the respective ATRi as single-agent). ** = p-values <0.001. *** =p-values <0.0001.
b) Representative images of spheroids treated as in a). Images were taken at a 40x magnification.

In p53-deficient H2087 and H1299 cells, inhibition of ATR or ATM alone caused only little to moderate decrease in spheroid growth and viability. On the other hand, inhibition of both ATM and ATR resulted in substantial cytotoxicity with reduction of spheroid size and viability by 80-90% for H1299 and 40-70% for H2087 ($p<0.0001$ for all combination treatments compared with the respective ATRi single treatments; Figure 5.5a, b).

These findings are consistent with the observation that ATM- and p53-deficient cell lines (H23 and GM16666B) are highly sensitive to ATR inhibitors and led us to conclude that concomitant disruption of both ATM and p53 function increases sensitivity of NSCLC cells to pharmacological ATR inhibition *in vitro*.

5.2 The increased sensitivity of ATM- and p53-deficient NSCLC cells to pharmacological inhibition of ATR is not caused by replication stress

ATR activity is required in all proliferating cells during normal S-phase progression where it plays a major role in the maintenance of genome stability through protection and restart of stalled replication forks and prevention of excessive origin firing (Friedel *et al*, 2009; Paulsen & Cimprich, 2007). Several studies have indicated that genetic depletion of ATR results in the induction of replication stress (Ruzankina *et al*, 2009, 2007). We therefore investigated, whether the observed differential sensitivity of p53-proficient and -deficient cells to inhibition of ATR and ATM could be related to the induction of DNA replication stress.

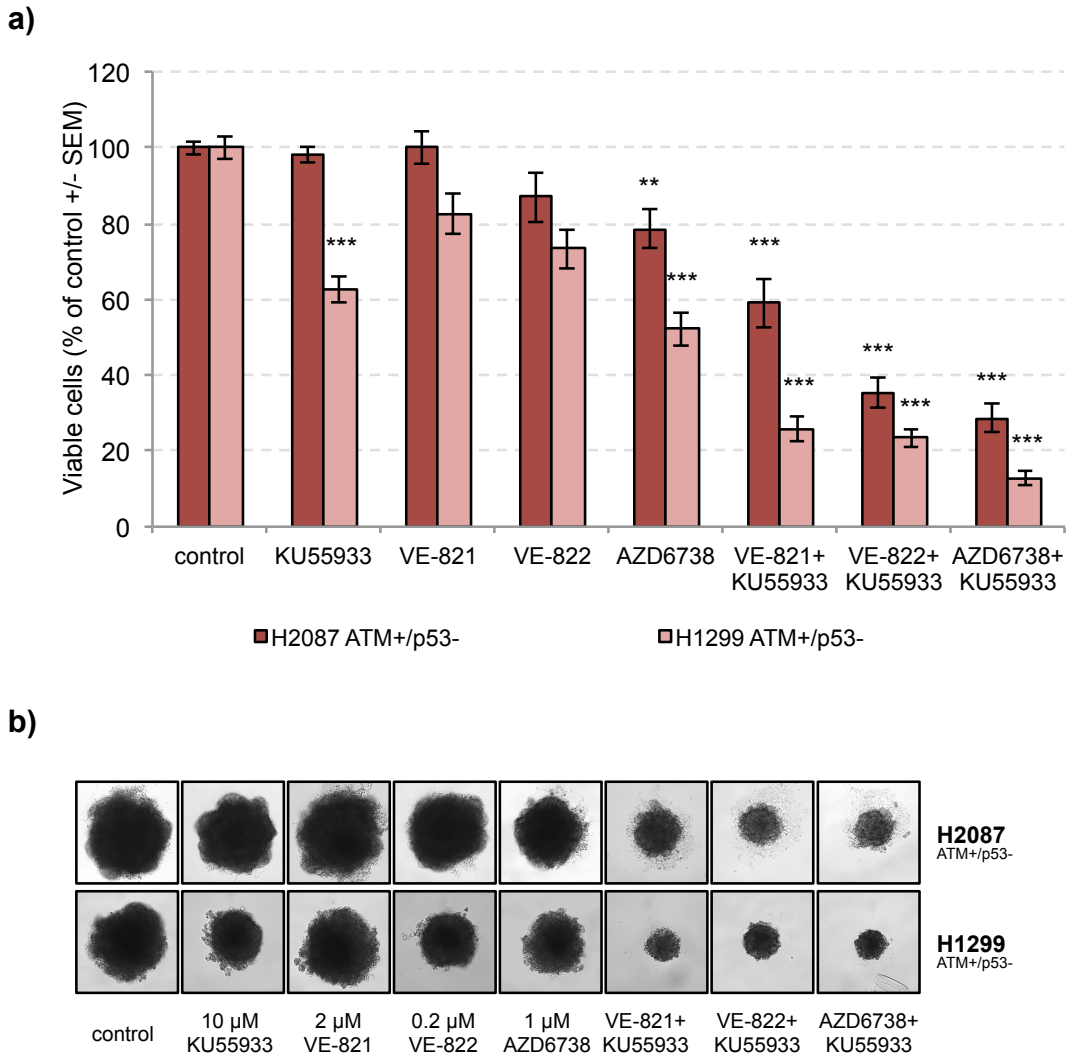

Figure 5.5: Combined inhibition of ATM and ATR is selectively cytotoxic for NSCLC cells deficient in p53.

a) Spheroids of H2087 and H1299 cells were treated with DMSO (control), 2 μM VE-821, 0.2 μM VE-822, 1 μM AZD6738 or 10 μM KU55933, or a combination of the ATM inhibitor with each of the ATR inhibitors, respectively. Treatment was carried out for 72 h. Following a 7-day recovery period in drug-free culture medium, cell viability was assessed by quantification of resazurin metabolism. Bars show means of three independent experiments, each performed in triplicate, ± SEM. ** = p-values <0.001. ***= p-values <0.0001 (calculated by Student's t-test comparing single treatments with control and combination treatments with the respective ATRi single-agent).
b) Representative images of spheroids treated as in a). Images were taken at a 40x magnification.

When replisome progression is halted during DNA replication, helicases continue to unwind the DNA ahead of the replication fork resulting in long stretches of single stranded DNA which is then coated by RPA (Byun *et al*, 2005; Wold, 1997). Therefore, quantification of RPA foci formation can be used as a biomarker for the identification of cells undergoing replication stress.

We used the topoisomerase I inhibitor camptothecin (CPT) as a positive control to assess RPA32 foci formation. CPT inhibits topoisomerase I by blocking the re-joining step of the DNA cleavage/re-ligation reaction, which results in the formation of covalently bound DNA/topoisomerase I reaction intermediates. During S-phase, such adducts hinder the progression of replisomes thereby causing replication stress.

The NSCLC cell lines A549, COR-L105, H2087 and H1975 were exposed to camptothecin (10 μM) for 3 h, followed by fixation, immunofluorescence staining for RPA32 and automated image acquisition on the InCell analyser. As expected, CPT treatment led to the induction of RPA32 foci in all cell lines tested (Figure 5.6a, b). Using the InCell 1000 image analysis software, we determined that a threshold of ≥15 RPA32 foci per cell could reliably differentiate between CPT-treated (replication stress-positive) and DMSO-treated (replication stress-negative) cells. In three out of the four cell lines (A549, H1975 and H2087), CPT treatment led to the induction of replication stress in approximately one third of the cells. In COR-L105 this percentage was much lower (8.4%), though compared with vehicle control, an almost 40-fold increase in the number of cells with ≥15 RPA32 foci was evident.

Next, we measured RPA32 foci formation in cells treated with the ATR inhibitors VE-821, VE-822 or AZD6738 alone or in combination with the ATM inhibitor KU55933 for 48 h. We found that exposure of cells to the ATR inhibitors only minimally

increased the percentage of cells with ≥15 RPA32 foci. In the case of VE-821, only very few cells showed signs of replication stress and we found no correlation with functional status of p53 (Figure 5.6d). VE-822 and AZD6738 were more potent in the induction of RPA32 foci formation (Figure 5.6e, f). However, the overall percentage of cells undergoing replication stress was still rather low in both cases (< 3% for VE-822 and <5% for AZD6738). Furthermore, addition of KU55933 did not significantly alter the amount of replication stress induced by any of the ATR inhibitors. Nor could we see any association between the sensitivity of cells to the combination of ATM and ATR inhibitors and the percentage of RPA32 foci-positive cells. For example, while the H2087 cell line is highly sensitive to combined ATM and ATR inhibition (Figure 5.1b; Figure 5.2b; Figure 5.5), only about 1% of cells showed signs of replication stress as measured by RPA foci formation (Figure 5.6e, f). A similar proportion of cells showed replication stress in A549 and COR-L105 cell lines, which are both rather insensitive to the combination treatment (Figure 5.1a; Figure 5.2a; Figure 5.4).

This observation suggests that induction of replication stress may not be a major contributing factor in conferring the observed high cytotoxicity of the treatment.

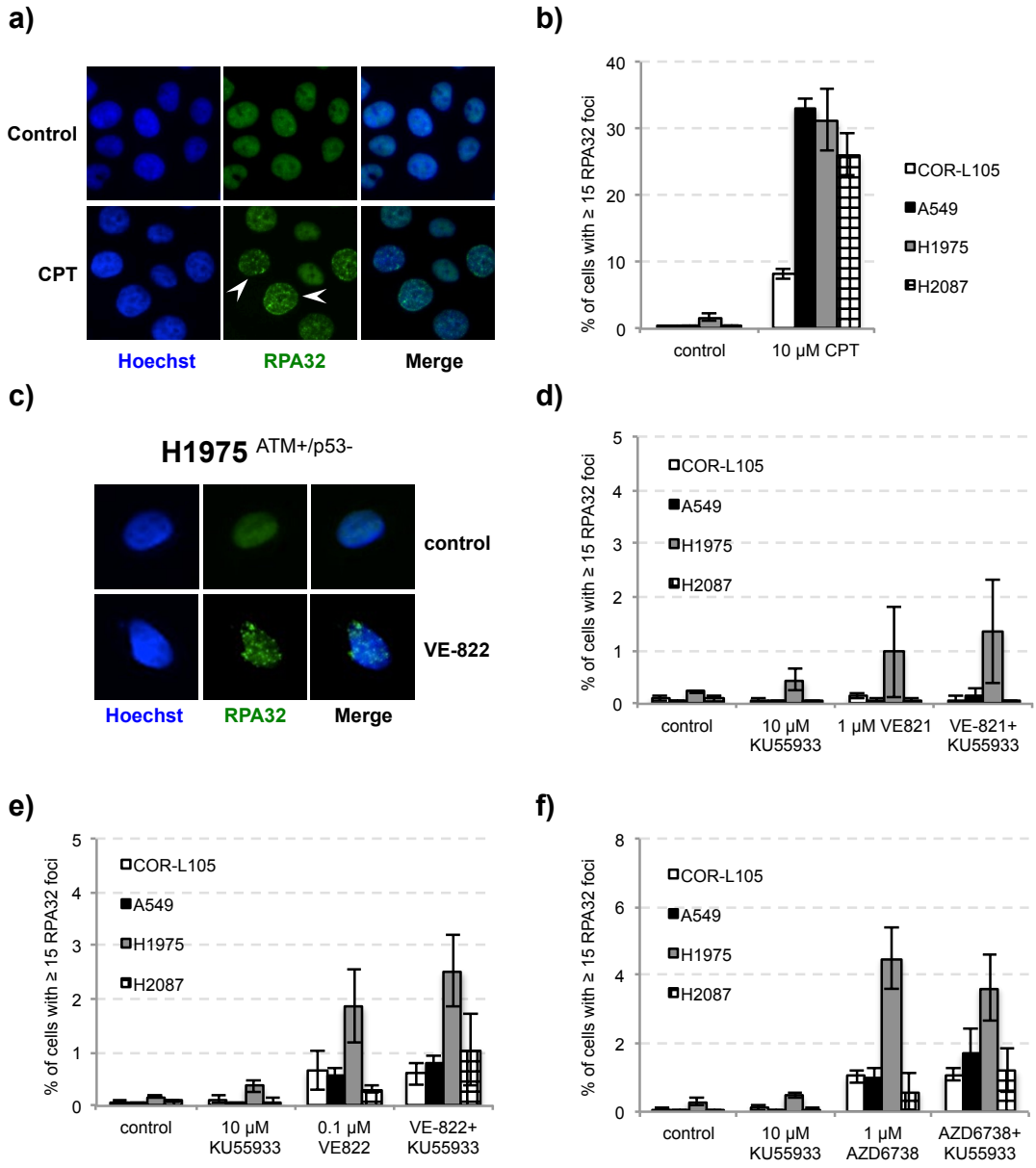

Figure 5.6: Induction of replication stress by pharmacological inhibition of ATR.

a) Representative images of RPA32 foci staining in H1975 cells treated with DMSO (control) or 10 μM CPT for 3 h. Arrowheads indicate cells with >15 RPA32 foci.
b) Quantification of RPA32 foci formation after 3 h treatment as in a). Bars represent the mean percentage of cells with ≥ 15 RPA32 foci ± SEM calculated from two independent experiments, each performed in triplicate.
c) Representative images of a H1975 cell undergoing replication stress following treatment with 0.1 μM VE-822 for 48 h (lower panel). DMSO treated control is also shown (upper panel).
d) to f) COR-L105, A549, H1975 and H2087 cells were treated with 10 μM KU55933, 1 μM VE-821 (d), 0.1 μM VE-822 (e), 1 μM AZD6738 (f) or a combination of the respective ATR inhibitor and KU55933 (48 h). Bars represent the mean percentage of cells with ≥ 15 RPA32 foci ± SEM calculated from three independent experiments each performed in triplicate.

5.3 Concomitant deficiency in ATM, ATR and p53 causes aberrations in mitosis and cell death through mitotic catastrophe.

According to our initial hypothesis, ATR inhibition in ATM depleted cells would lead to an accumulation of DNA DSBs resulting from collapse of stalled replication forks paired with DNA repair defects. Attenuation of the G2/M cell cycle checkpoint through loss or inhibition of both ATM and ATR would then allow cells to enter mitosis in the presence of DNA damage causing errors in mitosis and cell death through mitotic catastrophe.

To address this hypothesis and investigate the mode of cell death associated with the increased sensitivity of p53-deficient cells to combined ATM and ATR inhibition, H2087 cells were exposed to VE-821 and KU55933 for 48 h, followed by preparation of whole cell lysates (including dead cells floating in the media) or fixation for immunofluorescence staining. To investigate, whether cells undergo apoptosis, we monitored cleavage of caspase-3 and of PARP by western blot analysis. Both are prominent characteristics of apoptosis induction. However, we were unable to detect an increase in either marker.

At the same time, we found a substantial increase in the number of aberrant mitoses following concomitant inhibition of both ATM and ATR (Figure 5.7a, b), supporting the concept that cell death might be linked to errors in mitosis. Importantly, mitotic aberrations were confined to p53-mutated cells. Furthermore, ATR inhibitor treatment was accompanied by the formation of micronuclei within 48 hours of initiating treatment (Figure 5.8a, b).

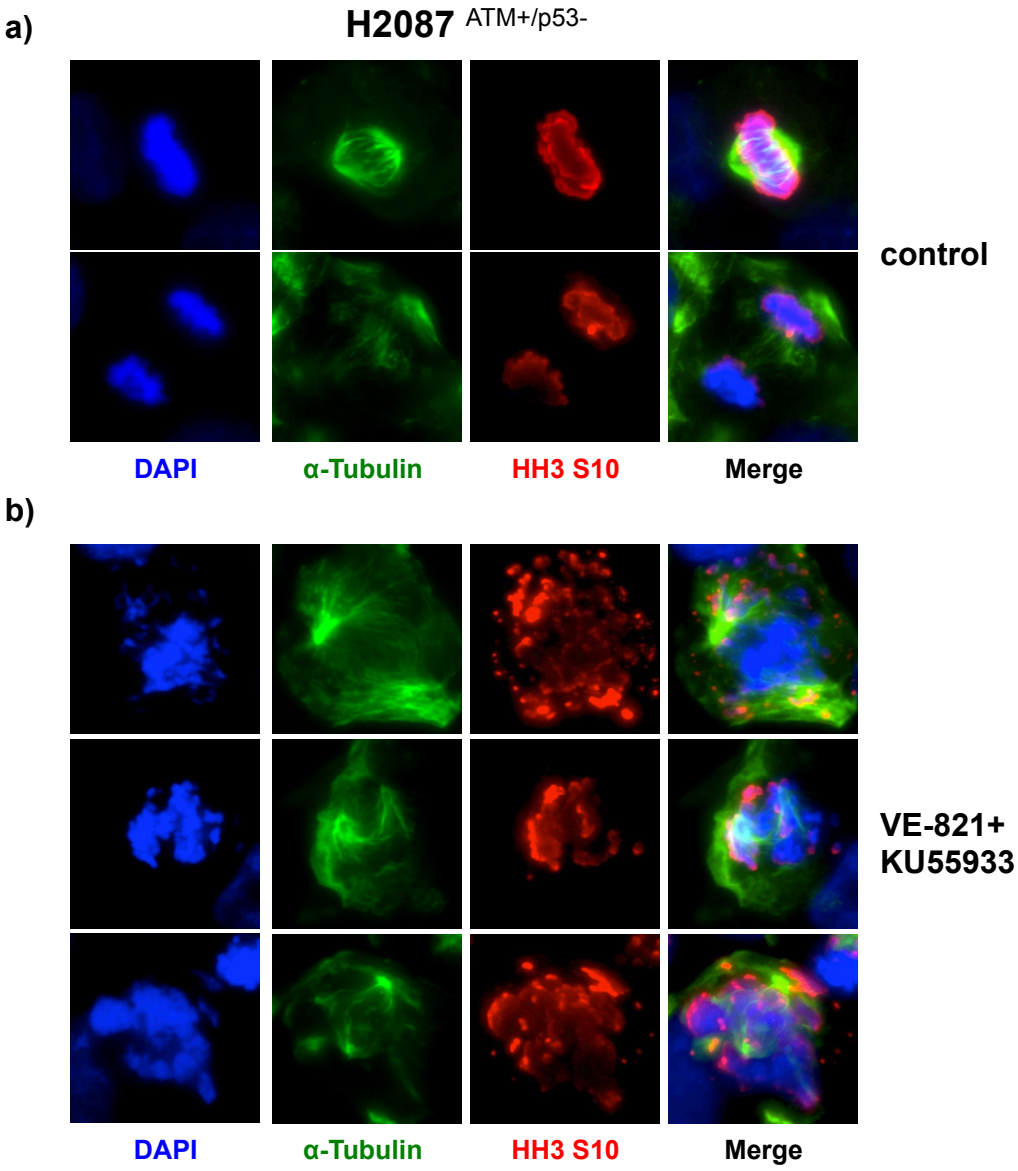

Figure 5.7: Concomitant inhibition of ATM and ATR results in mitotic aberrations and induction of mitotic catastrophe in p53-deficient cells.

a) Representative images of mitotic DMSO treated (control) H2087 cells following immunofluorescence (IF) staining for phospho-Histone H3 (S10) and α-Tubulin.
b) H2087 cells were treated with KU55933 (10 μM) and VE-821 (1 μM) for 48 h followed by IF staining as in a).

Micronuclei result from anaphase lagging chromosomes or can be generated from acentric fragments of chromosomes (Terradas *et al*, 2010) and are, like the occurrence of aberrant mitosis, an established sign of mitotic catastrophe (Portugal *et al*, 2010). Consistently, ATR inhibition induced this phenotype only in cell lines with genetic loss and/or inhibition of both ATM and p53 (H23, H1299, H2087). Cell lines with functional p53 (COR-L105and H1395) on the other hand, showed no signs of micronuclei-formation (Figure 5.8a, b).

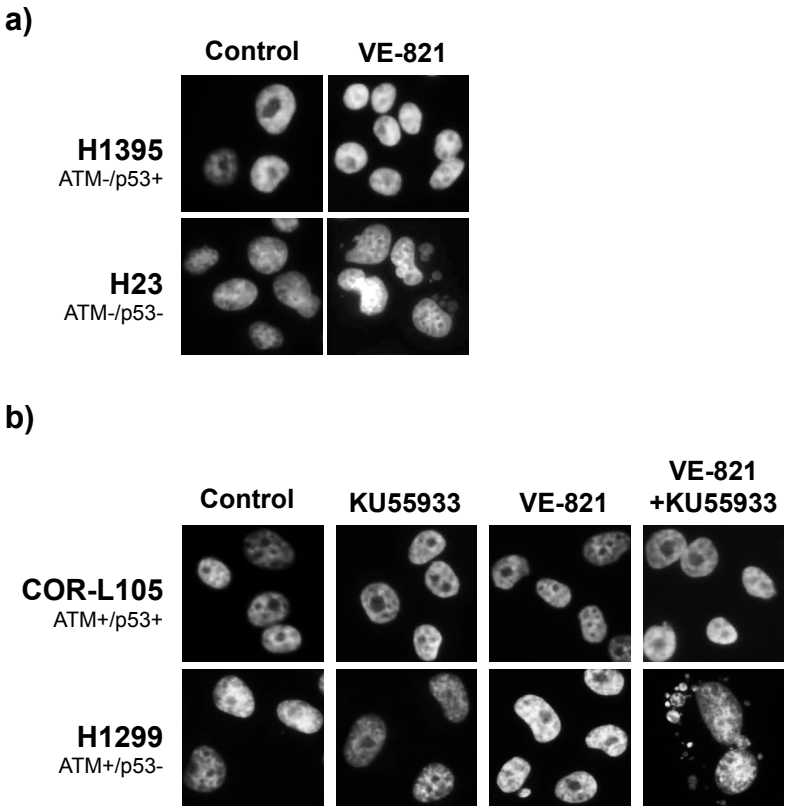

Figure 5.8: Pharmacological ATR inhibition induces micronuclei formation in cells with concomitant deficiency in ATM and p53.

a) DAPI staining demonstrates the induction of micronucleation in ATM- and p53-deficient cells (H23) following 48 h of treatment with VE-821 (1 μM). Cells with retained p53 function (H1395) show no micronuclei formation.
b) Representative images of DAPI nuclear staining of COR-L105 and H1299 cells following 48 h treatment with KU55933 (10 μM), VE-821 (1 μM) or a combination of both.

To further address the question, in which stage of the cell cycle cell death is induced and if it could be linked to errors in mitosis, we generated cell lines, which stably express a red-fluorescent (mCherry-tagged) version of histone H2B. This allows an indirect visualisation of chromosomes in live cell imaging.

First, we followed the cellular response to pharmacological ATR and/or ATM inhibition over a period of 24 h immediately after addition of the drugs and following 48 h pre-treatment. While combined ATM and ATR inhibition had no impact on the fidelity of mitotic segregation of chromosomes in p53-proficient A427 cells, severe mitotic aberrations occurred in p53 null mutant H1299 cells (Figure 5.9a, b). The first signs of mitotic aberrations occurred within 10 h of commencing treatment with VE-821 (1 μM) or VE-822 (0.1 μM) in combination with KU55933 (10 μM). A considerable number of H1299 cells going through mitosis appeared unable to properly align condensed chromosomes in a defined metaphase plate, but rather exhibited irregular masses of chromosomes (Figure 5.9b). Cell death occurred predominantly in mitosis or shortly after mitotic exit and was only rarely observed in interphase cells.

To study the kinetics of mitosis in more detail, cells were followed for 72 h after addition of the drugs (as above), with pictures taken every 15 min. The pictures acquired during live cell imaging were used for single-cell tracking of 50 mitotic cells per cell line and treatment condition. Following combined ATR and ATM inhibition, 54% (VE-821+ KU55933) and 88% (VE-822+ KU55933) of H1299 cells progressing through mitosis exhibited obvious nuclear fragmentation or micronuclei formation around chromosomal material, which may be fragments of chromosomes or lagging chromosomes (Figure 5.9e). 2% (VE-821+ KU55933) and 16% (VE-822+ KU55933)

of H1299 cells underwent mitosis-associated cell death[32] following combined ATM and ATR inhibition (Figure 5.9f; Figure 5.10b).

In p53-proficient A427 cells, only minimal micronuclei formation was observed and most cells exhibited normal metaphase and anaphase figures (Figure 5.9e; Figure 5.11a, b). It should be noted that the combination of VE-822 and KU55933 also induced a considerable increase in mitosis associated cell death in A427 cells compared with control (Figure 5.9f). However, the mitotic index (cells going through mitosis) was notably decreased in this cell line following ATM and ATR inhibition compared with control, suggesting that a proportion of cells might arrest cell cycle progression before mitotic entry.

The median time cells spent in mitosis was also markedly increased in p53-deficient cells treated with a combination of ATM and ATR inhibitors (2.4 h ± 0.3 h for VE-821+ KU55933 and 3.4 h ± 0.4 h for VE-822+ KU55933) compared with control cells (1.1 h ± 0.1 h; Figure 5.9d). In p53-proficient cells, only a small increase in the mitotic residence time was evident (0.58 h ± 0.02 h in control versus 0.63 h ± 0.02 h in VE-821+ KU55933 treated or 1 h ± 0.3 h in VE-822 + KU55933 treated; Figure 5.9c).

Treatment with ATM or ATR inhibitors alone had little or no effect on the kinetics of mitotic progression in either cell line (Figure 5.9c, d). Single-agent ATM or ATR inhibitor treatment induced some micronuclei formation in p53-deficient cells and cell death following mitotic entry, however, the size of the effect was considerably bigger in the combination treatments (Figure 5.9e, f).

32. defined as the fragmentation of the condensed chromatin during mitosis or shortly after mitotic exit, followed by loss of cell movement, indicting cell death (see Figure 5.10b).

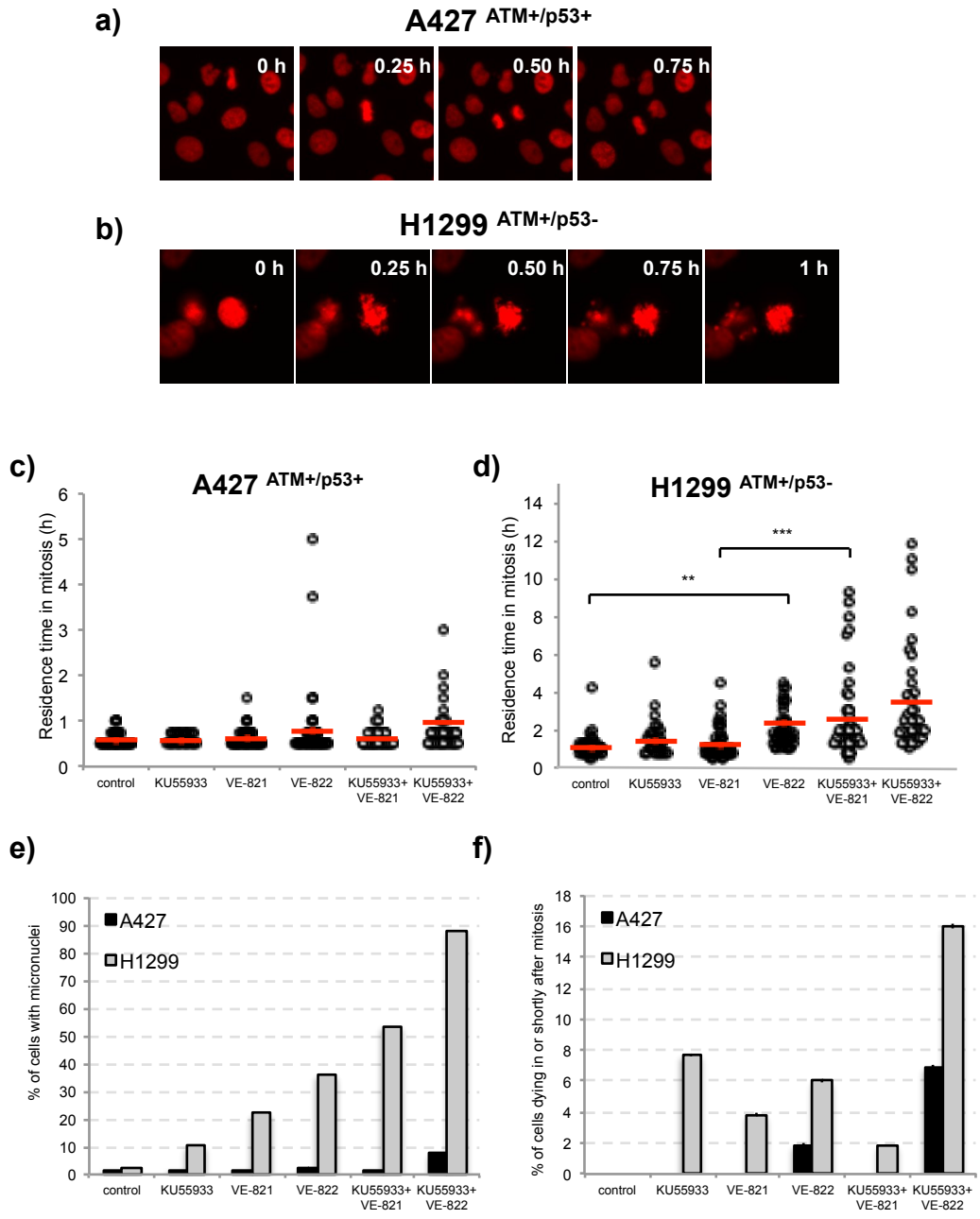

Figure 5.9: Combined ATM and ATR inhibition prolongs the mitotic residence time, induces micronuclei formation and cell death in p53-deficient NSCLC cells.

a) A time-lapse series of an A427 cell going through mitosis after 24 h of pre-treatment with a combination of KU55933 (10 μM) and VE-821 (1 μM). **b)** A time-lapse series of a H1299 cell entering mitosis (treatment as in a). Note the inability of the cell to form a proper metaphase plate and separate its chromosomes. **c) and d)** Quantification of the mitotic residence time following treatment of c) A427 and d) H1299 cells with KU55933 (10 μM), VE-821 (1 μM) or a combination of both. Images were taken in 15 min intervals over a period of 72 h. At least 50 mitotic cells were analysed per treatment condition. Each dot represents one cell, red lines indicate the mean time spent in mitosis for each condition. **= $p<0.001$; ***= $p<0.0001$ calculated by Student's t-test. **e)** Quantification of the percentage of cells showing micronuclei formation after mitotic exit. Treatment as in c) and d). **f)** Quantification of the percentage of cells undergoing cell death during mitosis or shortly after mitotic exit. Treatment as in c) and d).

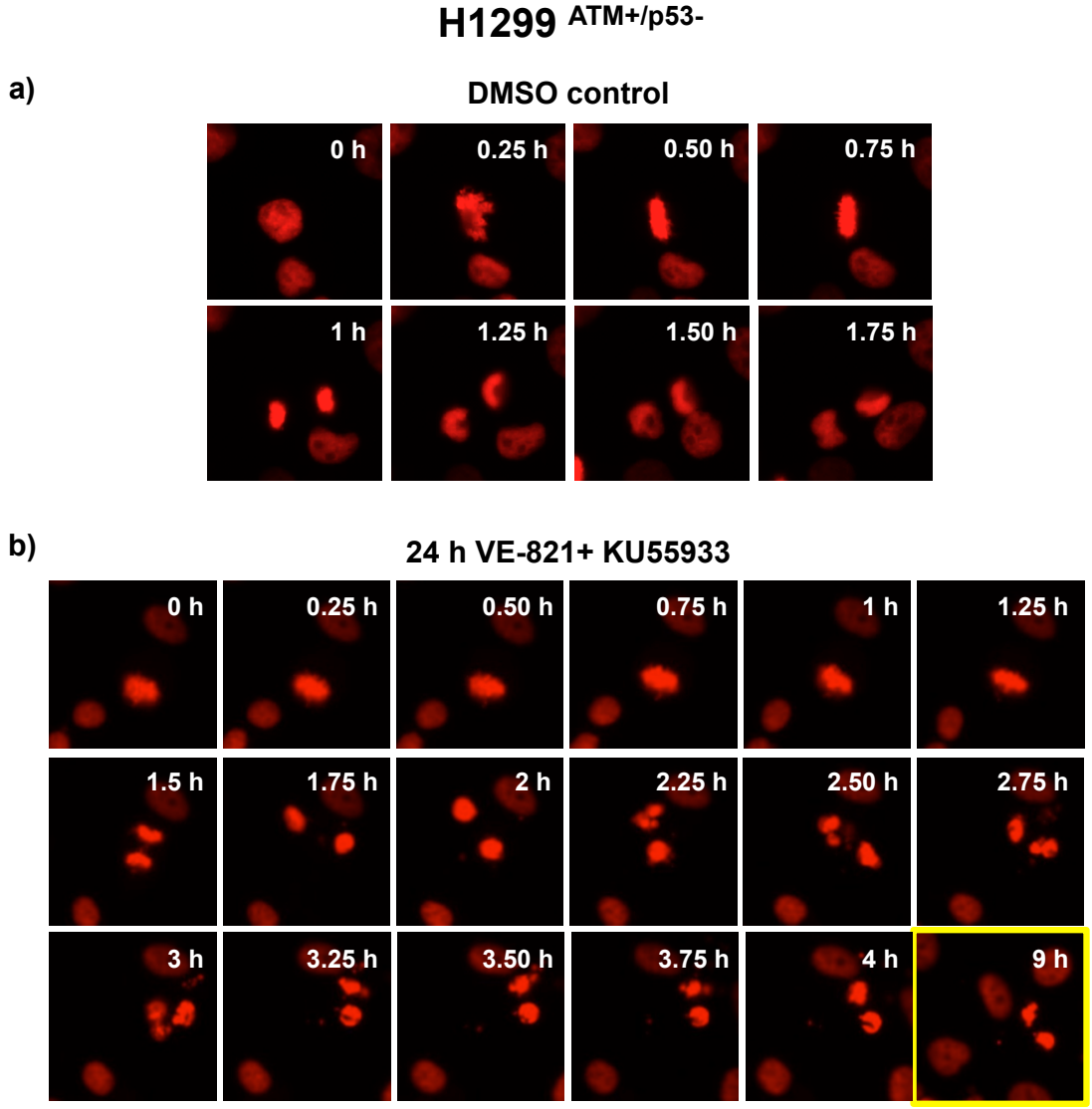

Figure 5.10: Combined ATM and ATR inhibition in p53-deficient cells prolongs the mitotic residence time and induces cell death.

Time-lapse images of H2B-mCherry transfected H1299 cells pre-treated for 24 h with a) DMSO (control) or b) a combination of KU55933 (10 μM) and VE-821 (1 μM).
a) A H1299 cell showing normal progression through mitosis.
b) A H1299 cell progressing through mitosis, but then undergoing cell death following mitotic exit.

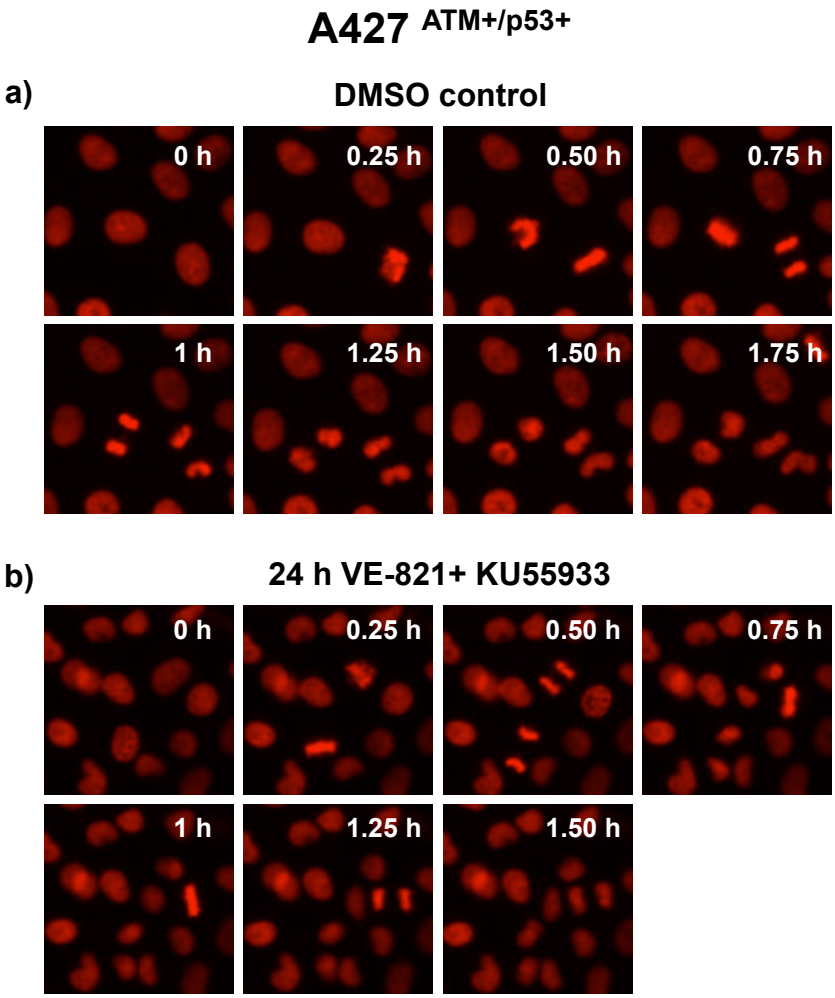

Figure 5.11 Combined ATM and ATR inhibition does not affect mitotic fidelity or residence time in p53-proficient cells.

Time-lapse images of H2B-mCherry transfected A427 cells going through mitosis following 24 h pre-treatment with **a)** DMSO (control) or **b)** a combination of KU55933 (10 μM) and VE-821 (1 μM).

It should also be noted that combined ATM and ATR inhibition not only increased the percentage of cells with formation of micronuclei in H1299 cells, but also generally induced more severe nuclear fragmentation and a higher number of micronuclei per cell compared with either single-treatment[33].

33. The data in Figure 5.9e is presented as % of micronuclei positive cells and does not differentiate between cells with only one micronucleus and those with severe nuclear fragmentation.

These observations suggested that cells undergo a form of cell death which is linked to errors in mitosis and which is likely caspase-independent, as no increase in caspase or PARP cleavage could be detected in western blot analysis.

5.4 Combined inhibition of ATM and ATR induces DNA damage in p53-deficient cells predominantly in mitosis

Given the important roles of ATM and ATR in the detection and repair of DNA damage, we next sought to address the question, whether ATR inhibition leads to the induction of DNA damage, particularly DNA DSBs, through assessment of H2AX S139 phosphorylation, an established marker of DNA DSBs (Scully & Xie, 2013; Löbrich *et al*, 2010).

We found that a large proportion of the micronuclei induced by VE-821 treatment in cells with genetic loss and/or inhibition of both ATM and p53 stained positive for γH2AX (Figure 5.12a). We also found subpopulations of cells with pan-nuclear γH2AX in all cell lines treated with ATR inhibitors (Figure 5.12b-d). This phenotype has been described in connection with loss or inhibition of ATR (Murga *et al*, 2010; Toledo *et al*, 2011; Jacq *et al*, 2012; Guichard *et al*, 2013; Chen *et al*, 2014) or CHK1 (Syljuåsen *et al*, 2005) activity and has been associated with the induction of replication stress.

Notably, the observed γH2AX staining pattern was not focal but evenly distributed throughout the entire nucleus, very similar to the staining pattern observed in micronuclei. Furthermore, the occurrence of 53BP1 foci, also a marker for DNA DSBs (Stewart, 2009), and pan-nuclear γH2AX were mutually exclusive (Figure 5.12b).

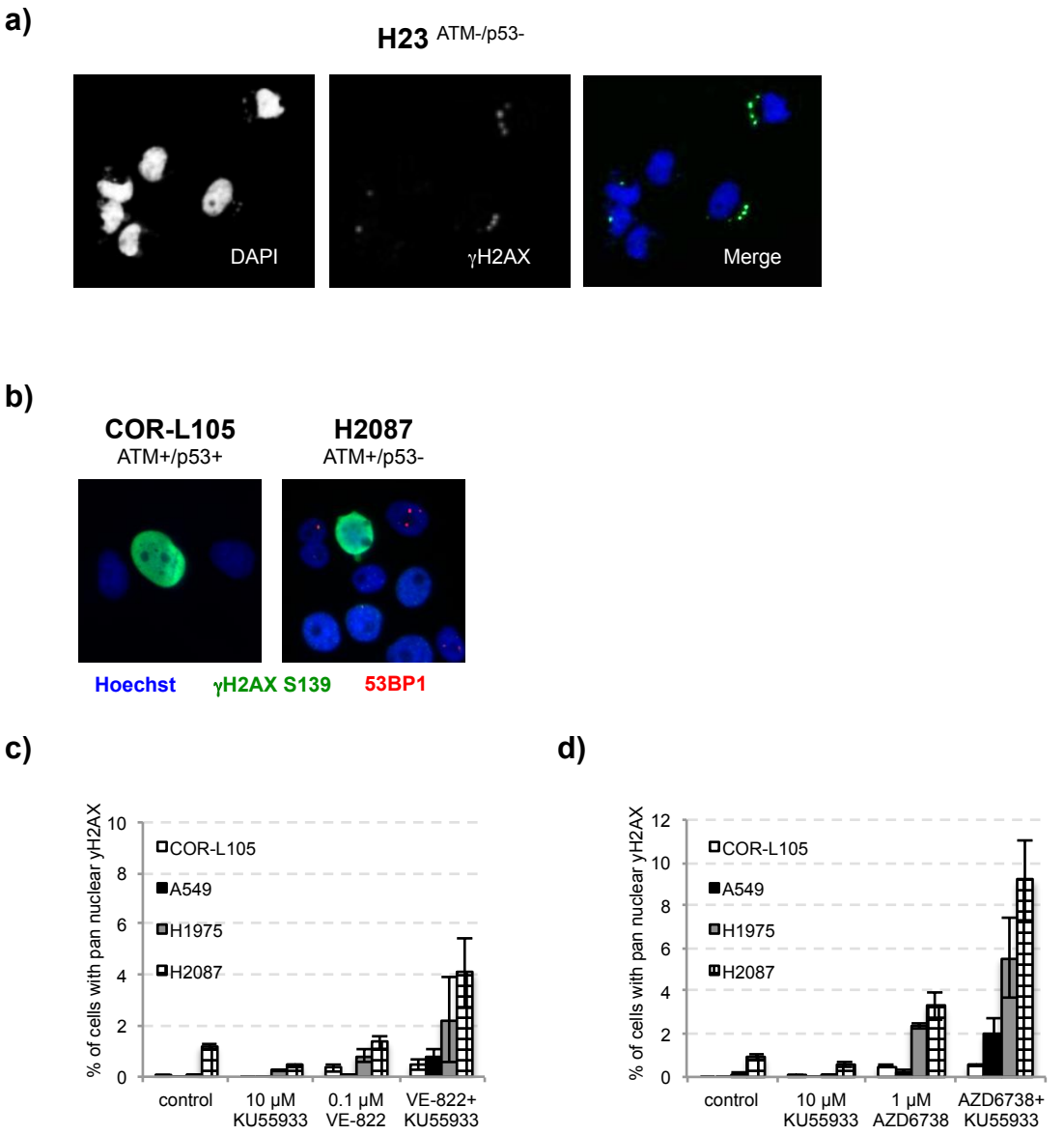

Figure 5.12: ATR inhibition induces pan-nuclear and pan-micronuclear H2AX phosphorylation, particularly in cells deficient in both ATM and p53.

a) Micronuclei formed in H23 cells after 48 h treatment with 1 μM VE-821 stain positive for γH2AX in immunofluorescence (IF).

b) IF staining for γH2AX and 53BP1 shows the induction of pan-nuclear H2AX phosphorylation in COR-L105 and H2087 cells treated with 0.1 μM VE-822 for 48 h. Notice the lack of 53BP1 foci in cells exhibiting pan-nuclear H2AX phosphorylation.

c) Quantification of the induction of pan-nuclear γH2AX in COR-L105, A549, H2087 and H1975 cells following 48 h of treatment with 0.1 μM VE-822, 10 μM KU55933 or a combination of both. The bars represent the mean ± SEM of three independent experiments each performed in triplicate.

d) Quantification of the percentage of cells with pan-nuclear γH2AX induced by 48 h treatment with 1 μM AZD6738, 10 μM KU55933 or a combination of both as in c).

We found that the percentage of cells exhibiting pan-nuclear γH2AX considerably exceeded the percentage of cells that showed signs of replication stress under the same treatment conditions (see Figure 5.6). And, unlike our previous results from RPA32 foci formation, the degree of pan-nuclear H2AX phosphorylation appeared to correlate with the sensitivity of cells to the respective ATR inhibitors or the combination treatment with KU55933. Firstly, this phenotype was more frequently observed in p53-mutated cell lines. Secondly, out of the three ATR inhibitors, AZD6738 induced the highest amount of pan-nuclear H2AX phosphorylation, particularly in combination with KU55933, consistent with the observed increased cytotoxicity of this combination compared with the other ATR inhibitors (Figure 5.12c, d). These results suggest that the observed phenotype of pan-nuclear H2AX phosphorylation might be linked to the cytotoxicity of ATR inhibitors alone and in combination with ATM depletion.

Interestingly, it has been suggested that phosphorylation of H2AX in micronuclei could be a marker for aberrant DNA replication, as micronuclei tend to undergo uncoordinated DNA synthesis, which results in the induction of DNA damage (Crasta *et al*, 2012). This raises the intriguing possibility that the observed diffuse pan-nuclear H2AX phosphorylation could be a sign of uncoordinated or aberrant DNA replication, rather than DNA DSBs or replication stress in form of stalled replication forks.

Despite the occurrence of pan-nuclear and micronuclear γH2AX, only a small increase in γH2AX levels could be observed in immunoblot analysis, for treatment with VE-821 alone as well as in combination with KU55933. Notably, p53-proficient and –deficient cells exhibited a similar increase (Figure 5.13a, b).

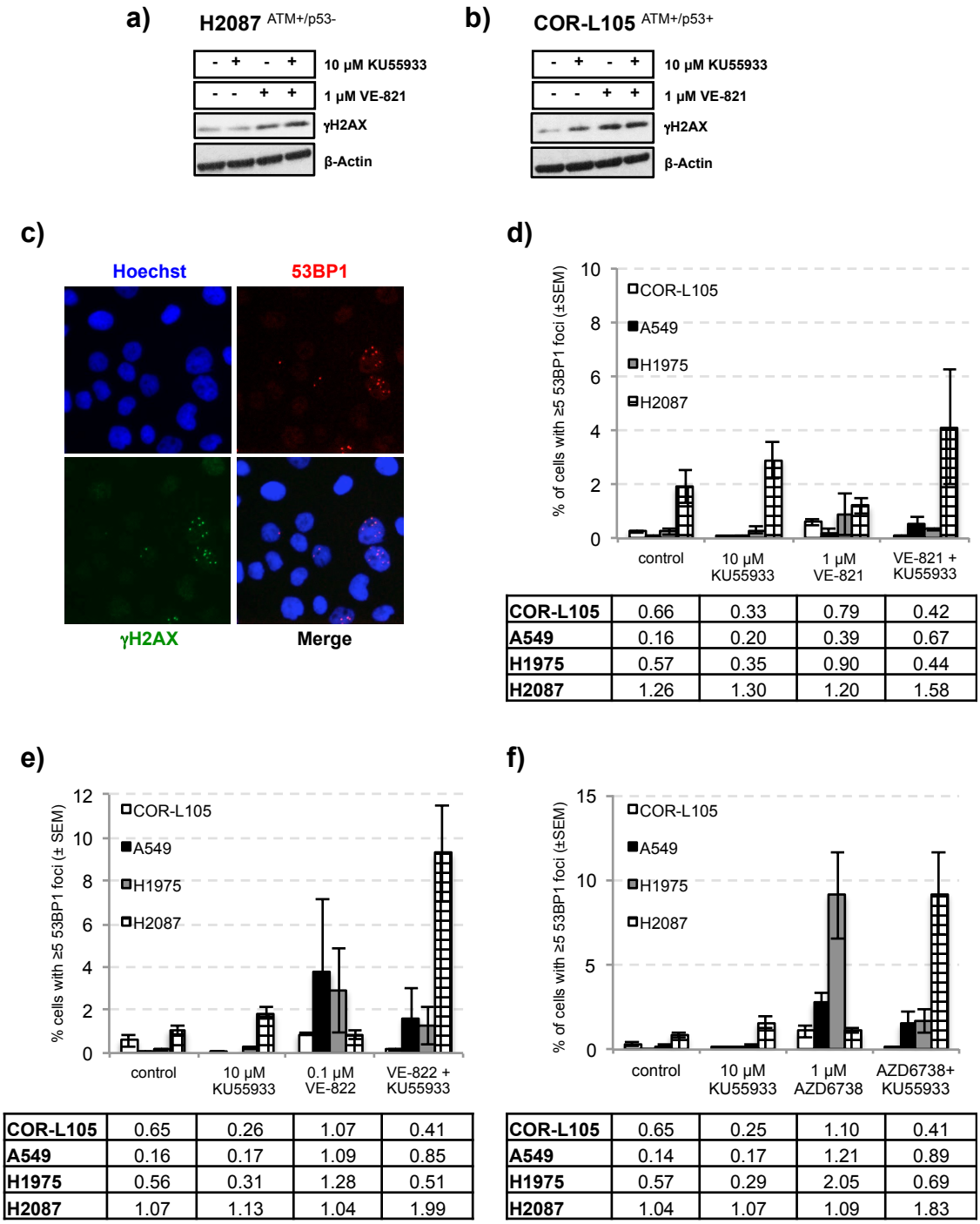

COR-L105	0.66	0.33	0.79	0.42
A549	0.16	0.20	0.39	0.67
H1975	0.57	0.35	0.90	0.44
H2087	1.26	1.30	1.20	1.58

COR-L105	0.65	0.26	1.07	0.41
A549	0.16	0.17	1.09	0.85
H1975	0.56	0.31	1.28	0.51
H2087	1.07	1.13	1.04	1.99

COR-L105	0.65	0.25	1.10	0.41
A549	0.14	0.17	1.21	0.89
H1975	0.57	0.29	2.05	0.69
H2087	1.04	1.07	1.09	1.83

Figure 5.13: Interphase cells show only a moderate increase in DNA DSB formation following combined inhibition of ATM and ATR.

Western blot analysis of γH2AX induction in **a)** H2087 and **b)** COR-L105 cells following 48 h of treatment with KU55933, VE-821 or a combination of both.
c) Example images of IF staining for γH2AX and 53BP1 in A549 cells treated with AZD6738 (1 μM) and KU55933 (10 μM) for 48 h. Pictures were taken at a 200x magnification.
d) to f) Quantification of 53BP1 foci formation in COR-L105, A549, H1975 and H2087 cells following 48 h treatment as indicated (mean ± SEM of three independent experiments each performed in triplicate). The tables summarise the mean number of 53BP1 foci per cell for each condition and cell line.

Consistently, we observed only a small increase in the formation of 53BP1 foci following treatment with KU55933, VE-821/VE-822, or a combination of both (Figure 5.13c-f). Similar to RPA32 foci formation, the observed increase in 53BP1 foci did not reflect the sensitivity of the cell lines to the respective ATR inhibitors alone or in combination with the ATM inhibitor.

Strikingly, even though the vast majority of interphase cells showed no substantial increase in γH2AX or 53BP1 foci formation under these conditions, a substantial amount of γH2AX foci was apparent in mitotic (pHH3 S10 positive) p53-mutated cells (H2087; Figure 5.14). An increase in DNA DSBs in mitosis was not observed in p53 wt COR-L105 (Figure 5.15a) or normal bronchial epithelial cells (NBE1; Figure 5.15b).

Taken together these data suggest that pharmacological inhibition of ATR, alone or in combination with ATMi, induces a small amount of DNA damage in both p53-proficient and –deficient cells. A substantial increase in the formation of DNA DSBs, can only be found in mitotic cells and only when ATM, ATR and p53 function are impaired.

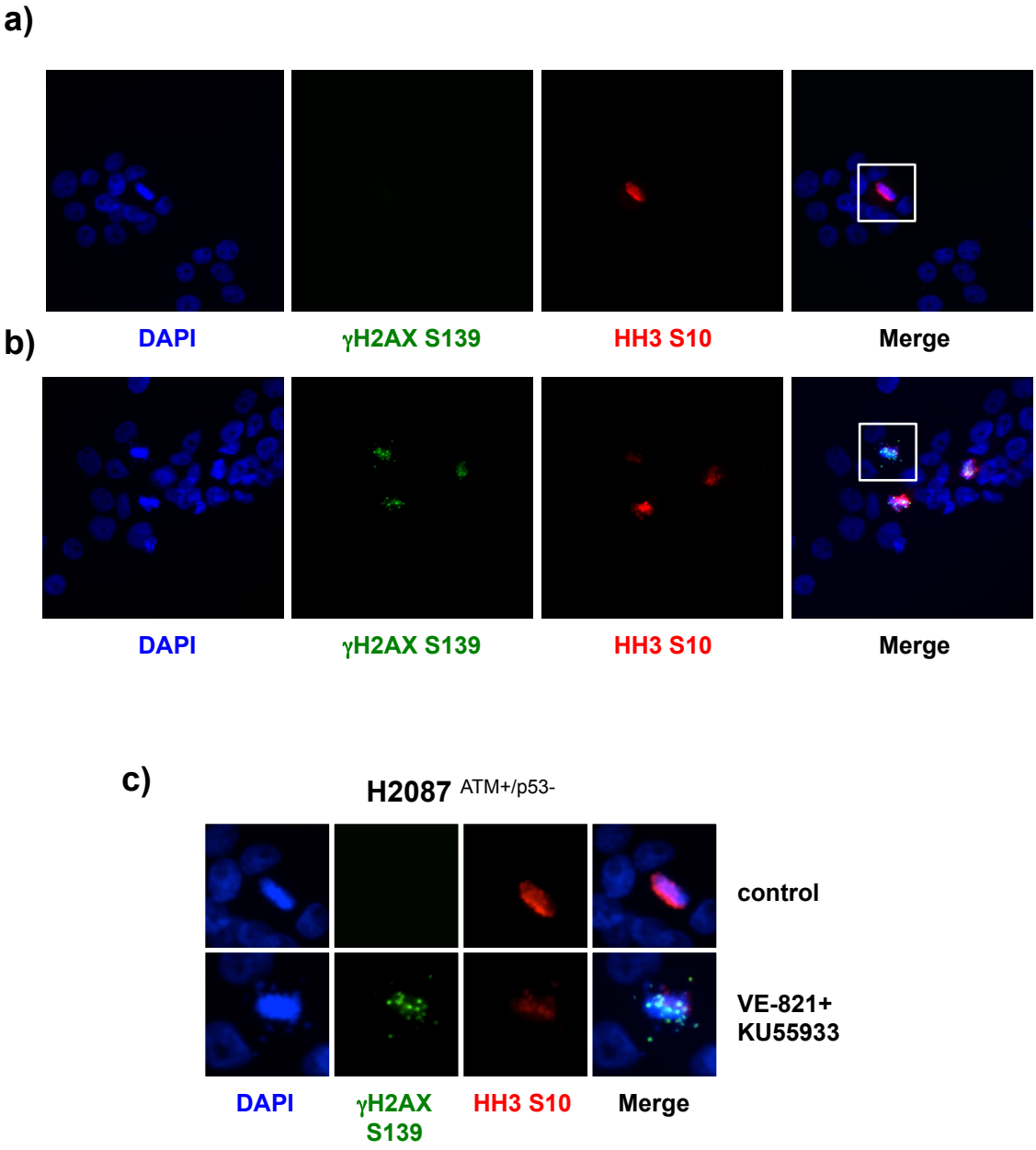

Figure 5.14: Concomitant inhibition of ATM and ATR induces γH2AX foci formation in p53-deficient cells particularly in mitosis.

a) Representative images of vehicle control (DMSO) treated H2087 cells stained for γH2AX and phospho- Histone H3 (pHH3). Nuclear counterstain was performed with Hoechst. Images were taken at a 100x magnification.
b) Representative images of immunofluorescence staining as in a) following 48 h treatment of H2087 cells with 1 μM VE-821 and 10 μM KU55933. Notice the high number of γH2AX foci in mitotic (pHH3 positive) cells.
c) The mitotic cells encircled in a) and b) shown at a higher magnification (400x).

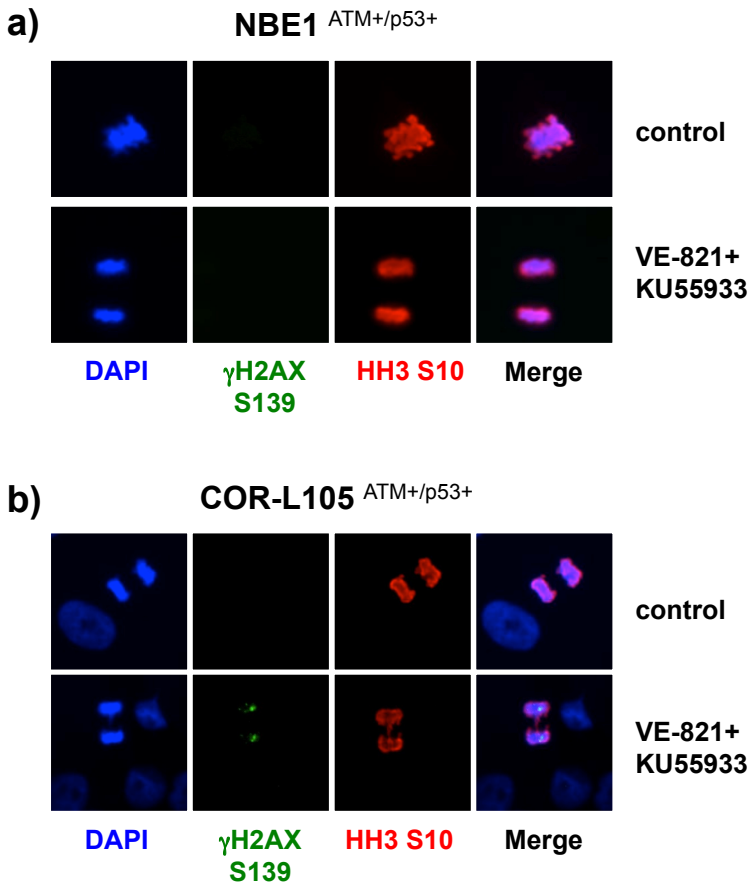

Figure 5.15: Cells with retained p53 function show no increase in γH2AX foci formation in mitosis.

Representative images of IF staining for phospho-Histone H3 (Ser10) and γH2AX in **a)** NBE1 and **b)** COR-L105 cells after 48 h treatment with DMSO (control) or a combination of KU55933 (10 μM) and VE-821 (1 μM). Pictures were taken at a 400x magnification.

5.5 ATR inhibition in cells with functional loss of both ATM and p53 induces severe chromosomal damage

As H2AX is a direct downstream target of both ATM and ATR, this raised the question whether the observed overall low level of H2AX phosphorylation following combined ATM and ATR inhibition could be a consequence of the inhibitors used.

53BP1 foci formation as readout for DNA DSBs also has its shortcomings, as 53BP1 does not localise to DNA DSBs in mitosis (Giunta *et al*, 2010).

In order to validate the induction of DNA DSBs in response to concomitant loss or inhibition of ATM, ATR and p53 and to further quantify DNA DSBs carried through into or induced during mitosis following ATR inhibition, we performed chromosome analysis in metaphase spreads. To assess the effect of ATR inhibition in cells with genetic loss of ATM, metaphase spreads were prepared from H1395 and H23 cells following treatment with VE-821 for 48 h. To investigate the effect of combined inhibition of ATM and ATR, COR-L105 and H2087 cells were treated with VE-821, KU55933 or a combination of both (48 h). For the last two hours of treatment before harvest of the cells, colcemid was added to the culture media. Importantly, while colcemid arrests cells at metaphase, it does not induce premature chromosome condensation and it also does not force cells into mitosis (e.g. through abrogation of the G2/M cell cycle checkpoint). Following counterstain with Giemsa, metaphase spreads were assessed for the presence of chromosomal aberrations.

Consistent with the data obtained from γH2AX foci formation, which showed an increase in DNA DSBs in mitotic p53-deficient cells (H2087) following inhibition of ATM and ATR, we found a marked increase in the formation of chromosome breaks in VE-821 treated $H23^{ATM-/p53-}$ cells (average of 5 aberrations/100 chromosomes in control treated vs. 38.4 in VE-821 treated; $p<0.0001$; Figure 5.16a, b). The majority of chromosomal aberrations detected were chromosome and chromatid breaks. The degree of chromosomal damage following loss of ATM, ATR and p53 function varied greatly between spreads with some cells exhibiting severe fragmentation of chromosomes (Figure 5.16c).

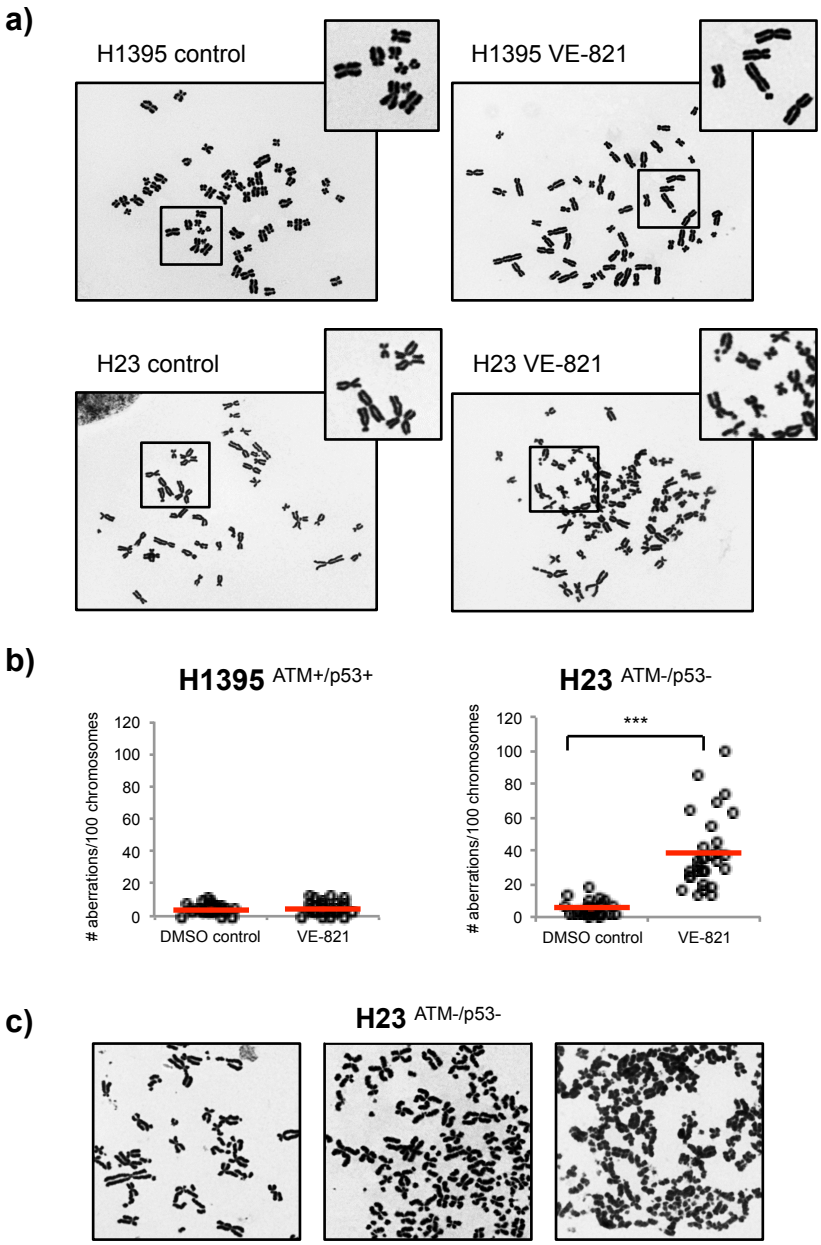

Figure 5.16: VE-821 induces chromosomal damage and fragmentation in cells with functional loss of both ATM and p53.

a) Representative images of metaphase spreads of H1395 and H23 cells treated with vehicle control (DMSO) or VE-821 (1 μM) for 48 h.
b) Diagram summarising the quantification of chromosome aberrations found in 30 metaphase spreads of H1395 and H23 cells treated as in a) The bar indicates the mean while the dot cloud emphasises the variation found between spreads. Asterisks indicate statistically significant differences between treatment groups (***= $p<0.0001$ calculated by 2-sided Student's t-test).
c) Representative images of metaphase spreads of H23 cells treated with 1 μM VE-821 (48 h) demonstrating the high degree of chromosomal breakage and even fragmentation observed in some cells. Spreads exhibiting severe fragmentation were not included in the quantification.

A similar increase in chromosome aberrations was observed in p53-deficient H2087 cells co-treated with VE-821 and KU55933 (control=3.5; VE-821=7.3; KU55933=8; VE-821+KU55933=44.6 aberrations/100 chromosomes; Figure 5.17c, d). In p53-proficient cells (H1395 and COR-L105), however, no significant increase in chromosome damage was observed (Figure 5.16a, b and Figure 5.17a, b).

To assess a potential activation of cell cycle checkpoints, we determined the mitotic index (MI) for each condition. For this purpose, the nuclei of 1,000 cells were assessed (interphase, pro- and metaphase) and the percentage of mitotic cells was calculated. Notably, in p53-proficient cells ($A549^{ATM+/p53+}$, $COR\text{-}L105^{ATM+/p53+}$ and $H1395^{ATM-/p53+}$) a decrease in the percentage of mitotic cells following ATR inhibition, ATM inhibition or the combination was observed, presumably in response to the induction of low levels of replication stress and DNA damage prior to mitotic entry (Figure 5.18a, b). P53-deficient cells ($H2087^{ATM+/p53-}$ and $H23^{ATM-/p53-}$), on the other hand, showed no decrease in the number of mitotic cells (Figure 5.18a, b).

This observation provides further evidence for the hypothesis that p53 performs ATM and ATR independent checkpoint functions, including the inhibition of G2 to M transition. It also suggests that in the absence of functional ATM and p53, exposure of cells to VE-821 either allows cells to enter mitosis in the presence of DNA damage, or leads to the induction of DNA damage in mitotic cells.

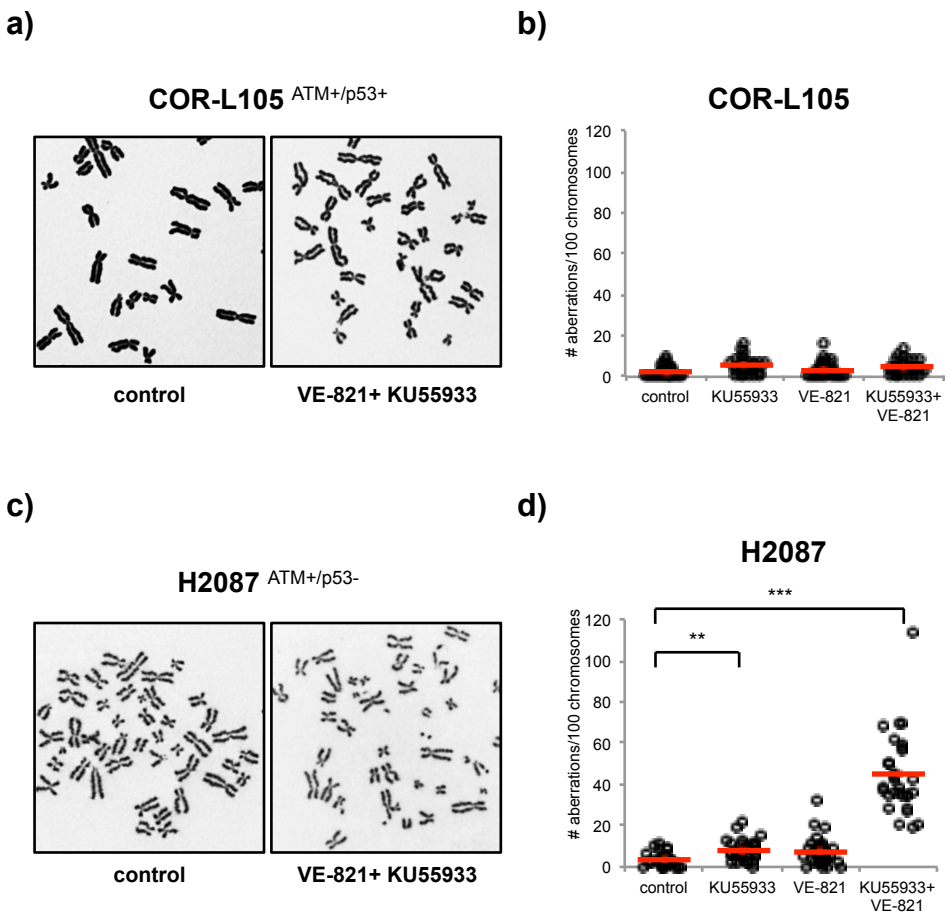

Figure 5.17: Concomitant disruption of ATM and ATR function induces chromosomal damage selectively in p53-deficient cells.

a) and c) Representative images of metaphase spreads of p53-proficient COR-L105 and p53-deficient H2087 cells after treatment with vehicle control, or a combination of 1 μM VE-821 and 10 μM KU55933 for 48 h.
b) and d) Diagrams summarising the quantification of chromosome aberrations found in 30 metaphase spreads of COR-L105 and H2087 cells treated with vehicle control, 1 μM VE-821, 10 μM KU55933 or a combination of both for 48 h. Bars indicate the mean while each dot represents the number of aberrations found in one metaphase spread. Statistically significant differences in the amount of chromosome aberrations between treatment groups, calculated by 2-sided Student's t-test, are indicated by asterisks: **= $p<0.001$; ***= $p<0.0001$.

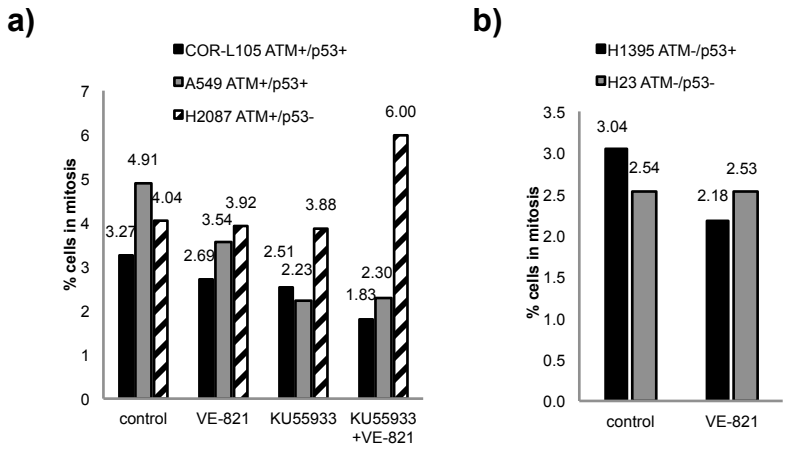

Figure 5.18: P53-proficient cells show a decrease in the percentage of mitotic cells when ATM and/or ATR signalling are disrupted.

a) Diagram summarising the total percentage of mitotic cells found in p53-proficient COR-L105 and A549 cells, and in p53-deficient H2087 cells following 48 h treatment with VE-821 (1 μM), KU55933 (10 μM) or the combination. The percentages were calculated from the number of metaphases and early mitotic nuclei observed in a total number of 1,000 nuclei (including interphase nuclei).
b) Diagram summarising the total percentage of mitotic cells found in H1395 and H23 cells following 48 h treatment with VE-821 (1 μM). Data calculation and presentation as in a).

5.6 ATM contributes to the regulation of CHK1 phosphorylation under physiological conditions

In our previous experiments, checkpoint activation was assayed under conditions when ATR inhibition was combined with DNA damage-inducing IR (see section 4.4.1). However, the observed high sensitivity of p53-deficient cells to combined ATM and ATR inhibition raised the possibility that in p53-deficient cells and under conditions of no additional genotoxic stress, ATM and ATR may perform important checkpoint functions, which are essential to maintain cell viability. We sought to address this question and investigated whether we could detect phosphorylation of the ATM and ATR downstream targets CHK1 (S345, S296) and CHK2 (Thr68), in p53-

deficient H2087 cells under unperturbed growth conditions (DMSO control) and following inhibition of ATM (KU55933, 10 μM), ATR (VE-821, 1 μM) or the combination.

Treatment with VE-821 alone or in combination with ATMi induced low levels of γH2AX, indicating a small increase in DNA DSB formation (Figure 5.19a). However, consistent with our previous results, the increase in H2AX phosphorylation was small and only detectable following long film exposure. We found low background levels of CHK2 phosphorylation, which were, as expected, reduced following ATM inhibition. Surprisingly, however, the background levels of CHK1 autophosphorylation (Ser296), which are generally present in untreated cells, were markedly decreased following inhibition of ATM and not ATR. CHK1 Ser345 phosphorylation was not detectable (Figure 5.19a).

Under the same treatment condition, pCHK1 and pCHK2 were below detectable levels in COR-L105 cells. However, we observed a decrease in cyclin A levels in cells treated with the ATM inhibitor, or with the ATM/ATR inhibitor combination, indicating a reduction in the S/G2 cell populations (Figure 5.19b). This decrease in cyclin A levels was accompanied by an increase in cyclin D1 levels, suggesting an increase in G1 cell populations. This observation indicates activation of an ATM-independent, yet p53-dependent, G1 cell cycle arrest, consistent with our previous results. Furthermore, we found an increase in p21 levels following treatment with VE-821 (Figure 5.19b). This increase in p21 levels was attenuated following addition of an ATM inhibitor, suggesting a role of ATM in p53 activation and G1 cell cycle checkpoint activation in cells exposed to ATR inhibitors.

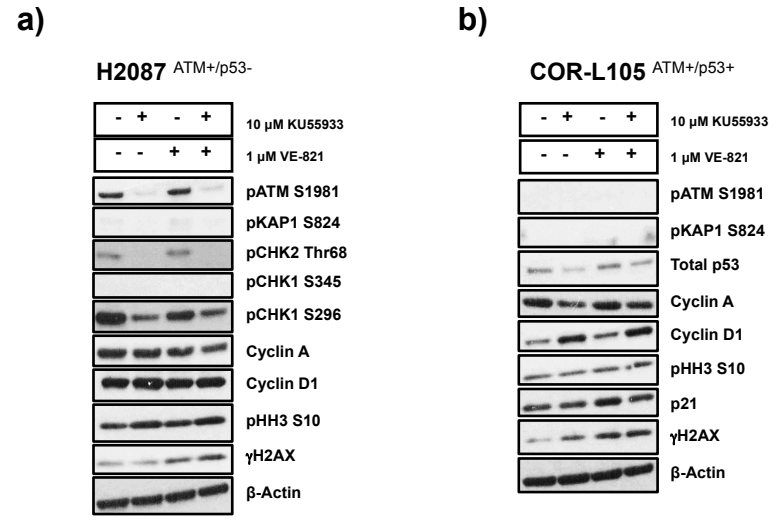

Figure 5.19: ATM contributes to the regulation of CHK1 phosphorylation and activity under physiological conditions.

a) Western blot analysis monitoring the phosphorylation of components of the ATM (ATM S1981 and CHK2 Thr68) and ATR (CHK1 S345 and S296) signalling pathways in H2087 cells following 48 h of treatment with KU55933 (10 μM), VE-821 (1 μM) or a combination of both. γH2AX levels were determined to assess the induction of DNA damage.
b) WB analysis of proteins involved in cell cycle checkpoint regulation in COR-L105 cells following 48 h of treatment with KU55933 (10 μM), VE-821 (1 μM) or a combination of both. β-Actin serves as loading control.

In contrast, H2087 cells showed no increase in cyclin D1 levels, though cells exhibited a small decrease in cyclin A levels. This was, however, accompanied by an increase in pHH3 levels, indicating an increase in mitotic cell populations following G2/M checkpoint abrogation rather than a G1 cell cycle delay.

Taken together these observations suggest that in normal replicating cells (at least in those which are p53-deficient) and without addition of genotoxic agents, ATM directly or indirectly contributes to the regulation of CHK1 autophosphorylation at serine 296. Interestingly, phosphorylation of CHK1 at S296 has been reported to be essential for CHK1 to perform its G2/M cell cycle checkpoint functions (Kasahara *et al*, 2010).

Furthermore, in cells with functional ATM and p53 (COR-L105), the levels of cell cycle specific biomarkers and their changes in response to ATM and/or ATR inhibition suggest important cell cycle checkpoint functions of both ATM and p53 in response to pharmacological inhibition of ATR.

5.7 DISCUSSION

Our previous results indicated that concomitant disruption of ATR and ATM signalling is selectively cytotoxic to p53-deficient cells. We were able to confirm this observation in both 2D and 3D models, where ATM inhibition sensitised p53-deficient cancer cells to ATR inhibitor treatment, while barely affecting the sensitivity of cells with retained p53 function.

This increased cytotoxicity was associated with the induction of mitotic aberrations, aneuploidy, and formation of micronucleated cells, suggesting errors in the separation of chromosomes during mitosis. Micronuclei tend to undergo aberrant DNA replication, which results in the induction of DNA damage (Crasta *et al*, 2012). In agreement with this, we found that a large proportion of the micronuclei induced by ATRi in a combined ATM-/p53-deficient background stained positive for γH2AX. We also found a large proportion of cells exhibiting diffuse pan-nuclear H2AX phosphorylation in response to ATR inhibition, particularly in p53-deficient cells. This phenotype has been described previously in connection with loss or inhibition of ATR (Murga *et al*, 2010; Chen *et al*, 2014) or CHK1 (Syljuåsen *et al*, 2005) activity and has been attributed to the induction of replication stress. Furthermore, the occurrence of γH2AX positive micronuclei has been connected to replication stress induced micronuclei formation and it has been suggested that the phosphorylation of H2AX in

micronuclei could be a marker for aberrant DNA replication (Xu *et al*, 2011; Crasta *et al*, 2012). We therefore assessed the induction of replication stress by ATR inhibition, alone or in combination with an ATM inhibitor through quantification of RPA foci formation, a marker of ssDNA formation following replication fork stalling (Wold, 1997). However, we found an only moderate increase in the percentage of cells exhibiting RPA foci formation suggesting that increased replication fork stalling was not a major factor in the induction of pan-nuclear H2AX phosphorylation or the increased sensitivity of p53-deficient cells to combined inhibition of ATM and ATR. This raises the possibility that the observed diffuse pan-nuclear H2AX phosphorylation could be a sign of uncoordinated or aberrant DNA replication, rather than replication fork stalling. However, further studies are required to assess the mechanisms and causes underlying pan-nuclear H2AX phosphorylation in response to ATR inhibition.

Micronuclei result from anaphase lagging chromosomes or can be generated from acentric fragments of chromosomes caused by DNA DSB formation (Terradas *et al*, 2010). We assessed the induction of DNA DSBs through quantification of 53BP1 foci formation and γH2AX levels, but found no significant increase in the induction of DNA DSBs in interphase cell populations. At the same time, high levels of γH2AX foci occurred in mitotic cells following loss or inhibition of ATM, ATR and p53 signalling. This finding was further supported by the marked increase in chromosome breaks observed in metaphase spreads from $H23^{ATM-/p53-}$ cells treated with ATRi, or $H2087^{ATM+/p53-}$ cells treated with a combination of ATRi and ATMi. However, none of these effects of ATRi were observed in cells with retained p53 and/or ATM function. This data suggests that DNA DSBs may not be induced until the cells enter mitosis.

A possible explanation for these observations could be that following functional loss of ATM, ATR and p53, cells enter mitosis prematurely while DNA synthesis is incomplete, resulting in substantial chromosome breakage when cells attempt to align and separate their chromosomes during mitosis. This breakage could be caused by mechanical forces during chromosome condensation, alignment and segregation or be the result of cleavage of under-replicated DNA by endonucleases (Ying *et al*, 2013; Naim *et al*, 2013). Following addition of genotoxic stress (e.g. IR or replication stress) these phenotypes would be further exacerbated.

Numerous studies have demonstrated that ATR is an important mediator of the intra-S-phase and G2/M cell cycle checkpoints that prevent the premature entry of cells into mitosis - during normal S-phase progression or in the presence of DNA damage (Xiao *et al*, 2003; Bartek *et al*, 2004; Sørensen *et al*, 2003; Zhao *et al*, 2002; Peng *et al*, 1997; Sanchez *et al*, 1997; Kumagai & Dunphy, 1999; Graves *et al*, 2001). Interestingly, it has been suggested that ATR acts together with p53 in the replication checkpoint to block cells from premature chromatin condensation (Nghiem *et al*, 2002). In agreement with this concept, we identified p53 as an important factor in the response of cells to ATRi. As demonstrated in section 4.4.1, ATR inhibition results in attenuation of the IR-induced G2/M cell cycle checkpoint. However, p53-proficient cells showed induction of an ATM-independent post-mitotic G1 cell cycle arrest following induction of DNA damage by IR. Following treatment of cells with ATRi, ATMi or a combination of both, we further observed a decrease in the mitotic subpopulation in cell lines with functional p53, suggesting that p53 supports the enforcement of the G2/M cell cycle checkpoint in response to replication stress or DNA damage, independently of ATM or ATR.

Furthermore, several studies have demonstrated that, depending on the cellular context and type of DNA damage, ATM contributes to the activation and maintenance of the intra-S-phase and G2/M cell cycle arrest, suggesting a functional overlap of ATM and ATR signalling in checkpoint activation (Abraham, 2001; Shiloh, 2001; Falck *et al*, 2001; Xiao *et al*, 2003; Bartek *et al*, 2004; Sørensen *et al*, 2003; Shiloh, 2003; Matsuoka *et al*, 1998). Our results support this concept as we found that following ATM inhibition background levels of both CHK2 Thr68 and CHK1 S296 phosphorylation were substantially reduced. Both kinases play important roles in the enforcement of the G2/M cell cycle checkpoint through targeting of CDC25C (see section 1.7.3). This data further indicates that under normal cell growth conditions, ATM contributes to the regulation of CHK1 activity. Interestingly, a previous study demonstrated that genetic inhibition of CHK1 S296 phosphorylation induces premature mitotic entry following replication stress (Kasahara *et al*, 2010). Further studies have documented a role for CHK1 in preventing premature mitotic entry in the absence of exogenous replication stress (Zachos & Gillespie, 2007; Krämer *et al*, 2004). This supports our hypothesis that during unperturbed cell cycle progression, ATM might cooperate with ATR in preventing premature mitotic entry through regulation of CHK1 activity.

Replication stress in tumour cells can be induced through aberrant oncogene activation (Bartkova *et al*, 2006; Di Micco *et al*, 2006), or through chemotherapeutic agents. But, even in the absence of replication stress-inducing agents, some fork stalling can occur during normal DNA replication, for example at common fragile sites (CFSs) or repetitive sequences (Mirkin & Mirkin, 2007). CFSs are large chromosomal regions that are thought to be particularly difficult to replicate; they replicate late during S-phase and undergo frequent breakage (Debatisse *et al*, 2012; Glover *et al*, 2005; Hills

& Diffley, 2014). They are thought to arise through incomplete DNA replication given that they are usually observed after various sources of replication stress, including low-dose aphidicolin treatment or oncogenic transformation (Harrigan *et al*, 2011; Le Beau *et al*, 1998; Hellman *et al*, 2000). Although clearly triggered by replication stress or abnormal DNA replication, the breakage of CFS only occurs in mitosis and not during S-phase (Naim *et al*, 2013; Harrigan *et al*, 2011). Both ATR and ATM have been shown to be critical for fragile-site stability (Casper *et al*, 2002; Ozeri-Galai *et al*, 2008). Of particular interest is the finding that the contribution of ATM in this process is only revealed in the absence of functional ATR (Ozeri-Galai *et al*, 2008). The overlapping functions of ATM and ATR in the regulation of fragile site stability were attributed to their effect on CHK1 activation, as both kinases were found to phosphorylate CHK1 under conditions of replication stress (Ozeri-Galai *et al*, 2008). Importantly, several studies have demonstrated that low levels of replication stress (e.g. induced by aberrant oncogene activation) are sufficient to induce chromosomal breakage at fragile sites (Tsantoulis *et al*, 2008; Wilson *et al*, 2015; Glover *et al*, 2005). This raises the possibility that the low levels of replication stress induction that we have observed in our studies might be sufficient to induce under-replication of CFS chromosomal regions.

Based on the data presented here and the findings described in the above-mentioned studies we propose the following model: In normal replicating cells without addition of genotoxic agents, ATM and ATR work together to ensure that mitotic entry is delayed until DNA synthesis is completed through enforcement of the intra-S and G2/M cell cycle checkpoints, presumably at least in part via their effect on CHK1 activation (Figure 5.20a, b). Inhibition of ATR in ATM deficient cells would therefore lead to an uncoupling of DNA replication and cell cycle transition, resulting in the

occurrence of regions of under-replicated DNA (e.g. at CFSs). In p53-proficient cells, induction of a p53-mediated G2/M cell cycle arrest could allow sufficient time to complete DNA synthesis before mitotic entry (Figure 5.20). It is likely that in the absence of functional ATR and ATM, some cells would slip through the p53 mediated G2/M cell cycle arrest. However, we have demonstrated that p53 can induce an ATM-independent post-mitotic G1 cell cycle arrest in response to DNA damage, which may allow cells enough time to repair and resolve DNA damage induced during the preceding mitosis, before proceeding into the next S-phase.

Our data is consistent with a model whereby functional loss or inhibition of ATM, ATR and p53 leads to pre-mature mitotic entry, before DNA replication is complete, which results in the generation of chromosome breaks during mitosis and eventually cell death (Figure 5.20d).

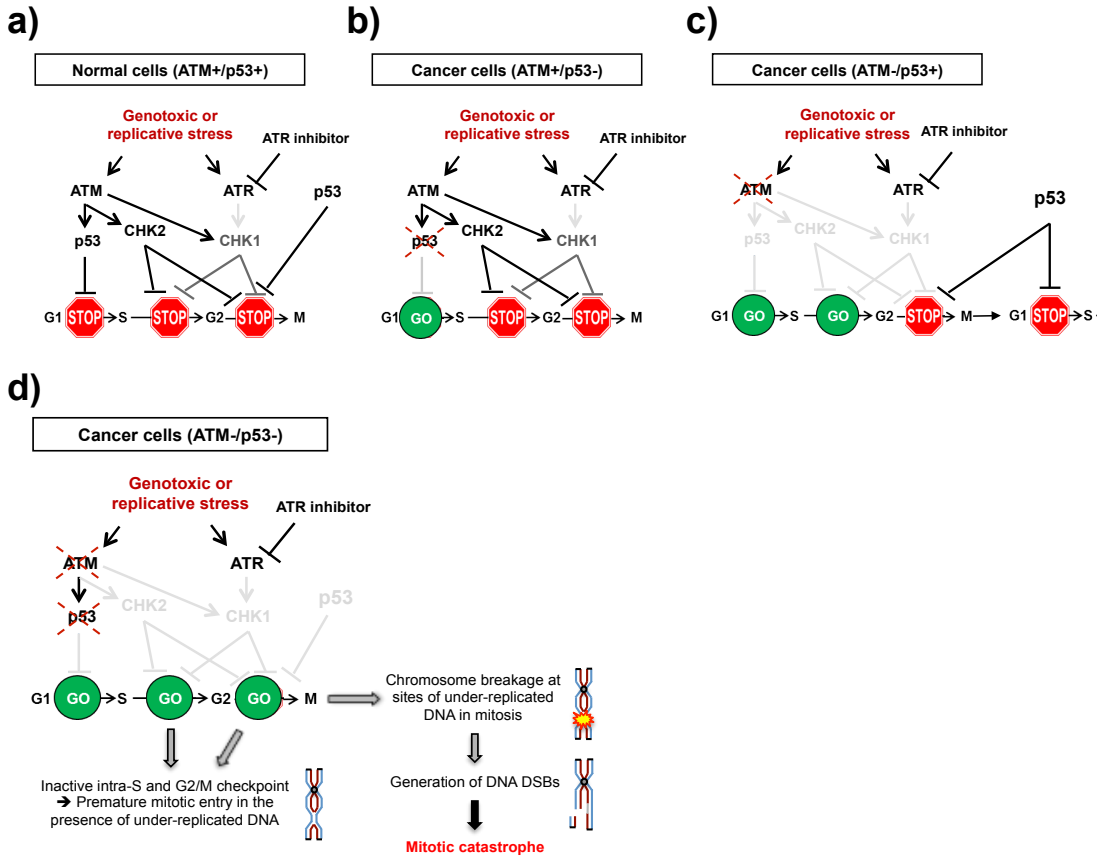

Figure 5.20: Proposed mechanism underlying the increased sensitivity of ATM and p53 deficient cells to pharmacological ATR inhibition.

a) In normal replicating cells exposure to genotoxic stress induces cell cycle checkpoint activation mediated via p53, ATM (through p53, CHK1 and CHK2) and ATR (through CHK1), allowing time to repair the damage before cells enter mitosis. Replication stress occurring endogenously during S-phase progression or induced exogenously through genotoxic agents induces activation of the intra-S-phase and G2/M cell cycle arrest, enforced by both ATM and ATR. In the presence of an ATR inhibitor, ATM and p53 are able to maintain checkpoint functions.
b) Cells deficient in p53 are unable to activate the G1 cell cycle arrest in response to genotoxic stress. However, ATM acts to enforce the intra-S and G2/M cell cycle checkpoints, even in the absence of functional ATR, to prevent premature mitotic entry in the presence of DNA damage or before DNA replication is completed
c) Treatment of ATM-deficient cells with an ATR inhibitor leads to abrogation of the G1/S and intra-S-phase cell cycle checkpoints. However, p53 maintains cell viability through activation of the G2/M and/or a post-mitotic G1 cell cycle arrest to allow for DNA damage to be resolved.
d) Following functional loss or inhibition of ATM, ATR and p53, cells are unable to slow cell cycle progression in response to genotoxic or replication stress (occurring endogenously e.g. through oncogene activation, or induced exogenously). This leads to pre-mature mitotic entry, before DNA replication is complete, which results in the generation of chromosome breaks during mitosis and eventually cell death.

CHAPTER 6

6 Combined pharmacological inhibition of ATR and PARP for the treatment of NSCLC

Poly(ADP-ribose)-polymerase (PARP) is an enzyme centrally involved in the detection and repair of DNA single strand breaks (SSB) by BER. Several small molecule inhibitors of PARP are currently in clinical development for cancer treatment. One of these inhibitors, olaparib (AZD2281, LYNPARZA™), has shown great promise in clinical trials, particularly for the treatment of BRCA1/2 mutated breast or ovarian cancer (Fong *et al*, 2009; Tutt *et al*, 2010; Audeh *et al*, 2010) and was FDA approved in the EU and USA in 2014. Recent studies have demonstrated that the cytotoxicity of several PARP inhibitors, including olaparib, is not merely based on the blocking of the DNA repair function of PARP, but also on the trapping of PARP at sites of DNA damage (Murai *et al*, 2012) (Figure 6.1). Such PARP/DNA complexes are cytotoxic to the cells, partly due to the induction of replication stress through stalling of replication forks. As ATR is required to prevent the collapse of stalled replication forks (Cimprich Cortez 2008) we hypothesised that combined inhibition of ATR and PARP would enhance the induction of DNA damage, particularly DNA DSBs, through collapse of stalled replication forks (Figure 6.1b). This would ultimately lead to cell death, particularly in cells with checkpoint defects, e.g. due to deficiency in ATM, p53 or both.

The studies described in this chapter aimed to address this hypothesis and to investigate the therapeutic potential of combined ATR and PARP inhibition for the treatment of NSCLC.

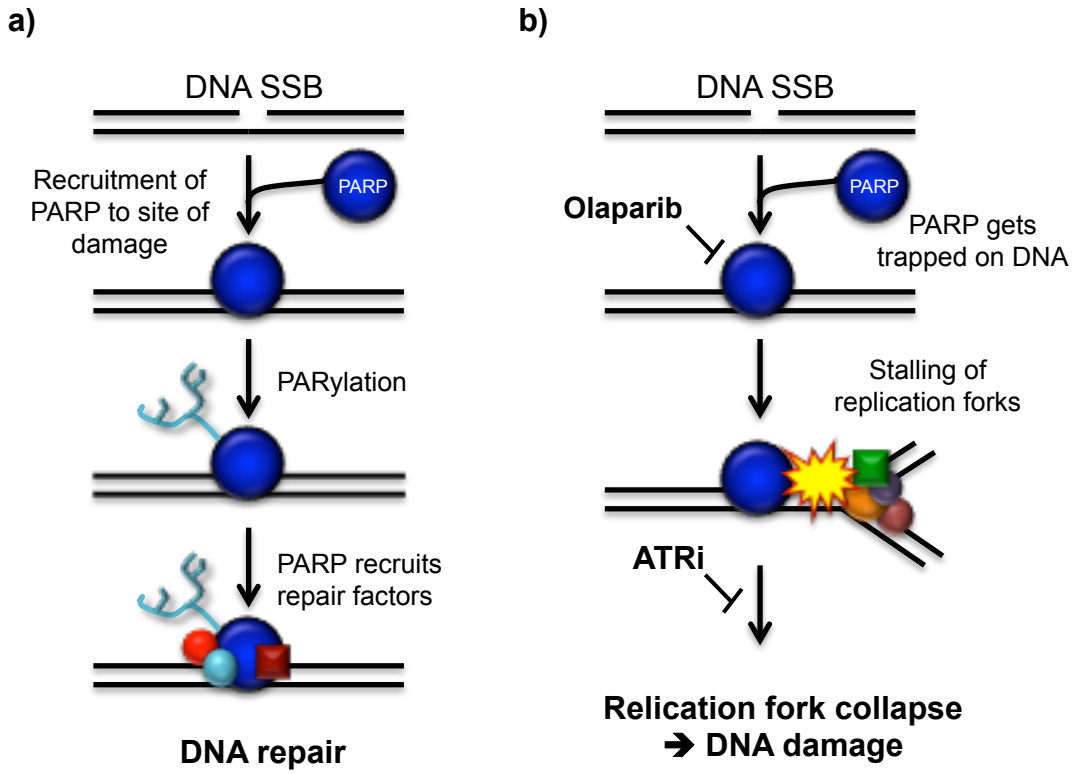

Figure 6.1: Mode of action of olaparib and rationale for the combination with pharmacological ATR inhibition.

a) PARP is recruited to sites of DNA SSBs and synthesises poly(ADP-ribose) chains (PAR). This PARylation serves as a signal for the recruitment of other DNA repair factors, which in turn resolve the DNA lesion.
b) Addition of a PARP inhibitor (olaparib) prevents PARylation and traps PARP on the DNA at the site of DNA damage. During S-phase this can cause a collision of ongoing replication forks with the trapped PARP/DNA complexes leading to replication fork stalling. Addition of an ATR inhibitor would then cause the collapse of such stalled forks leading to the induction of DNA damage in form of DSBs.

6.1 PARP inhibition sensitises p53-deficient NSCLC cells to ATR inhibitors

First, we investigated whether addition of olaparib enhances the cytotoxicity of pharmacological ATR inhibition in proliferation assays. For this purpose, a panel of NSCLC cell lines were exposed to dilution series of VE-821 or AZD6738 with or without addition of olaparib at a fixed concentration (1 μM AZD2281). Following 5 days of treatment, cell viability was assessed through quantification of resazurin metabolism.

We found that addition of olaparib generated no or only modest sensitisation to either one of the ATR inhibitors in p53 wild-type cells (A549 and COR-L105 for VE-821 and A427, COR-L105 or A549 for AZD6738; Figure 6.2a, c; Table 6.1; Table 6.2).

An exception was A549, which showed a 2.8-fold decrease in the IC_{50} value of VE-821 when olaparib was added (Figure 6.2a). For AZD6738, however, this cell line showed no sensitisation by olaparib (Figure 6.2c). In contrast, more marked reductions in the IC_{50} values of VE-821 were observed in p53-deficient NSCLC cell lines following addition of olaparib (fold-sensitisation: 3.7 for H1975, 8.2 for H2087 and 2.5 for PC-9; Figure 6.2b; Table 6.1).

The cell line H23 was markedly sensitised to both ATR inhibitors by olaparib (3.3-fold for VE-821 and 6.3-fold for AZD6738), as would be expected given the hypersensitivity of ATM- and p53-deficient cells to PARP (Williamson *et al*, 2012) and ATR inhibitors (see chapters 4 and 5).

For AZD6738, olaparib-mediated sensitisation also only occurred in p53-mutated NSCLC cells (Figure 6.2d; Table 6.2). However, the size of the sensitising effect was much smaller for AZD6738 compared with VE-821. Furthermore, several p53-

deficient cell lines (e.g. PC-9) showed no sensitisation, but over all much higher sensitivity to the ATR inhibitor AZD6738 than VE-821. This raised the question whether the lack of sensitisation could be due to AZD6738 alone already achieving maximal growth inhibition under these conditions, possibly due to the length of exposure to the drugs.

Table 6.1: IC_{50} values for VE-821 alone or in combination with olaparib.

Cell line	ATM status	p53 status	VE-821 mean IC_{50} [μM] (-/+ SEM, range)	VE-821 mean IC_{50} [μM] in the presence of AZD2281[34] (-/+ SEM, range)	SR [35]
A549	wt (+)	wt (+)	**13.8** (11.5-16.5)	**4.9** (4.4-5.5)	2.8
COR-L105	wt (+)	wt (+)	**12.2** (10.9-13.6)	**6.7** (6.2-7.3)	1.8
H2087	wt (+)	mut. (-)	**10.6** (9.4-12.0)	**1.3** (1.2-1.4)	8.2
H1975	wt (+)	mut. (-)	**12.4** (10.7-14.3)	**3.4** (3.2-3.7)	3.6
HCC827	wt (+)	mut. (-)	**8.2** (7.3-9.1)	**4.4** (4.1-4.7)	1.9
PC-9	wt (+)	mut. (-)	**4.5** (4.1-4.9)	**1.8** (1.6-1.9)	2.5
H23	mut. (-)	mut. (-)	**1.3** (1.2-1.4)	**0.4** (0.41-0.47)	3.3

34. Values were normalised to 1 μM AZD2281 treated cells.
35. SR (sensitisation ratio) represents the -fold sensitisation of VE-821+olaparib treatment compared with VE-821 treatment alone based on the mean IC_{50} values.

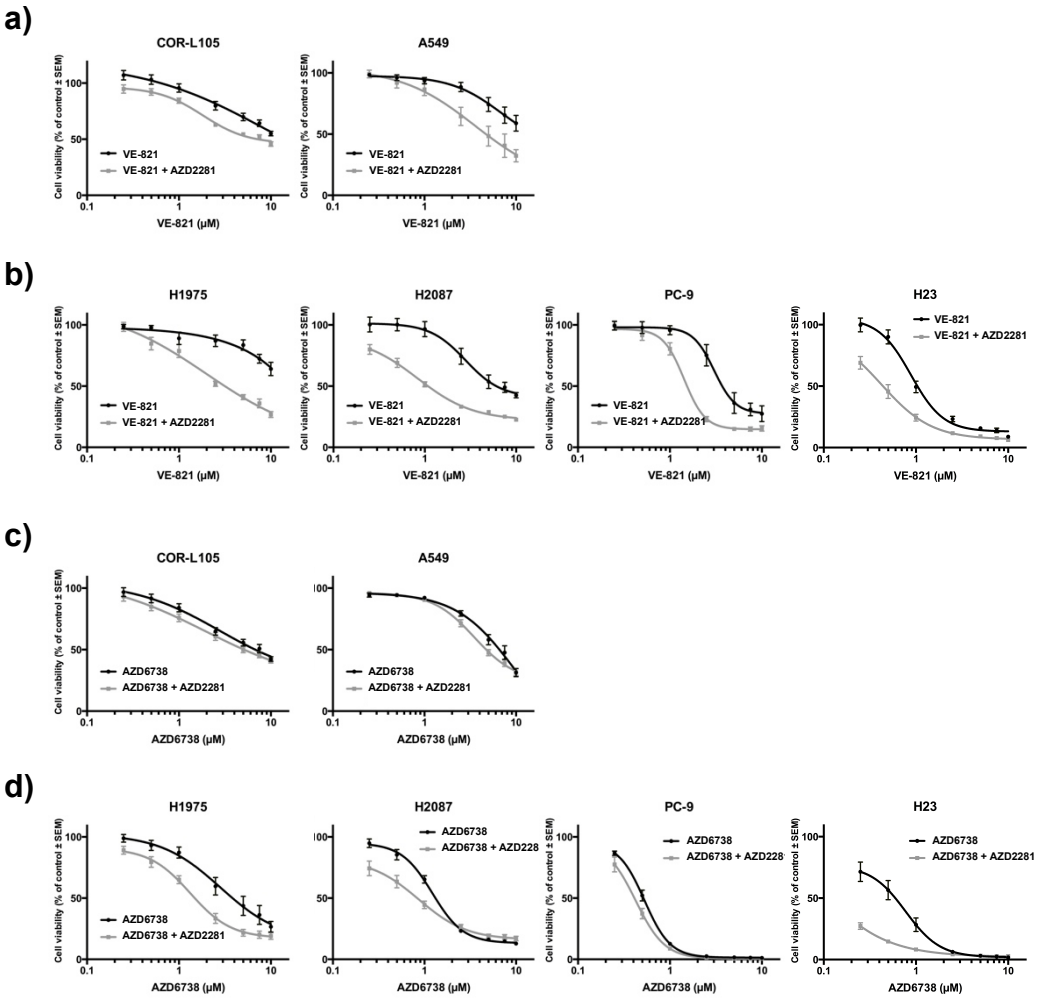

Figure 6.2: Effect of olaparib on the sensitivity of p53-proficient and -deficient NSCLC cells to AZD6738 treatment.

Assessment of the proliferation response of **a) and c)** p53 wild-type (COR-L105 and A549) and **b) and d)** p53-mutated NSCLC cells to combined inhibition of PARP and ATR. Cells were treated with a dilution series of the ATR inhibitors VE-821 (a and b) or AZD6738 (c and d) alone or in combination with olaparib at a fixed concentration of 1 μM. Cell viability was assessed through quantification of resazurin metabolism 5 days after beginning treatment. Points represent the means of at least two (a and b) or three (c and d) independent experiments each performed in triplicate ± SEM.

Table 6.2: IC_{50} values for AZD6738 alone or in combination with olaparib.

Cell line	ATM status	p53 status	AZD6738 mean IC_{50} [μM] (-/+ SEM, range)	AZD6738 mean IC_{50} [μM] in the presence of 1 μM AZD2281 (-/+ SEM, range)[36]	SR[37]
A549	wt (+)	wt (+)	**5.2** (5.0-5.5)	**5.1** (4.9-5.3)	1.0
A427	wt (+)	wt (+)	**7.0** (6.5-7.5)	**7.7** (7.1-8.4)	0.9
COR-L105	wt (+)	wt (+)	**5.5** (5.1-5.8)	**5.4** (5.0-5.8)	1.0
H2087	wt (+)	mut. (-)	**1.7** (1.65-1.8)	**0.9** (0.8-1.0)	1.9
H1975	wt (+)	mut. (-)	**2.2** (2.1-2.4)	**1.7** (1.6-1.8)	1.3
HCC827	wt (+)	mut. (-)	**1.8** (1.6-1.9)	**1.9** (1.7-2.1)	1.0
Calu-6	wt (+)	mut. (-)	**0.7** (0.64-0.72)	**0.5** (0.51-0.55)	1.4
PC-9	wt (+)	mut. (-)	**0.5** (0.5-0.52)	**0.4** (0.39-0.42)	1.3
H1395	mut. (-)	wt (+)	**3.8** (3.7-3.9)	**3.5** (3.4-3.7)	1.1
H23	mut. (-)	mut. (-)	**0.5** (0.47-0.52)	**0.08** (0.07-0.09)	6.25

To address this possibility, we next assessed the impact of PARP inhibition on the cytotoxicity of AZD6738 in 3D spheroid models. Spheroids of COR-L105 and H2087 cells were exposed to AZD6738, olaparib or the combination of both. Treatment was carried out for 48 h with an 8-day recovery period in drug-free culture media, or continuously for 10 days at the end of which proliferation and cell viability was assessed.

36. Values were normalised to 1 μM AZD2281 treated cells.
37. SR (sensitisation ratio) represents the -fold sensitisation of AZD6738+olaparib treatment compared with AZD6738 treatment alone based on the mean IC_{50} values.

Spheroid growth of p53-proficient COR-L105 cells was only minimally altered by exposure to AZD6738 alone, or in combination with olaparib (Figure 6.3a, c). Furthermore, this effect was reversible as spheroids appeared viable and resumed growth following removal of the drugs. In p53-deficient H2087 cells, both AZD2281 and AZD6738 moderately inhibited spheroid growth as single agents. The combination of both drugs appeared to have an additive effect on spheroid growth inhibition and significantly reduced spheroid size and viability to approximately 40% compared with vehicle-treated controls ($p<0.0001$). Notably, 48 h treatment led to a similar reduction in spheroid size and viability as 10-day continuous treatment (Figure 6.3b, c).

Together, these data demonstrate preferential sensitisation of p53-defective cells to pharmacological ATR inhibition by olaparib.

6.2 Olaparib enhances ATRi-mediated replication stress and DNA DSB induction, particularly in p53-deficient NSCLC cells

We next sought to investigate the mechanism underlying the observed sensitisation of p53-deficient NSCLC cells to ATRi by olaparib. Our initial hypothesis assumed the induction of replication stress through trapped PARP/DNA complexes and the subsequent induction of DNA DSBs following ATR inhibition. We therefore assessed the induction of replication stress through quantification of RPA32 foci formation in a panel of p53 wild-type (A549 and COR-L105) and p53 mutated (H1975, H2087, Calu-6 and PC-9) NSCLC cell lines following 48 h treatment with olaparib (AZD2281), AZD6738 or the combination of both.

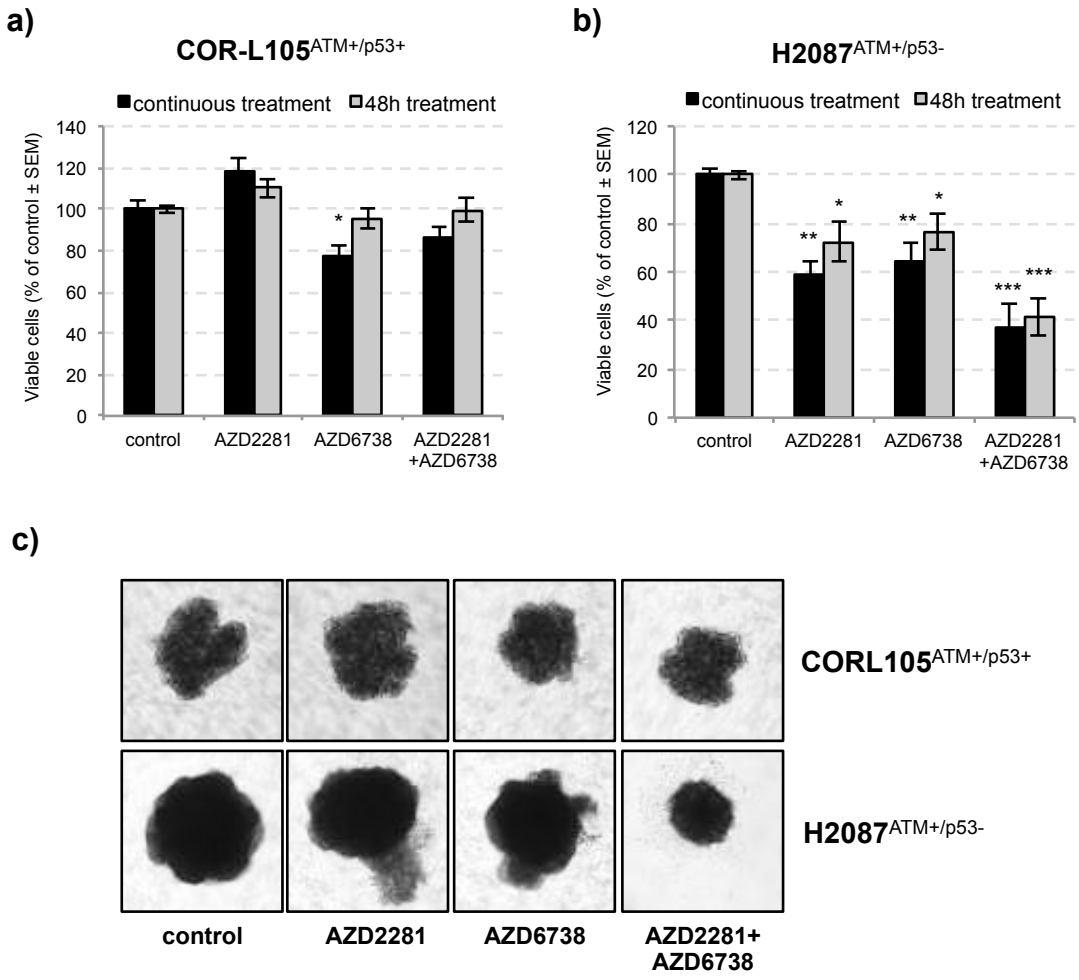

Figure 6.3: Olaparib selectively sensitises p53-mutated NSCLC cells to AZD6738 in 3D spheroid models.

Spheroids of **a)** COR-L105 and **b)** H2087 cells were treated with 1 μM AZD2281 (olaparib), 1 μM AZD6738 or a combination of both for 48 h with 8-days recovery in drug-free culture medium, or continuously for 10 days. Viability of cells was assessed by resazurin assay 10 days after beginning treatment. Means of three experiments, each performed in triplicate are shown. Error bars = SEM. Asterisks indicate statistically significant differences between treatment groups calculated by Student's t-test. *=p-values <0.01; ** = p<0.001; *** =p<0.0001 compared with control. **c)** Representative images of spheroids treated for 48 h as in a) and b).

We found that exposure of cells to olaparib alone minimally increased the percentage of cells with ≥15 RPA32 foci. AZD6738 was more potent at inducing replication stress and consistent with our previous results (see chapter 5) this phenotype was more prominently induced in p53-deficient cells. The combination of the two drugs further increased the percentage of cells exhibiting replication stress in Calu-6 and PC-9, but not the other cell lines (Figure 6.4a).

As our previous results had shown the induction of pan-nuclear H2AX phosphorylation in response to AZD6738 treatment, we investigated whether there was a correlation between the percentage of cells exhibiting this phenotype and the sensitivity of the respective cell lines to the combination of AZD6738 and olaparib. There was a significant increase in the percentage of cells with pan-nuclear γH2AX in the p53-deficient cell lines Calu-6 and PC-9 in response to AZD6738 treatment (Figure 6.4b). However, addition of olaparib did not affect the extent of this phenotype. In contrast, while only a small number of H2087 cells showed pan-nuclear γH2AX when treated with AZD6738, the addition of olaparib markedly increased this percentage (Figure 6.4b). This is an interesting observation, as H2087 cells, unlike PC-9 or Calu-6, are further sensitised to AZD6738 treatment by the addition of olaparib. Consistently, the p53-proficient cell lines A549 and COR-L105, which are both rather insensitive to each of the drugs alone as well as the combination, showed no significant increase in pan-nuclear γH2AX. H1975 cells, which show only minimal sensitisation to AZD6738 by olaparib, also exhibited no noteworthy up-regulation of γH2AX under any of the treatment conditions (Figure 6.4b).

VE-821 did not induce pan-nuclear H2AX phosphorylation in any of the cell lines (except H2087). Not even when VE-821 was combined with olaparib, even though olaparib markedly sensitises p53-deficient cells to VE-821 (Figure 6.4c).

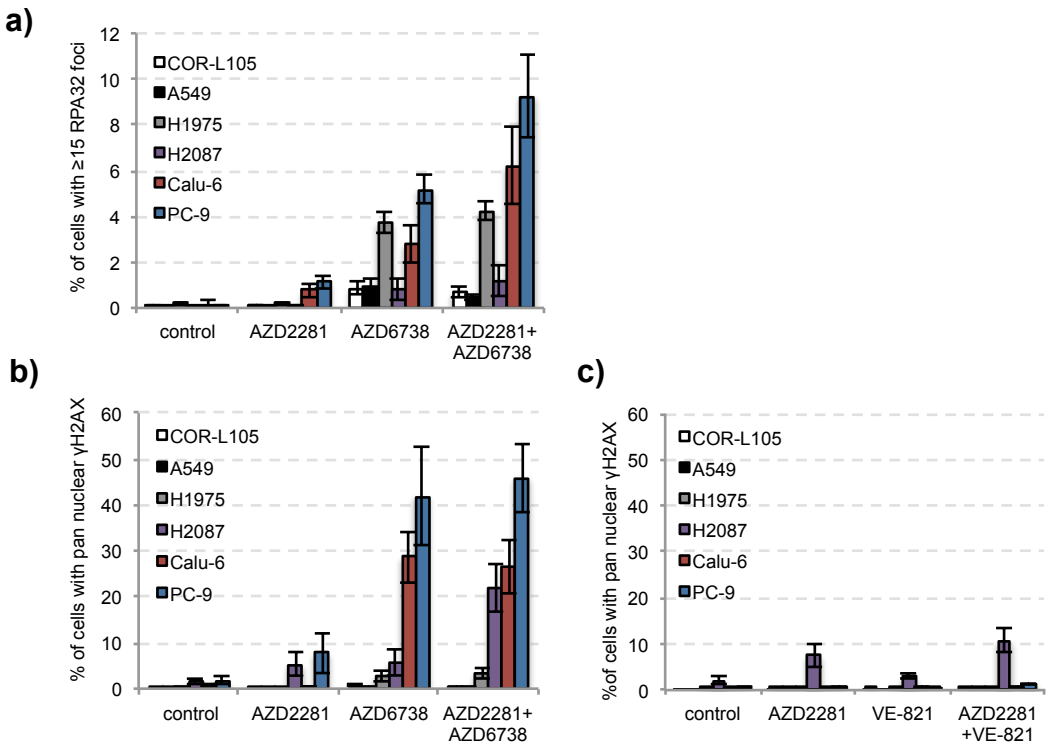

Figure 6.4: Combined ATR and PARP inhibition induces replication stress and pan-nuclear H2AX phosphorylation.

a) Quantification of RPA32 foci formation in COR-L105, A549, H1975, H2087, Calu-6 and PC-9 cells after 48 h treatment with 1 μM AZD2281, 1 μM AZD6738 or the combination of both.
b) Quantification of the induction of pan-nuclear γH2AX following 48 h of treatment as in a).
c) Quantification of the induction of pan-nuclear γH2AX following 48 h of treatment with 1 μM AZD2281, 1 μM VE-821 or the combination of both.

The bars represent the mean ± SEM calculated from three (a and b) or two (c) independent experiments each performed in triplicate.

Despite the fact that pan-nuclear H2AX phosphorylation and the induction of replication stress preferentially occurred in p53-deficient cells, we found no evidence for a causal relationship between the two. H1975 cells, for example, showed a marked increase in the number of cells undergoing replication stress following AZD6738 +/-

AZD2281 treatment, but no increase in pan-nuclear γH2AX could be observed. For H2087, the opposite observation was made (Figure 6.4a, b).

Taken together we conclude that even though the occurrence of pan-nuclear H2AX phosphorylation appears to be linked to ATR inhibitor treatment, particularly AZD6738, there is no clear correlation between the extent of this phenotype and the cytotoxicity conferred by combined ATRi and olaparib treatment. Furthermore, we found no clear correlation between the induction of replication stress and the occurrence of pan-nuclear γH2AX, in line with our previous results (see section 5.2).

6.3 Combined inhibition of ATR and PARP induces DNA damage and mitotic defects in p53-deficient NSCLC cells.

Next, we aimed to address the question, whether combined ATR and PARP inhibition causes the induction of DNA damage in form of DNA DSBs. For this purpose, p53-proficient (COR-L105) and p53-deficient (H2087[38]) cells were treated with olaparib (AZD2281), VE-821, AZD6738 or the combinations for 48 h and processed for western blot analysis.

Compared with vehicle treated control, no significant increase in γH2AX levels was evident in COR-L105 cells following treatment with either of the drugs alone or the combinations (Figure 6.5a). However, we observed activation of the ATM signalling pathway in response to AZD6738 treatment, as seen by an increase in phospho-ATM, phospho-KAP1 and phospho-p53 levels, which was further increased following addition of olaparib. This increase in ATM activity was accompanied by a decrease in

38. As we included analysis of γH2AX, we chose the H2087 cell line rather than Calu-6 or PC-9, to avoid a possible impairment of the results due to the high percentage of cells with pan-nuclear H2AX phosphorylation observed in these cell lines following AZD6738 treatment.

cyclin A levels, suggesting activation of the G1 cell cycle checkpoint. Cells treated with olaparib alone or with VE-821 and olaparib also showed a decrease in cyclin A levels.

This observation suggests that treatment of p53-proficient cells with olaparib, AZD6738 or the combinations of VE-821/AZD6738 and olaparib induces low levels of DNA damage, which in turn activate the ATM signalling pathway and cause G1 cell cycle arrest to prevent accumulation of DNA damage.

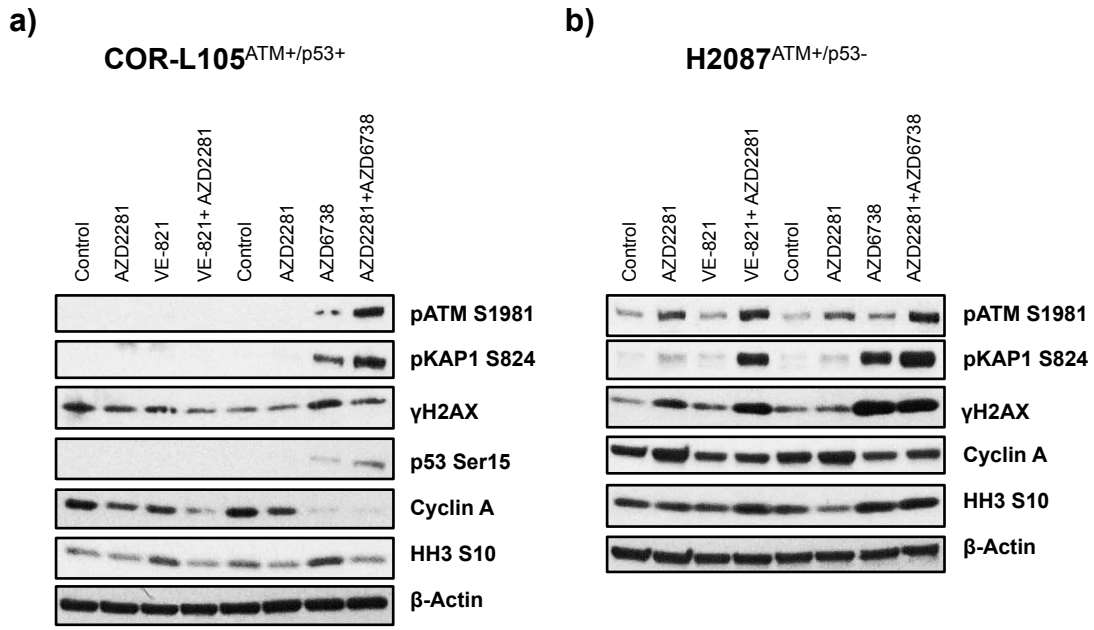

Figure 6.5: Comparison of DNA DSB induction and cell cycle checkpoint activation by VE-821 +/- olaparib or AZD6738 +/- olaparib treatment.

Western blot analysis monitoring the phosphorylation of components of the ATM signalling pathway (ATM S1981, KAP1 S824 and p53 S15) in **a)** p53-proficient COR-L105 and **b)** p53-deficient H2087 cells following 48 h treatment with AZD2281 (1 μM), VE-821 (1 μM), AZD6738 (1 μM) or the combinations as indicated. γH2AX levels were determined to assess the induction of DNA DSBs. Levels of cyclin A and phospho-histone H3 (HH3 S10) were determined to assess cell cycle distribution and potential activation of DNA damage-induced cell cycle checkpoints.

In contrast, p53-deficient H2087 cells showed a marked increase in the levels of γH2AX following treatment with AZD6738 alone or the combinations of VE-821 and olaparib or AZD6738 and olaparib (Figure 6.5b). This increase in γH2AX was accompanied by a marked increase in phospho-ATM and phospho-KAP1 levels, indicating activation of the ATM signalling pathway. Interestingly, treatment of cells with AZD6738 alone induced similar levels of γH2AX and phospho-KAP1 as the combination of VE-821 and olaparib, suggesting that AZD6738 alone causes comparably high levels of DNA damage. This observation may explain why in the case of VE-821, olaparib confers significant sensitisation in p53-deficient cells, while this sensitising effect is much smaller when olaparib is combined with AZD6738.
It further raises the question why the two ATR inhibitors show such different potency in the induction of DNA damage. Possible explanations include different modes of action of the two ATR inhibitors, differences in off-target effects as well as differences in the extent and duration of ATR inhibition. However, further studies are required to address this question.

Contrarily to the response observed in COR-L105, H2087 cells showed only a minimal decrease in cyclin A levels when exposed to the combinations of ATR and PARP inhibitors (Figure 6.5b). At the same time an increase in the level of phospho-histone H3 was evident, consistent with an increase in the mitotic cell population following G2/M checkpoint abrogation through ATR inhibition.

Taken together these data suggest that concomitant inhibition of ATR and PARP leads to the induction of DNA DSBs, in agreement with our hypothesis. Furthermore it provides evidence that p53-proficient cells respond to this DNA damage induction with activation of the G1 cell cycle checkpoint, which in turn prevents accumulation

of DNA damage. P53-deficicient cells, on the other hand, accumulate DNA DSBs, presumably due to the defective G1 cell cycle checkpoint and attenuation of the intra-S and G2/M checkpoints following inhibition of ATR.

6.4 Cell death in combination treated cells is driven by multiple modes of death.

We obtained consistent results in A549 (p53+) and H1975 (p53-) cells, where treatment with AZD6738 alone or in combination with olaparib caused an increase in the activity of the ATM signalling pathway. This increase was, however, more prominent in H1975 cells. Furthermore, a significant increase in γH2AX levels could only be observed in p53-deficient cells (Figure 6.6).

We further investigated, whether combined treatment of cells with AZD6738 and olaparib causes the induction of apoptosis. For this purpose, we monitored levels of cleaved caspase-3 and cleaved-PARP by western blot analysis. Both are established markers of apoptosis induction. Interestingly, 48 h exposure to a combination of AZD6738 and olaparib led to a marked increase in the levels of both markers in H1975 cells, indicating that cells undergo apoptosis (Figure 6.6b). However, despite the fact that H2087 cells are more sensitive to the combination of AZD6738 and olaparib, we found no signs of apoptosis induction (Figure 6.6a). This finding suggests that the mode of cell death may differ between cell lines.

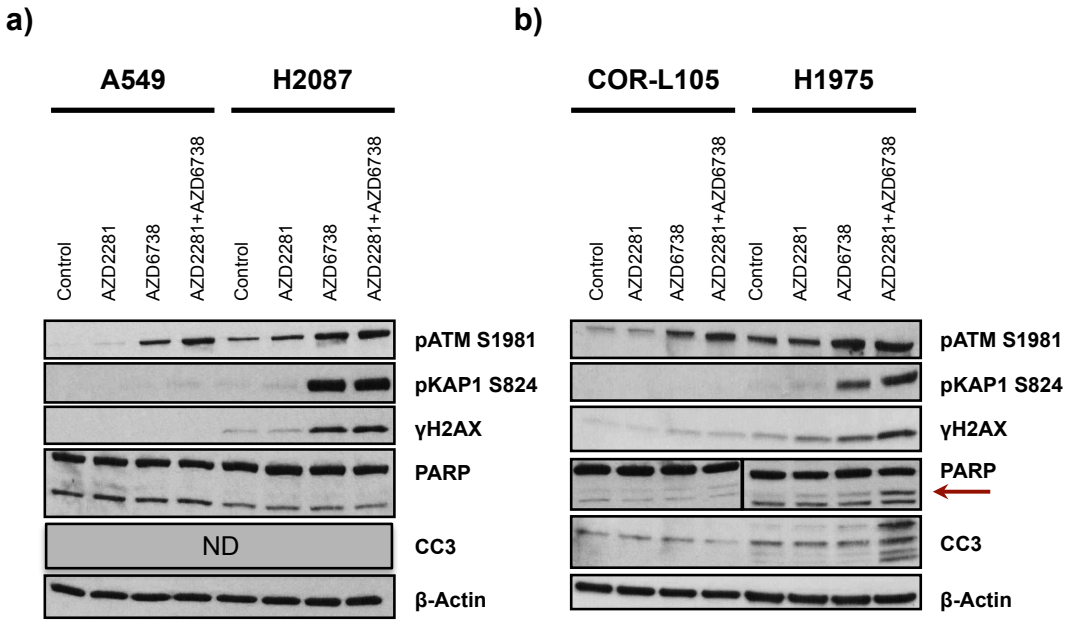

Figure 6.6: AZD6738 treatment alone or in combination with olaparib causes the induction of DNA DSBs and activation of the ATM signalling pathway selectively in p53-deficient NSCLC cells.

a) A549 and H2087, as well as **b)** COR-L105 and H1975 cells were treated with AZD2281 (1 μM), AZD6738 (1 μM) or the combination of both for 48 h followed by preparation of protein lysates and western blot analysis. Levels of γH2AX, pATM (S1981) and pKAP1 (S824) were determined to assess induction of DNA DSBs and activation of the ATM signalling pathway. Levels of cleaved PARP (see arrow) and cleaved caspase-3 (CC3) served for the assessment of apoptosis induction. ND= not detectable. It should be noted that in COR-L105 and A549 cells, low levels of pKAP1 and γH2AX were detectable at longer exposures (see Figure 6.5 for COR-L105).

In agreement with this notion, we found that in p53-deficient cell lines (H1975, H2087, Calu-6 and PC-9), formation of micronuclei was evident within 48 h of beginning treatment with AZD6738 (Figure 6.7). This observation suggests errors in the segregation of chromosomes during mitosis, possibly due to DNA damage, and induction of cell death through mitotic catastrophe. Micronucleation was, however, more prominent in Calu-6 and PC-9 than in H2087 or H1975.

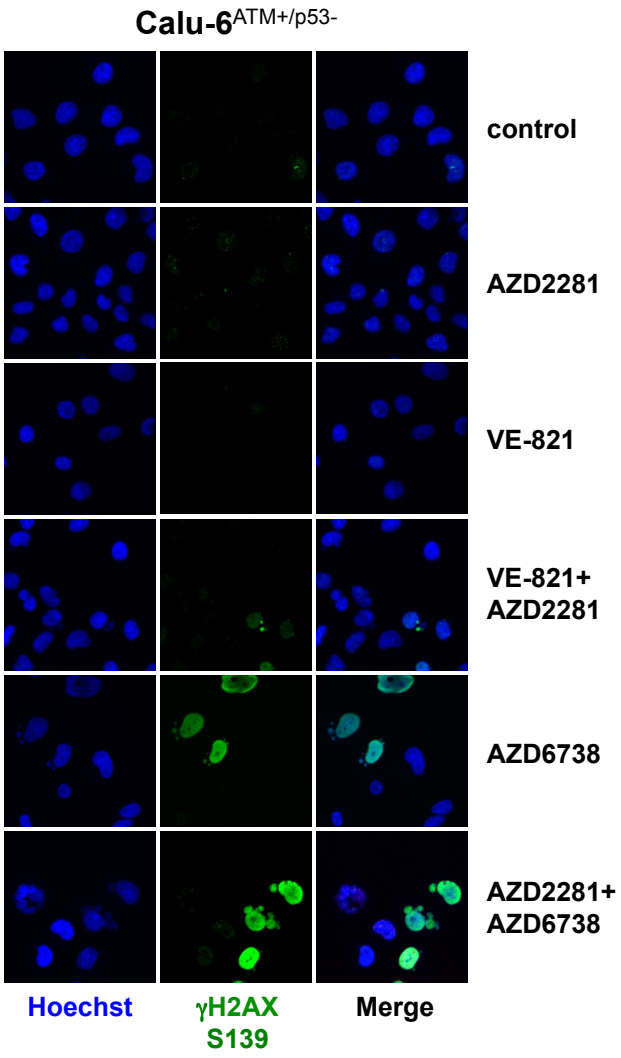

Figure 6.7: Combined ATR and PARP inhibition causes formation of micronuclei in p53-deficient NSCLC cells.

Calu-6 cells were treated with DMSO (control), AZD2281 (1 μM), VE-821 (1 μM), AZD6738 (1 μM) or the combinations of ATR and PARP inhibitors for 48 h. Cells were then fixed and stained for γH2AX. DNA was counter-stained with Hoechst. Images were acquired with the InCell analyser at a 200x magnification. Representative images of three (for AZD6738) or two (VE-821) independent experiments are shown.

Following addition of olaparib, this phenotype was exacerbated in all four p53-deficient cell lines. VE-821 treatment alone caused no formation of micronuclei in any of the cell lines. Combination treatment of VE-821 and olaparib, on the other hand,

induced micronuclei formation in all p53-deficent cells, albeit to a lesser extent than AZD6738 +/- olaparib (Figure 6.7). Cell lines with retained p53-function (A549 and COR-L105), showed no or only minimal signs of micronuclei formation under any of the treatment conditions (Figure 6.8). It should be noted that out of the four p53 mutated cell lines analysed, H1975 showed the least formation of micronuclei when treated with the ATR +/- PARP inhibitor combinations.

This data suggests, that concomitant disruption of PARP and ATR induces mitotic aberrations predominantly in p53-deficient cells, which could then lead to cell death through mitotic catastrophe.

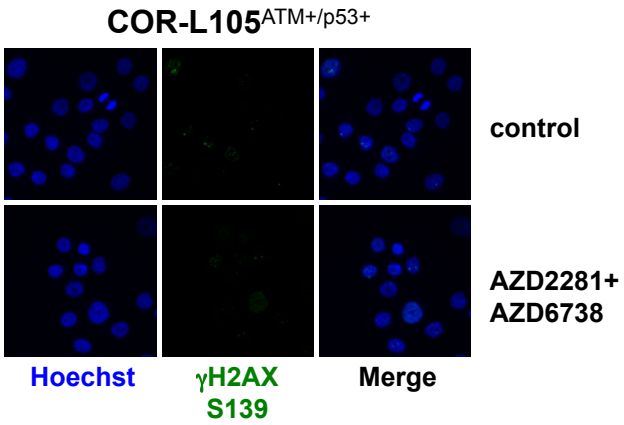

Figure 6.8: P53-proficient NSCLC cells show no micronuclei formation following combined inhibition of ATR and PARP.

COR-L105 cells were treated with DMSO (control) or a combination of AZD2281 (1 μM) and AZD6738 (1 μM) for 48 h. Cells were then fixed and stained for γH2AX. DNA was counter-stained with Hoechst. Images were acquired with the InCell analyser at a 200x magnification. Representative images of three independent experiments are shown.

6.5 *In vivo* anti-tumour activity of combined ATR and PARP inhibition in p53-deficient human NSCLC tumour xenografts

Next, we aimed to assess whether combined ATR and PARP inhibition has the potential to inhibit growth of p53-deficient NSCLC cells *in vivo*.

In our first study, we tested the tumour growth inhibitory activity of AZD6738 and olaparib in Balb/c nude mice bearing H1975 xenografts. H1975 cells were subcutaneously implanted onto the lower back of 6-8 weeks old female Balb/c nude mice (n=20) and tumour size was measured in three dimensions three times per week. Once tumours reached a volume of 100 mm^3, mice were randomised into four groups: (i) group 1 (vehicles alone, p.o. days 0-2, n=5), (ii) group 2 (olaparib, p.o. 50 mg/kg, days 0-2, n=5), (iii) group 3 (AZD6738, p.o. 50 mg/kg, days 0-2, n=5) or (iv) group 4 (AZD6738 and 2 hours later olaparib, each p.o. 50 mg/kg, days 0-2, n=5). Mice were schedule 1 sacrificed when tumours reached a volume of approximately 400 mm^3. Due to non-procedure related events, two of the mice in group 2 (olaparib alone) were culled prematurely. Given the small number of remaining animals in this group, the anti-tumour activity of olaparib alone was assessed in a separate study (which was performed by Dr. John Moore who repeated groups 1 and 2 with n=4 animals per group).

No difference in body weight was observed between olaparib (AZD2281), AZD6738 or combination-treated mice and vehicle-treated control, suggesting that both compounds alone and in combination were well tolerated at the administered doses.

Neither AZD6738, nor olaparib showed any significant single-agent anti-proliferative activity *in vivo* (Figure 6.9b, c).

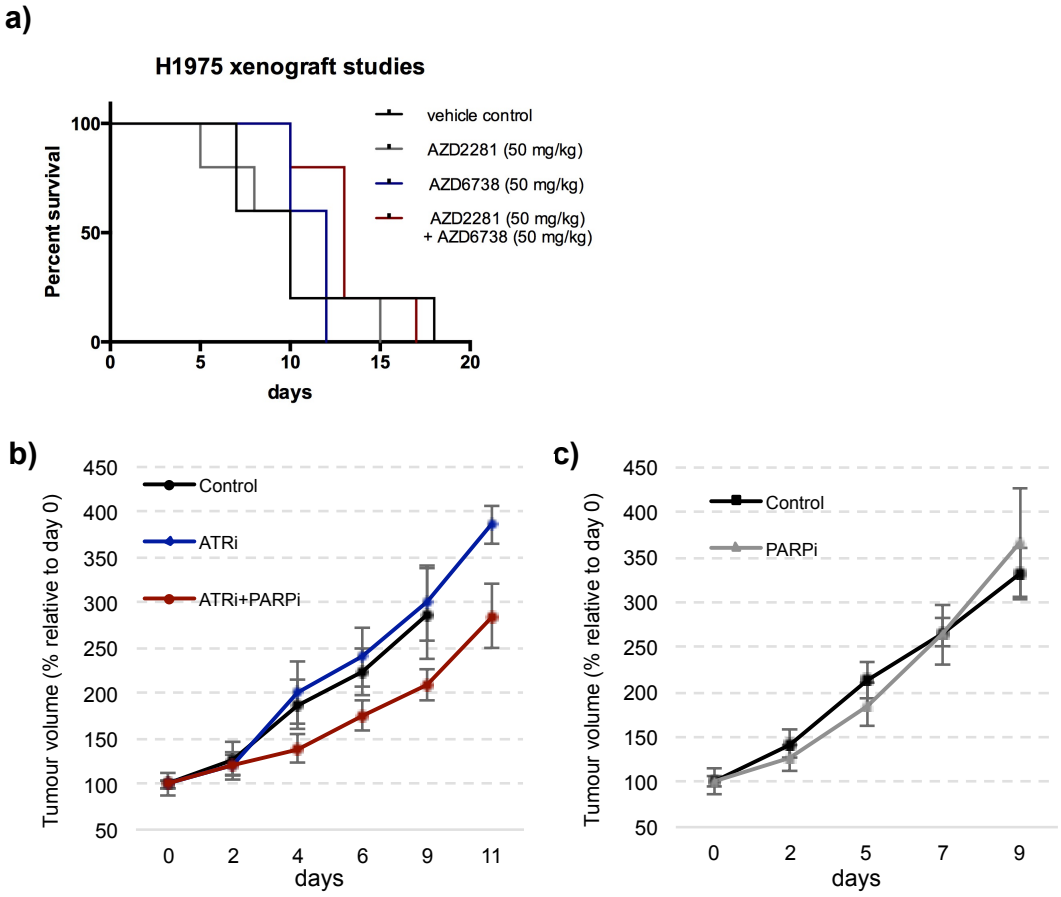

Figure 6.9: *In vivo* anti-tumour activity of AZD6738 and AZD2281 alone and in combination in a human xenograft model of H1975 NSCLC cells.

H1975 xenograft bearing Balb/c nude mice were treated once daily for three consecutive day with: group 1: vehicle control; group 2: 50 mg/kg AZD2281; group 3: 50 mg/kg AZD6738 and group 4: 50 mg/kg AZD6738 followed by 50 mg/kg AZD2281 2 h later.
a) Kaplan-Meier curve showing the survival of mice from each of the 4 treatment groups (mice were sacrificed by schedule 1 when they reached the endpoint = tumour size of ≥400 mm^3).
b) Graph representing the mean tumour volumes for treatment groups 1, 3 and 4 normalised to day 0 (=100%; first day of treatment) ± SEM. Data is shown up to the day where at least 3 animals per group were still included in the study.
c) Graph representing the mean relative tumour size for treatment groups 1 and 2 as in b). Data was obtained in a separate study and kindly provided by Dr. John Moore.

Adding olaparib to AZD6738 moderately delayed tumour growth and slightly prolonged the life span (time to sacrifice) of the animals[39] (Figure 6.9a, b). However, the size of the effect did not reach statistical significance[40].

Nevertheless, the observation that some tumour growth inhibition was achieved through combined ATR and PARP inhibition in this model raised the possibility that longer treatment with the drugs might increase the effect. We therefore planned a second *in vivo* study with an extended treatment schedule. As the fast growth rate of H1975 xenografts would not allow to extend the treatment duration over the course of several weeks, we chose a Calu-6 xenograft model for the second study. Mice (n=48; n=8 mice for efficacy and n=4 for pharmacodynamics studies per group) were implanted with Calu-6 tumour cells and randomised into the four treatment groups when tumours reached a volume of 100 mm^3 as before. Mice were treated with the compounds once daily on days 0-4 and 7-11 (groups and dosing were the same as in the first study). For the combinations, AZD6738 was administered first followed by olaparib (AZD2281) 2 h later. 3-4 mice per group were sacrificed two hours after administration of the last dose on day 11 for pharmacodynamics and biomarker studies (see section 6.6).

Similar to the results obtained in H1975 xenograft models, olaparib treatment alone did not affect tumour growth compared with vehicle controls. AZD6738, on the other hand, moderately delayed tumour growth (Figure 6.10b).

---

39. meaning the time until tumours reached a size of approximately 400 mm^3.
40. Treatment groups were compared by univariate ANOVA with day and treatment as factors, and relative tumour size as the variable; Bonferroni and Tukey corrections for multiple testing were included.

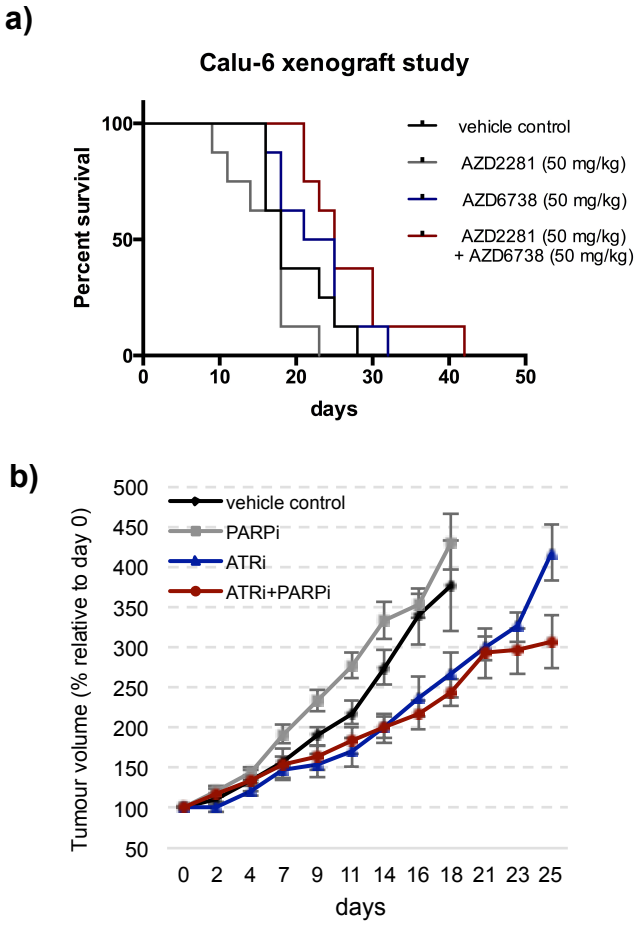

Figure 6.10: *In vivo* anti-tumour activity of AZD6738 and AZD2281 alone and in combination in a human xenograft model of Calu-6 NSCLC cells.

Calu-6 xenograft bearing Balb/c nude mice were treated for 5 consecutive days, followed by a 2-day treatment break and then another 5 days of treatment as follows: group 1: vehicle control; group 2: 50 mg/kg AZD2281; group 3: 50 mg/kg AZD6738 and group 4: 50 mg/kg AZD6738 followed by 50 mg/kg AZD2281 2 h later.
a) Kaplan-Meier curve showing the survival of mice from each of the 4 treatment groups. Mice were schedule 1 sacrificed when tumours reached a size of ≥400 mm^3.
b) Tumour volumes for each treatment group. Data are presented as mean relative tumour volume of each treatment group normalised to day 0 (=100%; first day of treatment) ± SEM. Data is shown up to the day where at least 4 animals per group were still included in the study.

Adding olaparib to AZD6738 treatment increased the anti-tumour effect in several of the mice in the group and prolonged the life span of the animals when compared with the vehicle control group (Figure 6.10a). However, the overall tumour growth inhibitory effect across the group did not reach statistical significance compared with AZD6738 treatment alone[41] (Figure 6.10b).

6.6 *In vivo* pharmacodynamics and biomarkers of ATR inhibition in Calu-6 xenograft models

To assess the cellular responses to pharmacological inhibition of ATR and/or PARP *in vivo*, we performed immunohistochemical (IHC) analysis for several of the biomarkers we had previously tested *in vitro*. Calu-6 tumour xenografts were collected two hours after administration of the last dose on day 11 (n=3-4 per group; see section 6.5) and following processing and sectioning were stained for cleaved caspase-3 (CC3; apoptosis marker), phospho-histone H3 (pHH3; mitosis marker), cyclin A (S/G2-phase marker) and γH2AX.

CC3-positive cells were found in all tumours, but were mostly located around necrotic areas and no difference in the percentage of CC3-positive cells could be found between treatment groups (data not shown). Quantification of cells staining positive for pHH3 also showed no significant differences between tumours treated with AZD6738, olaparib or the combination and vehicle-treated control (Figure 6.11a). Olaparib (AZD2281) treatment led to a small, yet statistically significant ($p<0.001$) reduction in the percentage of cyclin A positive cells. AZD6738 treatment alone or in

41. Comparison of treatment groups was performed by univariate ANOVA including Bonferroni and Tukey corrections for multiple testing

combination with olaparib, on the other hand, had no marked effect on the expression of cyclin A (Figure 6.11b).

However, consistent with the *in vitro* data, AZD6738 and AZD6738+olaparib treated tumours showed significantly greater levels of pan-nuclear γH2AX (Figure 6.12a, b). This observation suggests that pan-nuclear H2AX phosphorylation might be a useful biomarker to assess the pharmacological activity of AZD6738 *in vivo*.

Interestingly, in several of the tumours treated with AZD6738 alone or in combination with olaparib, we observed small areas with much greater abundance of cells exhibiting pan-nuclear γH2AX than in the rest of the tumour (Figure 6.13a). Calu-6 xenografts are generally poorly vascularised and show areas of extensive hypoxia and necrosis. However, areas with the highest percentage of γH2AX appeared to have a greater density of blood vessels than the remaining tumour areas.

This observation suggests that the concentration of AZD6738 reached in the tumour tissue might depend greatly on the vascular density and that less well-perfused tumour areas are thus less affected by the drug.

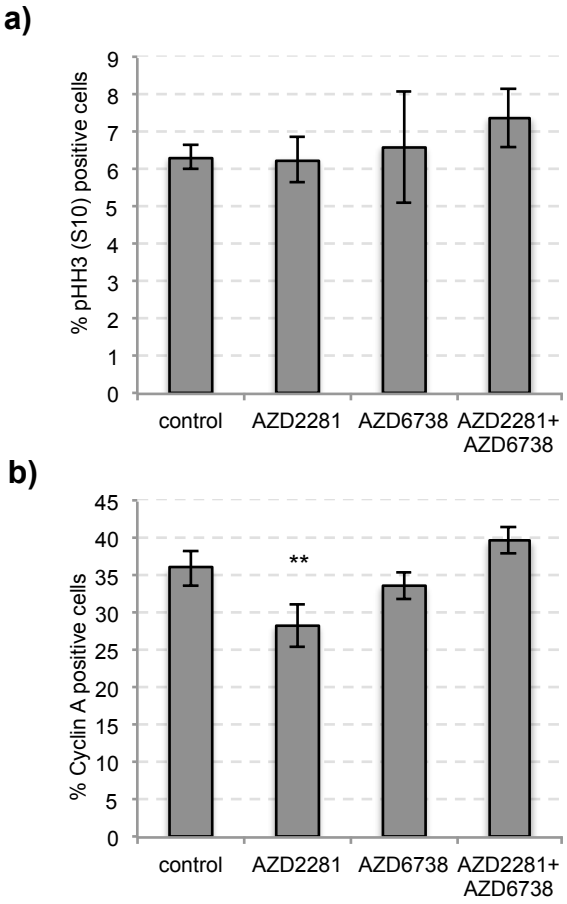

Figure 6.11: Effect of AZD6738 and/or olaparib treatment on tumour cyclin A and phospho-histone H3 levels in Calu-6 human NSCLC xenografts.

Quantification of the percentage of tumour cells staining positive for **a)** phospho-histone H3 (S10) and **b)** Cyclin A in IHC staining of Calu-6 xenografts following treatment with vehicle (control), AZD2281 (50 mg/kg), AZD6738 (50 mg/kg) or the combination. Mice were treated on days 0-4 and 7-11. Tumours were collected 2 h after administration of the last dose. Bars represent the means ± SEM.
Statistically significant differences between treatment groups are indicated by ** (= p-value <0.001 compared with control, calculated by 2-sided Student's t-test).

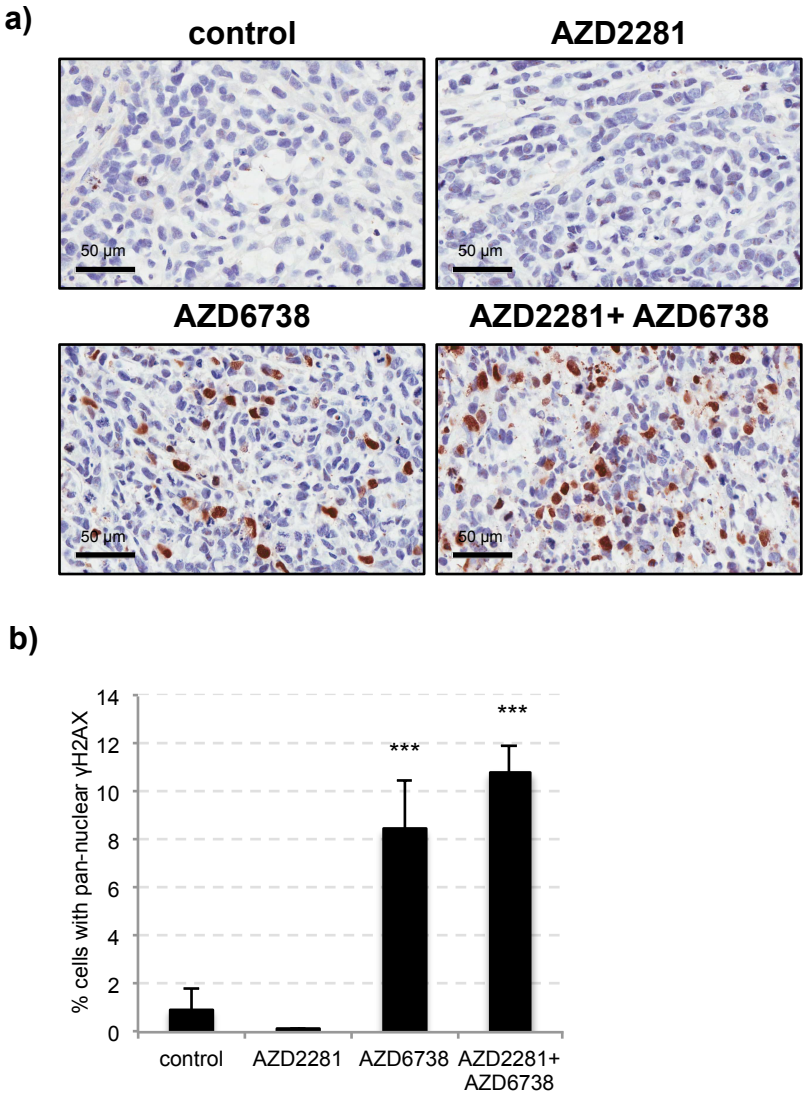

Figure 6.12: AZD6738 treatment alone and in combination with olaparib induces pan-nuclear H2AX phosphorylation in Calu-6 xenografts *in vivo*.

a) Representative images of γH2AX IHC staining in Calu-6 xenografts following treatment with vehicle (control), AZD2281 (50 mg/kg), AZD6738 (50 mg/kg) or the combination. Mice were treated on days 0-4 and 7-11. Tumours were collected 2 h after administration of the last dose. Pictures were taken at a 400x magnification. Scale bar = 50 μm.
b) Quantification of the percentage of tumour cells exhibiting pan-nuclear H2AX phosphorylation in Calu-6 xenografts treated as in a). Error bars = SEM.
Statistically significant differences between treatment groups are indicated by *** (= p-value <0.0001 compared with control, calculated by 2-sided Student's t-test).

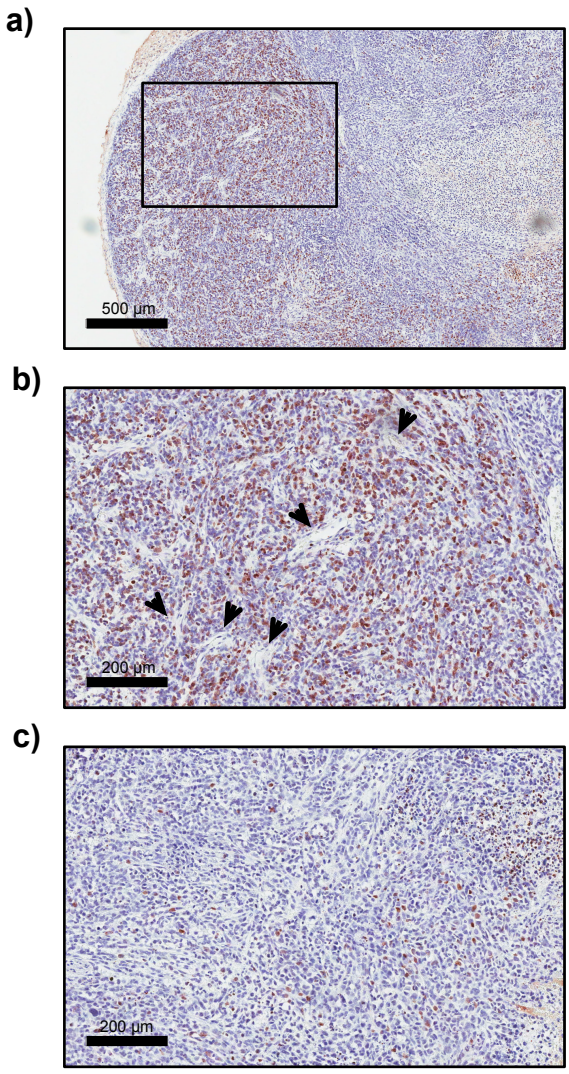

Figure 6.13: Pan-nuclear H2AX phosphorylation in Calu-6 xenograft cells in response to AZD6738+olaparib treatment occurs more frequently in highly vascularised tumour areas.

a) Representative image of a Calu-6 xenograft derived from a mouse treated with AZD6738 and olaparib (as in Figure 6.12a) stained for γH2AX by IHC. Note the significantly higher number of γH2AX positive cells in the tumour area on the left, compared with the area on the right. The encircled area is shown at a higher magnification in **b)** to illustrate the high abundance of blood vessels in this area (arrows).
c) Representative image of a poorly vascularised area from the same tumour as in b), showing significantly less cells with pan-nuclear γH2AX.
Pictures were taken at a 40x (a) or 100x (b, c) magnification. Scale bar = 500 (a) or 200 μm (b, c), respectively.

6.7 Discussion

In this study we aimed to assess the potential of the PARP inhibitor olaparib to sensitise NSCLC cells to pharmacological ATR inhibition. We found that olaparib selectively sensitises p53-deficient NSCLC cells to the ATR inhibitor VE-821 *in vitro*. For the ATR inhibitor AZD6738 we also observed preferential sensitisation of p53-defective cells by olaparib, however, the sensitising effect was much smaller for AZD6738. Interestingly, we found that while addition of olaparib to VE-821 treatment markedly increased the induction of DNA DSBs (measured by γH2AX levels) compared with either single treatment, AZD6738 treatment alone caused a substantial increase in γH2AX levels, which was only minimally increased by olaparib. This difference in the ability of ATR inhibitors to induce DNA DSB formation could explain why addition of olaparib causes significantly greater sensitisation of cells to VE-821 compared with AZD6738. It further raises the question whether the observed differences in the induction of DNA damage by the different inhibitors are merely due to the levels of ATR inhibition achieved (potency) or if there might be other reasons like, for example, different modes of action or off-target effects. The observed difference in the cellular responses to the two ATR inhibitors alone and in combination with olaparib might have clinical implication, as it suggests that the addition of PARP inhibitors might increase the efficacy of some ATR inhibitors, but not others.

We also found that the response of cells to treatment with ATR inhibitors alone, or in combination with olaparib, differed between p53-mutated NSCLC cell lines: while some cell lines were greatly sensitised to VE-821 by olaparib, the effect was much smaller in other cell lines. This observation suggests that different types of p53

mutations may have differential effects on the sensitivity of cancer cells to combined ATR and PARP inhibition and this question will need to be addressed in further studies.

Despite the generally smaller effect size in 2D models, we found selective sensitisation of p53-deficient cells to AZD6738 by olaparib in 3D spheroid models, suggesting that there might still be a benefit of the drug combination for the treatment of p53-deficient tumours.

We aimed to further investigate the cellular responses to combined pharmacological ATR and PARP inhibition, particularly the mode of cell death. While some cell lines showed signs of apoptosis induction, other cell lines predominantly exhibited signs of mitotic aberrations and mitotic catastrophe, particularly the formation of micronuclei. This observation suggests that the mode of cell death might differ between cell lines. Furthermore, we found induction of replication stress and pan-nuclear H2AX phosphorylation preferentially in p53-deficient cells. However, there was no evidence for a causal relationship between the two. The induction of replication stress was generally greater in p53-deficient cells and might be a contributing factor in the observed cytotoxicity of AZD6738 +/- olaparib.

Of note, H23 cells, which are deficient in both ATM and p53, were markedly sensitised to both ATR inhibitors by olaparib, suggesting that functional ATM may ameliorate the effects of combined ATR and PARP inhibition, potentially at least in part via checkpoint activation. In addition to the loss of DNA damage checkpoints, functional impairment of homologous recombination could be a contributing factor. Both ATM and ATR are involved in homologous recombination repair and defects in either protein cause recombination defects and lower HR efficiency (Beucher *et al*,

2009; Wang *et al*, 2004). It is possible that functional loss of both proteins would exacerbate the HR defects. As HR is particularly important for the repair of replication-associated DNA DSBs (see section 1.12), which would be induced following combined PARP and ATR inhibition, and considering the known high sensitivity of HR defective cells to PARP inhibition, this might explain the hypersensitivity of H23 cells to the combination of ATR and PARP inhibition.

This hypothesis is consistent with a recent study, which demonstrated that NU6027[42] is synthetically lethal with PARP inhibition in an ATR-dependent manner (Peasland *et al*, 2011). The authors hypothesised that this toxicity is caused by HR repair defects following ATR inhibition.

We also investigated the *in vivo* anti-tumour activity of the olaparib/AZD6738 combination in human NSCLC xenograft models. Both agents alone as well as the combination were well tolerated with <10% body weight loss observed. Based on our *in vitro* data we anticipated single agent AZD6738 activity in both H1975 and Calu-6 xenografts, and some (modest) enhancement by olaparib. However, the observed anti-tumour effects of AZD6738 alone and in combination with olaparib were small in both models. A limiting factor for the combination studies might have been the short half-life of olaparib *in vivo*. It has been shown previously that a single oral administration of olaparib at 100 mg/kg (twice the dose that we used) produces a significant decrease of intra-tumoral PAR levels at 2 h post-dosing. However, a partial recovery to approximately 20% of normal levels was evident at 8 h after administration and complete recovery within 24 h (Shen *et al*, 2013). The half-life of AZD6738 in mice is not reported. A recent study testing the *in vivo* anti-tumour activity of a small

42. NU6027 was originally developed as CDK inhibitor, but was subsequently shown to also potently inhibit ATR.

molecule ATR inhibitor[43] demonstrated, that prolonged inhibition of ATR is required to achieve anti-tumour efficacy in an ATM-deficient mantle cell lymphoma xenograft model (the authors used a treatment schedule of 3x daily administration of the ATR inhibitor for 4 consecutive days) (Menezes *et al*, 2014). Whether this long treatment period is required due to the presence of functional p53 or due to short half-life of the ATR inhibitor is not certain. However, our *in vitro* results indicate that the cytotoxic effects of ATR +/- PARP inhibition may be cell cycle dependent and therefore require sustained target inhibition as cells might escape the toxic effects of the combination treatment if ATR and/or PARP function is restored too soon. Our data obtained from 3D spheroid models suggests that 48 h might be sufficient. However, treatment duration experiments to determine the minimum time required to achieve an effect have not been performed yet.

In agreement with our *in vitro* data and the findings of other laboratories (Jacq *et al*, 2012; Guichard *et al*, 2013; Chen *et al*, 2014), ATR inhibition induced pan-nuclear H2AX phosphorylation *in vivo*, suggesting that pan-nuclear γH2AX phosphorylation might be useful biomarker for the assessment of AZD6738 activity *in vivo*. We observed a clear effect of AZD6738 treatment on γH2AX levels 2 h after administration of the last dose in pharmacodynamics studies, however we do not yet know if this effect is sustained between doses. We also found evidence of higher γH2AX levels in well vascularised tumour areas, suggesting that perfusion affects the concentrations of AZD6738 reached in the tissue and thus duration of inhibition. This finding further raises the possibility that less well-vascularised areas, including hypoxic regions of the tumour, may be less affected by the treatment.

---

43. It is not specified in the publication which ATR inhibitor was used, only that it belongs to the same series of pyrimidine indole derivatives as AZD6738 (patent ID# WO2010/073034).

Further studies are required to better evaluate the potential of this drug combination *in vivo* in both p53 wild-type and mutant tumours. Detailed PK/PD analysis following AZD6738 dosing, and exchanging olaparib for an alternative PARP inhibitor with longer half-life, for example BMN 673 (Shen *et al*, 2013), would help to address the question of the treatment duration required to achieve anti-tumour efficacy. Alternatively treatment schedules would need to be optimised to match *in vivo* target inhibition profiles over longer time periods.

CHAPTER 7

7 General discussion and conclusion

The DDR kinases ATM and ATR have sparked considerable scientific interest in recent years as potential targets for cancer therapy. Selective ATR inhibitors are currently in Phase I clinical development and it seems likely that ATM inhibitors with good pharmacological properties will become available in the near future. Several pre-clinical studies support the clinical development of ATM and ATR kinase inhibitors in two therapeutic approaches: as a monotherapy, aiming for synthetic lethal responses in tumours with DDR defects, and in combination with chemo- or radiotherapy. Each approach has its own set of challenges.

For synthetic lethal approaches to be successful, it will be critical to identify the right patient subsets with certain DDR defects that would confer sensitivity towards ATM and ATR inhibitors. Current sequencing techniques can identify mutations in DDR genes that may impact on the response of cancer cells to these treatments, for example p53. However, without functional studies, the consequences of these mutations are difficult to predict for proteins such as, for example, ATM. Developing biomarkers that can robustly determine the functional status of DDR pathways in tumours and help differentiate between deleterious and benign mutations will therefore be essential. In our studies we were able to demonstrate that somatic mutations in the ATM gene can lead to a reduction or loss of ATM protein expression, consistent with previous studies on loss-of-function ATM mutations in Ataxia-telangiectasia. Based on this observation we were able to develop an immunohistochemistry-based assay, which may allow for the identification of tumoral loss of ATM function in a clinical setting.

We have not yet investigated the correlation between loss of ATM protein expression in IHC analysis and the presence of ATM mutations or epigenetic changes in clinical samples. However, we would anticipate ATM IHC negative samples to be enriched for ATM mutations and possibly also markers of epigenetic silencing of ATM (e.g. promoter hypermethylation). An additional limitation of our studies thus far is that no data on pre-treatment of patients, treatment responses or survival outcome is available for the samples used in this study. Therefore no prediction for a potential correlation between ATM protein expression levels and response to chemo- and/or radiotherapy, or overall survival, can be made at this point.

Loss of ATM function has long been known to confer hypersensitivity to ionising radiation (Taylor *et al*, 1975), yet, to our knowledge, no studies investigating a potential link between ATM protein levels and tumour responses to radiotherapy have been carried to date. However, a recent study has demonstrated that elevated levels of ATM activity (measured by ATM autophosphorylation on S1981) prior to radiotherapy is associated with radioresistance and poor prognosis in cervical cancer (Roossink *et al*, 2012). This suggests that the response of tumours to radiotherapy might be associated with the levels of ATM activity and that reduced ATM expression or activity could confer radiosensitivity in a clinical setting. Furthermore, elevated levels of ATM protein expression or ATM activity in tumour tissues could serve as a potential biomarker to identify patients that might get the greatest benefit from a combination of ATM inhibitor treatment and radiotherapy.

Similar approaches may also prove useful for the detection of defects in other DDR components. For example, a study evaluating the protein expression of MRE11, a component of the MRN complex, by immunohistochemistry has demonstrated low

expression in bladder cancer, which was associated with worse survival following radiotherapy, but not surgery (Choudhury *et al*, 2010). This is of particular interest, as recent studies have suggested that cells with deficiency in MRE11 show increased sensitivity to ATR inhibitors *in vitro* and *in vivo* (Jacq *et al*, 2012; Foote *et al*, 2013; Guichard *et al*, 2013).

A recent study suggested that pharmacological ATR inhibition is selectively cytotoxic for cells with deficiency in either ATM or p53 when combined with genotoxic modalities (Reaper *et al*, 2011). The authors attributed this increased toxicity to the deficiency in G1 checkpoint activation observed in ATM- or p53-deficient cells and hypothesised that this checkpoint deficiency would drive a reliance of the cells on ATR-mediated intra-S and G2/M cell cycle checkpoints following DNA damage induction. In our studies we were unable to find a clear association between sensitivity of cells to pharmacological ATR inhibition (alone or in combination with genotoxic modalities such as IR and gemcitabine) and the functional status of either ATM or p53 alone. However, cells with combined functional loss of ATM and p53 showed substantial sensitivity to all three ATR inhibitors tested in this study, as single agents as well as in combination with IR. Our findings are supported by early studies assessing the radiosensitising properties of caffeine, a dual inhibitor of ATM and ATR, which showed improved radiosensitisation in p53-deficient cells (Bracey *et al*, 1997; Powell *et al*, 1995; Yao *et al*, 1996).

Our data suggests that ATM, ATR and p53 play important and partially overlapping roles in cell cycle checkpoint activation, which can act independently of each other – both following DNA damage induction, and also during normal cell cycle progression. We found that loss of all three signalling pathways led to excessive chromosomal

breakage during mitosis, chromosome mis-segregation (micronuclei formation) and eventually mitosis associated cell death, while retained activity of any one of these proteins is sufficient to ensure cell survival.

In addition to the identification of biomarkers for patient selection, another important challenge in the clinical development of ATM and ATR inhibitors will be the optimisation of treatment schedules and treatment duration. Particularly for combination studies a key issue is likely to be concern over the potential for increased normal tissue toxicity. Therefore, identifying the combinations and treatment schedules that have the greatest potential for tumour selective effects will be important. While several pre-clinical studies suggest that short-term treatment with ATM or ATR inhibitors may be sufficient to confer chemo- or radiosensitisation (Rainey *et al*, 2008; Batey *et al*, 2013; Fokas *et al*, 2012), synthetic lethal approaches may require prolonged target inhibition.

In live cell imaging studies we found that following treatment with a combination of ATM and ATR inhibitors, the first signs of mitotic aberrations and micronuclei formation – both important biomarkers for the sensitivity responses that we observed in p53-deficient cells – only became apparent approximately 10 hours after addition of the drugs. We also found evidence that chromosomal breakage and DNA damage induction occurred during mitosis and only following abrogation of DNA damage induced cell cycle checkpoints, suggesting that the cytotoxicity may be cell cycle dependent. Taken together these observations suggest that sustained target inhibition may be necessary to induce synthetic lethality in the absence of exogenous genotoxic stresses. Treatment duration experiments will be required to assess the minimum treatment time required to see anti-tumour activity.

In the early stages of clinical development, it is crucial to develop biomarkers for target inhibition, biological response and efficacy, to guide the further development of the compounds.

CHK1 phosphorylation is the most widely used preclinical biomarker of ATR kinase activity (Fokas *et al*, 2012; Hall *et al*, 2014; Pires *et al*, 2012; Chen *et al*, 2014). However, a recent study in ovarian cancer has suggested that CHK1 phosphorylation status may not offer a reliable marker for inhibition of the ATR-CHK1 pathway, as ATR inhibition was found to block gemcitabine-induced phosphorylation of CHK1 (Ser296 and Ser345) only in certain cell lines (Huntoon *et al*, 2013). Interestingly, a recent study assessing CHK1 phosphorylation following ATR knockdown has suggested that phospho-CHK1 levels may only reflect ATR kinase activity for a short period of time (3 h) after ATR depletion (Chen *et al*, 2014). Our results support these findings, as we also found that gemcitabine-induced phosphorylation of CHK1 was not consistently reduced by ATR inhibition. At the same time, we observed a marked increase in ATM activity and downstream signalling. As ATM can also phosphorylate CHK1, albeit to a lesser extent (Sørensen *et al*, 2003; Helt *et al*, 2005; Gatei *et al*, 2003; Ozeri-Galai *et al*, 2008), it is possible that the sustained phosphorylation of CHK1 could reflect a compensatory phosphorylation mediated by ATM. In agreement with this hypothesis, we found evidence that the background levels of CHK1 S296 phosphorylation observed under physiological conditions are decreased following ATM inhibition, supporting a role of ATM in the regulation of CHK1 phosphorylation and activity.

Another proposed biomarker for the biological activity of ATR inhibitors is the occurrence of pan-nuclear H2AX, a potential marker of induced replication stress (Murga *et al*, 2010; Jacq *et al*, 2012; Guichard *et al*, 2013; Chen *et al*, 2014). Our data

supports the utility of pan-nuclear H2AX phosphorylation as biomarker for ATR inhibitor efficacy, particularly for the ATR inhibitors AZD6738 and VE-822. We observed this phenotype both *in vitro* and *in vivo* and particularly in p53-defective cells, which were generally more sensitive to these ATR inhibitors. However, we could not confirm a causal relationship between the occurrence of pan-nuclear H2AX phosphorylation and the induction of replication stress.

The identification of biomarkers for ATM activity appears more straightforward. ATM autophosphorylation at S1981 has been shown to be a hallmark of activated human ATM (Shiloh & Ziv, 2013; Bakkenist & Kastan, 2003), and might thus have great utility to assess ATM kinase activity levels in tumour tissue (Roossink *et al*, 2012). IR-induced phosphorylation of the ATM downstream targets KAP1, SMC1 and CHK2 are additional widely used biomarkers of ATM kinase activity *in vitro* (Rainey *et al*, 2008; Olcina *et al*, 2013; Barone *et al*, 2009; Jacquemin *et al*, 2012; Verhagen *et al*, 2012; Guo *et al*, 2014). We found that IR-induced phospho-KAP1 (S824) and phospho-SMC1 (S966) levels correlated well with ATM S1981 levels and were consistently reduced following ATM knockdown as well as ATM kinase inhibition. Future studies will need to assess the utility of these biomarkers *in vivo*, for example in immunohistochemical approaches.

However, it should be noted that, in our studies, IR-induced phosphorylation of CHK2 (Thr68) was not consistently reduced after genetic depletion of ATM. At the same time, pharmacological ATM inhibition reduced the radiation-induced phosphorylation of CHK2 in a dose-dependent manner. These observations raise the possibility that alternative DDR pathways might be up-regulated after prolonged impairment of ATM function. Given the important function of CHK2 in cell cycle checkpoint activation,

such a compensatory mechanism could affect the response of cells to genotoxic agents or DDR modulators and might thus have clinical implications.

Small molecule inhibitors of poly(ADP-ribose)-polymerase were the first class of DDR modulating compounds to enter clinical development and the PARP inhibitor olaparib (LYNPARZA™) has recently been FDA approved as monotherapy for the treatment of BRCA-mutation positive advanced ovarian cancer. Several recent studies have focussed on identifying additional genes that might mediate sensitivity to PARP inhibition in BRCA wild-type cells and both ATM and ATR have been identified as potential targets (Dedes *et al*, 2011; Turner *et al*, 2008; Gilardini Montani *et al*, 2013; Kubota *et al*, 2014; Williamson *et al*, 2010, 2012). Therefore the wider clinical development of PARP inhibitors for the treatment of patients with non-BRCA mutated tumours could include combinations with ATR and ATM inhibitors.

We studied the potential of olaparib to enhance the efficacy of pharmacological ATR inhibition and found preferential sensitisation of p53-deficient NSCLC cells to the ATR inhibitors VE-821 and AZD6738 *in vitro*. Notably, cells with deficiency in both ATM and p53 were particularly sensitive to the combination, consistent with our finding that ATM and p53 play important roles in the cellular response to ATR inhibitors and a recent study which demonstrated that deficiency in both ATM and p53 confers high sensitivity to PARP inhibition (Williamson *et al*, 2012). At the same time, and contrary to previous reports (Williamson *et al*, 2010; Gilardini Montani *et al*, 2013), we found that cells with deficiency in ATM, but retained p53 function (H1395), were not particularly sensitive to single agent olaparib treatment (data not shown). Moreover, we found no sensitisation to AZD6738 by olaparib in these cells, further supporting the role of p53 in the response.

Despite the observed sensitisation of p53-deficient cells to AZD6738 by olaparib, particularly in 3D spheroid models, we found no significant enhancement of the anti-tumour activity of AZD6738 in *in vivo* xenograft models. Our *in vitro* data and the proposed mechanism underlying cancer cell sensitisation to ATR inhibitors by concomitant PARP inhibition suggest that prolonged target inhibition might be required to achieve efficacy. Therefore a potential explanation for the lack of *in vivo* activity of the AZD6738+olaparib combination could be the short half-life of olaparib in mouse models (Shen *et al*, 2013). We are planning further experiments to better evaluate the potential of ATR and PARP inhibitor combinations. These include additional *in vivo* studies to assess the efficacy of AZD6738 treatment in combination with an alternative PARP inhibitor (BMN 673), which possesses improved pharmacokinetic properties compared with olaparib and a longer half life (Shen *et al*, 2013).

We conclude from our studies that deficiency in p53 may identify cells that show increased sensitivity to combined ATR and PARP inhibition, a sensitivity that is further increased in cells with additional functional loss of ATM. However, there are limitations to the current work, which will require us to perform additional studies to confirm the role of p53 in the response to combined ATR and PARP inhibition. In our studies we used a panel of NSCLC cell lines and the presence of different types of p53 mutations and other somatic mutations may have been confounding factors. Therefore, the role of p53 should be studied further in isogenically matched cell lines with/without functional p53. Furthermore, studies to optimise treatment schedules, by assessing the minimum treatment time required to see anti-proliferative effects in treatment duration experiments, will need to be performed to assess whether clinically relevant anti-tumour activity can be achieved within a reasonable treatment period.

We are also planning to study the mechanism underlying the increased sensitivity of p53-deficient cells to combined ATM and ATR inhibition in more detail. We are particularly interested in cell cycle checkpoint functions of p53 in the absence of functional ATM and ATR. Furthermore, we aim to study the mechanism leading to chromosome fragmentation in more detail to address whether chromosomes condense before completion of DNA replication and whether the observed chromosomal breakage occurs at common fragile sites. These studies might also give further insight into the mechanisms and causes underlying the occurrence of pan-nuclear H2AX phosphorylation in response to ATR inhibition and the differences between different ATR inhibitors. As we observed this phenotype more frequently in cell lines with increased sensitivity to the respective ATR inhibitors, it might be useful as a biomarker of ATR inhibitor efficacy, and understanding the underlying mechanism could help identify additional cellular properties or somatic mutations that might mediate sensitivity to ATR inhibition.

Thus far, the knowledge about possible off-target effects, modes of action and kinetics of inhibition of the ATR inhibitors used in this study are incomplete. It would be interesting to compare our results from pharmacological ATR inhibition with cellular responses following downregulation of ATR protein levels. However, due to the observed strong reaction of cells to siRNA transfections (with regard to activation of the ATM signalling pathway), we were unable to study the effects of genetic depletion of ATR, which is a limitation of the current study. Nonetheless, we were able to validate the increased sensitivity of p53- and ATM-deficient cells to pharmacological ATR inhibition in several different assay types (2D and 3D cell viability assays, clonogenic survival assays and live cell imaging) and with three different small

molecule ATR inhibitors, which adds strength to the argument that ATM, ATR and p53 play vital and overlapping roles in maintaining cell viability.

We conclude that the therapeutic utility of ATR inhibitors alone or in combination with IR may depend on the functional status of both ATM and p53. Coexisting mutations in both ATM and p53 are not common in NSCLC (approx. 1.7-4.9% of cases (Cancer Genome Atlas Research Network, 2012b, 2014)). However, considering that approximately 1.5 million cases of NSCLC are diagnosed every year, a considerable number of patients with deficiencies in both pathways could get increased benefit from ATR inhibitor therapy. Furthermore, mutations in both ATM and p53 occur with a higher frequency in other types of cancer like, for example, in mantle cell lymphoma, where approximately 10% of cases harbour mutations in both genes (Greiner *et al*, 2006)). Our data also suggest that combining both ATR and ATM inhibition is selectively cytotoxic to p53-deficient tumour cells. Since mutations in p53 are very common in NSCLC (46-90% of cases (Cancer Genome Atlas Research Network, 2012b, 2014)), and many other tumour types, this combination approach might have broad utility for cancer treatment.

8 References

Abraham RT (2001) Cell cycle checkpoint signaling through the ATM and ATR kinases. *Genes Dev*. **15:** 2177–96

Adzhubei I a, Schmidt S, Peshkin L, Ramensky VE, Gerasimova A, Bork P, Kondrashov AS & Sunyaev SR (2010) A method and server for predicting damaging missense mutations. *Nat. Methods* **7:** 248–9

Ahnesorg P, Smith P & Jackson SP (2006) XLF interacts with the XRCC4-DNA Ligase IV complex to promote DNA nonhomologous end-joining. *Cell* **124:** 301–313

Al-Ahmadie H, Iyer G, Hohl M, Asthana S, Inagaki A, Schultz N, Hanrahan AJ, Scott SN, Brannon AR, McDermott GC, Pirun M, Ostrovnaya I, Kim P, Socci ND, Viale A, Schwartz GK, Reuter V, Bochner BH, Rosenberg JE, Bajorin DF, et al (2014) Synthetic lethality in ATM-deficient RAD50-mutant tumors underlie outlier response to cancer therapy. *Cancer Discov*. **4:** 1014–21

Alderton GK, Joenje H, Varon R, Børglum AD, Jeggo PA & O'Driscoll M (2004) Seckel syndrome exhibits cellular features demonstrating defects in the ATR-signalling pathway. *Hum Mol Genet*. **13:** 3127–38

Allen C, Halbrook J & Nickoloff JA (2003) Interactive competition between homologous recombination and non-homologous end joining. *Mol Cancer Res*. **1:** 913–920

American Cancer Society (2014) Cancer Facts & Figures 2014. *Atlanta Am. Cancer Soc*.

An J, Huang Y-C, Xu Q-Z, Zhou L-J, Shang Z-F, Huang B, Wang Y, Liu X-D, Wu D-C & Zhou P-K (2010) DNA-PKcs plays a dominant role in the regulation of H2AX phosphorylation in response to DNA damage and cell cycle progression. *BMC Mol Biol* **11:** 18

Arnaudeau C, Lundin C & Helleday T (2001) DNA double-strand breaks associated with replication forks are predominantly repaired by homologous recombination involving an exchange mechanism in mammalian cells. *J Mol Biol*. **307:** 1235–1245

Audebert M, Salles B & Calsou P (2004) Involvement of poly(ADP-ribose) polymerase-1 and XRCC1/DNA ligase III in an alternative route for DNA double-strand breaks rejoining. *J Biol Chem*. **279:** 55117–55126

Audeh MW, Carmichael J, Penson RT, Friedlander M, Powell B, Bell-McGuinn KM, Scott C, Weitzel JN, Oaknin A, Loman N, Lu K, Schmutzler RK, Matulonis U, Wickens M & Tutt A (2010) Oral poly(ADP-ribose) polymerase inhibitor olaparib in patients with BRCA1 or BRCA2 mutations and recurrent ovarian cancer: a proof-of-concept trial. *Lancet* **376:** 245–51

Aylon Y, Liefshitz B & Kupiec M (2004) The CDK regulates repair of double-strand breaks by homologous recombination during the cell cycle. *EMBO J*. **23:** 4868–4875

Bakkenist CJ & Kastan MB (2003) DNA damage activates ATM through intermolecular autophosphorylation and dimer dissociation. *Nature* **421:** 499–506

Banin S, Moyal L, Shieh S-Y, Taya Y, Anderson CW, Chessa L, Smorodinsky NI, Prives C, Reiss Y, Shiloh Y & Ziv Y (1998) Enhanced Phosphorylation of p53 by ATM in Response to DNA Damage. *Science*. **281:** 1674–1677

Bao S, Wu Q, McLendon RE, Hao Y, Shi Q, Hjelmeland AB, Dewhirst MW, Bigner DD & Rich JN (2006) Glioma stem cells promote radioresistance by preferential activation of the DNA damage response. *Nature* **444:** 756–60

Barlow C, Hirotsune S, Paylor R, Liyanage M, Eckhaus M, Collins F, Shiloh Y, Crawley JN, Ried T, Tagle D & Wynshaw-Boris A (1996) Atm-Deficient mice: A Paradigm of Ataxia Telangiectasia. *Cell* **86:** 159–71

Barone G, Groom A, Reiman A, Srinivasan V, Byrd PJ, Taylor A & R M (2009) Modeling ATM mutant proteins from missense changes confirms retained kinase activity. *Hum. Mutat.* **30:** 1222–30

Barretina J, Caponigro G, Stransky N, Venkatesan K, Margolin AA, Kim S, Wilson CJ, Lehár J, Kryukov G V., Sonkin D, Reddy A, Liu M, Murray L, Berger MF, Monahan JE, Morais P, Meltzer J, Korejwa A, Jané-Valbuena J, Mapa FA, et al (2012) The Cancer Cell Line Encyclopedia enables predictive modelling of anticancer drug sensitivity. *Nature* **483:** 603–307

Bartek J, Lukas C & Lukas J (2004) Checking on DNA damage in S phase. *Nat Rev Mol Cell Biol.* **5:** 792–804

Bartek J, Mistrik M & Bartkova J (2012) Thresholds of replication stress signaling in cancer development and treatment. *Nat Struct Mol Biol.* **19:** 5–7

Bartkova J, Horejsi Z, Koed K, Krämer A, Tort F, Zieger K, Guldberg P, Sehested M, Nesland JM, Lukas C, Ørntoft T, Lukas J & Bartek J (2005) DNA damage response as a candidate anti-cancer barrier in early human tumorigenesis. *Nature* **434:** 864–870

Bartkova J, Rezaei N, Liontos M, Karakaidos P, Kletsas D, Issaeva N, Vassiliou L-VF, Kolettas E, Niforou K, Zoumpourlis VC, Takaoka M, Nakagawa H, Tort F, Fugger K, Johansson F, Sehested M, Andersen CL, Dyrskjot L, Ørntoft T, Lukas J, et al (2006) Oncogene-induced senescence is part of the tumorigenesis barrier imposed by DNA damage checkpoints. *Nature* **444:** 633–7

Bartkova J, Tommiska J, Oplustilova L, Aaltonen K, Tamminen A, Heikkinen T, Mistrik M, Aittomäki K, Blomqvist C, Heikkilä P, Lukas J, Nevanlinna H & Bartek J (2008) Aberrations of the MRE11-RAD50-NBS1 DNA damage sensor complex in human breast cancer: MRE11 as a candidate familial cancer-predisposing gene. *Mol Oncol.* **2:** 296–316

Batey MA, Zhao Y, Kyle S, Richardson C, Slade A, Martin NMB, Lau A, Newell DR & Curtin NJ (2013) Preclinical evaluation of a novel ATM inhibitor, KU59403, in vitro and in vivo in p53 functional and dysfunctional models of human cancer. *Mol Cancer Ther.* **12:** 959–67

Baumann P, Benson FE & West SC (1996) Human Rad51 protein promotes ATP-dependent homologous pairing and strand transfer reactions in vitro. *Cell* **87:** 757–766

Beà S, Valdés-Mas R, Navarro A, Salaverria I, Martín-Garcia D, Jares P, Giné E, Pinyol M, Royo C, Nadeu F, Conde L, Juan M, Clot G, Vizán P, Di Croce L, Puente DA, López-Guerra M, Moros A, Roue G, Aymerich M, et al (2013) Landscape of somatic mutations and clonal evolution in mantle cell lymphoma. *Proc Natl Acad Sci U S A* **110:** 18250–5

Le Beau MM, Rassool F V., Neilly ME, Espinosa R, Glover TW, Smith DI & McKeithan TW (1998) Replication of a common fragile site, FRA3B, occurs late in S phase and is delayed further upon induction: Implications for the mechanism of fragile site induction. *Hum Mol Genet.* **7:** 755–761

Beck H, Nähse-Kumpf V, Larsen MSY, O'Hanlon KA, Patzke S, Holmberg C, Mejlvang J, Groth A, Nielsen O, Syljuasen RG & Sorensen CS (2012) Cyclin-Dependent Kinase Suppression by WEE1 Kinase Protects the Genome through Control of Replication Initiation and Nucleotide Consumption. *Mol Cell Biol.* **32:** 4226–4236

Bennett CB, Lewis AL, Baldwin KK & Resnick MA (1993) Lethality induced by a single site-specific double-strand break in a dispensable yeast plasmid. *Proc Natl Acad Sci U S A* **90:** 5613–7

Bennett RA, Wilson DM, Wong D & Demple B (1997) Interaction of human apurinic endonuclease and DNA polymerase beta in the base excision repair pathway. *Proc Natl Acad Sci U S A* **94:** 7166–7169

Berkovich E, Monnat RJ & Kastan MB (2007) Roles of ATM and NBS1 in chromatin structure modulation and DNA double-strand break repair. *Nat Cell Biol*. **9:** 683–690

Bermudez VP, Lindsey-Boltz L a, Cesare AJ, Maniwa Y, Griffith JD, Hurwitz J & Sancar A (2003) Loading of the human 9-1-1 checkpoint complex onto DNA by the checkpoint clamp loader hRad17-replication factor C complex in vitro. *Proc Natl Acad Sci U S A* **100:** 1633–1638

Beucher A, Birraux J, Tchouandong L, Barton O, Shibata A, Conrad S, Goodarzi AA, Krempler A, Jeggo PA & Löbrich M (2009) ATM and Artemis promote homologous recombination of radiation-induced DNA double-strand breaks in G2. *EMBO J*. **28:** 3413–3427

Biddlestone-Thorpe L, Sajjad M, Rosenberg E, Beckta JM, Valerie NCK, Tokarz M, Adams BR, Wagner AF, Khalil A, Gilfor D, Golding SE, Deb S, Temesi DG, Lau A, O'Connor MJ, Choe KS, Parada LF, Lim SK, Mukhopadhyay ND & Valerie K (2013) ATM kinase inhibition preferentially sensitizes p53-mutant glioma to ionizing radiation. *Clin Cancer Res*. **19:** 3189–200

Birmingham A, Anderson E, Sullivan K, Reynolds A, Boese Q, Leake D, Karpilow J & Khvorova A (2007) A protocol for designing siRNAs with high functionality and specificity. *Nat Protoc*. **2:** 2068–78

Blasina A, Hallin J, Chen E, Arango ME, Kraynov E, Register J, Grant S, Ninkovic S, Chen P, Nichols T, O'Connor P & Anderes K (2008) Breaching the DNA damage checkpoint via PF-00477736, a novel small-molecule inhibitor of checkpoint kinase 1. *Mol Cancer Ther*. **7:** 2394–404

Blasina A, Price BD, Turenne GA & McGowan CH (1999) Caffeine inhibits the checkpoint kinase ATM. *Curr Biol*. **9:** 1135–1138

Bobola MS, Kolstoe DD, Blank A, Chamberlain MC & Silber JR (2012) Repair of 3-methyladenine and abasic sites by base excision repair mediates glioblastoma resistance to temozolomide. *Front Oncol*. **2:176:**

De Bont R & van Larebeke N (2004) Endogenous DNA damage in humans: A review of quantitative data. *Mutagenesis*. **19:** 169–185

Bosotti R, Isacchi A & Sonnhammer EL (2000) FAT: a novel domain in PIK-related kinases. *Trends Biochem Sci*. **25:** 225–227

Boulton S, Pemberton LC, Porteous JK, Curtin NJ, Griffin RJ, Golding BT & Durkacz BW (1995) Potentiation of temozolomide-induced cytotoxicity: a comparative study of the biological effects of poly(ADP-ribose) polymerase inhibitors. *Br J Cancer*. **72:** 849–856

Bouwman P & Jonkers J (2012) The effects of deregulated DNA damage signalling on cancer chemotherapy response and resistance. *Nat Rev Cancer*. **12:** 587–598

Bracey TS, Williams AC & Paraskeva C (1997) Inhibition of radiation-induced G2 delay potentiates cell death by apoptosis and/or the induction of giant cells in colorectal tumor cells with disrupted p53 function. *Clin Cancer Res*. **3:** 1371–81

Brown EJ & Baltimore D (2000) ATR disruption leads to chromosomal fragmentation and early embryonic lethality. *Genes Dev*. **14:** 397–402

Brummelkamp TR, Bernards R & Agami R (2002) A system for stable expression of short interfering RNAs in mammalian cells. *Science*. **296:** 550–3

Bryant HE, Schultz N, Thomas HD, Parker KM, Flower D, Lopez E, Kyle S, Meuth M, Curtin NJ & Helleday T (2005) Specific killing of BRCA2-deficient tumours with inhibitors of poly(ADP-ribose) polymerase. *Nature* **434:** 913–7

Bugreev D V, Mazina OM & Mazin A V (2006) Rad54 protein promotes branch migration of Holliday junctions. *Nature* **442:** 590–593

Buis J, Stoneham T, Spehalski E & Ferguson DO (2012) Mre11 regulates CtIP-dependent double-strand break repair by interaction with CDK2. *Nat Struct Mol Biol*. **19:** 246–252

Buis J, Wu Y, Deng Y, Leddon J, Westfield G, Sekiguchi JM, Chang S & Ferguson DO (2009) Mre11 Nuclease Activity has Essential Roles in DNA Repair and Genomic Stability Distinct from ATM Activation. *Cell* **135:** 85–96

Bunz F, Dutriaux A, Lengauer C, Waldman T, Zhou S, Brown JP, Sedivy JM, Kinzler KW & Vogelstein B (1998) Requirement for p53 and p21 to sustain G2 arrest after DNA damage. *Science*. **282:** 1497–1501

Burma S, Chen BP, Murphy M, Kurimasa A & Chen DJ (2001) ATM phosphorylates histone H2AX in response to DNA double-strand breaks. *J Biol Chem*. **276:** 42462–7

Burzio LO, Riquelme PT & Koide SS (1979) ADP ribosylation of rat liver nucleosomal core histones. *J Biol Chem*. **254:** 3029–3037

Byun TS, Pacek M, Yee M, Walter JC & Cimprich KA (2005) Functional uncoupling of MCM helicase and DNA polymerase activities activates the ATR-dependent checkpoint. *Genes Dev*. **19:** 1040–52

Calabrese CR, Almassy R, Barton S, Batey M a, Calvert AH, Canan-Koch S, Durkacz BW, Hostomsky Z, Kumpf RA, Kyle S, Li J, Maegley K, Newell DR, Notarianni E, Stratford IJ, Skalitzky D, Thomas HD, Wang L-Z, Webber SE, Williams KJ, et al (2004) Anticancer chemosensitization and radiosensitization by the novel poly(ADP-ribose) polymerase-1 inhibitor AG14361. *J Natl Cancer Inst*. **96:** 56–67

Caldecott KW (2008) Single-strand break repair and genetic disease. *Nat Rev Genet*. **9:** 619–631

Cancer Genome Atlas Research Network (2012a) Comprehensive molecular characterization of human colon and rectal cancer. *Nature* **487:** 330–337

Cancer Genome Atlas Research Network (2012b) Comprehensive genomic characterization of squamous cell lung cancers. *Nature* **489:** 519–25

Cancer Genome Atlas Research Network (2012c) Comprehensive molecular portraits of human breast tumours. *Nature* **490:** 61–70

Cancer Genome Atlas Research Network (2014) Comprehensive molecular profiling of lung adenocarcinoma. *Nature* **511:** 543–550

Canman CE, Lim D-S, Cimprich KA, Taya Y, Tamai K, Sakaguchi K, Appella E, Kastan MB & Siliciano JD (1998) Activation of the ATM Kinase by Ionizing Radiation and Phosphorylation of p53. *Science*. **281:** 1677–1679

Carney DN (2002) Lung cancer - time to move on from chemotherapy. *N Engl J Med*. **346:** 126–128

Casper AM, Nghiem P, Arlt MF & Glover TW (2002) ATR regulates fragile site stability. *Cell* **111:** 779–89

Charrier J-D, Durrant SJ, Golec JMC, Kay DP, Knegtel RMA, MacCormick S, Mortimore M, O'Donnell ME, Pinder JL, Reaper PM, Rutherford AP, Wang PSH, Young SC & Pollard JR (2011) Discovery of potent and selective inhibitors of ataxia telangiectasia mutated and Rad3 related (ATR) protein kinase as potential anticancer agents. *J Med Chem*. **54:** 2320–30

Chehab NH, Malikzay A, Appel M & Halazonetis TD (2000) Chk2/hCds1 functions as a DNA damage checkpoint in G1 by stabilizing p53. *Genes Dev*. **14:** 278–288

Chehab NH, Malikzay A, Stavridi ES & Halazonetis TD (1999) Phosphorylation of Ser-20 mediates stabilization of human p53 in response to DNA damage. *Proc Natl Acad Sci U S A* **96:** 13777–82

Chen J (2000) Ataxia Telangiectasia-related Protein Is Involved in the Phosphorylation of BRCA1 following Deoxyribonucleic Acid Damage. *Cancer Res*. **60:** 5037–5039

Chen L, Nievera CJ, Lee AY-L & Wu X (2008) Cell cycle-dependent complex formation of BRCA1.CtIP.MRN is important for DNA double-strand break repair. *J Biol Chem*. **283:** 7713–7720

Chen T, Middleton FK, Falcon S, Reaper PM, Pollard JR & Curtin NJ (2014) Development of pharmacodynamic biomarkers for ATR inhibitors. *Mol Oncol*. **9:** 463–72

Choi S, Gamper AM, White JS & Bakkenist CJ (2010) Inhibition of ATM kinase activity does not phenocopy ATM protein disruption: Implications for the clinical utility of ATM kinase inhibitors. *Cell Cycle*. **9:** 4052–4057

Chou DM, Adamson B, Dephoure NE, Tan X, Nottke AC, Hurov KE, Gygi SP, Colaiácovo MP & Elledge SJ (2010) A chromatin localization screen reveals poly (ADP ribose)-regulated recruitment of the repressive polycomb and NuRD complexes to sites of DNA damage. *Proc Natl Acad Sci U S A* **107:** 18475–18480

Choudhury A, Nelson LD, Teo MTW, Chilka S, Bhattarai S, Johnston CF, Elliott F, Lowery J, Taylor CF, Churchman M, Bentley J, Knowles MA, Harnden P, Bristow RG, Bishop DT & Kiltie AE (2010) MRE11 expression is predictive of cause-specific survival following radical radiotherapy for muscle-invasive bladder cancer. *Cancer Res*. **70:** 7017–26

Chung C (2015) Tyrosine kinase inhibitors for epidermal growth factor receptor gene mutation-positive non-small cell lung cancers: an update for recent advances in therapeutics. *J Oncol Pharm Pr*. **Apr 8:** pii: 1078155215577810.

Ciccia A & Elledge SJ (2010) The DNA Damage Response : Making it safe to play with knives. *Mol Cell*. **40:** 179–204

Cimprich K & Cortez D (2008) ATR: An Essential Regulator of Genome Integrity. *Nat Rev Mol Cell Biol*. **9:** 616–627

Cliby WA, Roberts CJ, Cimprich KA, Stringer CM, Lamb JR, Schreiber SL & Friend SH (1998) Overexpression of a kinase-inactive ATR protein causes sensitivity to DNA-damaging agents and defects in cell cycle checkpoints. *EMBO J*. **17:** 159–69

Constantinou A, Tarsounas M, Karow JK, Brosh RM, Bohr VA, Hickson ID & West SC (2000) Werner's syndrome protein (WRN) migrates Holliday junctions and co-localizes with RPA upon replication arrest. *EMBO Rep*. **1:** 80–4

Cortez D, Guntuku S, Qin J & Elledge SJ (2001) ATR and ATRIP: partners in checkpoint signaling. *Science*. **294:** 1713–6

Cortez D, Wang Y, Qin J & Elledge SJ (1999) Requirement of ATM-dependent phosphorylation of brca1 in the DNA damage response to double-strand breaks. *Science*. **286:** 1162–1166

Crasta K, Ganem NJ, Dagher R, Lantermann AB, Ivanova E V, Pan Y, Nezi L, Protopopov A, Chowdhury D & Pellman D (2012) DNA breaks and chromosome pulverization from errors in mitosis. *Nature* **482:** 53–8

Cui Y, Palii SS, Innes CL & Paules RS (2014) Depletion of ATR selectively sensitizes ATM-deficient human mammary epithelial cells to ionizing radiation and DNA-damaging agents. *Cell Cycle*. **13:** 3541–3550

Curtin NJ (2005) PARP inhibitors for cancer therapy. *Expert Rev Mol Med*. **7:** 1–20

Curtin NJ (2012) DNA repair dysregulation from cancer driver to therapeutic target. *Nat. Rev Cancer*. **12:** 801–17

Curtin NJ & Szabo C (2013) Therapeutic applications of PARP inhibitors: anticancer therapy and beyond. *Mol Asp. Med*. **34:** 1217–56

Daley JM & Sung P (2014) 53BP1, BRCA1, and the choice between recombination and end joining at DNA double-strand breaks. *Mol Cell Biol*. **34:** 1380–8

Daniel J a., Pellegrini M, Lee BS, Guo Z, Filsuf D, Belkina N V., You Z, Paull TT, Sleckman BP, Feigenbaum L & Nussenzweig A (2012) Loss of ATM kinase activity leads to embryonic lethality in mice. *J Cell Biol*. **198:** 295–304

Daniel J a., Pellegrini M, Lee JH, Paull TT, Feigenbaum L & Nussenzweig A (2008) Multiple autophosphorylation sites are dispensable for murine ATM activation in vivo. *J Cell Biol*. **183:** 777–783

Dantzer F, de La Rubia G, Ménissier-De Murcia J, Hostomsky Z, de Murcia G & Schreiber V (2000) Base excision repair is impaired in mammalian cells lacking Poly(ADP-ribose) polymerase-1. *Biochemistry* **39:** 7559–7569

Davidovic L, Vodenicharov M, Affar EB & Poirier GG (2001) Importance of Poly(ADP-Ribose) Glycohydrolase in the Control of Poly(ADP-Ribose) Metabolism. *Exp Cell Res*. **268:** 7–13

Davidson MR, Gazdar AF & Clarke BE (2013) The pivotal role of pathology in the management of lung cancer. *J Thorac Dis*. **5:** S463–78

Davies AA, Masson J-Y, McIlwraith MJ, Stasiak AZ, Stasiak A, Venkitaraman AR & West SC (2001) Role of BRCA2 in Control of the RAD51 Recombination and DNA Repair Protein. *Mol Cell* **7:** 273–282

Davies H, Hunter C, Smith R, Stephens P, Greenman C, Bignell G, Teague J, Butler A, Edkins S, Stevens C, Parker A, O'Meara S, Avis T, Barthorpe S, Brackenbury L, Buck G, Clements J, Cole J, Dicks E, Edwards K, et al (2005) Somatic mutations of the protein kinase gene family in human lung cancer. *Cancer Res*. **65:** 7591–5

Debatisse M, Le Tallec B, Letessier A, Dutrillaux B & Brison O (2012) Common fragile sites: mechanisms of instability revisited. *Trends Genet*. **28:** 22–32

Dedes KJ, Wilkerson PM, Wetterskog D, Weigelt B, Ashworth A & Reis-Filho JS (2011) Synthetic lethality of PARP inhibition in cancers lacking BRCA1 and BRCA2 mutations. *Cell Cycle* **10:** 1192–1199

DeFazio LG, Stansel RM, Griffith JD & Chu G (2002) Synapsis of DNA ends by DNA-dependent protein kinase. *EMBO J*. **21:** 3192–3200

Delacroix S, Wagner JM, Kobayashi M, Yamamoto K & Karnitz LM (2007) The Rad9-Hus1-Rad1 (9-1-1) clamp activates checkpoint signaling via TopBP1. *Genes Dev*. **21:** 1472–7

Ding L, Getz G, Wheeler DA, Mardis ER, Mclellan MD, Sougnez C, Greulich H, Muzny DM, Morgan MB, Fulton L, Fulton RS, Zhang Q, Wendl MC, Michael S, Larson DE, Chen K, Dooling DJ, Sabo A, Alicia C, Shen H, et al (2009) Somatic mutations affect key pathways in lung adenocarcinoma. *Nature* **455:** 1069–1075

Doil C, Mailand N, Bekker-Jensen S, Menard P, Larsen DH, Pepperkok R, Ellenberg J, Panier S, Durocher D, Bartek J, Lukas J & Lukas C (2009) RNF168 Binds and Amplifies Ubiquitin Conjugates on Damaged Chromosomes to Allow Accumulation of Repair Proteins. *Cell* **136:** 435–446

El-Deiry WS, Harper JW, O'Connor PM, Velculescu VE, Canman CE, Jackman J, Pietenpol J a, Burrell M, Hill DE, Wang Y, Wiman KG, Mercer WE, Kastan MB, Kohn KW, Elledge SJ, Kinzler KW & Vogelstein B (1994) WAF1/CIP1 Is Induced in p53-mediated G1 Arrest and Apoptosis. *Cancer Res*. **54:** 1169–1174

El-Khamisy SF, Masutani M, Suzuki H & Caldecott KW (2003) A requirement for PARP-1 for the assembly or stability of XRCC1 nuclear foci at sites of oxidative DNA damage. *Nucleic Acids Res*. **31:** 5526–5533

Ellison V & Stillman B (2001) Biochemical characterization of DNA damage checkpoint complexes: clamp loader and clamp complexes with specificity for 5' recessed DNA. *PLoS Biol*. **1:** 231–243

Elson A, Wang Y, Daugherty CJ, Morton CC, Zhou F, Campos-Torres J & Leder P (1996) Pleiotropic defects in ataxia-telangiectasia protein-deficient mice. *Proc Natl Acad Sci U S A* **93:** 13084–9

Errico A & Costanzo V (2012) Mechanisms of replication fork protection: a safeguard for genome stability. *Crit Rev Biochem Mol Biol*. **47:** 222–35

Falck J, Mailand N, Syljuåsen RG, Bartek J & Lukas J (2001) The ATM-Chk2-Cdc25A checkpoint pathway guards against radioresistant DNA synthesis. *Nature* **410:** 842–7

Farmer H, McCabe N, Lord CJ, Tutt ANJ, Johnson DA, Richardson TB, Santarosa M, Dillon KJ, Hickson I, Knights C, Martin NMB, Jackson SP, Smith GCM & Ashworth A (2005) Targeting the DNA repair defect in BRCA mutant cells as a therapeutic strategy. *Nature* **434:** 917–21

Fedier A, Schlamminger M, Schwarz VA, Haller U, Howell SB & Fink D (2003) Loss of atm sensitises p53-deficient cells to topoisomerase poisons and antimetabolites. *Ann Oncol*. **14:** 938–945

Fekairi S, Scaglione S, Chahwan C, Taylor ER, Tissier A, Coulon S, Dong MQ, Ruse C, Yates JR, Russell P, Fuchs RP, McGowan CH & Gaillard PHL (2009) Human SLX4 Is a Holliday Junction Resolvase Subunit that Binds Multiple DNA Repair/Recombination Endonucleases. *Cell* **138:** 78–89

Fisher AEO, Hochegger H, Takeda S & Caldecott KW (2007) Poly(ADP-ribose) polymerase 1 accelerates single-strand break repair in concert with poly(ADP-ribose) glycohydrolase. *Mol Cell Biol*. **27:** 5597–5605

Flatt PM, Tang LJ, Scatena CD, Szak ST & Pietenpol JA (2000) p53 regulation of G(2) checkpoint is retinoblastoma protein dependent. *Mol Cell Biol*. **20:** 4210–4223

Fokas E, Prevo R, Pollard JR, Reaper PM, Charlton PA, Cornelissen B, Vallis KA, Hammond EM, Olcina MM, Gillies McKenna W, Muschel RJ & Brunner TB (2012) Targeting ATR in vivo using the novel inhibitor VE-822 results in selective sensitization of pancreatic tumors to radiation. *Cell Death Dis*. **3:e441:**

Fong PC, Boss DS, Yap TA, Tutt A, Wu P, Marja M-R, Mortimer P, Swaisland H, Lau A, O'Connor MJ, Ashworth A, Carmichael J, Kaye SB, Schellens JHM & de Bono JS (2009) Inhibition of poly(ADP-ribose) polymerase in tumors from BRCA mutation carriers. *N Engl J Med*. **361:** 123–134

Foote KM, Blades K, Cronin A, Fillery S, Guichard SS, Hassall L, Hickson I, Jacq X, Jewsbury PJ, Mcguire TM, Nissink JWM, Odedra R, Page K, Perkins P, Suleman A, Tam K, Thommes P, Broadhurst R & Wood C (2013) Discovery of 4-{4-[(3R)-3-Methylmorpholin-4-yl]-6-[1-(methylsulfonyl)cyclopropyl]pyrimidin-2-yl}-1H-indole (AZ20): a potent and selective inhibitor of ATR protein kinase with monotherapy in vivo antitumor activity. *J Med Chem*. **56:** 2125–2138

Friedel AM, Pike BL & Gasser SM (2009) ATR/Mec1: coordinating fork stability and repair. *Curr Opin Cell Biol*. **21:** 237–44

Friesner JD, Liu B, Culligan K & Britt AB (2005) Ionizing Radiation – dependent y-H2AX Focus Formation Requires Ataxia Telangiectasia Mutated and Ataxia Telangiectasia Mutated and Rad3-related. *Mol Biol Cell*. **16:** 2566–2576

Frosina G, Fortini P, Rossi O, Carrozzino F, Raspaglio G, Cox LS, Lane DP, Abbondandolo A & Dogliotti E (1996) Two Pathways for Base Excision Repair in Mammalian Cells. *J Biol Chem*. **271:** 9573–9578

Gatei M, Jakob B, Chen P, Kijas AW, Becherel OJ, Gueven N, Birrell G, Lee J-H, Paull TT, Lerenthal Y, Fazry S, Taucher-Scholz G, Kalb R, Schindler D, Waltes R, Dörk T & Lavin MF (2011) ATM protein-dependent phosphorylation of Rad50 protein regulates DNA repair and cell cycle control. *J Biol Chem*. **286:** 31542–56

Gatei M, Sloper K, Sorensen C, Syljuäsen R, Falck J, Hobson K, Savage K, Lukas J, Zhou B-B, Bartek J & Khanna KK (2003) Ataxia-telangiectasia-mutated (ATM) and NBS1-dependent phosphorylation of Chk1 on Ser-317 in response to ionizing radiation. *J Biol Chem*. **278:** 14806–11

Gatei M, Young D, Cerosaletti KM, Desai-Mehta A, Spring K, Kozlov S, Lavin MF, Gatti RA, Concannon P & Khanna K (2000) ATM-dependent phosphorylation of nibrin in response to radiation exposure. *Nat Genet*. **25:** 115–119

Gatei M, Zhou BB, Hobson K, Scott S, Young D & Khanna KK (2001) Ataxia telangiectasia mutated (ATM) kinase and ATM and Rad3 related kinase mediate phosphorylation of Brca1 at distinct and overlapping sites. *J Biol Chem*. **276:** 17276–17280

Gilad O, Nabet BY, Ragland RL, Schoppy DW, Smith KD, Durham AC & Brown EJ (2010) Combining ATR suppression with oncogenic Ras synergistically increases genomic instability, causing synthetic lethality or tumorigenesis in a dosage-dependent manner. *Cancer Res*. **70:** 9693–702

Gilardini Montani MS, Prodosmo A, Stagni V, Merli D, Monteonofrio L, Gatti V, Gentileschi MP, Barilà D & Soddu S (2013) ATM-depletion in breast cancer cells confers sensitivity to PARP inhibition. *J Exp Clin Cancer Res*. **32:** 95

Gillis LD, Leidal AM, Hill R & Lee PWK (2009) p21Cip1/WAF1 mediates cyclin B1 degradation in response to DNA damage. *Cell Cycle* **8:** 253–256

Giunta S, Belotserkovskaya R & Jackson SP (2010) DNA damage signaling in response to double-strand breaks during mitosis. *J. Cell Biol.* **190:** 197–207

Glover TW, Arlt MF, Casper AM & Durkin SG (2005) Mechanisms of common fragile site instability. *Hum Mol Genet.* **14:** R197–R205

Gnad F, Baucom A, Mukhyala K, Manning G & Zhang Z (2013) Assessment of computational methods for predicting the effects of missense mutations in human cancers. *BMC Genomics* **14:** S7

Golding S, Rosenberg E, Adams BR, Wignarajah S, Beckta JM, O'Connor MJ & Valerie K (2012) Dynamic inhibition of ATM kinase provides a strategy for glioblastoma multiforme radiosensitization and growth control. *Cell Cycle.* **11:** 1167–1173

Golding SE, Rosenberg E, Valerie N, Hussaini I, Frigerio M, Cockcroft XF, Chong WY, Hummersone M, Rigoreau L, Menear KA, O'Connor MJ, Povirk LF, van Meter T & Valerie K (2009) Improved ATM kinase inhibitor KU-60019 radiosensitizes glioma cells, compromises insulin, AKT and ERK prosurvival signaling, and inhibits migration and invasion. *Mol Cancer Ther.* **8:** 2894–902

Gorgoulis VG, Vassiliou LF, Karakaidos P, Zacharatos P, Kotsinas A, Liloglou T, Venere M, Jr RAD, Kastrinakis NG, Levy B, Kletsas D, Yoneta A, Herlyn M, Kittas C & Halazonetis TD (2005) Activation of the DNA damage checkpoint and genomic instability in human precancerous lesions. *Nature* **434:** 907–913

Gottlieb TM & Jackson SP (1993) The DNA-dependent protein kinase: requirement for DNA ends and association with Ku antigen. *Cell* **72:** 131–142

Graves PR, Lovly CM, Uy GL & Piwnica-Worms H (2001) Localization of human Cdc25C is regulated both by nuclear export and 14-3-3 protein binding. *Oncogene* **20:** 1839–51

Grawunder U, Wilm M, Wu X, Kulesza P, Wilson TE, Mann M & Lieber MR (1997) Activity of DNA ligase IV stimulated by complex formation with XRCC4 protein in mammalian cells. *Nature* **388:** 492–495

Greiner TC, Dasgupta C, Ho V V, Weisenburger DD, Smith LM, Lynch JC, Vose JM, Fu K, Armitage JO, Braziel RM, Campo E, Delabie J, Gascoyne RD, Jaffe ES, Muller-Hermelink HK, Ott G, Rosenwald A, Staudt LM, Im MY, Karaman MW, et al (2006) Mutation and genomic deletion status of ataxia telangiectasia mutated (ATM) and p53 confer specific gene expression profiles in mantle cell lymphoma. *PNAS* **103:** 2352–7

Griffith AJ, Blier PR, Mimori T & Hardin JA (1992) Ku polypeptides synthesized in vitro assemble into complexes which recognize ends of double-stranded DNA. *J Biol Chem.* **267:** 331–338

Gudmundsdottir K & Ashworth a (2006) The roles of BRCA1 and BRCA2 and associated proteins in the maintenance of genomic stability. *Oncogene* **25:** 5864–5874

Guichard S, Brown E, Odedra R, Hughes A, Heathcote D, Barnes J, Lau A, Powell S, Jones CD, Nissink W, Foote KM, Jewsbury PJ & Pass M (2013) The pre-clinical in vitro and in vivo activity of AZD6738: A potent and selective inhibitor of ATR kinase. [abstract]. In *Proceedings of the 104th Annual Meeting of the American Association for Cancer Research; 2013 Apr 6-10;* Washington, DC. Philadelphia (PA):AACR; Cancer Res. 2013; 73(8 Suppl):Abstract nr 3343; doi:10.1158/1538-7445.AM2013-3343

Guo K, Shelat A a, Guy RK & Kastan MB (2014) Development of a cell-based, high-throughput screening assay for ATM kinase inhibitors. *J Biomol Screen*. **19:** 538–46

Halazonetis TD, Gorgoulis VG & Bartek J (2008) An oncogene-induced DNA damage model for cancer development. *Science*. **319:** 1352–5

Hall AB, Newsome D, Wang Y, Boucher DM, Eustace B, Gu Y, Hare B, Johnson M a, Milton S, Murphy CE, Takemoto D, Tolman C, Wood M, Charlton P, Charrier J-D, Furey B, Golec J, Reaper PM & Pollard JR (2014) Potentiation of tumor responses to DNA damaging therapy by the selective ATR inhibitor VX-970. *Oncotarget* **5:** 5674–85

Hammond EM, Dorie MJ & Giaccia AJ (2003) ATR/ATM targets are phosphorylated by ATR in response to hypoxia and ATM in response to reoxygenation. *J Biol Chem*. **278:** 12207–13

Hanahan D & Weinberg RA (2011) Hallmarks of cancer: the next generation. *Cell* **144:** 646–74

Harrigan JA, Belotserkovskaya R, Coates J, Dimitrova DS, Polo SE, Bradshaw CR, Fraser P & Jackson SP (2011) Replication stress induces 53BP1-containing OPT domains in G1 cells. *J Cell Biol*. **193:** 97–108

Haupt Y, Maya R, Kazaz A & Oren M (1997) Mdm2 promotes the rapid degradation of p53. *Nature* **387:** 296–299

Helleday T, Lo J, van Gent DC & Engelward BP (2007) DNA double-strand break repair: From mechanistic understanding to cancer treatment. *DNA Repair* **6:** 923–935

Hellman A, Rahat A, Scherer SW, Darvasi A, Tsui LC & Kerem B (2000) Replication delay along FRA7H, a common fragile site on human chromosome 7, leads to chromosomal instability. *Mol Cell Biol*. **20:** 4420–4427

Helt CE, Cliby WA, Keng PC, Bambara RA & O'Reilly MA (2005) Ataxia telangiectasia mutated (ATM) and ATM and Rad3-related protein exhibit selective target specificities in response to different forms of DNA damage. *J Biol Chem*. **280:** 1186–92

Hermeking H & Benzinger A (2006) 14-3-3 Proteins in Cell Cycle Regulation. *Semin Cancer Biol*. **16:** 183–192

Hermeking H, Lengauer C, Polyak K, He T, Zhang L, Thiagalingam S, Kinzler KW & Vogelstein B (1997) 14-3-3σ is a p53-Regulated Inhibitor of G2/M Progression. *Mol Cell* **1:** 3–11

Hickson I, Zhao Y, Richardson CJ, Green SJ, Martin NMB, Orr AI, Reaper PM, Jackson SP, Curtin NJ & Smith GC (2004) Identification and Characterization of a Novel and Specific Inhibitor of the Ataxia-Telangiectasia Mutated Kinase ATM. *Cancer Res*. **64:** 9152–9159

Hills SA & Diffley JFX (2014) DNA replication and oncogene-induced replicative stress. *Curr Biol*. **24:** R435–44

Houldsworth J & Lavin M (1980) Effect of ionizing radiation on DNA synthesis in ataxia teleangiectasia cells. *Nucleic Acids Res*. **8:** 3709–3720

Howlader N, Noone AM, Krapcho M, Garshell J, Miller D, Altekruse SF, Kosary CL, Yu M, Ruhl J, Tatalovich Z, Mariotto A, Lewis DR, Chen HS, Feuer EJ, Cronin KA & (eds). (2013) SEER Cancer Statistics Review, 1975-2011. *based Novemb. 2013 SEER data submission; posted to SEER web site April 2014*.**:** http://seer.cancer.gov/csr/1975_2011/

Huertas P & Jackson SP (2009) Human CtIP mediates cell cycle control of DNA end resection and double strand break repair. *J Biol Chem*. **284:** 9558–9565

Huffman JL, Sundheim O & Tainer JA (2005) DNA base damage recognition and removal: New twists and grooves. *Mut Res*. **577:** 55–76

Huntoon CJ, Flatten KS, Wahner Hendrickson AE, Huehls AM, Sutor SL, Kaufmann SH & Karnitz LM (2013) ATR Inhibition Broadly Sensitizes Ovarian Cancer Cells to Chemotherapy Independent of BRCA Status. *Cancer Res*. **73:** 3683–3691

Hutter G, Nickenig C, Garritsen H, Hellenkamp F, Hoerning A, Hiddemann W & Dreyling M (2004) Use of polymorphisms in the noncoding region of the human mitochondrial genome to identify potential contamination of human leukemia-lymphoma cell lines. *Hematol. J*. **5:** 61–8

Ira G, Pellicioli A, Balijja A, Wang X, Fiorani S, Carotenuto W, Liberi G, Bressan D, Wan L, Hollingsworth NM, Haber JE & Foiani M (2004) DNA end resection, homologous recombination and DNA damage checkpoint activation require CDK1. *Nature* **431:** 1011–1017

Ishikawa Y, Kozakai T, Morita H, Saida K, Oka S & Masuo Y (2006) Rapid detection of mycoplasma contamination in cell cultures using SYBR Green-based real-time polymerase chain reaction. *Vitr. Cell Dev Biol Anim*. **42:** 63–69

Jackson SP & Bartek J (2010) The DNA-damage response in human biology and disease. *Nature* **461:** 1071–1078

Jacq X, Smith L, Brown E, Hughes A, Odedra R, Heathcote D, Barnes J, Powell S, Maguire S, Pearson V, Boros J, Caie P, Thommes PA, Nissink W, Foote K, Jewsbury PJ & Guichard SM (2012) AZ20, a novel potent and selective inhibitor of ATR kinase with in vivo antitumour activity. [abstract]. In *Proceedings of the 103rd Annual Meeting of the American Association for Cancer Research; 2012 Mar 31-Apr 4* Chicago, IL Philadelphia (PA): AACR; Cancer Res 2012; 72(8 Suppl): Abstract nr 1823; doi:1538-7445.AM2012-1823

Jacquemin V, Rieunier G, Jacob S, Bellanger D, D'Enghien CD, Laugé A, Stoppa-Lyonnet D & Stern M-H (2012) Underexpression and abnormal localization of ATM products in ataxia telangiectasia patients bearing ATM missense mutations. *Eur J Hum Genet*. **20:** 305–12

Jazayeri A, Falck J, Lukas C, Bartek J, Smith GCM, Lukas J & Jackson SP (2006) ATM- and cell cycle-dependent regulation of ATR in response to DNA double-strand breaks. *Nat Cell Biol*. **8:** 37–45

Jiang H, Reinhardt HC, Bartkova J, Tommiska J, Blomqvist C, Nevanlinna H, Bartek J, Yaffe MB & Hemann MT (2009) The combined status of ATM and p53 link tumor development with therapeutic response. *Genes Dev*. **23:** 1895–909

Jones CD, Blades K, Foote KM, Guichard SM, Jewsbury, Philip J. McGuire T, Nissink JW, Odedra R, Tam K, Thommes P, Turner P, Wilkinson G, Wood C & Yates JW (2013) Discovery of AZD6738, a potent and selective inhibitor with the potential to test the clinical efficacy of ATR kinase inhibition in cancer patients. [abstract]. In *Proceedings of the 104th Annual Meeting of the American Association for Cancer Research; 2013 Apr 6-10* Washington, DC. Philadelphia (PA): AACR; Cancer Res. 2013; 73(8 Suppl):Abstract nr 2348. doi:10.1158/1538-7445.AM2013-2348

Kaelin WGJ (2005) The concept of synthetic lethality in the context of anticancer therapy. *Nat Rev Cancer*. **5:** 689–98

Kakarougkas A & Jeggo PA (2014) DNA DSB repair pathway choice: an orchestrated handover mechanism. *Brit J Radiol*. **87:** 20130685

Kandoth C, McLellan MD, Vandin F, Ye K, Niu B, Lu C, Xie M, Zhang Q, McMichael JF, Wyczalkowski MA, Leiserson MDM, Miller CA, Welch JS, Walter MJ, Wendl MC, Ley TJ,

Wilson RK, Raphael BJ & Ding L (2013) Mutational landscape and significance across 12 major cancer types. *Nature* **502:** 333–9

Karnitz LM, Flatten KS, Wagner JM, Loegering D, Hackbarth JS, Arlander SJH, Vroman BT, Thomas MB, Baek Y-U, Hopkins KM, Lieberman HB, Chen J, Cliby W a & Kaufmann SH (2005) Gemcitabine-induced activation of checkpoint signaling pathways that affect tumor cell survival. *Mol Pharmacol*. **68:** 1636–44

Karve S, Werner ME, Sukumar R, Cummings ND, Copp JA, Wang EC, Li C, Sethi M, Chen RC, Pacold ME & Wang AZ (2012) Revival of the abandoned therapeutic wortmannin by nanoparticle drug delivery. *Proc Natl Acad Sci U S A* **109:** 8230–5

Kasahara K, Goto H, Enomoto M, Tomono Y, Kiyono T & Inagaki M (2010) 14-3-3gamma mediates Cdc25A proteolysis to block premature mitotic entry after DNA damage. *EMBO J*. **29:** 2802–12

Kastan MB & Bartek J (2004) Cell-cycle checkpoints and cancer. *Nature* **432:** 316–23

Kastan MB, Onyekwere O, Sidransky D, Vogelstein B & Craig RW (1991) Participation of p53 Protein in the Cellular Response to DNA Damage. *Cancer Res*. **51:** 6304–6311

Kastan MB, Zhan Q, El-Deiry WS, Carrier F, Jacks T, Walsh W V, Plunkett BS, Vogelstein B & Fornace AJJ (1992) A mammalian cell cycle checkpoint pathway utilizing p53 and GADD45 is defective in ataxia-telangiectasia. *Cell* **71:** 587–97

Keith CT & Schreiber SL (1995) PIK-related kinases: DNA repair, recombination, and cell cycle checkpoints. *Science*. **270:** 50–51

Kennedy RD, Chen CC, Stuckert P, Archila EM, De la Vega MA, Moreau LA, Shimamura A & D'Andrea AD (2007) Fanconi anemia pathway-deficient tumor cells are hypersensitive to inhibition of ataxia telangiectasia mutated. *J Clin Invest*. **117:** 1140–1149

Kennedy RD & D'Andrea AD (2006) DNA repair pathways in clinical practice: lessons from pediatric cancer susceptibility syndromes. *J Clin Oncol*. **24:** 3799–808

Khosravi R, Maya R, Gottlieb T, Oren M, Shiloh Y & Shkedy D (1999) Rapid ATM-dependent phosphorylation of MDM2 precedes p53 accumulation in response to DNA damage. *Proc Natl Acad Sci U S A* **96:** 14973–7

Kim S-T, Lim D-S, Canman CE & Kastan MB (1999) Substrate Specificities and Identification of Putative Substrates of ATM Kinase Family Members. *J Biol Chem*. **274:** 37538–37543

Kim W-J, Vo QN, Shrivastav M, Lataxes TA & Brown KD (2002) Aberrant methylation of the ATM promoter correlates with increased radiosensitivity in a human colorectal tumor cell line. *Oncogene* **21:** 3864–3871

Kitagawa R, Bakkenist CJ, McKinnon PJ & Kastan MB (2004) Phosphorylation of SMC1 is a critical downstream event in the ATM-NBS1-BRCA1 pathway. *Genes Dev*. **18:** 1423–38

De Klein A, Muijtjens M, van Os R, Verhoeven Y, Smit B, Carr AM, Lehmann AR & Hoeijmakers JH (2000) Targeted disruption of the cell-cycle checkpoint gene ATR leads to early embryonic lethality in mice. *Curr Biol*. **10:** 479–82

Klungland A & Lindahl T (1997) Second pathway for completion of human DNA base excision-repair: Reconstitution with purified proteins and requirement for DNase IV (FEN1). *EMBO J*. **16:** 3341–3348

Konstantinidou G, Bey EA, Rabellino A, Schuster K, Michael S, Gazdar AF, Amici A, Boothman DA & Scaglioni PP (2010) Dual PI3K/mTOR blockade is an effective radiosensitizing strategy for the treatment of non-small cell lung cancer harbouring K-RAS mutations. *Cancer Res*. **69:** 7644–7652

Kozlov S V, Graham ME, Peng C, Chen P, Robinson PJ & Lavin MF (2006) Involvement of novel autophosphorylation sites in ATM activation. *EMBO J*. **25:** 3504–3514

Krämer A, Mailand N, Lukas C, Syljuåsen RG, Wilkinson CJ, Nigg E a, Bartek J & Lukas J (2004) Centrosome-associated Chk1 prevents premature activation of cyclin-B-Cdk1 kinase. *Nat Cell Biol*. **6:** 884–91

Krejci L, Altmannova V, Spirek M & Zhao X (2012) Homologous recombination and its regulation. *Nucleic Acids Res*. **40:** 5795–5818

Kubota E, Williamson CT, Ye R, Elegbede A, Peterson L, Lees-Miller SP & Bebb DG (2014) Low ATM protein expression and depletion of p53 correlates with olaparib sensitivity in gastric cancer cell lines. *Cell Cycle*. **13:** 2129–37

Kubota Y, Nash R a, Klungland A, Schar P, Barnes DE & Lindahl T (1996) Reconstitution excision-repair purified proteins: polymerase protein. *EMBO J*. **15:** 6662–6670

Kumagai A & Dunphy WG (1999) Binding of 14-3-3 proteins and nuclear export control the intracellular localization of the mitotic inducer Cdc25. *Genes Dev*. **13:** 1067–1072

Kumagai A, Lee J, Yoo HY & Dunphy WG (2006) TopBP1 activates the ATR-ATRIP complex. *Cell* **124:** 943–55

Kurimasa A, Kumano S, Boubnov N V, Story MD, Tung CS, Peterson SR & Chen DJ (1999) Requirement for the kinase activity of human DNA-dependent protein kinase catalytic subunit in DNA strand break rejoining. *Mol Cell Biol*. **19:** 3877–3884

Kuzminov A (2001) Single-strand interruptions in replicating chromosomes cause double-strand breaks. *Proc Natl Acad Sci U S A* **98:** 8241–8246

Lakin ND, Hann BC & Jackson SP (1999) The ataxia-telangiectasia related protein ATR mediates DNA-dependent phosphorylation of p53. *Oncogene* **18:** 3989–3995

Landau DA & Wu CJ (2013) Chronic lymphocytic leukemia: molecular heterogeneity revealed by high-throughput genomics. *Genome Med*. **5:** 47

Lavin MF (2008) Ataxia-telangiectasia: from a rare disorder to a paradigm for cell signalling and cancer. *Nat Rev Mol Cell Biol*. **9:** 759–69

Lavin MF, Scott S, Gueven N, Kozlov S, Peng C & Chen P (2004) Functional consequences of sequence alterations in the ATM gene. *DNA Repair* **3:** 1197–205

Lee J, Kumagai A & Dunphy WG (2007) The Rad9-Hus1-Rad1 checkpoint clamp regulates interaction of TopBP1 with ATR. *J Biol Chem*. **282:** 28036–44

Lee J-H & Paull TT (2005) ATM activation by DNA double-strand breaks through the Mre11-Rad50-Nbs1 complex. *Science*. **308:** 551–4

Lee JW, Blanco L, Zhou T, Garcia-Diaz M, Bebenek K, Kunkel TA, Wang Z & Povirk LF (2004) Implication of DNA Polymerase λ in Alignment-based Gap Filling for Nonhomologous DNA End Joining in Human Nuclear Extracts. *J Biol Chem*. **279:** 805–811

Lees-Miller SP, Sakaguchi K, Ullrich SJ, Appella E & Anderson CW (1992) Human DNA-activated protein kinase phosphorylates serines 15 and 37 in the amino-terminal transactivation domain of human p53. *Mol Cell Biol*. **12:** 5041–5049

Lempiäinen H & Halazonetis TD (2009) Emerging common themes in regulation of PIKKs and PI3Ks. *EMBO J*. **28:** 3067–73

Leppard JB, Dong Z, Mackey ZB & Tomkinson AE (2003) Physical and functional interaction between DNA ligase IIIalpha and poly(ADP-Ribose) polymerase 1 in DNA single-strand break repair. *Mol Cell Biol*. **23:** 5919–5927

Levy-Lahad E & Friedman E (2007) Cancer risks among BRCA1 and BRCA2 mutation carriers. *Br J Cancer*. **96:** 11–5

Lim D-S, Kim S-T, Xu B, Maser RS, Lin J, Petrini JHJ & Kastan MB (2000) ATM phosphorylates p95/nbs1 in an S-phase checkpoint pathway. *Nature* **404:** 613–617

Lindahl T (1993) Instability and decay of the primary structure of DNA. *Nature* **362:** 709–715

Lindahl T & Barnes DE (2000) Repair of Endogenous DNA Damage. *Cold Spring Harb Symp Quant Biol*. **65:** 127–133

Löbrich M, Shibata A, Beucher A, Fisher A, Ensminger M, Goodarzi AA, Barton O & Jeggo PA (2010) γH2AX foci analysis for monitoring DNA double-strand break repair: Strengths, limitations and optimization. *Cell Cycle* **9:** 662–669

Lossaint G, Besnard E, Fisher D, Piette J & Dulić V (2011) Chk1 is dispensable for G2 arrest in response to sustained DNA damage when the ATM/p53/p21 pathway is functional. *Oncogene* **30:** 4261–74

Lundholm L, Hååg P, Zong D, Juntti T, Mörk B, Lewensohn R & K. V (2013) Resistance to DNA-damaging treatment in non-small cell lung cancer tumor-initiating cells involves reduced DNA-PK/ATM activation and diminished cell cycle arrest. *Cell Death Dis*. **4:e478:** doi: 10.1038/cddis.2012.211

Lynch TJ, Bell DW, Sordella R, Gurubhagavatula S, Okimoto RA, Brannigan BW, Harris PL, Haserlat SM, Supko JG, Haluska FG, Louis DN, Christiani DC, Settleman J & Haber DA (2004) Activating Mutations in the Epidermal Growth Factor Receptor Underlying Responsiveness of Non–Small-Cell Lung Cancer to Gefitinib. *N Engl J Med*. **350:** 2129–39

Ma Y, Pannicke U, Schwarz K & Lieber MR (2002) Hairpin Opening and Overhang Processing by an Artemis/DNA-Dependent Protein Kinase Complex in Nonhomologous End Joining and V(D)J Recombination. *Cell* **108:** 781–794

Maemondo M, Inoue A, Kobayashi K, Sugawara S, Oizumi S, Isobe H, Gemma A, Harada M, Yoshizawa H, Kinoshita I, Fujita Y, Okinaga S, Hirano H, Yoshimori K, Harada T, Ogura T, Ando M, Miyazawa H, Tanaka T, Saijo Y, et al (2010) Gefitinib or chemotherapy for non-small-cell lung cancer with mutated EGFR. *N Engl J Med*. **362:** 2380–2388

Mahajan KN, Nick McElhinny SA, Mitchell BS & Ramsden DA (2002) Association of DNA polymerase μ (pol μ) with Ku and ligase IV: role for pol μ in end-joining double-strand break repair. *Mol Cell Biol*. **22:** 5194–5202

Mahaney BL, Meek K & Lees-Miller SP (2009) Repair of ionizing radiation-induced DNA double strand breaks by non-homologoud end-joining. *Biochem J* **417:** 639–650

Mailand N, Bekker-Jensen S, Faustrup H, Melander F, Bartek J, Lukas C & Lukas J (2007) RNF8 Ubiquitylates Histones at DNA Double-Strand Breaks and Promotes Assembly of Repair Proteins. *Cell* **131:** 887–900

Maira S-M, Stauffer F, Brueggen J, Furet P, Schnell C, Fritsch C, Brachmann S, Chène P, De Pover A, Schoemaker K, Fabbro D, Gabriel D, Simonen M, Murphy L, Finan P, Sellers W & García-Echeverría C (2008) Identification and characterization of NVP-BEZ235, a new orally available dual phosphatidylinositol 3-kinase/mammalian target of rapamycin inhibitor with potent in vivo antitumor activity. *Mol Cancer Ther*. **7:** 1851–63

Malanga M & Althaus FR (2004) Poly(ADP-ribose) Reactivates Stalled DNA Topoisomerase I and Induces DNA Strand Break Resealing. *J Biol Chem*. **279:** 5244–5248

Mari PO, Florea BI, Persengiev SP, Verkaik NS, Brüggenwirth HT, Modesti M, Giglia-mari G, Bezstarosti K, Demmers JAA, Luider TM, Hourtsmuller AB & van Gent DC (2006) Dynamic assembly of end-joining complexes requires interaction between Ku70/80 and XRCC4. *Proc Natl Acad Sci U S A* **103:** 18597–602

Marine J-C & Lozano G (2010) Mdm2-mediated ubiquitylation: p53 and beyond. *Cell Death Differ*. **17:** 93–102

Martin LP, Hamilton TC & Schilder RJ (2008) Platinum resistance: the role of DNA repair pathways. *Clin Cancer Res*. **14:** 1291–5

Matsumoto Y, Kim K & Bogenhagen DF (1994) Proliferating cell nuclear antigen-dependent abasic site repair in Xenopus laevis oocytes: an alternative pathway of base excision DNA repair. *Mol Cell Biol*. **14:** 6187–6197

Matsuoka S, Ballif BA, Smogorzewska A, McDonald ER, Hurov KE, Luo J, Bakalarski CE, Zhao Z, Solimini N, Lerenthal Y, Shiloh Y, Gygi SP & Elledge SJ (2007) ATM and ATR substrate analysis reveals extensive protein networks responsive to DNA damage. *Science*. **316:** 1160–6

Matsuoka S, Huang M & Elledge SJ (1998) Linkage of ATM to Cell Cycle Regulation by the Chk2 Protein Kinase. *Science*. **282:** 1893–1897

Matthews DJ, Yakes FM, Chen J, Tadano M, Bornheim L, Clary DO, Tai A, Wagner JM, Miller N, Kim YD, Robertson S, Murray L & Karnitz LM (2007) Pharmacological abrogation of S-phase checkpoint enhances the anti-tumor activity of gemcitabine in vivo. *Cell Cycle*. **6:** 104–10

Maughan TS, Adams RA, Smith CG, Meade AM, Seymour MT, Wilson RH, Idziaszczyk S, Harris R, Fisher D, Kenny SL, Kay E, Mitchell JK, Madi A, Jasani B, James MD, Bridgewater J, Kennedy MJ, Claes B, Lambrechts D, Kaplan R, et al (2011) Addition of cetuximab to oxaliplatin-based first-line combination chemotherapy for treatment of advanced colorectal cancer: results of the randomised phase 3 MRC COIN trial. *Lancet* **377:** 2103–14

Mazouzi A, Velimezi G & Loizou JI (2014) DNA replication stress : Causes , resolution and disease. *Exp Cell Res*. **329:** 85–93

McCabe N, Turner NC, Lord CJ, Kluzek K, Białkowska A, Swift S, Giavara S, O'Connor MJ, Tutt AN, Zdzienicka MZ, Smith GCM & Ashworth A (2006) Deficiency in the repair of DNA damage by homologous recombination and sensitivity to poly(ADP-ribose) polymerase inhibition. *Cancer Res*. **66:** 8109–8115

McGowan CH & Russell P (1995) Cell cycle regulation of human WEE1. *EMBO J* **14:** 2166–2175

McIlwraith MJ, Vaisman A, Liu Y, Fanning E, Woodgate R & West SC (2005) Human DNA polymerase eta promotes DNA synthesis from strand invasion intermediates of homologous recombination. *Mol Cell* **20:** 783–792

Mendoza-Alvarez H & Alvarez-Gonzalez R (1993) Poly(ADP-ribose) polymerase is a catalytic dimer and the automodification reaction is intermolecular. *J Biol Chem*. **268:** 22575–22580

Menezes DL, Holt J, Tang Y, Feng J, Barsanti P, Pan Y, Ghoddusi M, Zhang W, Thomas G, Holash J, Lees E & Taricani L (2014) A Synthetic Lethal Screen Reveals Enhanced Sensitivity to ATR Inhibitor Treatment in Mantle Cell Lymphoma with ATM Loss-of-function. *Mol Cancer Res*.**:** pii: molcanres.0240.2014

Di Micco R, Fumagalli M, Cicalese A, Piccinin S, Gasparini P, Luise C, Schurra C, Garre' M, Nuciforo PG, Bensimon A, Maestro R, Pelicci PG & d'Adda di Fagagna F (2006) Oncogene-induced senescence is a DNA damage response triggered by DNA hyper-replication. *Nature* **444:** 638–42

Miknyoczki SJ, Jones-Bolin S, Pritchard S, Hunter K, Zhao H, Wan W, Ator M, Bihovsky R, Hudkins R, Chatterjee S, Klein-szanto A, Dionne C & Ruggeri B (2003) Chemopotentiation of Temozolomide, Irinotecan, and Cisplatin Activity by CEP-6800, a Poly(ADP-Ribose) Polymerase Inhibitor. *Mol Cancer Ther* **2:** 371–382

Mirkin E V & Mirkin SM (2007) Replication fork stalling at natural impediments. *Microbiol Mol Biol Rev*. **71:** 13–35

Mitchell JB, Choudhuri R, Fabre K, Sowers AL, Citrin D, Zabludoff SD & Cook JA (2010) In vitro and in vivo radiation sensitization of human tumor cells by a novel checkpoint kinase inhibitor, AZD7762. *Clin Cancer Res*. **16:** 2076–84

Mitsudomi T, Morita S, Yatabe Y, Negoro S, Okamoto I, Tsurutani J, Seto T, Satouchi M, Tada H, Hirashima T, Asami K, Katakami N, Takada M, Yoshioka H, Shibata K, Kudoh S, Shimizu E, Saito H, Toyooka S, Nakagawa K, et al (2010) Gefitinib versus cisplatin plus docetaxel in patients with non-small-cell lung cancer harbouring mutations of the epidermal growth factor receptor (WJTOG3405): an open label, randomised phase 3 trial. *Lancet Oncol*. **11:** 121–128

Mitui M, Nahas SA, Du LT, Yang Z, Lai CH, Nakamura K, Arroyo S, Scott S, Purayidom A, Concannon P, Lavin MF & Gatti RA (2009) Functional and Computational Assessment of Missense Variants in the Ataxia-Telangiectasia Mutated (ATM) Gene: Mutations with Increased Cancer Risk. *Hum. Mutat*. **30:** 12–21

Moding EJ, Lee C-L, Castle KD, Oh P, Mao L, Zha S, Min HD, Ma Y, Das S & Kirsch DG (2014) Atm deletion with dual recombinase technology preferentially radiosensitizes tumor endothelium. *J Clin Invest*. **124:** 3325–3338

Mok TS, Wu Y, Thongprasert S, Yang C-H, Saijo N, Sunpaweravong P, Han B, Margono B, Ichinose Y, Nishiwaki Y, Ohe Y, Yang J-J, Chewaskulyong B, Jiang H, Duffield EL, Watkins CL, Armour AA & Fukuoka M (2009) Gefitinib or Carboplatin–Paclitaxel in Pulmonary Adenocarcinoma. *N Engl J Med*. **361:** 947–957

Mol CD, Izumi T, Mitra S & Tainer JA (2000) DNA-bound structures and mutants reveal abasic DNA binding by APE1 and DNA repair coordination. *Nature* **403:** 451–456

Montano R, Chung I, Garner KM, Parry D & Eastman A (2012) Preclinical development of the novel Chk1 inhibitor SCH900776 in combination with DNA-damaging agents and antimetabolites. *Mol Cancer Ther*. **11:** 427–38

Murai J, Huang SYN, Das BB, Renaud A, Zhang Y, Doroshow JH, Ji J, Takeda S & Pommier Y (2012) Trapping of PARP1 and PARP2 by clinical PARP inhibitors. *Cancer Res*. **72:** 5588–5599

Murga M, Bunting S, Montaña MF, Soria R, Mulero F, Cañamero M, Lee Y, Mckinnon PJ, Nussenzweig A & Fernandez-Capetillo O (2010) A mouse model of ATR-Seckel shows embryonic replicative stress and accelerated aging. *Nat Genet*. **41:** 891–898

Murga M, Campaner S, Lopez-Contreras AJ, Toledo LI, Soria R, Montaña MF, D'Artista L, Schleker T, Guerra C, Garcia E, Barbacid M, Hidalgo M, Amati B & Fernandez-Capetillo O (2011) Exploiting oncogene-induced replicative stress for the selective killing of Myc-driven tumors. *Nat Struct Mol Biol*. **18:** 1331–5

Myers JS & Cortez D (2006) Rapid activation of ATR by ionizing radiation requires ATM and Mre11. *J Biol Chem*. **281:** 9346–9350

Myers K, Gagou ME, Zuazua-Villar P, Rodriguez R & Meuth M (2009) ATR and Chk1 suppress a caspase-3-dependent apoptotic response following DNA replication stress. *PLoS Genet*. **5:** e1000324

Naim V, Wilhelm T, Debatisse M & Rosselli F (2013) ERCC1 and MUS81-EME1 promote sister chromatid separation by processing late replication intermediates at common fragile sites during mitosis. *Nat Cell Biol*. **15:** 1008–15

Nam E a & Cortez D (2011) ATR signalling: more than meeting at the fork. *Biochem J*. **436:** 527–36

National Collaborating Centre for Cancer (UK) (2011) The diagnosis and treatment of lung cancer (update). NICE Clinical Guidelines, No. 121. *Cardiff Natl. Collab. Cent. Cancer*.

Negrini S, Gorgoulis VG & Halazonetis TD (2010) Genomic instability--an evolving hallmark of cancer. *Nat Rev Mol Cell Biol* **11:** 220–8

Nghiem P, Park PK, Kim Ys Y, Desai BN & Schreiber SL (2002) ATR is not required for p53 activation but synergizes with p53 in the replication checkpoint. *J Biol Chem*. **277:** 4428–34

Nimonkar A V, Ozsoy AZ, Genschel J, Modrich P & Kowalczykowski SC (2008) Human exonuclease 1 and BLM helicase interact to resect DNA and initiate DNA repair. *Proc Natl Acad Sci U S A* **105:** 16906–16911

Nishida H, Tatewaki N, Nakajima Y, Magara T, Ko KM, Hamamori Y & Konishi T (2009) Inhibition of ATR protein kinase activity by schisandrin B in DNA damage response. *Nucleic Acids Res*. **37:** 5678–89

Non-Small Cell Lung Cancer Collaborative Group (2010) Chemotherapy for non-small cell lung cancer (Review). *Cochrane Database Syst Rev*.

O'Brien J, Wilson I, Orton T & Pognan F (2000) Investigation of the Alamar Blue (resazurin) fluorescent dye for the assessment of mammalian cell cytotoxicity. *Eur J Biochem*. **267:** 5421–5426

O'Driscoll M & Jeggo P a (2006) The role of double-strand break repair - insights from human genetics. *Nat Rev Genet*. **7:** 45–54

O'Driscoll M, Ruiz-Perez VL, Woods CG, Jeggo PA & Goodship JA (2003) A splicing mutation affecting expression of ataxia-telangiectasia and Rad3-related protein (ATR) results in Seckel syndrome. *Nat. Genet*. **33:** 497–501

O'Neill T, Dwyer AJ, Ziv Y, Chan DW, Lees-Miller SP, Abraham RH, Lai JH, Hill D, Shiloh Y, Cantley LC & Rathbun GA (2000) Utilization of oriented peptide libraries to identify substrate motifs selected by ATM. *J Biol Chem*. **275:** 22719–27

O'Rourke N, Roque i Figuls M, Macbeth F & Farre Bernado N (2010) Concurrent chemoradiotherapy in non-small cell lung cancer. *Cochrane Database Syst Rev*.

Ohashi Y, Itaya A, Tanaka Y, Yoshihara K, Kamiya T & Matsukage A (1986) Poly(ADP-ribosyl)ation of DNA polymerase beta in vitro. *Biochem Biophys Res Commun*. **140:** 666–673

Okano S, Lan L, Caldecott KW, Mori T & Yasui A (2003) Spatial and temporal cellular responses to single-strand breaks in human cells. *Mol Cell Biol*. **23:** 3974–3981

Olcina MM, Foskolou IP, Anbalagan S, Senra JM, Pires IM, Jiang Y, Ryan AJ & Hammond EM (2013) Replication stress and chromatin context link ATM activation to a role in DNA replication. *Mol Cell*. **52:** 758–766

Oliver TG, Mercer KL, Sayles LC, Burke JR, Mendus D, Lovejoy KS, Cheng M, Subramanian A, Mu D, Powers S, Crowley D, Bronson RT, Whittaker CA, Bhutkar A, Lippard SJ, Golub T, Thomale J, Jacks T & Sweet-Cordero A (2010) Chronic cisplatin treatment promotes enhanced damage repair and tumor progression in a mouse model of lung cancer. *Genes Dev*. **24:** 837–852

Olivier M, Goldgar DE, Sodha N, Ohgaki H, Kleihues P, Hainaut P & Eeles RA (2003) Li-Fraumeni and Related Syndromes: Correlation between Tumor Type, Family Structure, and TP53 Genotype. *Cancer Res*. **63:** 6643–6650

Ottini L, Falchetti M, Saieva C, De Marco M, Masala G, Zanna I, Paglierani M, Giannini G, Gulino A, Nesi G, Mariani Costantini R & Palli D (2004) MRE11 expression is impaired in gastric cancer with microsatellite instability. *Carcinogenesis* **25:** 2337–43

Ozeri-Galai E, Schwartz M, Rahat A & Kerem B (2008) Interplay between ATM and ATR in the regulation of common fragile site stability. *Oncogene* **27:** 2109–17

Paez JG, Jänne PA, Lee JC, Tracy S, Greulich H, Gabriel S, Herman P, Kaye FJ, Lindeman N, Boggon TJ, Naoki K, Sasaki H, Fujii Y, Eck MJ, Sellers WR, Johnson BE & Meyerson M (2004) EGFR Mutations in Lung Cancer: Correlation with Clinical Response to Gefitinib Therapy. *Science*. **304:** 1497–1500

Pal T, Permuth-Wey J, Betts J a, Krischer JP, Fiorica J, Arango H, LaPolla J, Hoffman M, Martino M a, Wakeley K, Wilbanks G, Nicosia S, Cantor A & Sutphen R (2005) BRCA1 and BRCA2 mutations account for a large proportion of ovarian carcinoma cases. *Cancer* **104:** 2807–16

Parker LL & Piwnica-Worms H (1992) Inactivation of the p34cdc2-cyclin B complex by the human WEE1 tyrosine kinase. *Science*. **257:** 1955–7

Patel AG, Flatten KS, Schneider P a., Dai NT, McDonald JS, Poirier GG & Kaufmann SH (2012) Enhanced killing of cancer cells by poly(ADP-ribose) polymerase inhibitors and topoisomerase I inhibitors reflects poisoning of both enzymes. *J Biol Chem*. **287:** 4198–4210

Paull TT, Rogakou EP, Yamazaki V, Kirchgessner CU, Gellert M & Bonner WM (2000) A critical role for histone H2AX in recruitment of repair factors to nuclear foci after DNA damage. *Curr Biol*. **10:** 886–95

Paulsen RD & Cimprich KA (2007) The ATR pathway: Fine-tuning the fork. *DNA Repair* **6:** 953–966

Peasland A, Wang L-Z, Rowling E, Kyle S, Chen T, Hopkins A, Cliby W a, Sarkaria J, Beale G, Edmondson RJ & Curtin NJ (2011) Identification and evaluation of a potent novel ATR inhibitor, NU6027, in breast and ovarian cancer cell lines. *Br J Cancer* **105:** 372–381

Pellegrini M, Celeste A, Difilippantonio S, Guo R, Wang W, Feigenbaum L & Nussenzweig A (2006) Autophosphorylation at serine 1987 is dispensable for murine Atm activation in vivo. *Nature* **443:** 222–225

Peng C-Y, Graves PR, Thoma RS, Wu Z, Shaw AS & Piwnica-Worms H (1997) Mitotic and G2 Checkpoint Control: Regulation of 14-3-3 Protein Binding by Phosphorylation of Cdc25C on Serine-216. *Science*. **277:** 1501–1505

Phung YT, Barbone D, Broaddus VC & Ho M (2011) Rapid generation of in vitro multicellular spheroids for the study of monoclonal antibody therapy. *J. Cancer* **2:** 507–14

Pires IM, Olcina MM, Anbalagan S, Pollard JR, Reaper PM, Charlton PA, McKenna WG & Hammond EM (2012) Targeting radiation-resistant hypoxic tumour cells through ATR inhibition. *Br J Cancer* **107:** 291–9

Portugal J, Mansilla S & Bataller M (2010) Mechanisms of drug-induced mitotic catastrophe in cancer cells. *Curr. Pharm. Des.* **16:** 69–78

Povirk LF, Zhou T, Zhou R, Cowan MJ & Yannone SM (2007) Processing of 3'-phosphoglycolate-terminated DNA double strand breaks by Artemis nuclease. *J Biol Chem*. **282:** 3547–3558

Powell SN, DeFrank JS, Connell P, Eogan M, Preffer F, Dombkowski D, Tang W & Friend S (1995) Differential sensitivity of p53(-) and p53(+) cells to caffeine-induced radiosensitization and override of G2 delay. *Cancer Res*. **55:** 1643–8

Prevo R, Fokas E, Reaper PM, Charlton PA, Pollard JR, McKenna WG, Muschel RJ & Brunner TB (2012) The novel ATR inhibitor VE-821 increases sensitivity of pancreatic cancer cells to radiation and chemotherapy. *Cancer Biol Ther*. **13:** 1072–81

Price BD & Youmell MB (1996) The Phosphatidylinositol 3-Kinase Inhibitor Wortmannin Sensitizes Murine Fibroblasts and Human Tumor Cells to Radiation and Blocks Induction of p53 following DNA Damage. *Cancer Res*. **56:** 246–250

Rainey MD, Charlton ME, Stanton R V & Kastan MB (2008) Transient inhibition of ATM kinase is sufficient to enhance cellular sensitivity to ionizing radiation. *Cancer Res*. **68:** 7466–74

Raynard S, Bussen W & Sung P (2006) A double holliday junction dissolvasome comprising BLM, topoisomerase IIIalpha, and BLAP75. *J Biol Chem*. **281:** 13861–13864

Reaper PM, Griffiths MR, Long JM, Charrier J-D, Maccormick S, Charlton PA, Golec JMC & Pollard JR (2011) Selective killing of ATM- or p53-deficient cancer cells through inhibition of ATR. *Nat Chem Biol*. **7:** 428–30

Reck M, Heigener DF, Mok T, Soria J-C & Rabe KF (2013) Management of non-small-cell lung cancer: recent developments. *Lancet* **382:** 709–719

Riesterer O, Matsumoto F, Wang L, Pickett J, Molkentine D, Giri U, Milas L & Raju U (2011) A novel Chk inhibitor, XL-844, increases human cancer cell radiosensitivity through promotion of mitotic catastrophe. *Invest New Drugs*. **29:** 514–22

Roossink F, Wieringa HW, Noordhuis MG, ten Hoor KA, Kok M, Slagter-Menkema L, Hollema H, de Bock GH, Pras E, de Vries EGE, de Jong S, van der Zee AGJ, Schuuring E, Wisman GBA & van Vugt MATM (2012) The role of ATM and 53BP1 as predictive markers in cervical cancer. *Int J Cancer*. **131:** 2056–66

Roy K, Wang L, Makrigiorgos GM & Price BD (2006) Methylation of the ATM promoter in glioma cells alters ionizing radiation sensitivity. *Biochem Biophys Res Commun*. **344:** 821–6

Ruzankina Y, Pinzon-Guzman C, Asare A, Ong T, Pontano L, Cotsarelis G, Zediak VP, Velez M, Bhandoola A & Brown EJ (2007) Deletion of the developmentally essential gene ATR in adult mice leads to age-related phenotypes and stem cell loss. *Cell Stem Cell*. **1:** 113–26

Ruzankina Y, Schoppy DW, Asare A, Clark CE, Vonderheide RH & Brown EJ (2009) Tissue regenerative delays and synthetic lethality in adult mice after combined deletion of Atr and Trp53. *Nat. Genet*. **41:** 1144–9

Sancar A, Lindsey-Boltz LA, Unsal-Kaçmaz K & Linn S (2004) Molecular mechanisms of mammalian DNA repair and the DNA damage checkpoints. *Annu Rev Biochem*. **73:** 39–85

Sanchez Y, Wong C, Thoma RS, Richman R, Wu Z, Piwnica-Worms H & Elledge SJ (1997) Conservation of the Chk1 Checkpoint Pathway in Mammals: Linkage of DNA Damage to Cdk Regulation Through Cdc25. *Science*. **277:** 1497–1501

Sandhu SK, Yap T a. & de Bono JS (2010) Poly(ADP-ribose) polymerase inhibitors in cancer treatment: A clinical perspective. *Eur J Cancer*. **46:** 9–20

Sandoval N, Platzer M, Rosenthal A, Dörk T, Bendix R, Skawran B, Stuhrmann M, Wegner RD, Sperling K, Banin S, Shiloh Y, Baumer A, Bernthaler U, Sennefelder H, Brohm M, Weber BH & Schindler D (1999) Characterization of ATM gene mutations in 66 ataxia telangiectasia families. *Hum Mol Genet*. **8:** 69–79

Sarkaria JN, Busby EC, Tibbetts RS, Roos P, Taya Y, Karnitz LM & Abraham RT (1999) Inhibition of ATM and ATR Kinase Activities by the Radiosensitizing Agent, Caffeine. *Cancer Res*. **59:** 4375–4382

Sarkaria JN, Tibbetts RS, Busby EC, Kennedy AP, Hill DE & Abraham RT (1998) Inhibition of Phosphoinositide 3-Kinase Related Kinases by the Radiosensitizing Agent Wortmannin. *Cancer Res*. **58:** 4375–4382

Sartori A a, Lukas C, Coates J, Mistrik M, Fu S, Bartek J, Baer R, Lukas J & Jackson SP (2007) Human CtIP promotes DNA end resection. *Nature* **450:** 509–514

Satoh MS & Lindahl T (1992) Role of poly(ADP-ribose) formation in DNA repair. Role of poly(ADP-ribose) formation in DNA repair. *Nature* **356:** 356–8

Savitsky K, Bar-Shira A, Gilad S, Rotman G, Ziv Y, Vanagaite L, Tagle DA, Smith S, Uziel T, Sfez S, Ashkenazi M, Pecker I, Frydman M, Harnik R, Patanjali SR, Simmons A, Clines GA, Sartiel A, Gatti RA, Chessa L, et al (1995) A single ataxia telangiectasia gene with a product similar to PI-3 kinase. *Science*. **268:** 1749–53

Schiller JH, Harrington D, Belani CP, Langer C, Sandler A, Krook J, Zhu J & Johnson DH (2002) Comparison of four chemotherapy regimens for advanced non-small-cell lung cancer. *N Engl J Med*. **346:** 92–8

Schoppy DW, Ragland RL, Gilad O, Shastri N, Peters AA, Murga M, Fernandez-capetillo O, Diehl JA & Brown EJ (2012) Oncogenic stress sensitizes murine cancers to hypomorphic suppression of ATR. *J Clin Invest*. **122:** 241–252

Schultz N, Lopez E, Saleh-Gohari N & Helleday T (2003) Poly(ADP-ribose) polymerase (PARP-1) has a controlling role in homologous recombination. *Nucleic Acids Res*. **31:** 4959–4964

Scott SP, Bendix R, Chen P, Clark R, Dork T & Lavin MF (2002) Missense mutations but not allelic variants alter the function of ATM by dominant interference in patients with breast cancer. *PNAS* **99:** 925–30

Scully R & Xie A (2013) Double strand break repair functions of histone H2AX. *Mutat Res*. **750:** 5–14

Senra JM, Telfer B a., Cherry KE, McCrudden CM, Hirst DG, O'Connor MJ, Wedge SR & Stratford IJ (2011) Inhibition of PARP-1 by Olaparib (AZD2281) Increases the Radiosensitivity of a Lung Tumor Xenograft. *Mol Cancer Ther*. **10:** 1949–1958

Shang ZF, Huang B, Xu QZ, Zhang SM, Fan R, Liu XD, Wang Y & Zhou PK (2010) Inactivation of DNA-dependent protein kinase leads to spindle disruption and mitotic catastrophe with attenuated checkpoint protein 2 phosphorylation in response to DNA damage. *Cancer Res*. **70:** 3657–3666

Shen Y, Rehman FL, Feng Y, Boshuizen J, Bajrami I, Elliott R, Wang B, Lord CJ, Post LE & Ashworth A (2013) BMN 673, a novel and highly potent PARP1/2 inhibitor for the treatment of human cancers with DNA repair deficiency. *Clin Cancer Res*. **19:** 5003–15

Shibata A, Conrad S, Birraux J, Geuting V, Barton O, Ismail A, Kakarougkas A, Meek K, Taucher-Scholz G, Löbrich M & Jeggo PA (2011) Factors determining DNA double-strand break repair pathway choice in G2 phase. *EMBO J*. **30:** 1079–1092

Shibata A, Moiani D, Arvai AS, Perry J, Harding SM, Genois MM, Maity R, van Rossum-Fikkert S, Kertokalio A, Romoli F, Ismail A, Ismalaj E, Petricci E, Neale MJ, Bristow RG, Masson JY, Wyman C, Jeggo PA & Tainer JA (2014) DNA Double-Strand Break Repair Pathway Choice Is Directed by Distinct MRE11 Nuclease Activities. *Mol Cell* **53:** 7–18

Shieh SY, Ikeda M, Taya Y & Prives C (1997) DNA damage-induced phosphorylation of p53 alleviates inhibition by MDM2. *Cell* **91:** 325–34

Shih I, Zhou W, Goodman SN, Tumorigenesis C, Lengauer C, Kinzler KW & Vogelstein B (2001) Evidence That Genetic Instability Occurs at an Early Stage of Colorectal Tumorigenesis. *Cancer Res*. **61:** 818–822

Shiloh Y (2001) ATM and ATR : networking cellular responses to DNA damage. *Curr Opin Genet Dev*. **11:** 71–77

Shiloh Y (2003) ATM and related protein kinases: safeguarding genome integrity. *Nat Rev Cancer*. **3:** 155–68

Shiloh Y & Ziv Y (2013) The ATM protein kinase: regulating the cellular response to genotoxic stress, and more. *Nat Rev Mol Cell Biol*. **14:** 197–210

Shiotani B & Zou L (2009) ATR signaling at aglance. *J Cell Sci*. **2:** 301–304

Siliciano JD, Canman CE, Taya Y, Sakaguchi K, Appella E & Kastan MB (1997) DNA damage induces phosphorylation of the amino terminus of p53. *Genes Dev*. **11:** 3471–3481

So S, Davis AJ & Chen DJ (2009) Autophosphorylation at serine 1981 stabilizes ATM at DNA damage sites. *J Cell Biol*. **187:** 977–990

Sonnenblick A, de Azambuja E, Azim HA & Piccart M (2015) An update on PARP inhibitors-moving to the adjuvant setting. *Nat Rev Clin Oncol*. **12:** 27–41

Sørensen CS, Syljuåsen RG, Falck J, Schroeder T, Rönnstrand L, Khanna KK, Zhou B-B, Bartek J & Lukas J (2003) Chk1 regulates the S phase checkpoint by coupling the physiological turnover and ionizing radiation-induced accelerated proteolysis of Cdc25A. *Cancer Cell* **3:** 247–58

Stead LF, Berri S, Wood HM, Egan P, Conway C, Daly C & Rabbits P (2012) The Transcriptional Consequences of Somatic Amplifications, Deletions, and Rearrangements in a Human Lung Squamous Cell Carcinoma. *Neoplasia* **14:** 1075–1086

Steigemann P, Wurzenberger C, Schmitz MHA, Held M, Guizetti J, Maar S & Gerlich DW (2009) Aurora B-Mediated Abscission Checkpoint Protects against Tetraploidization. *Cell* **136:** 473–484

Stewart GS (2009) Solving the RIDDLE of 53BP1 recruitment to sites of damage. *Cell cycle* **8:** 1532–8

Stiff T, Driscoll MO, Rief N, Iwabuchi K, Lo M & Jeggo PA (2004) ATM and DNA-PK Function Redundantly to Phosphorylate H2AX after Exposure to Ionizing Radiation. *Cancer Res*. **64:** 2390–2396

Stracker TH & Petrini JHJ (2011) The MRE11 complex: starting from the ends. *Nat Rev Mol Cell Biol*. **12:** 90–103

Stratton MR, Campbell PJ & Futreal PA (2009) The cancer genome. *Nature* **458:** 719–724

Stucki M, Clapperton JA, Mohammad D, Yaffe MB, Smerdon SJ & Jackson SP (2005) MDC1 directly binds phosphorylated histone H2AX to regulate cellular responses to DNA double-strand breaks. *Cell* **123:** 1213–1226

Sullivan KD, Gallant-Behm CL, Henry RE, Fraikin J-L & Espinosa JM (2012) The p53 circuit board. *Biochim Biophys Acta*. **1825:** 229–44

Sultana R, Abdel-Fatah T, Abbotts R, Hawkes C, Albarakati N, Seedhouse C, Ball G, Chan S, Rakha E a, Ellis IO & Madhusudan S (2013a) Targeting XRCC1 deficiency in breast cancer for personalized therapy. *Cancer Res*. **73:** 1621–34

Sultana R, Abdel-Fatah T, Perry C, Moseley P, Albarakti N, Mohan V, Seedhouse C, Chan S & Madhusudan S (2013b) Ataxia telangiectasia mutated and Rad3 related (ATR) protein kinase inhibition is synthetically lethal in XRCC1 deficient ovarian cancer cells. *PLoS One* **8:** e57098

Sultana R, McNeill DR, Abbotts R, Mohammed MZ, Zdzienicka MZ, Qutob H, Seedhouse C, Laughton CA, Fischer PM, Patel PM, Wilson DM & Madhusudan S (2012) Synthetic lethal targeting of DNA double-strand break repair deficient cells by human apurinic/apyrimidinic endonuclease inhibitors. *Int J Cancer* **131:** 2433–44

Syljuåsen RG, Sørensen CS, Hansen LT, Fugger K, Lundin C, Helleday T, Sehested M & Lukas J (2005) Inhibition of Human Chk1 Causes Increased Initiation of DNA Replication, Phosphorylation of ATR Targets, and DNA Breakage. *Mol Cell Biol*. **25:** 3553–3562

Tarsounas M, Davies A a & West SC (2004) RAD51 localization and activation following DNA damage. *Philos Trans R Soc L. B Biol Sci*. **359:** 87–93

Taylor AMR, Harnden DG, Arlett CF, Harcourt SA, Lehmann AR, Stevens S & Bridges BA (1975) Ataxia teleangiectasia: a human mutation with abnormal radiation sensitivity. *Nature* **258:** 427–429

Teng P, Bateman NW, Darcy KM, Hamilton CA, Larry G, Bakkenist CJ & Conrads TP (2015) Pharmacologic inhibition of ATR and ATM offers clinically important distinctions to enhancing platinumor radiation response in ovarian, endometrial, and cervical cancer cells. *Gynecol Oncol*. **136:** 554–561

Terradas M, Martín M, Tusell L & Genescà A (2010) Genetic activities in micronuclei: is the DNA entrapped in micronuclei lost for the cell? *Mutat Res*. **705:** 60–7

The Information Centre for Health and Social Care (2006) National Clinical Audit Support Programme Lung Cancer NLCA Report 2005. *Leeds Inf. Cent. Heal. Soc. Care*

Tibbetts RS, Brumbaugh KM, Williams JM, Sarkaria JN, Cliby WA, Shieh S-Y, Taya Y, Prives C & Abraham RT (1999) A role for ATR in the DNA damage-induced phosphorylation of p53. *Genes Dev*. **13:** 152–157

Tibbetts RS, Cortez D, Brumbaugh KM, Scully R, Livingston D, Elledge SJ & Abraham RT (2000) Functional interactions between BRCA1 and the checkpoint kinase ATR during genotoxic stress. *Genes Dev*. **14:** 2989–3002

Toledo LI, Altmeyer M, Rask MB, Lukas C, Larsen DH, Povlsen LK, Bekker-Jensen S, Mailand N, Bartek J & Lukas J (2013) ATR prohibits replication catastrophe by preventing global exhaustion of RPA. *Cell* **155:** 1088–1103

Toledo LI, Murga M, Zur R, Soria R, Rodriguez A, Martinez S, Oyarzabal J, Pastor J, Bischoff JR & Fernandez-Capetillo O (2011) A cell-based screen identifies ATR inhibitors with synthetic lethal properties for cancer-associated mutations. *Nat Struct Mol Biol*. **18:** 721–7

Tsantoulis PK, Kotsinas A, Sfikakis PP, Evangelou K, Sideridou M, Levy B, Mo L, Kittas C, Wu X-R, Papavassiliou AG & Gorgoulis VG (2008) Oncogene-induced replication stress preferentially targets common fragile sites in preneoplastic lesions. A genome-wide study. *Oncogene* **27:** 3256–3264

Tuli R, Surmak AJ, Reyes J, Armour M, Hacker-Prietz A, Wong J, DeWeese TL & Herman JM (2014) Radiosensitization of Pancreatic Cancer Cells In Vitro and In Vivo through Poly (ADP-ribose) Polymerase Inhibition with ABT-888. *Transl Oncol*. **7:** 439–445

Turner NC, Lord CJ, Iorns E, Brough R, Swift S, Elliott R, Rayter S, Tutt AN & Ashworth A (2008) A synthetic lethal siRNA screen identifying genes mediating sensitivity to a PARP inhibitor. *EMBO J*. **27:** 1368–77

Tutt A, Robson M, Garber JE, Domchek SM, Audeh MW, Weitzel JN, Friedlander M, Arun B, Loman N, Schmutzler RK, Wardley A, Mitchell G, Earl H, Wickens M & Carmichael J (2010) Oral poly(ADP-ribose) polymerase inhibitor olaparib in patients with BRCA1 or BRCA2 mutations and advanced breast cancer: a proof-of-concept trial. *Lancet* **376:** 235–44

Uziel T, Savitsky K, Platzer M, Ziv Y, Helbitz T, Nehls M, Boehm T, Rosenthal A, Shiloh Y & Rotman G (1996) Genomic Organization of the ATM Gene. *Genomics* **33:** 317–320

Vance SM, Liu E, Zhao L, Parsels JD, Parsels LA, Brown JL, Maybaum J, Lawrence TS & Morgan MA (2011) Selective radiosensitization of p53 mutant pancreatic cancer cells by combined inhibition of Chk1 and PARP1. *Cell Cycle*. **10:** 4321–4329

Vaporciyan AA, Kies MS, Stevens CW, Komaki R & Roth JA (2003) Molecular pathogenesis. In *Holland-Frei Cancer Medicine. 6th edition*., Kufe DW Pollock RE Weichselbaum RR & Al. E (eds) p Available from: http://www.ncbi.nlm.nih.gov/books/. Hamilton (ON): BC Decker

Verhagen MMM, Last JI, Hogervorst FBL, Smeets DFCM, Roeleveld N, Verheijen F, Catsman-Berrevoets CE, Wulffraat NM, Cobben JM, Hiel J, Brunt ER, Peeters E a J, Gómez Garcia EB, van der Knaap MS, Lincke CR, Laan L a EM, Tijssen M a J, van Rijn M a, Majoor-Krakauer D, Visser M, et al (2012) Presence of ATM protein and residual kinase activity correlates with the phenotype in ataxia-telangiectasia: a genotype-phenotype study. *Hum. Mut*. **33:** 561–71

Di Virgilio M, Ying CY & Gautier J (2009) PIKK-dependent phosphorylation of Mre11 induces MRN complex inactivation by disassembly from chromatin. *DNA Repair* **8:** 1311–20

Vo QN, Kim W-J, Cvitanovic L, Boudreau DA, Ginzinger DG & Brown KD (2004) The ATM gene is a target for epigenetic silencing in locally advanced breast cancer. *Oncogene* **23:** 9432–7

Walker JR, Corpina RA & Goldberg J (2001) Structure of the Ku heterodimer bound to DNA and its implications for double-strand break repair. *Nature* **412:** 607–614

Wang H, Shi LZ, Wong CCL, Han X, Hwang PYH, Truong LN, Zhu Q, Shao Z, Chen DJ, Berns MW, Yates JR, Chen L & Wu X (2013) The Interaction of CtIP and Nbs1 Connects CDK and ATM to Regulate HR-Mediated Double-Strand Break Repair. *PLoS Genet*. **9:** 25–27

Wang H, Wang H, Powell SN, Iliakis G & Wang Y (2004) ATR Affecting Cell Radiosensitivity Is Dependent on Homologous Recombination Repair but Independent of Nonhomologous End Joining. *Cancer Res*. **64:** 7139–7143

Wang L, Mosel AJ, Oakley GG & Peng A (2012) Deficient DNA damage signaling leads to chemoresistance to cisplatin in oral cancer. *Mol Cancer Ther*. **11:** 2401–2409

Ward IM & Chen J (2001) Histone H2AX is phosphorylated in an ATR-dependent manner in response to replicational stress. *J. Biol. Chem*. **276:** 47759–62

Weber AM & Ryan AJ (2015) ATM and ATR as therapeutic targets in cancer. *Pharmacol Ther*. **149:** 124–138

West SC (2003) Molecular views of recombination proteins and their control. *Nat Rev Mol Cell Biol*. **4:** 435–45

Weston VJ, Oldreive CE, Skowronska A, Oscier DG, Pratt G, Dyer MJS, Smith G, Powell JE, Rudzki Z, Kearns P, Moss PAH, Taylor AMR & Stankovic T (2010) The PARP inhibitor olaparib induces significant killing of ATM-deficient lymphoid tumor cells in vitro and in vivo. *Blood* **116:** 4578–87

White JS, Choi S & Bakkenist CJ (2010) Transient ATM kinase inhibition disrupts DNA damage-induced sister chromatid exchange. *Sci Signal*. **3:** ra44

Williamson CT, Kubota E, Hamill JD, Klimowicz A, Ye R, Muzik H, Dean M, Tu L, Gilley D, Magliocco AM, McKay BC, Bebb DG & Lees-Miller SP (2012) Enhanced cytotoxicity of PARP inhibition in mantle cell lymphoma harbouring mutations in both ATM and p53. *EMBO Mol Med*. **4:** 515–527

Williamson CT, Muzik H, Turhan AG, Zamò A, O'Connor MJ, Bebb DG & Lees-Miller SP (2010) ATM deficiency sensitizes mantle cell lymphoma cells to poly(ADP-ribose) polymerase-1 inhibitors. *Mol Cancer Ther*. **9:** 347–57

Wilson TE, Arlt MF, Park SH, Rajendran S, Paulsen M, Ljungman M & Glover TW (2015) Large transcription units unify copy number variants and common fragile sites arising under replication stress. *Genome Res*. **25:** 189–200

Wold MS (1997) Replication protein A: a heterotrimeric, single-stranded DNA-binding protein required for eukaryotic DNA metabolism. *Annu Rev Biochem*. **66:** 61–92

Wold MS & Kelly T (1988) Purification and characterization of replication protein A, a cellular protein required for in vitro replication of simian virus 40 DNA. *Proc. Natl. Acad. Sci. U. S. A*. **85:** 2523–7

Woods D & Turchi JJ (2013) Chemotherapy induced DNA damage response: convergence of drugs and pathways. *Cancer Biol Ther*. **14:** 379–89

Wu L & Hickson ID (2003) The Bloom's syndrome helicase suppresses crossing over during homologous recombination. *Nature* **426:** 870–874

Xiao Z, Chen Z, Gunasekera AH, Sowin TJ, Rosenberg SH, Fesik S & Zhang H (2003) Chk1 mediates S and G2 arrests through Cdc25A degradation in response to DNA-damaging agents. *J Biol Chem*. **278:** 21767–73

Xu B, Sun Z, Liu Z, Guo H, Liu Q, Jiang H, Zou Y, Gong Y, Tischfield J a & Shao C (2011) Replication stress induces micronuclei comprising of aggregated DNA double-strand breaks. *PLoS One* **6:** e18618

Yamamoto K, Wang Y, Jiang W, Liu X, Dubois RL, Lin C-S, Ludwig T, Bakkenist CJ & Zha S (2012) Kinase-dead ATM protein causes genomic instability and early embryonic lethality in mice. *J Cell Biol*. **198:** 305–313

Yao S-L, Akhtar AJ, McKenna KA, C. BG, David S, Mack M, Rajani R, Collector MI, Jones RJ, Sharkis SJ, Fuchs EJ & Bedi A (1996) Selective radiosensitization of p53-deficient cells by ceffeine-mediated activation of p34 cdc2 kinase. *Nat. Med*. **2:** 1140–1143

Ying S, Minocherhomji S, Chan KL, Palmai-Pallag T, Chu WK, Wass T, Mankouri HW, Liu Y & Hickson ID (2013) MUS81 promotes common fragile site expression. *Nat Cell Biol*. **15:** 1001–7

You Z & Bailis JM (2010) DNA damage and decisions: CtIP coordinates DNA repair and cell cycle checkpoints. *Trends Cell Biol*. **20:** 402–409

You Z, Chahwan C, Bailis J, Hunter T & Russell P (2005) ATM Activation and Its Recruitment to Damaged DNA Require Binding to the C Terminus of Nbs1. *Mol Cell Biol*. **25:** 5363–5379

Zachos G & Gillespie DA (2007) Exercising Restraints: Role of Chk1 in Regulating the Onset and Progression of Unperturbed Mitosis in Vertebrate Cells. *Cell Cycle* **6:** 810–813

Zannini L, Delia D & Buscemi G (2014) CHK2 kinase in the DNA damage response and beyond. *J Mol Cell Biol*. **6:** 442–457

Zeman MK & Cimprich KA (2014) Causes and consequences of replication stress. *Nat Cell Biol*. **16:** 2–9

Zhao H & Piwnica-Worms H (2001) ATR-mediated checkpoint pathways regulate phosphorylation and activation of human Chk1. *Mol Cell Biol*. **21:** 4129–39

Zhao H, Watkins JL & Piwnica-Worms H (2002) Disruption of the checkpoint kinase 1/cell division cycle 25A pathway abrogates ionizing radiation- induced S and G2 checkpoints. *Proc Natl Acad Sci U S A* **99:** 14795–14800

Zhao Y, Thomas HD, Batey MA, Cowell IG, Richardson CJ, Griffin RJ, Calvert AH, Newell DR, Smith GCM & Curtin NJ (2006) Preclinical evaluation of a potent novel DNA-dependent protein kinase inhibitor NU7441. *Cancer Res*. **66:** 5354–62

Zhou Y & Paull TT (2013) DNA-dependent protein kinase regulates DNA end resection in concert with Mre11-Rad50-Nbs1 (MRN) and Ataxia Telangiectasia-mutated (ATM). *J Biol Chem*. **288:** 37112–37125

Ziv Y, Bar-Shira A, Pecker I, Russell P, Jorgensen TJ, Tsarfati I & Shiloh Y (1997) Recombinant ATM protein complements the cellular A-T phenotype. *Oncogene* **15:** 159–67

Zou L & Elledge SJ (2003) Sensing DNA damage through ATRIP recognition of RPA-ssDNA complexes. *Science*. **300:** 1542–8

9 Appendix

Supplementary Table 1: IHC evaluation of ATM protein expression in NSCLC cell lines.

A TMA containing FFPE cell pellet samples of 35 NSCLC cell lines was analysed for ATM protein expression by immunohistochemistry. The table summarises the cell lines included on the TMA and the staining results for each cell line; pos. = positive, neg. = negative for ATM staining. Representative images, taken at a 200x magnification on the Aperio ScanScope CS digital slide scanner, are shown for each cell line. GM05849F is a fibroblast cell line derived from an A-T patient and served as negative control. Cell lines showing no ATM protein expression (GM05849F, H1395 and H23) are highlighted in red.

Cell line	ATM IHC	Example image	Cell line	ATM IHC	Example image
PC9	pos.	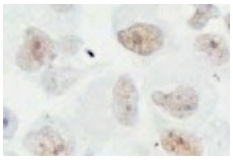	**H1975**	pos.	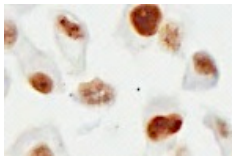
LouN91	pos.	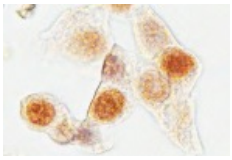	**H1915**	pos.	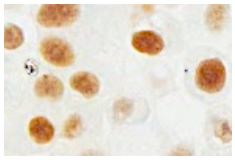
HCC827	pos.	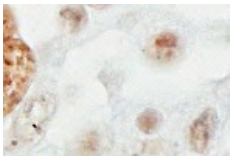	**H1819**	pos.	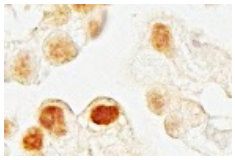
HCC366	pos.	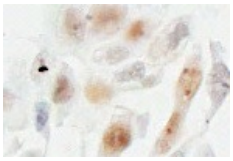	**H1792**	pos.	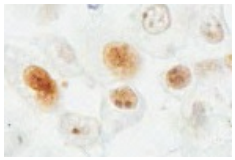
H596	pos.	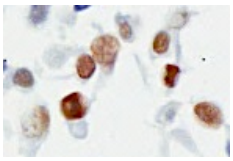	**H1781**	pos.	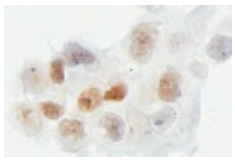
H520	pos.	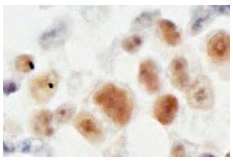	**H1755**	pos.	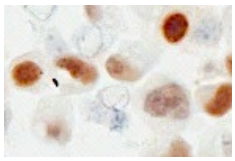

Cell line	ATM IHC	Example image	Cell line	ATM IHC	Example image
H460	pos.	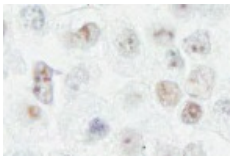	**H1734**	pos.	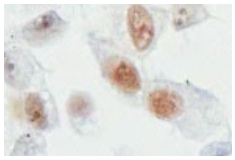
H441	pos.	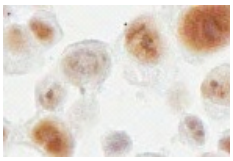	**H1651**	pos.	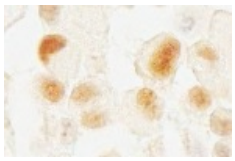
H3122	pos.	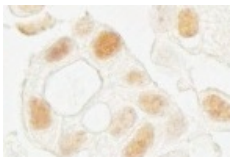	**H1650**	pos.	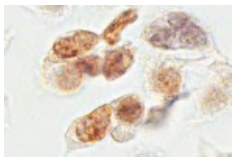
H2935	pos.	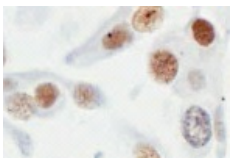	**H1648**	pos.	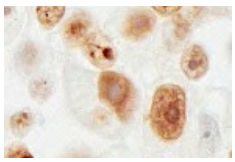
H23	neg.	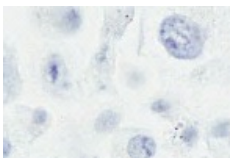	**H1568**	pos.	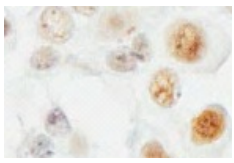
H2228	pos.	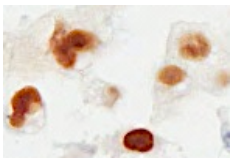	**H1563**	pos.	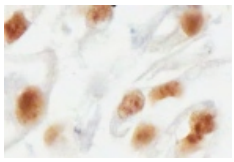
H2126	pos.	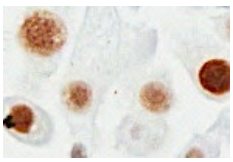	**H1395**	neg.	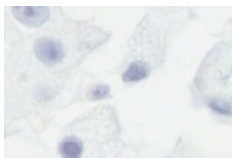
H2087	pos.	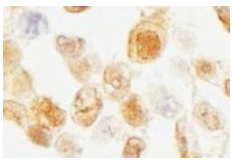	**H1299**	pos.	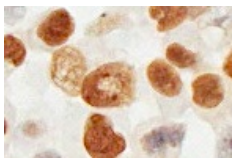
H2030	pos.	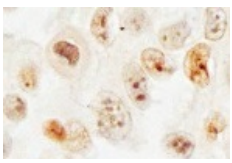	**COR-L105**	pos.	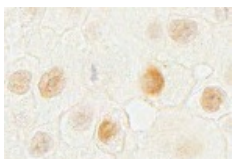

Cell line	ATM IHC	Example image	Cell line	ATM IHC	Example image
H2009	pos.	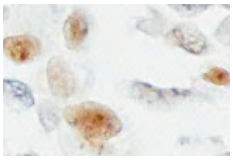	**Colo699**	pos.	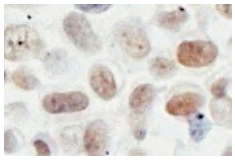
A549	pos.	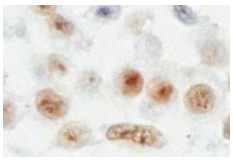	**Calu-6**	pos.	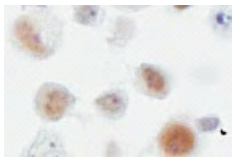
A427	pos.	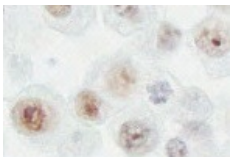	**GM05849F**	neg.